JSCSEN 77(7)859–981(2012)

ISSN 1820-7421 (Online)

Journal of the Serbian Chemical Society

Society 115th Anniversary
1897 - 2012

VOLUME 77
No 7
BELGRADE 2012

Available on line at
www.shd.org.rs/JSCS/

Journal of the Serbian Chemical Society
eVersion electronic
JSCS-info@shd.org.rs • www.shd.org.rs/JSCS

J. Serb. Chem. Soc. Vol. 77, No. 7 (2012)

CONTENTS

Organic Chemistry

Biochemistry and Biotechnology

Theoretical Chemistry

Electrochemistry

Analytical Chemistry

Polymers

Materials

Thermodynamics

Environmental

Published by the Serbian Chemical Society
Karnegijeva 4/III, 11000 Belgrade, Serbia
Printed by the Faculty of Technology and Metallurgy
Karnegijeva 4, P.O. Box 35-03, 11120 Belgrade, Serbia

Journal of the Serbian Chemical Society

JSCS-info@shd.org.rs • www.shd.org.rs/JSCS

J. Serb. Chem. Soc. 77 (7) 859–866 (2012)
JSCS–4314

UDC 547.814+547.853+66.095.3:
615.281.004.12
Original scientific paper

Synthesis and characterization of new 2-amino-4-(3,4-dihydro-7-methoxy-2,2-dimethyl-2*H*-benzopyran-6-yl)-6-(substituted phenyl)pyrimidines and their bioevaluation

YELLAJYOSULA LAKSHMI NARASIMHA MURTHY[1]*, KILARU PADMA SUHASINI[1]
and ANJALI JHA[2]

[1]Department of Organic Chemistry, Andhra University, Visakhapatnam, India
and [2]Department of Chemistry, Gitam Institute of Science,
GITAM University, Visakhapatnam, India

(Received 23 September 2011, revised 22 January 2012)

Abstract: A series of eight novel 2-amino-4-(3,4-dihydro-7-methoxy-2,2-dimethyl-2*H*-benzopyran-6-yl)-6-(substituted phenyl)pyrimidines were designed and synthesized by utilizing benzene-1,3-diol as the starting material. The structures of the isolated products (**6a–h**) were established through ^{1}H-NMR, ^{13}C-NMR, and FT-IR spectroscopic techniques and elemental analysis. The antimicrobial properties of the synthesized compounds were screened against gram positive (*Bacillus pumilus*, *Bacillus subtilis* and *Streptococcus faecalis*), gram negative bacteria (*Enterococcus faecalis*, *Escherchia coli* and *Proteus vulgaris)* and fungi *(Pencillium expansum, Aspergillus niger* and *Candida albicans)* using ampicillin and ketoconazole as reference compounds. Most of the compounds showed moderate to high antibacterial and antifungal activities against the studied strains, with inhibition zones between 8 and 30 mm.

Keywords: benzopyran; chalcones; Claisen–Schmidt condensation; 2-amino pyrimidine derivatives; antimicrobial activity.

INTRODUCTION

Antibiotics revolutionized medical care in the 20th century. However, the emergence of super bugs, *i.e.*, bacteria that resist the effects of the most powerful antibiotics, are posing a great challenge to the field of medicine.[1] In this sense, nitrogen-containing heterocycles are an important class of compounds in medicinal chemistry.[2] As pyrimidines seem to possess a wide spectrum of biological activity,[3] there has been considerable interest in the development of preparative methods for the production of pyrimidines.

---

* Corresponding author. E-mail: murthyyln@gmail.com

doi: 10.2298/JSC110923008M

On the other hand, pyrimidines, being an integral part of DNA and RNA, exhibit diverse pharmacological properties as effective bactericide, fungicide, viricide, insecticide and meticide,[4] antitubercular,[5] antineoplastic,[6] antitumor,[7] anti-inflammatory,[8] diuretic,[9] antimalarial,[10] cardiovascular,[11] calcium channel blockers[12] and many other classes of chemotherapeutic agents.[13]

The benzopyran ring occurs frequently in natural products. However 3,4-dihydro-2*H*-benzopyrans occur rarely in nature but are useful degradation products of a large number of natural products.[14] They have been reported to show marked pharmacological activities.[15] The biological activity of many of the naturally occurring compounds which incorporate a benzopyran ring has resulted in several applications of various levels of saturation and oxidation in synthesis.[16] Due to the various biological functions associated with this skeleton, it has been frequently employed as a key scaffold in drug research.[17]

In view of these observations and in continuation of our work[18] on biologically active heterocycles and their increasing importance in pharmaceutical and biological fields, it was considered of interest to synthesize some new chemical entities incorporating two active pharmacophores in a single molecular framework and to evaluate their biological activities. In this respect, eight novel 2-amino-4-(3,4-dihydro-7-methoxy-2,2-dimethyl-2*H*-benzopyran-6-yl)-6-(substituted phenyl)pyrimidines (**6a**–**h**) were synthesized *via* benzopyranylchalcones and the antimicrobial activities of the compact structures were screened.

EXPERIMENTAL

Materials, methods and instruments

All the chemicals and solvents used in this work were of analytical reagent grade (anhydrous) and purchased from Sigma–Aldrich. Melting points were determined using an electro-thermal apparatus in an open capillary tube and are uncorrected. The ^{1}H-NMR and ^{13}C-NMR spectra were recorded on a JEOL JNM Ex-90 instrument, at 90 and 22.5 MHz, respectively, using TMS as an internal reference in $CDCl_3$. The IR spectra were recorded in KBr discs on a Thermo Nicolet 6700 FTIR spectrophotometer. The HPLC was performed using a Shimadzu LC 6A instrument fitted with a Shimpack silica gel column using acetonitrile as the solvent. The mass spectra were obtained on a Varian Atlas CH-7 mass spectrometer. Elemental analyses were performed using an Elementar Vario EL elemental analyzer. Satisfactory C, H, N analyses were obtained for all the compounds.

The steps involved in the synthesis of the new series of 2-amino-4-benzopyran-6-yl pyrimidines from benzene-1,3-diol are depicted in Scheme 1.

*Synthesis of 3,4-dihydro-7-hydroxy-2,2-dimethyl-2*H*-benzopyran (**2**)*

To a solution of benzene-1,3-diol **1** (10 mmol) in dichloromethane (20 mL) was added polyphosphoric acid (0.1 eq.) followed by 2-methyl-3-buten-2-ol (5 mmol) and the mixture was stirred for 1 h at room temperature. The reaction mixture was heated at reflux for 4 h. After cooling, the mixture was neutralized with saturated $NaHCO_3$ and extracted with dichloromethane. The solvent was removed and the residue recrystallized from *n*-hexane to give a white crystalline solid in 68 % yield, which was characterized by its spectral data.[19]

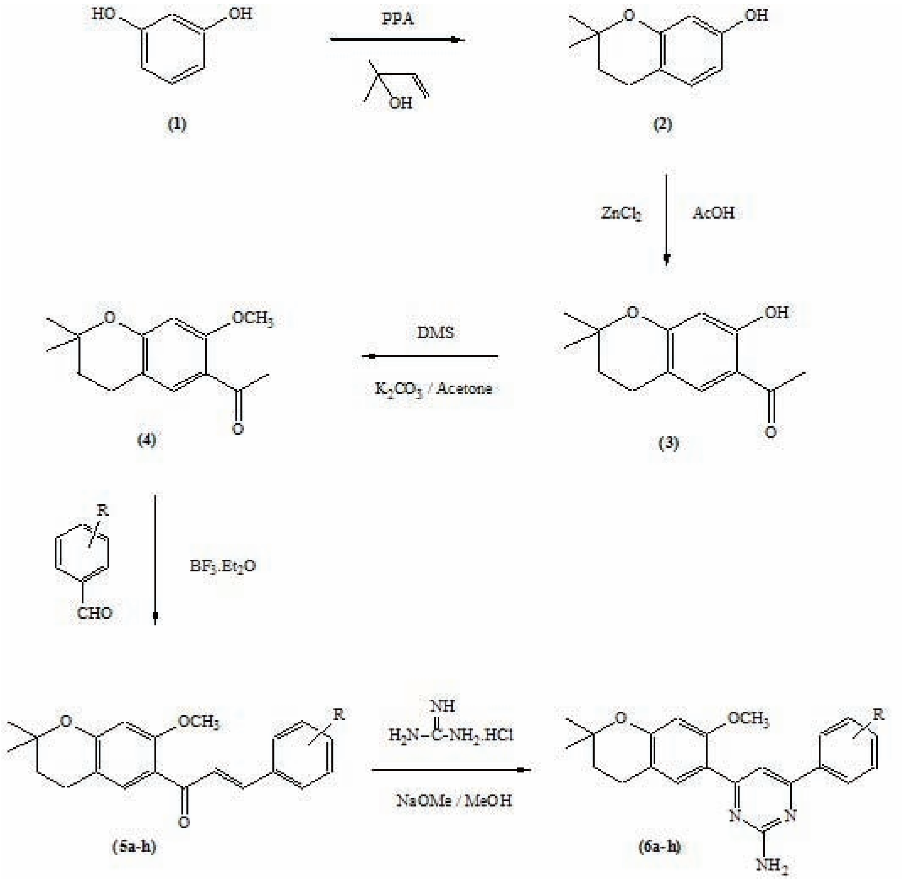

R: a) H, b) 4-CH_3, c) 4-OCH_3, d) 2,5-OCH_3, e) $N(Me)_2$, f) 4-Cl, g) 4-NO_2, h) 4-CN

Scheme 1. The synthetic pathway to the new 2-amino benzopyrano pyrimidines **6a–h**.

*Synthesis of 6-acetyl-3,4-dihydro-7-hydroxy-2,2-dimethyl-2*H*-benzopyran (**3**)*

3,4-Dihydro-7-hydroxy-2,2-dimethyl-2*H*-benzopyran (**2**) (8 mmol) was acetylated using acetic acid (8 mmol) in the presence of freshly fused $ZnCl_2$ (8 mmol) at 140–150 °C under stirring for 15 min. After cooling to room temperature, HCl was added to the reaction mixture to break the zinc chloride complex and in 5 min precipitation commenced. The precipitate was washed with very dilute HCl to afford colorless needles in 54 % yield. The product was characterized by its spectral data.[19]

*Synthesis of 6-acetyl-3,4-dihydro-7-methoxy-2,2-dimethyl-2*H*-benzopyran (**4**)*

To a solution of 6-acetyl-3,4-dihydro-7-hydroxy-2,2-dimethyl-2*H*-benzopyran **3** (8 mmol) in acetone (20 mL), anhydrous K_2CO_3 (16 mmol) and dimethyl sulfate (8 mmol) were added and the mixture was stirred at room temperature for 2 h. The reaction mixture was poured into water, extracted with diethyl ether and dried over anhydrous Na_2SO_4. The residue was chromatographed using *n*-hexane and ethyl acetate (9:1) to give the compound as a colorless oil.

General method for the synthesis of ***5a–h***

To a stirred solution of 6-acetyl-3,4-dihydro-7-methoxy-2,2-dimethyl-2*H*-benzopyran **4** (6 mmol) and a substituted benzaldehyde (6 mmol) was added gradually $BF_3 \cdot Et_2O$ (3 mmol) at room temperature in dioxane. The solution was stirred for 2–3 h at room temperature. The reaction was monitored by TLC. After completion of the reaction, the reaction mixture was cooled to room temperature and diluted with moist diethyl ether (50 mL), washed with water to discharge the color and the $BF_3 \cdot Et_2O$ complex. The extracted ethereal solution was dried over anhydrous Na_2SO_4, concentrated and recrystallized from dry ethanol to afford the appropriate pure chalcone.

General procedure for the synthesis of ***6a–h***

6-(Substituted cinnamoyl)-3,4-dihydro-7-methoxy-2,2-dimethyl-2*H*-benzopyran (5 mmol) and guanidine hydrochloride (5 mmol) were refluxed in presence of freshly prepared sodium methoxide (5 mmol) in methanol for 4–5 h. The solvent was evaporated and the residue was neutralized with 20 % HCl whereby a yellow solid separated out, which was filtered and crystallized from ethanol to give yellow crystals.

Antimicrobial activity

The *in vitro* antimicrobial activity determination was performed by the well-diffusion method[20] using 100 µg ml^{-1}. All the synthesized compounds (**6a**–**h**) were screened for antibacterial activity against 3 gram positive bacteria *Bacillus pumilus*, *Bacillus subtilis* and *Streptococcus faecalis*, 3 gram negative bacteria *Enterococcus faecalis*, *Escherichia coli* and *Proteus vulgaris* and 3 fungi *Pencillium expansum*, *Aspergillus niger* and *Candida albicans* using ampicillin and ketoconazole as standards in DMSO. DMSO showed no inhibition zone. Nutrient agar (NA) and potato dextrose agar (PDA) were used as the basal medium for test bacteria and fungi, respectively. Inhibition was recorded in millimeters by measuring the diameter of the inhibition zone at the end of 24 h for bacteria and 48 h for fungi with a Hi antibiotic zone scale at (35±2) °C. Each experiment was repeated twice and the average of the two determinations was recorded. The results are summarized in Tables I and II.

RESULTS AND DISCUSSIONS

The characterization data of all the synthesized compounds are given in the supplementary material to this paper.

Spectroscopy

According to the literature,[21] condensation of benzene-1,3-diol **1** with 2-methylbut-3-en-2-ol in presence of citric acid and phosphoric acid yielded 3,4-dihydro-7-hydroxy-2,2-dimethyl-*2H*-benzopyran in 55 and 43 % yield, respectively. In the present attempts to modify the reaction conditions, polyphosphoric acid was found to be a better condensing agent with 2-methyl-3-buten-2-ol leading to the cyclic benzopyran **2** in very good yield.

The preparation of 2-hydroxychalcones from 2-hydroxyacetophenones and benzaldehydes generally presents some difficulties because they always partially cyclize to flavanones during their synthesis, resulting in low yields.[22] Hence compound **3** was methylated to **4** using dimethyl sulfate to avoid byproducts and to obtain only chalcones in good yields. The sharp singlet at δ 3.71 in the ^{1}H-

-NMR, the peak at δ 53.6 in the ^{13}C-NMR and the disappearance of the band at 3433 cm^{-1} (OH) in the IR spectra confirmed the methoxy group of compound **4**. The synthesis of the title compounds was achieved *via* chalcone formation, which was generated *in situ* by the Claisen–Schmidt condensation of **4** with different aromatic aldehydes in presence of $BF_3 \cdot Et_2O$ within 2–3 h, without any side reactions.[23] Generally, in aqueous KOH- or NaOH-assisted synthesis of chalcones, the reaction times were much longer (1–2 days), with a high probability of side reactions, such as *via* the Cannizzaro reaction or aldol condensation. By using $BF_3 \cdot Et_2O$, the side reactions were reduced and chalcones were obtained exclusively, in good yields. The ^{1}H-NMR spectra of compounds **5a**–**h** show doublets of –CO–C**H**=CH–Ar and –CO–CH=C**H**–Ar at about δ 6.7 and 7.8 ppm, respectively, and the signals around δ 120 and 140 ppm in the ^{13}C-NMR spectra confirmed the presence of the chalcone moiety.

Finally, the target compounds were obtained by cyclization of **5a**–**h** in the presence of sodium methoxide in methanol with guanidine hydrochloride to give the products in good to excellent yields. The target compounds on purification and crystallization formed bright yellow crystalline solids of 99 % purity by HPLC. The synthesized 2-amino-4-benzopyran-6-ylpyrimidines (**6a–h**) exhibited characteristic primary amine bands at 3400–3100 cm^{-1} and did not show any absorption band in the region of 1700–1600 cm^{-1}, which indicates the absence of >C=O groups. The stretching peak of >C=N– appeared at 1600–1510 cm^{-1} and the absorption band at 855–800 cm^{-1} was characteristic of aromatic C–H bending vibrations. The ^{1}H-NMR spectrum showed the C_5-H proton as a singlet around δ 7.20–7.41 ppm and a broad signal around at δ 5.0 ppm due to the amino protons, which disappeared on D_2O exchange and the aromatic protons appeared between δ 7.2–7.9 ppm as a multiplet in all synthesized compounds as expected.[24] In the ^{13}C-NMR spectra of the pyrimidines, the C_2 carbon was the most deshielded carbon, appearing at δ 160 ppm, the C_4/C_6-carbons resonated at δ 157 ppm as expected.[25] The C_5 carbon resonated at δ 122 ppm nearer to the aromatic carbon shifts.

Antimicrobial screening

In the assay of the antimicrobial activity, all eight newly synthesized title compounds showed significant activity against *E. coli* with inhibition zones of 16 to 32 mm. Based on the inhibition zones shown by these compounds against all the tested bacterial strains, compound **6d** with methoxy groups at 2nd and 5th positions was found to be most effective against *E. coli* and *B. subtilis*, with activities nearly equal to those of the standard antibiotic ampicillin. This was explained as being due to the dimethoxy molecule being lipophilic[26] and good electron mobility in the aromatic ring may enhance the activity. It was demonstrated that increasing the number of methoxy groups on the phenyl ring or introducing an electronic donating substituent on the phenyl ring resulted in increased antibacterial activity.

TABLE I. Inhibition zone (mean diameter of inhibition in mm) as a criterion of the antibacterial activities of the newly synthesized compounds

Compound	Gram-positive bacteria			Gram-negative bacteria		
	B. pumilus	*B. subtilis*	*S. faecalis*	*E. faecalis*	*E. coli*	*P. vulgaris*
6a	11	14	12	13	16	9
6b	12	15	16	14	18	11
6c	20	23	21	18	27	14
6d	27	29	23	20	32	22
6e	15	18	16	17	21	16
6f	8	14	–	14	24	12
6g	11	19	15	16	22	11
6h	10	11	13	–	19	10
Ampicillin	25	28	24	22	31	20

TABLE II. Inhibition zone (mean diameter of inhibition in mm) as a criterion of the antifungal activities of the newly synthesized compounds

Compound	Fungi		
	P. expansom	*A. niger*	*C. albicans*
6a	8	13	11
6b	–	16	11
6c	11	15	10
6d	17	16	–
6e	15	15	16
6f	21	24	18
6g	24	22	21
6h	18	17	15
Ketoconazole	22	23	19

From the screening results, it was observed that the presence of nitro and chloro groups at the phenyl ring in compounds **6f** and **6g** increased the antifungal activity against *A. niger* and their activity was equipotent to those of the standard ketoconazole. The other compounds, **6a**–**e** and **6h,** exhibited lower activities compared with those of the standard ketoconazole.

CONCLUSIONS

In conclusion, eight novel 2-amino-4-benzopyran-6-yl pyrimidines (**6a**–**h**) were synthesized from benzene-1,3-diol and were subjected to *in vitro* antimicrobial activity screening against various pathogenic bacteria and fungi. The screening results indicated that all the compounds exhibited moderate activity against bacteria and fungi, except the **6d, 6f** and **6g** compounds. These differences in activity depended on the substitution of different reactive groups on the pyrimidine moiety. Further studies to explore the structure–activity relationship by structural modifications of the final investigated compounds to improve their biological activity are in progress.

SUPPLEMENTARY MATERIAL

Analytical and spectral data of the synthesized compounds are available electronically from http://www.shd.org.rs/JSCS/, or from the corresponding author on request.

ИЗВОД

СИНТЕЗА И КАРАКТЕРИЗАЦИЈА НОВИХ 2-АМИНО-4-(3,4-ДИХИДРО-2,2-ДИМЕТИЛ-7-МЕТОКСИ-2*H*-БЕНЗОПИРАН-6-ИЛ)-6-(СУПСТИТУИСАНИ ФЕНИЛ)ПИРИМИДИНА И ИСПИТИВАЊЕ ЊИХОВЕ БИОЛОШКЕ АКТИВНОСТИ

YELLAJYOSULA LAKSHMI NARASIMHA MURTHY[1], KILARU PADMA SUHASINI[1] и ANJALI JHA[2]

[1]*Department of Organic Chemistry, Andhra University, Visakhapatnam, India и* [2]*Department of Chemistry, Gitam Institute of Science, GITAM University, Visakhapatnam, India*

Синтетисана је нова серија од осам деривата 2-амино-4-(3,4-дихидро-2,2-диметил-7-метокси-2*H*-бензопиран-6-ил)-6(супституисани фенил)пиримидина, употребом бензен 1,3-диола као полазног једињења. Структура изолованих производа (**6a–h**) утврђена је спектроскопским техникама ^{1}H-NMR, ^{13}C-NMR и FT-IR и елементалном анализом. Испитана је биолошка активност синтетисаних једињења према грам-позитивним (*Bacillus pumilus*, *Bacillus subtilis* и *Streptococcus faecalis*) и грам-негативним (*Enterococcus faecalis*, *Escherichia coli* и *Proteus vulgaris)* бактеријама и гљивама *(Pencillium expansum*, *Aspergillus niger* и *Candida albicans*). Већина деривата показује умерену до високу антибактеријску и фунгицидну активност, са зонама инхибиције између 8 и 30 mm.

(Примљено 23. септембра 2011, ревидирано 22. јануара 2012)

REFERENCES

1. C. O. Wilson, J. H. Block, O. Gisvold, *Wilson and Gisvold's Text Book of Organic Medicinal and Pharmaceutical Chemistry*, XI ed., Lippincott Williams & Wilkins, Philadelphia, 2004, Chap. 10, p. 299
2. a) M. Garcia, Valverde, T. Torroba, *Molecules* **10** (2005) 318; b) J. U. Yuhong, R. S. Varma, *J. Org. Chem.* **71** (2006) 135
3. K. S. Jain, T. S. Chitre, P. B. Miniyar, M. K. Kathiravan, V. S. Bendre, V. S. Veer, S. R. Shahane, C. J. Shishoo, C*urr. Sci.* **90** (2006) 793
4. C. C. Cheng, *Prog. Med. Chem.* **6** (1969) 67
5. a) V. K. Ahluwalia, B. Madhu, *Indian J. Chem., Sect. B* **35** (1996) 742; b) A. A. Siddiqui, R. Rajesh, Mojahid-Ul-Islam, V. Alagarsamy, E. De Clercq, *Arch. Pharm. Chem. Life Sci*. **340** (2007) 95
6. E. J. Pease, G. A. Breault, E. J. Williams, R. H. Bradbury, J. J. Morris (AstraZeneca AB), U.S. 6649608 (2003)
7. M. G. Mostafa, A. R. Fatma, I. H. Helmy, Y. A. Ammar, G. E. Marwa, *Bioorg. Med. Chem. Lett*. **20** (2010) 6316
8. A. S. Said, E. A. Abd El-Galil, M. S. Nermien, M. Mohamed, *Eur. J. Med. Chem*. **44** (2009) 4787
9. V. S. Modi, T. S. Basuri, *Int. J. Pharm. Pharm. Sci*. **3** (2011) 13

10. N. Azas, P. Rathelot, S. Djekou, F. Delmas, A. Gellis, C. Di-Giorgio, P. Vanelle, P. Timon-David, *Farmaco* **58** (2003) 1263
11. V. L. Rusinov, A. Yu. Petrov, T. L. Pilicheva, O. N. Chupakhin, G. V. Kovalev, E. R. Komina, *Pharm. Chem. J.* **20** (1986) 113
12. K. S. Atwal, G. C. Roynyk, S. D. Kimball, D. M. Floyd, S. Moreland, *J. Med. Chem.* **33** (1990) 2629
13. a) H .G. Garg, C. Prakash, *J. Med. Chem.* **14** (1971) 175; b) V. J. Ram, *Arch. Pharm.* **323** (1990) 895
14. a) K. C. Nicolaou, J. A. Pfefferkorn, A. J. Roecker, G. Q. Cao, S. Barluenga, H. J. Mitchell, *J. Am. Chem. Soc.* **122** (2000) 9939; b) P. Pittayakhajonwut, M. Theerasilp, P. Kongsaeree, A. Rungrod, M. Tanticharoen, Y. Thebtaranonth, *Planta Med.* **68** (2002) 1017; c) K. H. Jang, B. H. Lee, B. W. Choi, H. Lee, J. Shin, *J. Nat. Prod.* **68** (2005) 716
15. a) X. Wu, X. Liu, Y. Lin, J. Luo, Z. She, H. Li, W. Chan, S. Antus, T. Kurtan, B. Elsasser, K. Krohn, *Eur. J. Org. Chem.* **19** (2005) 4061; b) W. Chen, Y. Qian, W. Meng, J. Pang, Y. Lin, Y. Guan, S. Chen, J. Liu, Z. Pei, G. Wang, *Biochem. Pharmacol.* **78** (2009) 941; c) J. Zhao, L. Li, L. Chen, J. Li, J. Pang, Y. Lin, J. Liu, R. Huang, G. Wang, Z. Pei, J. Zeng, *Brain Res.* **1302** (2009) 240
16. a) M. G. Murugesh, K. Subburaj, G. K. Trivedi, *Tetrahedron* **52** (1996) 2217; b) B. Lesch, J. Toräng, M. Nieger, S. Bräse, *Synthesis* **2005** (2005) 1888
17. a) D. Xie, S. Sharma, N. Paiva, D. Ferreira, R. Dixon, *Science* **299** (2003) 396; b) A. Saito, M. Emoto, A. Tanaka, Y. Doi, K. Shoji, Y. Mizushina, H. Ikawa, H. Yoshida, N. Atsuura, N. Nakajima, *Tetrahedron* **60 (**2004) 12043
18. a) Y. L. N. Murthy, R. Nanda, P. Ellaiah, R. Devi, Bhavani, *Heterocycl. Commun.* **11** (2005) 189; b) Y. L. N. Murthy, R. Nanda, P. S Rao, R. Suryaprabha, V. V. Lakshmi, P. V. N. Acharyulu, *Chem.: An Indian J.* **1** (2003) 246
19. Q. Wang, X. She, X. Ren, J. Ma, X. Pan, *Tetrahedron: Asymmetry* **15** (2004) 29
20. F. C. Odds, *J. Antimicrob. Chemother.* **24** (1989) 533
21. R. J. Molyneux, L. Jurd, *Tetrahedron* **26** (1970) 4743
22. a) Y. Hoshino, N. Takeno, *Bull. Chem. Soc. Jpn.* **59** (1986) 2903; b) A. R. Alcantara, J. M. Marinas, J. V. Sinisterra, *Tetrahedron Lett.* **28** (1987) 1515
23. T. Narender, K. Papi Reddy, *Tetrahedron Lett.* **48** (2007) 3177
24. a) F. C. Baddar, F. H. Al-Hajjar, N. R. El-Rayyes, *J. Heterocycl. Chem.* **13** (1976) 257; b) N. R. El-Rayyes, F. H. Al-Hajjar, *J. Heterocycl. Chem.* **14** (1977) 367
25. A. S. R. Anjaneyulu, G. Sudha Rani, K. G, Annapurna, U. V. Mallavadhani, Y. L. N. Murthy, *Indian J. Chem., B* **34** (1995) 933
26. B. Roth, E. Aig, B. S. Rauckman, J. Z. Sterlitz, R. Ferone, P. Arthur, S. R. M. Bushby, C. W. Sigel, *J. Med. Chem.* **24** (1981) 933.

Journal of the Serbian Chemical Society
JSCS@tmf.bg.ac.rs • www.shd.org.rs/JSCS
J. Serb. Chem. Soc. 77 (7) S97–S101 (2012)
Supplementary material

SUPPLEMENTARY MATERIAL TO

Synthesis and characterization of new 2-amino-4-(3,4-dihydro-7-methoxy-2,2-dimethyl-2*H*-benzopyran-6-yl)-6-(substituted phenyl)pyrimidines and their bio evaluation

YELLAJYOSULA LAKSHMI NARASIMHA MURTHY[1]*, KILARU PADMA SUHASINI[1] and ANJALI JHA[2]

[1]Department of Organic Chemistry, Andhra University, Visakhapatnam, and [2]Department of Chemistry, Gitam Institute of Science, GITAM University, Visakhapatnam, India

J. Serb. Chem. Soc. 77 (7) (2012) 865–872

ANALYTICAL AND SPECTRAL DATA OF THE SYNTHESIZED COMPOUNDS

*3,4-Dihydro-7-hydroxy-2,2-dimethyl-2*H*-benzopyran* (**2**). Yield: 68 %; m.p.: 66 °C; Anal. Calcd. for $C_{11}H_{14}O_2$: C, 74.13; H, 7.92 %. Found: C, 74.09; H, 7.94 %; IR (KBr, cm^{-1}): 3315; ^{1}H-NMR (90 MHz, $CDCl_3$, δ / ppm): 1.31 (6H, *s*, C_2-methyls), 1.77 (2H, *t*, J = 7.0 Hz, CH_2), 2.69 (2H, *t*, J = 7.0 Hz, CH_2), 5.01 (1H, *s*, Ar–OH), 6.2–6.94 (3H, *m*, Ar-H); ^{13}C-NMR (22.5 MHz, $CDCl_3$, δ / ppm): 22.8, 27.2, 48.1, 73.7, 101.2, 107.1, 117.7, 130.3, 155.1; MS (*m/z*): 178 (M$^+$).

*6-Acetyl-3,4-dihydro-7-hydroxy-2,2-dimethyl-2*H*-benzopyran* (**3**). Yield: 65 %; m.p.: 115 °C; Anal. Calcd. for $C_{13}H_{16}O_3$: C, 70.89; H, 7.32 %. Found: C, 70.79; H, 7.29 %; IR (KBr, cm^{-1}): 3350, 1609; ^{1}H-NMR (90 MHz, $CDCl_3$, δ / / ppm): 1.31 (6H, *s*, C_2-methyls), 1.82 (2H, *t*, J = 7.0 Hz, CH_2), 2.54 (3H, *s*, CH_3CO), 2.73 (2H, *t*, J = 7.0 Hz, CH_2), 6.26 (1H, *s*, Ar–H), 7.44 (1H, *s*, Ar–H); 13.1 (1H, *s*, OH); ^{13}C-NMR (22.5 MHz, $CDCl_3$, δ / ppm): 17.05, 21.62, 26.79, 32.67, 77.00, 111.73, 119.83, 129.13, 156.06, 198.37; MS (*m/z*): 220 (M$^+$).

*6-Acetyl-3,4-dihydro-7-methoxy-2,2-dimethyl-2*H*-benzopyran* (**4**). Yield: 72 %; Anal. Calcd. for $C_{14}H_{18}O_3$: C, 71.77; H, 7.74 %. Found: C, 71.70; H, 7.76 %; IR (KBr, cm^{-1}): 1685, 1592, 1425, 1092; ^{1}H-NMR (90 MHz, $CDCl_3$, δ / ppm): 1.33 (6H, *s*, C_2-methyls), 1.77 (2H, *t*, J = 7.0 Hz, CH_2), 2.51 (3H, *s*, CH_3CO), 2.72 (2H, *t*, J = 7.0 Hz, CH_2), 3.71 (3H, *s*, OCH_3), 6.26 (1H, *s*, Ar–H), 7.42 (1H, *s*, Ar–H); ^{13}C-NMR (22.5 MHz, $CDCl_3$, δ / ppm): 21.8, 22.9, 28.4, 46.1, 53.6, 71.6, 100.1, 113.8, 114.3, 128.0, 150.2, 162.7, 193.6; MS (*m/z*): 234 (M$^+$).

---

* Corresponding author. E-mail: murthyyln@gmail.com

*6-Cinnamoyl,3,4-dihydro-7-methoxy-2,2-dimethyl-2*H*-benzopyran* (**5a**). Yellow crystals; Yield: 68 %; m.p.: 123 °C; Anal. Calcd. for $C_{21}H_{22}O_3$: C, 78.23; H 6.88 %. Found: C, 78.19; H, 6.87 %; IR (KBr, cm^{-1}): 2979, 2934, 1727, 1594, 1455, 1372, 1244, 1115, 1036, 933, 748, 645, 568; ^{1}H-NMR (90 MHz, $CDCl_3$, δ / ppm): 1.3 (6H, *s*, C_2-methyls), 1.81 (2H, *t*, J = 7.0 Hz, CH_2), 2.58 (2H, *t*, J = = 7.0 Hz, CH_2), 3.11 (3H, *s*, OCH_3), 6.95 (1H, *d*, J = 15.4 Hz, –CO–C**H**=CH–), 7.65 (1H, *d*, J = 15.4 Hz, –CO–CH=C**H**–), 7.11 (5H, *m*, Ar–H); ^{13}C-NMR (22.5 MHz, $CDCl_3$, δ / ppm): 21.3, 25.8, 31.4, 56.1, 72.8, 102.4, 114.6, 116.2, 124.7, 129.0, 134.9, 140.9, 161.0, 171.3; MS (*m*/*z*): 322 (M$^+$).

*3,4-Dihydro-7-methoxy-2,2-dimethyl-6-(4-methylcinnamoyl)-2*H*-benzopyran* (**5b**). Bright yellow crystals; Yield: 70 %; m.p.: 105 °C; Anal. Calcd. for $C_{22}H_{24}O_3$: C, 78.54; H, 7.19 %. Found: C, 78.58; H, 7.17 %; IR (KBr, cm^{-1}): 2997, 2943, 1733, 1599, 1457, 1375, 1246, 1182, 1058, 943, 789, 654; ^{1}H-NMR (90 MHz, $CDCl_3$, δ / ppm): 1.34 (6H, *s*, C_2-methyls), 1.79 (2H, *t*, J = 7.0 Hz, CH_2), 2.35 (3H, *s*, CH_3), 2.68 (2H, *t*, J = 7.0 Hz, CH_2), 3.15 (3H, *s*, OCH_3); 6.86 (1H, *d*, J = 15.5 Hz, –CO–CH=CH–), 7.85 (1H, *d*, J = 15.5 Hz, –CO–CH=CH–), 7.3–7.7 (4H, *m*, Ar–H); ^{13}C-NMR (22.5 MHz, $CDCl_3$, δ / ppm): 20.9, 21.5, 26.4, 33.5, 53.8, 74.6, 100.8, 111.3, 115.9, 126.7, 129.1, 136.9, 140.5, 158.6, 168.9; MS (*m*/*z*): 336 (M$^+$).

*3,4-Dihydro-7-methoxy-6-(4-methoxycinnamoyl)-2,2-dimethyl-2*H*-benzopyran* (**5c**). Brown crystals; Yield: 77 %; m.p.: 116 °C; Anal. Calcd. for $C_{22}H_{24}O_4$: C, 74.98; H, 6.86 %. Found: C, 74.92; H, 6.84 %; IR (KBr, cm^{-1}): 3009, 2977, 2945, 1722, 1611, 1455, 1393, 1191, 1160, 1118, 1092, 884, 853; ^{1}H-NMR (90 MHz, $CDCl_3$, δ / ppm): 1.37 (6H, *s*, C_2-methyls), 1.80 (2H, *t*, J = 7.0 Hz, CH_2), 2.67 (2H, *t*, J = 7.0 Hz, CH_2), 3.39 (3H, *s*, OCH_3), 3.48 (3H, *s*, OCH_3), 6.74 (1H, *d*, J = 15.5 Hz, –CO–CH=CH–), 7.62 (1H, *d*, J = 15.5 Hz, –CO–CH=CH–), 7.2 (4H, *m*, Ar–H); ^{13}C-NMR (22.5 MHz, $CDCl_3$, δ / ppm): 22.8, 27.1, 31.9, 54.8, 56.2, 75.2, 109.4, 112.1, 114.1, 126.0, 128.7, 129.6, 140.2, 160.7, 161.0, 184.6; MS (*m*/*z*): 352 (M$^+$).

*6-(2,5-dimethoxycinnamoyl)-3,4-dihydro-7-methoxy-2,2-dimethyl-2*H*-benzopyran* (**5d**). Brown oil; Yield: 72 %; Anal. Calcd. for $C_{23}H_{26}O_5$: C, 72.23; H, 6.85 %. Found: C, 72.20; H, 6.84 %; IR (KBr, cm^{-1}): 3008, 2962, 2955, 1726, 1610, 1458, 1396, 1153, 1109, 1033, 929, 885, 650, 601, 541; ^{1}H-NMR (90 MHz, $CDCl_3$, δ / ppm): 1.38 (6H, *s*, C_2-methyls), 1.79 (2H, *t*, J = 7.0 Hz, CH_2), 2.78 (2H, *t*, J = 7.0 Hz, CH_2), 3.83 (3H, *s*, OCH_3), 3.89 (6H, *s*, OCH_3), 6.85 (1H, *d*, J = 15.6 Hz, –CO–CH=CH–), 7.59 (1H, *d*, J = 15.6 Hz, –CO–CH=CH–), 7.3 (3H, *m*, Ar–H); ^{13}C-NMR (22.5 MHz, $CDCl_3$, δ / ppm): 21.9, 25.36, 31.5, 52.4, 53.2, 56.7, 73.1, 105.6, 110.1, 112.6, 113.4, 125.0, 125.3, 140.1, 154.2, 158.3, 172.8; MS (*m*/*z*): 382 (M$^+$).

*6-[4-(Dimethylamino)cinnamoyl]-3,4-dihydro-7-methoxy-2,2-dimethyl-2*H*-benzopyran* (**5e**). Yellow crystals; Yield: 69 %; m.p.: 112 °C; Anal. Calcd. for

$C_{23}H_{27}O_3N$: C, 75.59; H, 7.45; N, 3.83 %. Found: C, 75.57; H, 7.49; N, 3.80 %; IR (KBr, cm^{-1}): 3020, 2983, 2944, 1722, 1614, 1456, 1383, 1186, 1123, 1093; ^{1}H-NMR (90 MHz, $CDCl_3$, δ / ppm): 1.35 (6H, *s*, C_2-methyls), 1.82 (2H, *t*, *J* = = 7.0 Hz, CH_2), 2.78 (2H, *t*, *J* = 7.0 Hz, CH_2), 3.03 (3H, *s*, OCH_3), 4.01 (6H, *s*, $N(CH_3)_2$), 6.70 (1H, *d*, *J* = 15.6 Hz, –CO–CH=CH–) 7.93 (1H, *d*, *J* = 15.6 Hz, –CO–CH=CH–), 7.2 (4H, *m*, Ar–H); ^{13}C-NMR (22.5 MHz, $CDCl_3$, δ / ppm): 22.4, 27.1, 41.5, 43.6, 56.4, 76.3, 101.6, 112.4, 116.9, 127.1, 124.4, 131.2, 142.8, 156.8, 179.5; MS (*m*/*z*): 365 (M^+).

*6-(4-Chlorocinnamoyl)-3,4-dihydro-7-methoxy-2,2-dimethyl-2*H*-benzopyran (**5f**)*. Brown crystals; Yield: 65 %; m.p.: 99 °C; Anal. Calcd. for $C_{21}H_{21}ClO_3$: C, 70.68; H, 5.93. Found: C, 70.71; H, 5.97; IR (KBr, cm^{-1}): 3012, 2927, 2915, 1791, 1611, 1494, 1364, 1112, 1150, 1001, 923, 864; ^{1}H-NMR (90 MHz, $CDCl_3$, δ / ppm): 1.36 (6H, *s*, C_2-methyls) , 1.78 (2H, *t*, *J* = 7.0 Hz, CH_2), 2.69 (2H, *t*, *J* = 7.0 Hz, CH_2), 3.21 (3H, *s*, OCH_3); 7.03 (1H, *d*, –CO–CH=CH–), 7.51 (1H, *d*, –CO–CH=CH–), 7.3 (4H, *m*, Ar–H); ^{13}C-NMR (22.5 MHz, $CDCl_3$, δ / ppm): 22.8, 27.2, 44.6, 56.0, 77.3, 102.9, 131.1, 113.7, 127.6, 128.8, 133.0, 143.1, 158.2, 181.0; MS (*m*/*z*): 356 (M^+).

*3,4-Dihydro-7-methoxy-2,2-dimethyl-6-(4-nitrocinnamoyl)-2*H*-benzopyran (**5g**)*. Yellow crystals; Yield: 63 %; m.p.: 120 °C; Anal. Calcd. for $C_{21}H_{21}NO_5$: C, 68.65; H, 5.76 %; N, 3.81 %. Found: C, 68.67; H, 5.79 %, N, 3.79 %; IR (KBr, cm^{-1}): 3018, 2978, 2934, 1729, 1709, 1626, 1363, 1260, 1159, 1100, 1070; ^{1}H-NMR (90 MHz, $CDCl_3$, δ / ppm): 1.34 (6H, *s*, C_2-methyls), 1.82 (2H, *t*, *J* = 7.0 Hz, CH_2), 2.71 (2H, *t*, *J* = 7.0 Hz, CH_2), 3.14 (3H, *s*, OCH_3), 6.87 (1H, *d*, *J* = 15.7 Hz, –CO–CH=CH–), 8.00 (1H, *d*, *J* = 15.7 Hz, –CO–CH=CH–), 7.4 (4H, *m*, Ar–H); ^{13}C-NMR (22.5 MHz, $CDCl_3$, δ / ppm): 23.1, 28.3, 34.6, 44.8, 57.1, 100.5, 112.6, 114.8, 126.4, 127.3, 129.0, 147.6, 166.4, 186.2; MS (*m*/*z*): 367 (M^+).

*6-(4-Cyanocinnamoyl)-3,4-dihydro-7-methoxy-2,2-dimethyl-2*H*-benzopyran (**5h**)*. Light brown crystals; Yield: 59 %; m.p.: 128 °C; Anal. Calcd. for $C_{22}H_{21}O_3N$: C, 76.06; H, 6.09; N, 4.04 %. Found: C, 76.07; H, 6.05; N, 4.01 %; IR (KBr, cm^{-1}): 3021, 2998, 2957, 1788, 1676, 1393, 1206, 1109, 1043; ^{1}H--NMR (90 MHz, $CDCl_3$, δ / ppm): 1.37 (6H, *s*, C_2-methyls), 1.85 (2H, *t*, *J* = 7.0 Hz, CH_2), 2.73 (2H, *t*, *J* = 7.0 Hz, CH_2), 3.41 (3H, *s*, OCH_3), 6.88 (1H, *d*, *J* = = 15.7 Hz, –CO–CH=CH–), 7.98 (1H, *d*, *J* = 15.7 Hz, –CO–CH=CH–), 7.5 (4H, *m*, Ar–H); ^{13}C-NMR (22.5 MHz, $CDCl_3$, δ / ppm): 22.9, 29.1, 35.4, 56.3, 100.8, 112.9, 113.4, 116.5, 126.8, 128.0, 139.2, 142.8, 165.4, 186.1; MS (*m*/*z*): 347 (M^+).

*2-Amino-4-(3,4-dihydro-7-methoxy-2,2-dimethyl-2*H*-benzopyran-6-yl)-6--phenylpyrimidine (**6a**)*. Yellow crystals; Yield: 55 %; m.p.: 210 °C; Anal. Calcd. for $C_{22}H_{23}O_2N_3$: C, 73.11; H, 6.41; N, 11.63 %. Found: C, 73.09; H, 6.43; N, 11.72 %; IR (KBr, cm^{-1}): 3301, 3146, 2978, 2944, 1579, 1461, 1363, 1299, 1157, 1123, 1034, 921; ^{1}H-NMR (90 MHz, $CDCl_3$, δ / ppm): 1.32 (6H, *s*, C_2-methyls), 1.79 (2H, *t*, *J* = 7.0 Hz, CH_2), 2.67 (2H, *t*, *J* = 7.0 Hz, CH_2), 3.65 (3H, *s*, OCH_3), 5.23 (2H, *s*, NH_2), 7.5 (6H, *m*, Ar–H); ^{13}C-NMR (22.5 MHz, $CDCl_3$, δ / ppm): 17.22, 23.11, 33.65, 56.30, 75.02, 108.4, 110.68, 113.5, 117.9, 126.9, 129.7, 137.7, 158.3, 159.6, 164.3, 167.5; MS (*m*/*z*): 361 (M^+).

*2-Amino-4-(3,4-dihydro-7-methoxy-2,2-dimethyl-2*H*-benzopyran-6-yl)-6-(4-methylphenyl)pyrimidine (**6b**)*. Light yellow crystals; Yield: 56 %; m.p.: 205 °C; Anal. Calcd. for $C_{23}H_{25}O_2N_3$: C, 73.57; H, 6.71; N 11.19 %. Found: C, 73.69; H, 6.78; N, 11.12 %; IR (KBr, cm^{-1}): 3316, 3147, 2985, 2869, 1547, 1368, 1147, 968; ^{1}H-NMR (90 MHz, $CDCl_3$, δ / ppm): 1.35 (6H, *s*, C_2-methyls), 1.80 (2H, *t*, *J* = 7.0 Hz, CH_2), 2.65 (2H, *t*, *J* = 7.0 Hz, CH_2), 3.75 (3H, *s*, OCH_3), 5.91 (2H, *s*, NH_2), 7.56 (5H, *m*, Ar–H); ^{13}C-NMR (22.5 MHz, $CDCl_3$, δ / ppm): 17.09, 20.09, 26.18, 31.77, 56.50, 74.97, 110.13, 111.98, 112.64, 121.98, 134.69, 143.32, 150.06, 150.70, 165.08; MS (*m*/*z*): 375 (M^+).

*2-Amino-4-(3,4-dihydro-7-methoxy-2,2-dimethyl-2*H*-benzopyran-6-yl)-6-(4-methoxyphenyl)pyrimidine (**6c**)*. Brown solid; Yield: 59 %; m.p.: 223 °C, Anal. Calcd. for $C_{23}H_{25}O_3N_3$: C, 70.57; H, 6.44; N, 10.73 %. Found: C, 70.58; H, 6.41; N, 10.69 %; IR (KBr, cm^{-1}): 3346, 3184, 2978, 2929, 1514, 1456, 1378, 1167, 1113, 1024, 946, 887; ^{1}H-NMR (90 MHz, $CDCl_3$, δ / ppm): 1.33 (6H, *s*, C_2-methyls), 1.78 (2H, *t*, *J* = 7.0 Hz, CH_2), 2.66 (2H, *t*, *J* = 7.0 Hz, CH_2), 3.74 (3H, *s*, OCH_3), 3.93 (3H, *s*, OCH_3), 5.16 (2H, *s*, NH_2), 7.2 (5H, *m*, Ar–H); ^{13}C-NMR (22.5 MHz, $CDCl_3$, δ / ppm): 18.01, 22.69, 33.98, 56.67, 54.02, 73.51, 110.56, 111.64, 112.71, 115.58, 118.14, 120.89, 124.75, 145.63, 152.85, 159.03, 166.32; MS (*m*/*z*): 391 (M^+).

*2-Amino-4-(3,4-dihydro-7-methoxy-2,2-dimethyl-2*H*-benzopyran-6-yl)-6-(2,5-dimethoxyphenyl)pyrimidine (**6d**)*. Brown oil; Yield: 52 %; Anal. Calcd. for $C_{24}H_{27}O_4N_3$: C, 68.39; H, 6.46; N, 9.97 %. Found: C, 68.28; H, 6.41; N, 9.90 %; IR (KBr, cm^{-1}): 3377, 3186, 2978, 2934, 1572, 1459, 1295, 1126, 1044, 700, 618; ^{1}H-NMR (90 MHz, $CDCl_3$, δ / ppm): 1.32 (6H, *s*, C_2-methyls), 1.82 (2H, *t*, *J* = 7.0 Hz, CH_2), 2.65 (2H, *t*, *J* = 7.0 Hz, CH_2), 3.82 (3H, *s*, OCH_3), 3.85 (3H, *s*, OCH_3), 3.90 (3H, *s*, OCH_3), 5.01 (2H, *s*, NH_2), 7.15 (4H, *m*, Ar–H); ^{13}C-NMR (22.5 MHz, $CDCl_3$, δ / ppm): 17.14, 21.67, 31.75, 55.01, 55.93, 56.23, 73.80, 109.22, 111.54, 112.88, 115.32, 118.08, 128.84, 151.48, 153.55, 162.83, 162.96; MS (*m*/*z*): 421 (M^+).

*2-Amino-4-(3,4-dihydro-7-methoxy-2,2-dimethyl-2*H*-benzopyran-6-yl)-6-[4-(dimethylamino)phenyl]pyrimidine (**6e**)*. Bright yellow solid; Yield: 53 %; m.p.: 202 °C; Anal. Calcd. for $C_{24}H_{28}O_2N_4$: C, 71.26; H, 6.98; N, 13.85 %. Found: C, 71.28; H, 6.93; N, 13.87 %; IR (KBr, cm^{-1}): 3382, 3180, 3022, 2912, 2841, 1596, 1530, 1289, 1093, 665; ^{1}H-NMR (90 MHz, $CDCl_3$, δ / ppm): 1.31 (6H, *s*, C_2-methyls), 1.77 (2H, *t*, *J* = 7.0 Hz, CH_2), 2.69 (2H, *t*, *J* = 7.0 Hz, CH_2), 3.85 (3H, *s*, OCH_3), 4.04 (6H, *s*, $N(CH_3)_2$), 5.52 (2H, *s*, NH_2), 7.4–7.8 (5H, *m*, Ar–H);

^{13}C-NMR (22.5 MHz, CDCl$_3$, δ / ppm): 14.60, 26.80, 31.77, 40.01, 53.21, 74.95, 104.98, 112.37, 127.95, 128.31, 129.66, 152.19, 160.73, 165.08, 165.39; MS (*m*/*z*): 404 (M$^+$).

*2-Amino-4-(4-chlorophenyl)-6-(3,4-dihydro-7-methoxy-2,2-dimethyl-2*H*-benzopyran-6-yl)pyrimidine* (***6f***). Yellow solid; Yield: 51 %; m.p.: 176 °C; Anal. Calcd. for $C_{22}H_{22}ClO_2N_3$: C, 66.75; H, 5.60; N, 10.61 %. Found: C, 66.71; H, 5.64; N, 10.63 %; IR (KBr, cm^{-1}): 3408, 3159, 2957, 2864, 1598, 1382, 1148, 1026, 965; ^{1}H-NMR (90 MHz, CDCl$_3$, δ / ppm): 1.35 (6H, *s*, C$_2$-methyls), 1.82 (2H, *t*, *J* = 7.0 Hz, CH$_2$), 2.78 (2H, *t*, *J* = 7.0 Hz, CH$_2$), 3.79 (3H, *s*, OCH$_3$), 5.37 (2H, *s*, NH$_2$); 7.3 (5H, *m*, Ar–H); ^{13}C-NMR (22.5 MHz, CDCl$_3$, δ / ppm): 18.62, 28.36, 34.23, 55.38, 76.77, 110.95, 113.77, 122.02, 130.20, 130.49, 131.22, 131.35, 136.02, 136.69, 140.01, 154.73, 157.68; MS (*m*/*z*): 395 (M$^+$).

*2-Amino-4-(3,4-dihydro-7-methoxy-2,2-dimethyl-2*H*-benzopyran-6-yl)-6-(4--nitrophenyl)pyrimidine* (***6g***). Brown solid; Yield 50 %; m.p.: 194 °C; Anal. Calcd. for $C_{22}H_{22}O_4N_4$: C, 65.01; H, 5.46; N, 13.78 %. Found: C, 64.98; H, 5.41; N, 13.72 %; IR (KBr, cm^{-1}): 3410, 3022, 2889, 2814, 1527, 1383, 1246, 1039, 1142, 842; ^{1}H-NMR (90 MHz, CDCl$_3$, δ / ppm): 1.34 (6H, *s*, C$_2$-methyls), 1.79 (2H, *t*, *J* = 7.0 Hz, CH$_2$), 2.65 (2H, *t*, *J* = 7.0 Hz, CH$_2$), 3.83 (3H, *s*, OCH$_3$), 5.10 (2H, *s*, NH$_2$), 7.49 (5H, *m*, Ar–H); ^{13}C-NMR (22.5 MHz, CDCl$_3$, δ / ppm): 16.60, 25.90, 33.33, 74.24, 110.55, 111.65, 116.32, 125.71, 126.66, 129.66, 134.74, 148.50, 152.63, 153.37, 162.96; MS (*m*/*z*): 406 (M$^+$).

*4-[2-Amino-4-(4-dihydro-7-methoxy-2,2-dimethyl-2*H*-benzopyran-6-yl)pyrimidin-4-yl]benzonitrile* (***6h***). Bright brown solid; Yield: 48 %; m.p.: 211 °C; Anal. Calcd. for $C_{23}H_{22}O_2N_4$: C, 71.48; H, 5.74; N, 14.50 %. Found: C, 71.37; H, 5.79; N, 14.53 %; IR (KBr, cm^{-1}): 3501, 3246, 3016, 2912, 2841, 1590, 1405, 1209, 954, 746, 685; ^{1}H-NMR (90 MHz, CDCl$_3$, δ / ppm): 1.35 (6H, *s*, C$_2$-methyls), 1.82 (2H, *t*, *J* = 7.0 Hz, CH$_2$), 2.78 (2H, *t*, *J* = 7.0 Hz, CH$_2$), 3.90 (3H, *s*, OCH$_3$), 5.5 (2H, *s*, NH$_2$), 7.5 (5H, *m*, Ar–H); ^{13}C-NMR (22.5 MHz, CDCl$_3$, δ / ppm): 18.3 28.35, 36.87, 56.34, 77.26, 110.21, 119.63, 125.24, 136.95, 137.10, 138.25, 147.14, 155.34, 159.47, 163.58; MS (*m*/*z*): 386 (M$^+$).

Journal of the Serbian Chemical Society

JSCS-info@shd.org.rs • www.shd.org.rs/JSCS

J. Serb. Chem. Soc. 77 (7) 867–871 (2012)
JSCS–4315

UDC 547.7+547–304.9+66.095.25:542.913:
535.33.004.12
Short communication

SHORT COMMUNICATION

Synthesis and spectral properties of novel thiadiazolotriazinone derivatives

DEMET GÜRBÜZ* and SÜLEYMAN TANYOLAÇ

Istanbul University, Faculty of Engineering, Department of Chemistry,
34320, Avcilar, Istanbul, Turkey

(Received 30 September, revised 7 December 2011)

Abstract: A series of new 7-substitued-4*H*-1,3,4-thiadiazolo[2,3-*c*][1,2,4]-triazin-4-ones were synthesized in good yields by the reaction of 4-amino-3-mercapto-1,2,4-triazin-5(4*H*)-one with various aromatic carboxylic acids in the presence of phosphorus oxychloride. All the synthesized compounds were confirmed by FT-IR, NMR (^{1}H and ^{13}C) and ESI-MS spectroscopic techniques and analytical methods.

Keywords: heterocyclic; 1,2,4-triazine; cyclization; thiadiazolotriazinones.

INTRODUCTION

Triazines and their derivatives are important groups of heterocyclic compounds. They have attracted considerable interest because of their great biological importance, such as their antitumor,[1,2] anti-HIV,[3] antiviral,[4] antimalarial,[5] antibacterial,[6] antifungal[7] and antioxidant activities.[8]

Triazines have also found wide applications as herbicides[9,10] and pesticides[11] in the field of agriculture. In addition, a number of thiadiazole derivatives exhibit a broad range of biological activities due to the presence of the NCS moiety.[12]

Herein, the synthesis of 7-substitued-4*H*-1,3,4-thiadiazolo[2,3-*c*][1,2,4]triazin-4-ones **3** (Scheme 1) by condensation of 4-amino-3-mercapto-1,2,4-triazin-5(4*H*)-one **1** with various aromatic carboxylic acids **2** and their characterization using analytical and spectroscopic techniques are described.

---

* Corresponding author. E-mail: demet@istanbul.edu.tr

doi: 10.2298/JSC110930217G

RESULTS AND DISCUSSION

For the present work, 4-amino-3-mercapto-1,2,4-triazin-5(4*H*)-one **1** was prepared by the reaction of thiocarbohydrazide with glyoxalic acid monohydrate following a literature method.[13] Thirteen novel thiadiazolotriazine derivatives were synthesized for the first time in this study. The physical and chemical data of the synthesized compounds are given in Table I.

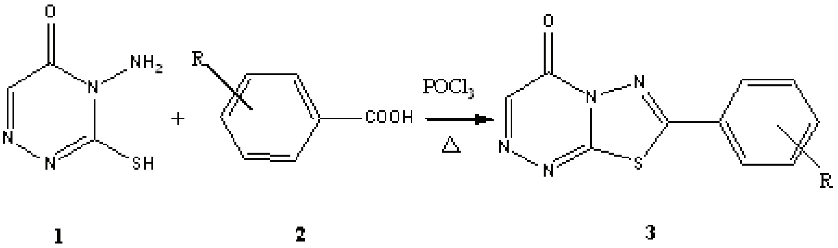

Scheme 1. Synthesis of 7-substitued-4*H*-[1,3,4]thiadiazolo[2,3-*c*][1,2,4]triazin-4-ones.

TABLE I. Physical and chemical data of the synthesized compounds

Compound	R^1	Formula	M.p., °C	Yield, %	Solvent for crystallization
3a	2-Cl	$C_{10}H_5ClN_4OS$	200–201.5	52	Dioxane
3b	4-F	$C_{10}H_5FN_4OS$	190–192	62	Dioxane
3c	4-CH_3	$C_{11}H_8N_4OS$	217–219	75	Dioxane
3d	3-OCH_3	$C_{11}H_9N_4O_2S$	208–209	92	Dioxane
3e	4-OCH_3	$C_{11}H_9N_4O_2S$	240–241.5	55	Dioxane
3f	4-SCH_3	$C_{11}H_9N_4OS_2$	183–184	87	Dioxane–ethanol (1:1)
3g	4-CF_3	$C_{11}H_6F_3N_4OS$	219.5–221	55	Dioxane–ethanol (1:1)
3h	3-CH_3-4-NO_2	$C_{11}H_7N_5O_3S$	249–250	79	Dioxane
3i	2,4-Cl	$C_{10}H_4Cl_2N_4OS_2$	205–207	65	Dioxane
3j	3,4-Cl	$C_{10}H_4Cl_2N_4OS_2$	246–248	87	Dioxane
3k	3,4-OH	$C_{10}H_6N_4O_3S$	307–308.5	40	Dioxane
3l	3,4-CH_3	$C_{12}H_{10}N_4OS$	212–214	80	Dioxane
3m	3,4-OCH_3	$C_{12}H_{12}N_4O_3S$	245–247	83	Dioxane

The IR spectra of all cyclized compounds (**3a**–**m**) showed no absorption band due to the NH_2 and SH groups. These observations gave clear evidence for the formation of a fused ring system. The IR spectrum of **3c** showed absorption bands at 1715 cm^{-1} due to carbonyl group and 1615 cm^{-1} assigned to the C=N stretching mode. The characteristic C–H modes of the ring residues were observed at 3061 cm^{-1}. The C–H stretching vibration bands of the CH_3 group were at 2984–2938 cm^{-1}. The presence of aromatic rings was identified by their characteristic ring vibrations at 1461 cm^{-1} and in the 821–715 cm^{-1} range. Similarly, the IR spectrum of **3i** exhibited absorption bands at 3092 cm^{-1} due to aromatic protons and at 1707 cm^{-1} due to the C=O of the triazine carbonyl group.

Other absorption bands were observed at 1584 (C=N), 1469 (C=C) and at 869 and 715cm^{-1} (C–Cl).

In the ^{1}H-NMR spectra of the cyclized compounds, peaks due to NH_2 and SH groups were absent, which confirmed the involvement of these functional groups in the cyclization of triazine to thiadiazolotriazines. The ^{1}H-NMR (DMSO-d_6) spectrum of compound **3c** showed a singlet at δ 2.40 ppm, integrating for three protons arising from CH_3 groups. The protons of the *p*-methylphenyl ring resonated as two doublets at δ 7.45 ppm (*J* = 8.3 Hz) and 7.91 ppm (*J* = 8.29 Hz), each integrating for two protons. The signal due to the triazine ring proton appeared as a singlet at 8.58 ppm. The ^{13}C-NMR (DMSO-d_6) spectrum of compound **3c** showed signals at 21.88, 125.42, 128.46, 131.03, 144.89, 146.06, 148.57, 160.53 and 162.03 ppm. According to this APT spectral data, $C^{2\prime}$ and $C^{6\prime}$ as well as $C^{3\prime}$ and $C^{5\prime}$ are magnetically equivalent to each other. They exhibited a single signal at 128.46 and 131.03 ppm, respectively. The ^{1}H-NMR (DMSO-d_6) spectrum of compound **3i** showed a doublet of doublets at 6.73 ppm (*J* = 1.96, 8.79) and two doublets at 8.01 ppm (*J* =1.96 Hz) and 8.10 ppm (*J* = 8.79 Hz), confirming the presence of the aromatic group. The signal due to the triazine ring appeared as a singlet at 8.63 ppm. The ^{13}C-NMR (DMSO-d_6) spectrum of **3i** showed the following signals 126.06, 129.41, 131.38, 133.17, 134.05, 138.97, 146.01, 148.45, 156.62 and 161.92 ppm, which account for the ten different carbon atoms present in the molecule.

The molecular ion peaks were determined for all the synthesized compounds. The mass spectrum of **3c** showed a protonated molecular ion peak at *m*/*z* = = 245.15 (100, $[M+1]^+$), which is consistent with molecular formula $C_{11}H_8N_4OS$. The mass spectrum of **3i** showed the presence of a molecular ion peak at *m*/*z* = = 299.27 (100, $[M]^+$), which is in agreement with the molecular formula $C_{10}H_4Cl_2N_4OS$. The spectral data of all the newly synthesized compounds are presented in the Supplementary Material to this paper.

EXPERIMENTAL

All chemicals and solvents were of reagent grade and used without further purification. The reactions were monitored by thin layer chromatography (TLC) using Merck silica gel 60 F_{254} coated alumina plates with ultraviolet light detection. The elemental data were obtained with a Thermo Finnigan Flash EA 1112 analyzer. The melting points were determined using a Büchi melting point apparatus. The FT-IR spectra were recorded in KBr disks on a Mattson 1000 FT-IR spectrometer. The ^{1}H- and ^{13}C-NMR spectra were recorded on a Varian Unity Inova instrument operating at 500 MHz. The residual DMSO-d_6 signal was also used as an internal reference. The Electron Spray Ionization-Mass Spectroscopy (ESI–MS) analyses were realized in positive ion modes using a Thermo Finnigan LCQ Advantage MAX LC/MS/MS spectrometer.

General procedure for the synthesis of compounds ***3a–m***

A mixture of 4-amino-3-mercapto-1,2,4-triazin-5(4*H*)-one **1** (0.001 mol) and mono- or di-substituted carboxylic acids **2** (0.001 mol) in 10 mL phosphorus oxychloride was refluxed on a water bath for about 8–10 h. The extent of the reaction was monitored by TLC. After cooling, the excess of phosphorus oxychloride was removed under vacuum. The reaction mixture was poured onto crushed ice. The precipitate was filtered, washed with sodium bicarbonate and water. The crude product was recrystallized from appropriate solvents, given in Table I.

CONCLUSIONS

In conclusion, thirteen novel 7-substitued-4*H*-1,3,4-thiadiazolo[2,3-*c*]1,2,4-triazin-4-ones (**3a**–**m**) were synthesized for the first time in this study. The structures of products were determined by FT-IR, NMR (^{1}H and ^{13}C) and ESI-MS spectroscopic techniques and analytical methods.

SUPPLEMENTARY MATERIAL

Analytic and spectral data of the synthesized compounds are available electronically from http://www.shd.org.rs/JSCS/, or from the corresponding author on request.

Acknowledgement. This work was supported by the Research Fund of Istanbul University, Project No.: 2085.

ИЗВОД

СИНТЕЗА И СПЕКТРАЛНЕ КАРАКТЕРИСТИКЕ НОВИХ ДЕРИВАТА ТИЈАДИАЗОЛОТРИАЗИНОНА

DEMET GÜRBÜZ и SÜLEYMAN TANYOLAÇ

Istanbul University, Faculty of Engineering, Department of Chemistry, 34320, Avcilar, Istanbul, Turkey

Синтетисана је серија 7-супституисаних деривата 4*H*-1,3,4-тијадиазоло[2,3-*c*][1,2,4]-триазин-4-она, у добром приносу, реакцијом 4-амино-3-меркапто-1,2,4-триазин-5(4*H*)-она са различитим ароматичним карбоксилним киселинама у присуству фосфор-оксихлорида. Структура свих добијених деривата потврђена је помоћу FT-IR, NMR (^{1}H и ^{13}C) и ESI-MS спектроскопских и аналитичких метода.

(Примљено 30. септембра, ревидирано 7. децембра 2011)

REFERENCES

1. Z. El-Gendy, J. M. Morsy, H. A. Allimony, A. R. Abdel-Monem, R. M. Abdel-Rahman, *Pharmazie* **56** (2001) 376
2. K. Sztanke, K. Pasternak, M. Sztanke, M. Kandefer-Szerszeń, A. E. Kozioł, I. Dybała, *Bioorg. Med. Chem. Lett.* **19** (2009) 5095
3. R. M. Abdel-Rahman, M. Seada, M. Fawzy, I. el Baz, *Boll. Chim. Farm.* **133** (1994) 381
4. V. L. Rusinov, O. N. Chupakhin, S. L. Deev, T. S. Shestakova, E. N. Ulomskii, L. I. Rusinova, O. I. Kiselev, E. G. Deeva, *Russ. Chem. Bull.* **59** (2010) 136
5. C. M. Louis, S. B. Gurdip, L. Jessie, W. Khizar, M. J. Madeleine, *J. Med. Chem.* **19** (1976) 845

6. B. S. Holla, B. K. Sarojini, R. Gonsalves, *Farmaco* **53** (1998) 395
7. W. M. Davidson, W. D. Boykin, *J. Pharm. Sci*. **65** (1978) 737
8. L. S. Pustoshnaya, V. P. Pustoshnyi, A. K. Mazitova, V. K. Khamaev, E. Y. Davydov, G. E. Zaikov, K. S. Minsker, *Polym. Degrad. Stab.* **70** (2000) 39
9. W. Oettmeier, U. Hilp, *Pestic. Sci.* **33** (1991) 399
10. C. Olmeda, L. Deban, E. Barrado, Y. Castrillejo, L. Herrero, *Electrochim. Acta* **39** (1994) 2237
11. L. Kang-Chieu, S. Bi-Jane, L. Chuen-Hsiang, *J. Heterocycl. Chem*. **29** (1992) 97
12. M. Onar, M. E. Omaima, M. Aboulwafa, *J. Heterocycl. Chem.* **23** (1986) 1339
13. A. Dornow, H. Menzel, P. Marx. *Chem. Ber*. **97** (1964) 2173.

JSCS@tmf.bg.ac.rs • www.shd.org.rs/JSCS

J. Serb. Chem. Soc. 77 (7) S102–S105 (2012)

Supplementary material

SUPPLEMENTARY MATERIAL TO

Synthesis and spectral properties of novel thiadiazolotriazinone derivatives

DEMET GÜRBÜZ* and SÜLEYMAN TANYOLAÇ

Istanbul University, Faculty of Engineering, Department of Chemistry,
34320, Avcilar, Istanbul, Turkey

J. Serb. Chem. Soc. 77 (7) (2012) 859–863

ANALYTIC AND SPECTRAL DATA

*7-(2-Chlorophenyl)-4*H*-[1,3,4]thiadiazolo[2,3-*c*][1,2,4]triazin-4-one* (**3a**). Yield: 52 %; Anal. Calcd. for $C_{10}H_5ClN_4OS$ (FW = 264.69): C, 45.38; H, 1.90; N, 21.17; S, 12.11 %. Found: C, 45.16; H, 1.97; N, 20.98; S, 12.02 %; IR (KBr, cm^{-1}): 3092 (C–H stretching of aromatic ring), 1707 (C=O stretching of triazine ring), 1592 (C=N), 1469 (C=C), 1200 (C–O), 792, 669 (C–H); ^{1}H-NMR (499.74 MHz, DMSO-d_6, δ / ppm): 7.72 (1H, *ddd*, *J* = 1.46, 7.32, 7.81 Hz, aromatic H-5'), 7.81 (1H, *ddd*, *J* = 1.95, 7.32, 7.81 Hz, aromatic H-4'), 7.88 (1H, *dd*, *J* =1.46, 8.29 Hz, aromatic H-6'), 8.20 (1H, *dd*, *J* =1.46, 7.81 Hz, aromatic H-3'), 8.71 (1H, *s*, triazine H-3); ^{13}C-NMR (125.66 MHz, DMSO-d_6, δ / ppm): 126.92, 129.11, 131.86, 132.00, 132.93, 135.00, 145.97, 148.50, 157.35, 162.07; MS (*m*/*z*): 265.13 (100, $[M+1]^+$).

*7-(4-Fluorophenyl)-4*H*-[1,3,4]thiadiazolo[2,3-*c*][1,2,4]triazin-4-one* (**3b**). Yield: 62 %; Anal. Calcd. for $C_{10}H_5FN_4OS$ (FW = 248.23): C, 48.38; H, 2.03; N, 22.57; S, 12.92 %. Found: C, 48.15; H, 2.01; N, 22.30; S, 12.80 %; IR (KBr, cm^{-1}): 3064 (C–H stretching of aromatic ring), 1715 (C=O stretching of triazine ring), 1595 (C=N), 1461 (C=C), 1253 (C–O), 853, 746 (C–H); ^{1}H-NMR (499.74 MHz, DMSO-d_6, δ / ppm): 7.45 (2H, *dd'*, *J* = 1.95, 5.37 Hz, aromatic H-3' and H-5), 8.55 (2H, *dd*, *J* = 1.95, 5.37 Hz, aromatic H-2' and H-6'), 8.60 (1H, *s*, triazine H-3); ^{13}C-NMR (125.66 MHz, DMSO-d_6, δ / ppm): 117.69, 117.87, 124.79, 131.30, 131.38, 146.15, 148.58, 159.50, 162.14, 164.70; MS (*m*/*z*): 249.16 (100, $[M+1]^+$).

*7-(4-Methylphenyl)-4*H*-[1,3,4]thiadiazolo[2,3-*c*][1,2,4]triazin-4-one* (**3c**). Yield: 75 %; Anal. Calcd. for $C_{11}H_8N_4OS$ (FW = 244.27): C, 54.09; H, 3.30; N,

---

* Corresponding author. E-mail: demet@istanbul.edu.tr

doi: 10.2298/JSC110930217G

22.94; S, 13.13 %. Found: C, 53.90; H, 3.21; N, 22.75; S, 13.05 %; IR (KBr, cm^{-1}): 3063 (C–H stretching of aromatic ring), 2984, 2938 (C–H stretching of CH_3 group), 1715 (C=O stretching of triazine ring), 1615 (C=N), 1461 (C=C), 1376 (C–H vibration of CH_3 group), 1276 (C–O), 823, 715 (C–H); ^{1}H-NMR (499.74 MHz, DMSO-*d*$_6$, δ / ppm): 2.40 (3H, *s*, $–CH_3$), 7.45 (2H, *d*, *J* = 8.3 Hz, aromatic H-3' and H-5'), 7.91 (1H, *d*, *J* =8.29 Hz, aromatic H-2' and H-6'), 8.58 (1H, *s*, triazine H-3); ^{13}C-NMR (125.66 MHz, DMSO-*d*$_6$, δ / ppm): 21.88, 125.42, 128.46, 131.03, 144.89, 146.06, 148.57, 160.53, 162.03; MS (*m*/*z*): 245.15 (100, [M+1]$^+$).

7-(3-Methoxyphenyl)-4H-[1,3,4]thiadiazolo[2,3-c][1,2,4]triazin-4-one (**3d**). Yield: 92 %; Anal. Calcd. for $C_{11}H_8N_4O_2S$ (FW = 260.27): C, 50.76; H, 3.10; N, 21.53; S, 12.32 %. Found: C, 50.67; H, 3.02; N, 22.51; S, 12.23 %; IR (KBr, cm^{-1}): 3100 (C–H stretching of aromatic ring), 2976, 2889 (C–H stretching of OCH_3 group), 1707 (C=O stretching of triazine ring), 1584 (C=N), 1461 (C=C), 1376 (C–H vibration of OCH_3 group), 1284 (C–O), 800, 692 (C–H); ^{1}H-NMR (499.74 MHz, DMSO-*d*$_6$, δ / ppm): 3.83 (3H, *s*, $–OCH_3$), 7.29–7.60 (4H, *m*, aromatic C–H), 8.76 (1H, *s*, triazine H-3); ^{13}C-NMR (125.66 MHz, DMSO-*d*$_6$, δ / ppm): 56.37, 112.88, 120.30, 121.11, 129.35, 131.81, 146.12, 148.60, 160.41, 160.61, 162.06; MS (*m*/*z*): 261.13 (100, [M+1]$^+$).

*7-(4-Methoxyphenyl)-*4H-*[1,3,4]thiadiazolo[2,3-*c*][1,2,4]triazin-4-one* (**3e**). Yield: 55 %; Anal. Calcd. for $C_{11}H_8N_4O_2S$ (FW = 260.27): C, 50.76; H, 3.10; N, 21.53; S, 12.32 %. Found: C, 50.56; H, 3.08; N, 22.46; S, 12.26 %; IR (KBr, cm^{-1}): 3076 (C–H stretching of aromatic ring), 2976, 2861 (C–H stretching of OCH_3 group), 1707 (C=O stretching of triazine ring), 1607 (C=N), 1469 (C=C), 1323 (C–H vibration of OCH_3 group), 1269 (C–O), 846, 715 (C–H); ^{1}H-NMR (499.74 MHz, DMSO-*d*$_6$, δ / ppm): 3.83 (3H, *s*, $–OCH_3$), 7.19 (2H, *dd*, *J* = 1.95, 6.83 Hz, aromatic H-3' and H-5'), 7.98 (2H, *dd*, *J* = 1.95, 6.83 Hz, aromatic H-2' and H-6'), 8.56 (1H, *s*, triazine H-3); ^{13}C-NMR (125.66 MHz, DMSO-*d*$_6$, δ / ppm): 56.48, 115.94, 120.43, 130.49, 146.12, 148.56, 160.10, 162.06, 164.08; MS (*m*/*z*): 260.26 (100, [M]$^+$).

*7-[4-(Methylthio)phenyl]-*4H-*[1,3,4]thiadiazolo[2,3-*c*][1,2,4]triazin-4-one* (***3f***). Yield: 87 %; Anal. Calcd. for $C_{11}H_8N_4OS_2$ (FW = 276.33): C, 47.81; H, 2.92; N, 20.27; S, 23.21 %. Found: C, 47.76; H, 2.90; N, 20.05; S, 23.23 %; IR (KBr, cm^{-1}): 3061 (C–H str. of aromatic ring), 2969, 2946 (C–H str. of CH_3 group), 1707 (C=O str.), 1592 (C=N str.), 1463 (C=C str.), 1300 (str. of OCH_3 group), 1276 (C–O str.), 830, 753 (C–H); ^{1}H-NMR (499.74 MHz, DMSO-*d*$_6$, δ / ppm): 2.65 (3H, *s*, $–SCH_3$), 7.56 (2H, *dd*, *J* = 1.95, 6.83 Hz, aromatic H-3' and H-5'), 8.05 (2H, *dd*, *J* = 1.95, 6.83 Hz, aromatic H-2' and H-6'), 8.65 (1H, *s*, triazine H-3); ^{13}C-NMR (125.66 MHz, DMSO-*d*$_6$, δ / ppm): 14.76, 124.0, 125.74, 126.57, 127.77, 128.75, 128.96, 145.85, 146.07, 151.44, 164.31; MS (*m*/*z*): 277.338 (100, [M+1]$^+$).

*7-[4-(Trifluoromethyl)phenyl]-4*H*-[1,3,4]thiadiazolo[2,3-*c*][1,2,4]triazin-4--one (**3g**)*. Yield: 55 %; Anal. Calcd. for $C_{11}H_5F_3N_4OS$ (FW = 298.24): C, 44.30; H, 1.69; N, 18.79; S, 10.75 %. Found: C, 44.21; H, 1.56; N, 18.75; S, 10.59 %; IR (KBr, cm^{-1}): 3076 (C–H stretching of aromatic ring), 1723 (C=O stretching of triazine ring), 1530 (C=N), 1469 (C=C), 1176 (C–O), 853, 723 (C–H); ^{1}H-NMR (499.74 MHz, DMSO-d_6, δ / ppm): 8.02 (2H, *d*, *J* = 8.30 Hz, aromatic H-3' and H-5'), 8.26 (2H, *d*, *J* = 8.30 Hz, aromatic H-2' and H-6'), 8.62 (1H, *s*, triazine H-3); ^{13}C-NMR (125.66 MHz, DMSO-d_6, δ / ppm): 123.81, 127.38, 127.40, 129.53, 131.94, 133.34, 146.26, 148.60, 159.30, 162.05; MS (*m*/*z*): 299.10 (100, $[M+1]^+$).

*7-(3-Methyl-4-nitrophenyl)-4*H*-[1,3,4]thiadiazolo[2,3-*c*][1,2,4]triazin-4-one (**3h**)*.Yield: 79 %; Anal. Calcd. for $C_{11}H_7N_5O_3S$ (FW = 289.27): C, 45.67; H, 2.44; N, 24.21; S, 11.08 %. Found: C, 45.02; H, 2.79; N, 23.87; S, 10.45 %; IR (KBr, cm^{-1}): 3076 (C–H stretching of aromatic ring), 2946, 2876 (C–H stretching of CH_3 group), 1715 (C=O stretching of triazine ring), 1538 (C=N), 1461 (C=C), 1323 (C–H vibration of CH_3 group), 1250 (C–O), 853 (C–H); ^{1}H-NMR (499.74 MHz, DMSO-d_6, δ / ppm): 2.61 (3H, *s*, –CH_3), 8.00–8.20 (3H, *m*, aromatic C–H), 8.63 (1H, *s*, triazine H-3); ^{13}C-NMR (125.66 MHz, DMSO-d_6, δ / / ppm): 19.69, 126.35, 127.27, 131.88, 132.77, 135.0, 146.28, 148.58, 152.12, 158.80, 162.09; MS (*m*/*z*): 289.95 (100, $[M]^+$)

*7-(2,4-Dichlorophenyl)-4*H*-[1,3,4]thiadiazolo[2,3-*c*][1,2,4]triazin-4-one (**3i**)*. Yield: 65 %; Anal. Calcd. for $C_{10}H_4Cl_2N_4OS$ (FW = 299.13): C, 40.15; H, 1.35; N, 18.73; S, 10.72 %. Found: C, 44.02; H, 1.23; N, 18.70; S, 10.65 %; IR (KBr, cm^{-1}): 3092 (C–H stretching of aromatic ring), 1707 (C=O stretching of triazine ring), 1584 (C=N), 1469 (C=C), 1284 (C–O), 869, 715 (C–Cl); ^{1}H-NMR (499.74 MHz, DMSO-d_6, δ / ppm): 6.73 (1H, *dd*, *J* = 1.96, 8.79 Hz, aromatic H-5'), 8.01 (1H, *d*, *J* = 1.96 Hz, aromatic H-6'), 8.10 (1H, *d*, *J* = 8.79 Hz, aromatic H-3'), 8.63 (1H, *s*, triazine H-3); ^{13}C-NMR (125.66 MHz, DMSO-d_6, δ / ppm): 126.06, 129.41, 131.38, 133.17, 134.05, 138.97, 146.01, 148.45, 156.62, 161.92; MS (*m*/*z*): 299.27 (100, $[M]^+$).

*7-(3,4-Dichlorophenyl)-4*H*-[1,3,4]thiadiazolo[2,3-*c*][1,2,4]triazin-4-one (**3j**)*. Yield: 87 %; Anal. Calcd. for $C_{10}H_4Cl_2N_4OS$ (FW = 299.13): C, 40.15; H, 1.35; N, 18.73; S, 10.72 %. Found: C, 40.09; H, 1.32; N, 18.65; S, 10.58 %; IR (KBr, cm^{-1}): 3084 (C–H stretching of aromatic ring), 1707 (C=O stretching of triazine ring), 1528 (C=N), 1469 (C=C), 1276 (C–O), 892, 776 (C–Cl); ^{1}H-NMR (499.74 MHz, DMSO-d_6, δ / ppm): 8.0 (1H, *d*, *J* = 6.34 Hz, aromatic H-3'), 8.11 (1H, *dd*, *J* = 0.98, 6.34 Hz, aromatic H-2'), 8.36 (1H, *d*, *J* = 0.98 Hz, aromatic H-6'), 8.63 (1H, *s*, triazine H-3); ^{13}C-NMR (125.66 MHz, DMSO-d_6, δ / ppm): 128.47, 128.61, 130.14, 132.69, 133.42, 136.95, 146.23, 148.52, 148.50, 162.11; MS (*m*/*z*): 299.01 (100, $[M]^+$).

*7-(3,4-Dihydroxyphenyl)-4*H-*[1,3,4]thiadiazolo[2,3-*c*][1,2,4]triazin-4-one* (***3k***). Yield: 35 %; Anal. Calcd. for $C_{10}H_6N_4O_3S$ (FW = 262.24): C, 45.80; H, 2.31; N, 21.36; S, 12.23 %. Found: C, 45.69; H, 2.27; N, 21.15; S, 12.12 %; IR (KBr, cm^{-1}): 3423 (O–H stretching), 3061 (C–H stretching of aromatic ring), 1700 (C=O stretching of triazine ring), 1512 (C=N), 1461 (C=C), 1207 (C–O), 830, 676 (C–H); ^{1}H-NMR (499.74 MHz, DMSO-d_6, δ / ppm): 6.93 (1H, *d*, J = = 8.29 Hz, aromatic H–5’), 7.34 (1H, *dd*, J = 1.95, 8.29 Hz, aromatic H–6’), 7.41 (1H, *d*, J = 2.39 Hz, aromatic H–2’), 8.56 (1H, *s*, triazine H-3), 9.73, 10.15 (1H, *s*, $OH_{(1)}$ and $OH_{(2)}$); ^{13}C-NMR (125.66 MHz, DMSO-d_6, δ / ppm): 114.40, 117.07, 119.03, 121.73, 145.93, 146.96, 151.83, 148.55, 160.34, 162.03; MS (*m*/*z*): 261.26 (100, [M–1]$^+$)

*7-(3,4-Dimethylphenyl)-4*H-*[1,3,4]thiadiazolo[2,3-*c*][1,2,4]triazin-4-one* (***3l***). Yield: 80 %; Anal. Calcd. for $C_{12}H_{10}N_4OS$ (FW = 258.29): C, 55.8; H, 3.90; N, 21.69; S, 12.41 %. Found: C, 55.63; H, 3.88; N, 21.65; S, 12.36 %; IR (KBr, cm^{-1}): 3076 (C–H stretching of aromatic ring), 2976 (C–H stretching of CH_3 group), 1715 (C=O stretching of triazine ring), 1530 (C=N), 1469 (C=C), 1315 (C–H vibration of CH_3 group), 1276 (C–O), 846, 610 (C–H); ^{1}H-NMR (499.74 MHz, DMSO-d_6, δ / ppm): 2.32, 2.35 (3H, *s*, $–CH_{3(1)}$ and $–CH_{3(2)}$), 7.40 (1H, *d*, J = = 7.81 Hz, aromatic H-5’), 7.75 (1H , *dd*, J = 1.95, 7.81 Hz, aromatic H-6’), 7.80 (1H, *d*, J = 1.95 Hz, aromatic H-2’), 8.57 (1H, *s*, triazine H-3); ^{13}C-NMR (125.66 MHz, DMSO-d_6, δ / ppm): 19.81, 20.03, 125.68, 129.47, 129.03, 130.30, 131.43, 142.19, 146.02, 148.58, 160.61, 162.03; MS (*m*/*z*): 259.21 (100, [M+1]$^+$).

*7-(3,4-Dimethoxyphenyl)-4*H-*[1,3,4]thiadiazolo[2,3-*c*][1,2,4]triazin-4-one* (***3m***). Yield: 83 %; Anal. Calcd. for $C_{12}H_{10}N_4O_3S$ (FW = 290.29): C, 49.65; H, 3.47; N, 19.30; S, 11.05 %. Found: C, 49.58; H, 3.41; N, 19.25; S, 10.90 %; IR (KBr, cm^{-1}): 3061 (C–H stretching of aromatic ring), 2946, 2838 (C–H stretching of OCH_3 group), 1700 (C=O stretching of triazine ring), 1560 (C=N), 1469 (C=C), 1320 (C–H vibration of OCH_3 group), 1276 (C–O), 850, 769 (C–H); ^{1}H-NMR (499.74 MHz, DMSO-d_6, δ / ppm): 3.81, 3.82 (3H, *s*, $OCH_{3(1)}$ and $OCH_{3(2)}$), 7.19 (1H , *d*, J = 8.39 Hz, aromatic H-5′), 7.58 (1H , *d*, J = 2.01 Hz, aromatic H-2′), 7.60 (1H, *dd*, J = 2.01, 8.39 Hz, aromatic H-6′), 8.57 (1H, *s*, triazine H-3); ^{13}C-NMR (125.66 MHz, DMSO-d_6, δ / ppm): 56.4, 56.6, 111.62, 112.85, 122.25, 123.95, 146.03, 149.16, 151.51, 153.25, 160.24, 162.11; MS (*m*/*z*): 291.17 (100, [M+1]$^+$).

Journal of the Serbian Chemical Society
version electronic

JSCS-info@shd.org.rs • www.shd.org.rs/JSCS

J. Serb. Chem. Soc. 77 (7) 873–877 (2012) UDC 547.324+547.261+546.814:543.422.25
JSCS–4316 *Note*

NOTE

Reaction of (iodomethyl)tin(IV) compounds with (2*S*)-2,5-dihydro-2-isopropyl-3,6-dimethoxy-pyrazine

KARIN DÖLLING*

Biozentrum, Martin-Luther-Universität Halle, 06099 Halle, Germany

(Received 15 December 2011, revised 24 January 2012)

Abstract: Following the Schöllkopf methodology, the reaction of (2*S*)-2,5-dihydro-2-isopropyl-3,6-dimethoxy-pyrazine **1** with (iodomethyl)trimethylstannane gives (2*S*,5*S*)-2,5-dihydro-2-isopropyl-3,6-dimethoxy-5-[(trimethylstannyl)methyl]pyrazine **2** in good yields. The obtained compound was characterized by elemental analysis and multinuclear (^{1}H, ^{13}C and ^{119}Sn)-NMR spectroscopy.

Keywords: Schöllkopf reaction; 2,5-dihydro-2-isopropyl-3,6-dimethoxy-pyrazine; stannylmethylation; NMR-spectroscopy.

INTRODUCTION

Among the synthetic methods for the preparation of optically active amino acids, compounds that contain a structural element producing a high asymmetric induction in the alkylation step and that can be separated after the reaction are the most important.[1,2] One of them is the Schöllkopf bis-lactim ether methodology,[3] which has proved to be of enormous utility in the preparation of a wide range of α-substituted and α,α-disubstituted amino acids in both enantiomeric forms. The most popular and extensively studied bis-lactim ether is 2,5-dihydro -2-isopropyl-3,6-dimethoxy-pyrazine **1**, which is derived from valine and glycine and is commercially available in both enantiopure (*R*)- and (*S*)-forms. The metalation of the bis-lactim ether with *n*-butyllithium in THF at a low temperature followed by alkylation with an electrophile proceeds with a high degree of stereoselectivity. The electrophile reacts at the side opposite to the alkyl group at the 2-position of the pyrazine ring.

The Schöllkopf method is widely used for the synthesis of (*R*)- and (*S*)-enantiomers of unnatural amino acids, such as β-(trimethylsilyl)alanine and β-(trimethylgermyl)alanine,[4–6] which due to their C/Si/Ge bioisosterism are of interest as

---

* E-mail: karin.doelling@medizin.uni-halle.de

doi: 10.2298/JSC111215007D

precursors of drugs and plant-protective agents. For example, *β*-(trimethylsilyl)-alanine derivatives are used as renin inhibitions.[7]

Stannylated alanine derivatives of the type $R_3SnCH_2CH(NHCOR')COOR''$ were previously synthesized using different procedures[8–10] but, in all cases, the products were mixtures of stereoisomers. However, the stereoselective reaction of (iodomethyl)tin(IV) compounds with (*S*)-1-(*t*-butoxycarbonyl)-2-*t*-butyl-3-methyl-4-imidazolidinone (Boc-BMI) yielded a pure product, (2*S*,5*R*)-*t*-butyl,2-t-butyl-3-methyl-4-oxo-5-[(trimethylstannyl)-methyl]-1imidaazolidine-carboxylate of high stereoselectivity.[11]

Therefore, it seemed of interest to investigate stereoselectively produced C-stannylated amino acids based on the Schöllkopf procedure. Herein, the reaction of (iodomethyl)trimethylstannane with (2*S*)-2,5-dihydro-2-isopropyl-3,6-dimethoxy-pyrazine **1** is described.

EXPERIMENTAL

Materials and methods

All operations were performed under dry nitrogen. THF of analytical purity was dried over Na/benzophenone prior to use. (2*S*)-2,5-Dihydro-2-isopropyl-3,6-dimethoxy-pyrazine was purchased from Merck. (Iodomethyl)trimethylstannane was obtained as described previously.[12] The elemental microanalyses were realized using a Carlo Erba Elemental Analyzer. All the NMR spectra were recorded in $CDCl_3$ solution by means of a Bruker AC 80, WP 200 or a Varian Unity 500 spectrometer.

*Synthesis of (2*S*,5*S*)-2,5-dihydro-2isopropyl-3,6-dimethoxy-5-[(trimethylstannyl)-lmethyl]pyrazine (**2**)*

An equimolar amount of butyl-lithium in hexane (15 mmol, 16.7 ml of a 0.9 M solution in hexane) was added to a stirred solution of (2*S*)-2,5-dihydro -2-isopropyl-3,6-dimethoxy-pyrazine (**1**) (2.5 ml, 13.9 mmol) in dry THF (10 ml) at –70 °C. After stirring for 10 min, a precooled solution (–70 °C) of (iodomethyl)trimethylstannane (4.24 g, 13.9 mmol) in dry THF (10 ml) was added dropwise. After stirring at –70 °C for about 24 h, the reaction mixture was allowed to warm to room temperature. The solvent was removed under reduced pressure, the residue treated with diethyl ether and then extracted with 20 ml water. The aqueous phase was extracted three times with diethyl ether (10 ml). The ether phases were combined and dried over $MgSO_4$. The solvent was removed after filtration and the crude yellow oil was chromatographically separated over silica gel (Merck Kieselgel 60; solvent ligroin:ether 3:1). *Rf*: 0.83 (ligroin/ether 3:1).

RESULTS

*Analytic and spectral data of the obtained compound **2***

Yield: 60 %; Anal. Calcd. for $C_{13}H_{26}N_2O_2Sn$: C, 43.25; H, 7.26; N, 7.76 %. Found: C, 43.27, H, 7.42, N, 7.81 %; ^{1}H-NMR (500 MHz, $CDCl_3$, 30 °C, δ / ppm): 0.05 (9H, *s*, ^2J (^{119}Sn, C^{1}H) = 54.0 Hz, $SnMe_3$), 0.66 (3H, *d*, ^3J = 7.0 Hz, $CH(C\mathbf{H}_3)_2$), 1.00 (3H, *d*, ^3J = 7.0 Hz, $CH(C\mathbf{H}_3)_2$), 1.13 (1H, *dd*, ^2J (H_A, H_B) = = –12.77 Hz, ^3J (H_A, H-5) = 9.22 Hz, $SnCH_A$), 1.42 (1H, *dd*, ^2J (H_B, H_A) =

= –12.77 Hz, ^3J (H_B, H-5) = 5.96 Hz, $SnCH_B$), 2.17–2.25 (1H, *m*, C**H**(CH_3)$_2$), 3.62 (3H, *s*, OCH_3), 3.65 (3H, *s*, OCH_3), 3.92 (1H, *t*, ^5J (C^2H, H-5) = 3.55 Hz, H-2), 4.03–4.13 (1H, *sept*, ^3J (^{119}Sn, C^1H) = 55.0 Hz, ^3J ($SnCH_A$, H-5) = 9.22 Hz, ^3J ($SnCH_B$, H-5) = 5.96 Hz, ^5J (H-2, H-5) = 3.55 Hz, H-5); ^{13}C-NMR (125.7 MHz, $CDCl_3$, 30 °C, δ / ppm): –9.17 (^1J (^{119}Sn, ^{13}C) = 334.3 Hz, Sn(CH_3)$_3$), 16.7 (CH(**C**H_3)$_2$), 19.0 (CH(**C**H_3)$_2$), 19.25 (^1J (^{119}Sn, ^{13}C) = 368.9 Hz, $SnCH_2$), 31.8 (**C**(CH_3)$_2$), 52.27 (OCH_3), 52.29 (OCH_3), 54.2 (^2J (^{119}Sn, ^{13}C) = 21.9 Hz, C-5), 61.1 (C-2), 162.97 (C-3), 165.59 (^3J (^{119}Sn ^{13}C) = 18.5 Hz, C-6); ^{119}Sn-NMR ($CDCl_3$, ^{1}H decoupled, internal standard (CH_3)$_4$Sn, δ / ppm): –6.3.

DISCUSSION

Following the standard reaction conditions (Experimental part), 2,5-dihydro-2-isopropyl-3,6-dimethoxy-5-[(trimethylstannyl)methyl]pyrazine was formed in 60 % yield (Scheme 1). Analysis of the crude reaction mixture by ^{119}Sn-NMR spectroscopy revealed the presence of two signals at –6.3 and –5.6 ppm in a ratio of 10:1, corresponding to the (2*S*,5*S*)- and the (2*S*,5*R*)-derivatives, **2** and **3**, respectively; both identified by ^{1}H-NMR spectroscopy of the raw product.

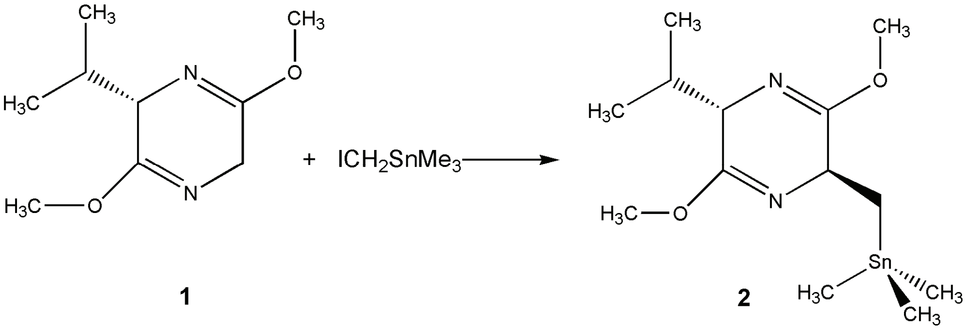

Scheme 1. Reaction of (2*S*)-2,5-dihydro-2-isopropyl-3,6-dimethoxy-pyrazine **1** with (iodomethyl)trimethylstannane.

The mixture was separated by column chromatography on silica gel yielding **2** as diastereomerically pure and colorless oil soluble in common organic solvents such as diethyl ether, chloroform and methanol. Attempts to prepare the stannylated alanine by hydrolysis of **2**, analogously to the preparation of β-(trimethylsilyl)alanine ethyl ester,[4] failed. Under the acidic reaction conditions, Sn–C bond cleavage was observed. Compound **2** was studied in detail by multinuclear NMR spectroscopy. The δ^{119}Sn at –6.3 ppm is situated in the region for tetramethyl tin compounds,[13] indicating tetra coordination at the tin atom. The non-equivalence of both protons of the $SnCH_2$ group in the neighbourhood of the C^5H proton leads to an AMX spin system in which the X-part becomes still more complicated because of the higher order coupling to the homoallylic standing C^2H proton atom. This long range coupling constant through five bonds was used to determine the orientation of the protons at C^2 and C^5, and to serve thereby for differentiation of the diastereomers. The determination of the configuration of the diastereomer **2** was based on the specific ^5J coupling constants in the ^{1}H-NMR spectra, which corresponds very well with literature data.[14] The configuration of **2** can also be explained based on the accepted model for the alkylation reactions of the Schöllkopf reagent,[3] verified by a large number of examples.

CONCLUSIONS

Following the Schöllkopf methodology, the reaction of (2*S*)-2,5-dihydro-2-isopropyl-3,6-dimethoxy-pyrazine **1** with (iodomethyl)trimethylstannane gives (2*S*,5*S*)-2,5-dihydro-2-isopropyl-3,6-dimethoxy-5-[(trimethylstannyl)methyl]pyrazine **2** in good yields. Compound **2** was studied in detail by multinuclear NMR spectroscopy. The determination of the configuration of **2** was based on the specific ^5J coupling constants between protons at C^2 and C^5, which correspond very well with literature data.[14] The configuration can also be explained based on the accepted model for the alkylation reaction of the Schöllkopf reagent.[3]

ИЗВОД

РЕАКЦИЈА ЈЕДИЊЕЊА (ЈОДМЕТИЛ)КАЛАЈА(IV) И (2*S*)-2,5-ДИХИДРО-2-ИЗОПРОПИЛ-3,6-ДИМЕТОКСИ-ПИРАЗИНА

KARIN DÖLLING

Biozentrum, Martin-Luther-Universität Halle, 06099 Halle, Germany

Пратећи методологију Schöllkopf-a реакцијом (2*S*)-2,5-дихидро-2-изопропил-3,6-диметокси-пиразина **1** и (јодметил)триметилстанана добијен је (2*S*,5*S*)-2,5-дихидро-2-изопропил-3,6-диметокси-5-[(триметилстанил)метил]пиразин **2** у добром приносу. Производ је окарактерисан елементалном анализом и (^{1}H, ^{13}C и ^{119}Sn)-NMR спектроскопијом.

(Примљено 15. децембра 2011, ревидирано 24. јануара 2012)

REFERENCES

1. R. M. Williams, *Synthesis of Optically Active a-Amino Acids*, Pergamon Press, Oxford, 1989
2. L. A. Paquette, *Chiral Reagents for Asymmetric Synthesis*, Wiley, New York, 2003, p. 220
3. U. Schöllkopf, *Tetrahedron* **39** (1983) 2085
4. B. Weidmann, *Chimia* **46** (1992) 312
5. R. Tacke, M. Merget, R. Bertermann, M. Bernd, T. Beckers, T. Reissmann, *Organometallics* **19** (2000) 3486
6. M. Merget, K. Günther, M. Bernd, E. Günther, R. Tacke, *J. Organomet. Chem.* **628** (2001) 183
7. Sandoz-Patent- GmbH (B. Weidmann) DE 3841319 (June 1989)
8. K. Dölling, H. Hartung, D. Schollmeyer, H. Weichmann, *Z. Anorg. Allg. Chem.* **600** (1991) 153
9. K. Dölling, A. Krug, H. Hartung, H. Weichmann, *Z. Anorg. Allg. Chem.* **621** (1995) 63
10. K. Dölling, K. Merzweiler, C. Wagner, H. Weichmann, *Z. Naturforsch.* **54b** (1999) 293

11. K. Dölling, A. Krug, H. Hartung, H. Weichmann, *Z. Naturforsch.* **51b** (1996) 619
12. F. Richter, H. Weichmann, *J. Organomet. Chem.* **466** (1994) 77
13. B. Wrackmeyer, *Annu. Rep. NMR Spectrosc.* **16** (1985) 73
14. N. G. Akhmedov, C. A. Dacko, A. Güven, B. C. G. Söderberg, *Magn. Reson. Chem.* **48** (2010) 134.

Journal of the Serbian Chemical Society
JSCS-info@shd.org.rs • www.shd.org.rs/JSCS

J. Serb. Chem. Soc. 77 (7) 879–886 (2012)
JSCS–4317

UDC 638.16+615.33:66.022.362
Original scientific paper

Stability of tetracycline residues in honey

MONICA CRISTINA CARA[1], GABRIELA-ALINA DUMITREL[2]*,
MIREL GLEVITZKY[3] and DELIA PERJU[2]

[1]Sanitary-Veterinary and Food Safety Directorate of Timis County, Martir Caceu No.4, 300585, Timişoara, [2]Politehnica University of Timişoara, Faculty of Industrial Chemistry and Environmental Engineering, 2 Victoriei Square, 300006, Timişoara, and [3]Sanitary-Veterinary and Food Safety Directorate of Alba County, 7A Lalelelor Street, 510217 Alba Iulia, Romania

(Received 2 October, revised 14 December 2011)

Abstract: The problem of the availability of veterinary medicines to treat honeybees is discussed extensively worldwide. An uncontrolled administration of antibiotics may lead to contamination of beehive products and contribute to the problem of food safety. In this study, the kinetics of tetracycline (TC) degradation in honey was studied for samples provided by four beekeepers located in the west region of Romania. The samples of honey were stored in the dark at room temperature for 30 days and sub-samples were analyzed every 3 days by the Elisa method. The results of the study revealed that the level of tetracycline decreased with time in all the honey samples. The tetracycline degradation followed a first-order kinetic model with reaction rate constants between 1.2×10^3–2×10^3 days^{-1}. The half-life time, $\tau_{1/2}$, of tetracycline in monofloral honeys: acacia and lime was 251 and 232 days, respectively. Tetracycline degradation in the polyfloral honey was accelerated, exhibiting a $\tau_{1/2}$ of 151 days.

Keywords: honey; antibiotics; storage; degradation; kinetics.

INTRODUCTION

The general aim of the European Union (EU) 2007–2013 Health Strategy is to improve and protect human health. One of the actions under this Strategy is to support safe, innovative and cost-efficient health products and technologies.[1]

Honey is a valuable bee product used frequently as food but also as therapeutic product. From ancient times, the antibacterial effect of honey was perceived due to its ability to stimulate rapid wound healing and the inhibition of wound pathogens. In addition to antibacterial activity, honeys are known to have antioxidant capacities, which may act to modulate the production of free radicals.

---

* Corresponding author. E-mail: alina.dumitrel@chim.upt.ro

doi: 10.2298/JSC111002214C

The use of antibiotics, for example tetracyclines, in apiculture for the treatment of bacterial brood diseases, such as American foulbrood (*Paenibacillus larvae*) and European foulbrood (*Melissococcus plutonius*) leads to contamination of honey with drugs.

The presence of tetracycline (TC) and its degradation products in honey may have harmful effects on consumers, such as possible allergic reactions, liver damage, yellowing of teeth and gastro–intestinal disturbance due to the selective pressure of antibiotics on the micro flora of human gut.[2]

According to Regulation (EC) No 470/2009[3] and Regulation (EU) No 37/ /2010,[4] in the European Union, no maximum residue level (MRL) for tetracycline in honey has been set. This means that the presence of tetracycline residues in honey is not allowed. Despite this decision, some countries have established action limits or tolerated levels for tetracycline in honey. For instance, in Belgium, the action limit for the group of tetracycline has been fixed at 20 μg kg^{-1}. France applies a nonconformity limit for tetracycline in honey of 15 μg kg^{-1}; the reporting limit in Great Britain is 50 μg kg^{-1}, while the tolerance level in Switzerland is 20 μg kg^{-1}.[5]

The Community Reference Laboratories proposed 20 μg kg^{-1} as the recommended concentration for screening for tetracyclines in honey.[6] Romania has adopted this action level as an acceptable limit for tetracycline residue detection in honey.

Little information about the stability of tetracycline residues in honey during storage is available in the literature. The first study was published by Landerkin *et al*. in 1957.[7] They reported that after nine months storage at 34 °C, the concentration of tetracycline residues in honey had decreased from the initial concentration of 100 to 2 mg kg^{-1}.

In the study performed by Martel *et al*.,[8] tetracycline was very stable in honey; the half-lives of tetracycline hydrochloride in honey stored at 4, 20 and 35 °C in the dark were 520, 242 and 121 days, respectively. Čuláková *et al*.[9] stored honey fortified with 209.4 mg kg^{-1} of tetracycline in the dark, semi-dark and daylight at a temperature of 25 °C. The half-life of tetracycline in the dark was 210 days and because it is light-sensitive, the half-life decreased to 147 days under semi-dark conditions and to 19.3 days in daylight.

Recently, Tayar *et al*.[10] reported that the residual level of tetracycline in honey was reduced by 76 % after 60-day storage and according to Molino *et al*.[11] after 90 days of storage at 20 °C in the dark, the tetracycline level had decreased by 50 %.

The aim of this study was to determine the contamination of honey samples by tetracycline and to characterize from a kinetic viewpoint the degradation of tetracycline in different types of honey during storage.

EXPERIMENTAL

Honey samples

Three types of honey (two monofloral, acacia and lime, and one polyfloral) were collected in 2009 from four beekeepers located in the west region of Romania.

In all cases, three replicates were analyzed for the presence of tetracycline residues (TC).

Antibacterial residues analyses

A commercially enzyme immunoassay (ELISA) (Ridascreen® tetracycline, R-Biopharm GmbH, Darmstadt, Germany) was used to analyze for tetracycline (TC) in honey. The detection system for the ELISA was a Sunrise Absorbance Microplate Reader from Tecan AG. In order to demonstrate the reliability of the method, the following parameters were investigated according to the European Commission Decision 2002/657/EC: repeatability, reproducibility, recovery, specificity and precision. The values of these parameters are presented in Table I. From the specification of the Ridascreen® kit, chlortetracycline (CTC) could give cross-reactions with tetracycline. Therefore a specificity test was performed for these two compounds and it was proved that the method has the ability to distinguish between TC and CTC.

TABLE I. Parameters showing the reliability of the employed analytic method

Parameter		TC added to the sample, μg·kg^{-1}			CTC added to the sample, μg·kg^{-1}
		20	30	40	30
Repeatability[a]	Mean ±*SD*, μg·kg^{-1}	20.3±0.67	30.5±0.54	39.8±0.28	–
Recovery[a]	%	101.5	101.6	99.5	–
Reproducibility[a]	Analyst 1 Mean ±*SD*, μg·kg^{-1}	20.3±0.67	30.5±0.54	39.8±0.28	–
	Analyst 2 Mean ±*SD*, μg·kg^{-1}	19.66±0.33	28.44±0.91	39.85±0.20	–
Precision[b]	Mean ±*SD*, μg·kg^{-1}	20.23±0.5	–	–	–
	CV, %	2.47	–	–	–
Specificity[a]	Mean ±*SD*, μg·kg^{-1}	–	29.65±0.18	–	ND[c]

[a]Number of replicated samples, *n* = 6; [b]number of replicated samples, *n* = 15; [c]not detectable

Reagent preparation

All the reagents and standards are prepared according to the instructions given by the manufacturer of the test kit.

Sample preparation

A honey sample (1 g) was dissolved with 49 ml 10 mM phosphate buffered saline (PBS buffer, pH 7.4). In order to achieve a better dissolution, the sample solution was vortexed and then kept for 5 min in an ultrasonic bath.

Testing protocol

According to the procedure described for the kit, 50 µl of each standard solution and prepared sample were added in duplicate into different sample wells. Into each well, 50 µl of anti-tetracycline antibody solution was added, mixed gently by shaking the plate manually and incubated for 1 h at room temperature (20–25 °C). Subsequently, the liquid was poured out of the wells and the wells were washed 3 times with 250 µl washing buffer. 100 µl of enzyme conjugate was added to each well and the plate incubated at room temperature (20–25 °C). After 15 min incubation, the liquid was poured and the washing procedure was repeated. In the next step, 50 µl of substrate and 50 µl of chromogen were added to each well and after mixing, the plate was incubated for 15 min at room temperature (20–25 °C) in the dark. In the last step, 100 µl of the stop solution was added to each well. The absorbance of the sample was read on a plate reader at 450 nm. The limit of detection was 15 µg kg^{-1}.

pH Measurement

The pH of the honey was determined with an InoLab level 1 type pH-meter and a pH electrode for viscous samples.

Storage study

Honey samples were poured into a glass bottle with a metal screw and stored at room temperature (21±1) °C in the dark, for 30 days. Sub-samples from each type of honey were analyzed three times every 3 days by the Elisa method.

RESULTS AND DISCUSSION

The results of the determination of tetracycline residues in the honey samples collected from four beekeepers located in the west region of Romania are summarized in Table II as the mean value of three replicates per sample and the standard deviation (*SD*).

TABLE II. Tetracycline concentrations (mean ± *SD*, µg·kg^{-1}) in the tested honey and the Romania action limit for tetracycline in honey; MRL: 20 ppb

Honey type	1st Apiary	2ndApiary	3rd Apiary	4th Apiary
Acacia	38.32±0.18	19.14±0.18	27.03±0.16	16.18±0.21
Lime	15.47±0.45	21.27±0.11	18.04±0.26	60.67±0.47
Polyfloral	16.63±0.46	30.72±0.42	15.47±0.45	22.89±0.43

Tetracycline residues were found in 50 % of the examined honey samples. The highest detected tetracycline contamination level was 60.67 µg $kg^{–1}$ for a lime honey sample. For the other types of honey, the maximum tetracycline contents found were 38.32 µg $kg^{–1}$ in acacia honey and 30.72 µg $kg^{–1}$ in polyfloral honey. The corresponding mean pH values of the initial samples were 4.2 for the acacia honey, 4.1 for the lime honey and 3.8 for the polyfloral honey.

In order to study the rate of the degradation of the tetracycline residues, samples with the highest tetracycline concentration from each honey type were placed into Erlenmeyer flasks and stored at laboratory temperature (21±1) °C in the dark. The experiments were performed from the beginning of August 2009 until September 2009.

The results of the effect of storage time on the tetracycline level (expressed as percent of the initial tetracycline concentration in the sample) are summarized in Fig. 1, from which it can be seen that the tetracycline concentration continuously decreased in all the honey samples.

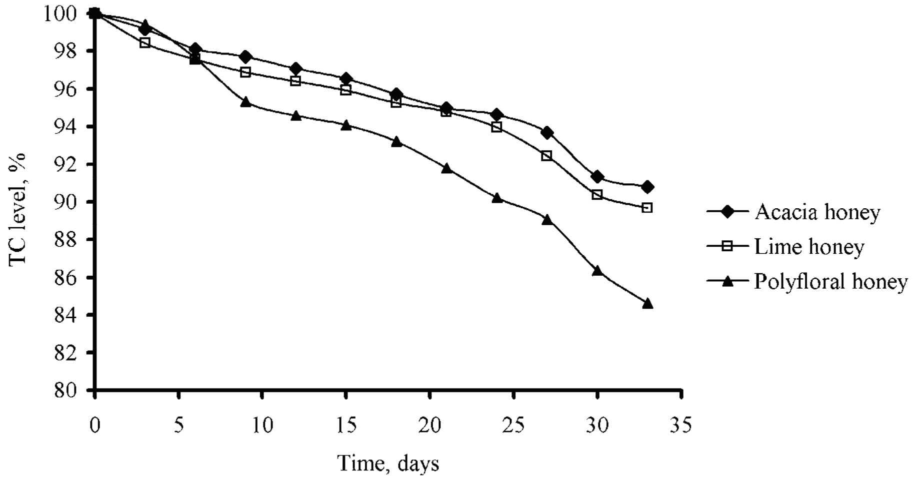

Fig. 1. Decrease in the tetracycline level in different types of honey during storage at room temperature in the dark.

After 3 days of storage, the tetracycline level was reduced by 2.5 % in all three honey samples. This decrease continued but was more pronounced in the polyfloral honey. At day 30, the tetracycline level in the monofloral honeys (acacia and lime) had decreased by 10 % while a 15 % decrease was registered in the polyfloral honey.

Molino *et al.*[11] reported a 21 % decrease of the tetracycline level in honey after 30 days of storage at 20 °C, but the type of honey was not specified. Similar results were obtained by Čuláková *et al.*[9] and Martel *et al.*[8]

In order to describe the degradation of tetracycline in the different types of honey, a first order kinetic model (1) was proposed:

$$c = c_0 e^{-kt} \tag{1}$$

where c is the concentration of tetracycline in the honey at time t, c_0 is the initial concentration of tetracycline in the honey and k is the first-order kinetic rate constant.

For the determination of the values of the rate constant k, the results of the decrease in the tetracycline concentration in the different types of honey during storage at room temperature and darkness were used. From these data, the values of k were evaluated by plotting $-\ln (c/c_0)$ *vs*. time t (Fig. 2). The plots of $-\ln (c/c_0)$ *vs*. time t gave straight lines, the slopes of which were equal to the respective first order rate constant k.

The half-life of the TC degradation process is independent of the starting concentration and is given by:

$$t_{1/2} = \ln 2 / k \tag{2}$$

The first-order reaction rate constants (k) and the half-lives ($t_{1/2}$) of the model are given in Table III.

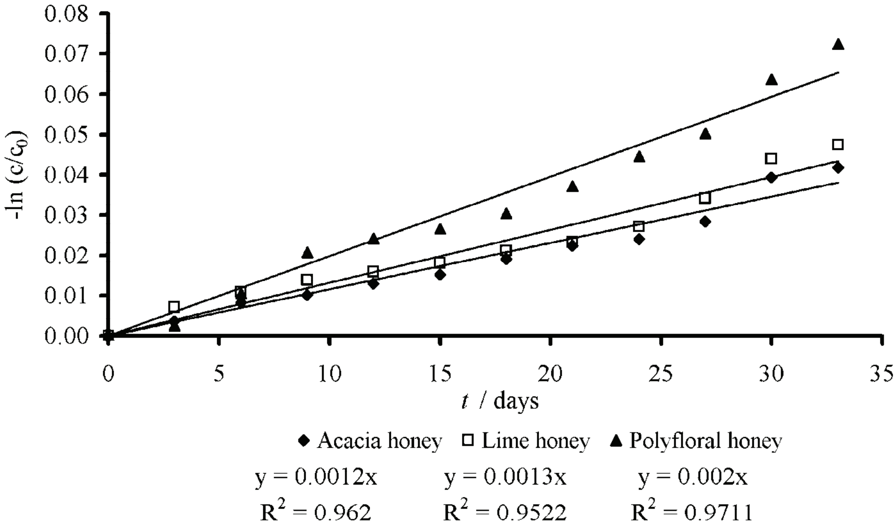

Fig. 2. Determination of the values of the rate constant for tetracycline degradation in different types of honey with time.

TABLE III. Effect of honey type on the k and $t_{1/2}$ values of tetracycline degradation in honey stored at room temperature in the dark

Honey type	$k\times10^3$ / days^{-1}	$t_{1/2}$ / days	R^2
Acacia	1.2	251	0.9620
Lime	1.3	232	0.9522
Polyfloral	2.0	151	0.9711

In all cases, the R^2 values were higher than 0.95, indicating a good fit of the data to the first-order kinetic model. The k values were almost the same for the two types of monofloral honey, acacia and lime honeys. When comparing the rate constants of tetracycline degradation in the monofloral honeys with that in the polyfloral honey, it can be seen that the degradation in the polyfloral sample was about 1.6 times faster that in the monofloral samples. This can be due to the different qualitative and quantitative composition of the monofloral and polyfloral honey, as well as to the pH of the samples. Tetracycline degradation in the polyfloral honey may also be increased by the presence of enzymes.

The values of half-life time of tetracycline show that it is very stable in honey. In the study of Čuláková *et al.*,[9] the half-life of tetracycline in honey stored at 25 °C in the dark was 210 days. Martel *et al.*[8] reported the half-lives at 20 and 35 °C as 242 and 121 days, respectively. These values are similar to the values obtained in the present study of tetracycline degradation.

On analyzing the initial pH values of the samples and the half-life values of tetracycline in the different types of honeys, it was noticed that the increase in the pH of the samples was accompanied by an increase of the TC half-life. The linear correlation between these two parameters is presented in Fig. 3.

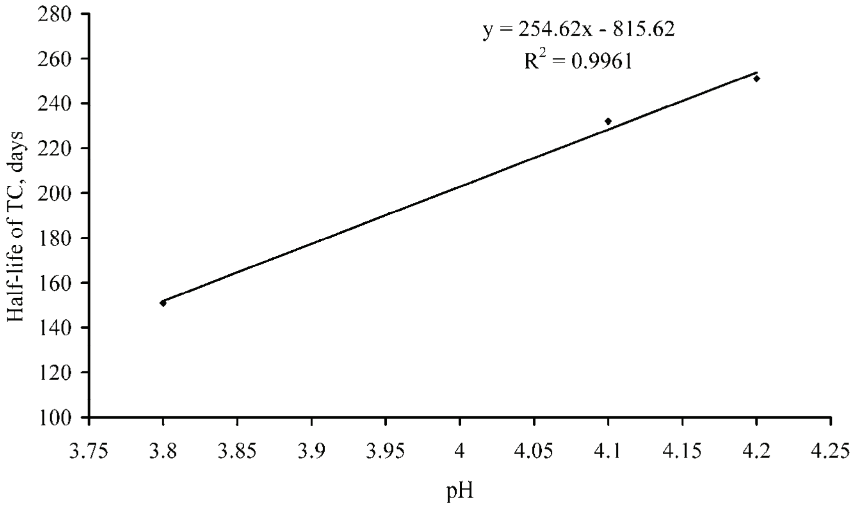

Fig. 3. Variation of the half-life of TC with pH.

The very good linear correlation between the two parameters was confirmed by the correlation coefficient R^2 of 0.9961. The values of pH were also measured at the end of the storage study and the results revealed that the pH of samples were constant during the 30 days of the experiment. These findings are in accordance with the studies of Jimenez *et al.*[12] and Cavia *et al.*[13]

CONCLUSIONS

The results presented in this paper showed that the concentration of tetracycline decreased with time in all the honey samples and that it was more rapidly degraded in the polyfloral honey. Based on the experimental results, it was found that first-order reaction kinetics adequately described the degradation of tetracycline residues in all the types of analyzed honey. The different values of the half-life of tetracycline in the three types of honeys were shown to be due to the pH of the samples.

Although studies of tetracycline degradation in honey are quite rare in the literature, the results presented in this work corresponded with those reported by other authors.

All these emphasize the need to improve the education of beekeepers in order to avoid any use and misuse of antibacterial drugs and to prevent honey contamination.

Acknowledgments. This work was partially supported by the strategic grant POSDRU/ /21/1.5/G/13798, inside POSDRU Romania 2007–2013, co-financed by the European Social Fund – Investing in People.

ИЗВОД

СТАБИЛНОСТ ОСТАТАКА ТЕТРАЦИКЛИНА У МЕДУ

MONICA CRISTINA CARA[1], GABRIELA-ALINA DUMITREL[2], MIREL GLEVITZKY[3] и DELIA PERJU[2]

[1]*Sanitary-Veterinary and Food Safety Directorate of Timis County, Timişoara,* [2]*Politehnica University of Timişsoara, Faculty of Industrial Chemistry and Environmental Engineering, Timişsoara и* [3]*Sanitary-Veterinary and Food Safety Directorate of Alba County, Alba Iulia, Romania*

Познато је да постоји проблем у коришћењу ветеринарских медикамената у лечењу медоносних пчела. Неконтролисана примена антибиотика може довести до контаминације пчелињих производа и угрожавања безбедности хране. У овом раду је проучавана кинетика деградације тетрациклина у узорцима меда из западне Румуније. Узорци меда су чувани у мраку, на собној температури, 30 дана и анализирани ELISA методом свака 3 дана. Резултати су показали да концентрација тетрациклина опада с временом. Деградација тетрациклина одговара моделу реакције првог реда, са константама брзине реакције $1{,}2\times10^{-3}$–$2{,}0\times10^{-3}$ дан$^{-1}$. Полуживот тетрациклина у багремовом меду је 251 дан, а у меду од липе 232 дана. Деградација тетрациклина у полифлоралном меду је бржа и полуживот износи 151 дан.

(Примљено 2. октобра, ревидирано 14. децембра 2011)

REFERENCES

1. Directorate General for Health & Consumers, *DG Health and Consumers Management Plan 2011 and beyond*, 2010, p. 55
2. W. Thanasarakhan, S. Kruanetr, R. L. Deming, B. Liawruangrath, S. Wangkarn, S. Liawruangrath, *Talanta* **84** (2011) 1401
3. Regulation (EC) No. 470/2009 of the European Parliament and of the Council, *Official Journal of the European Union* **L 152** (2009) 11
4. Regulation (EU) No. 37/2010, *Official Journal of the European Union* **L15/1** (2010) 1
5. J. Li, L. Chen, X. Wang, H. Jin, L. Ding, K. Zhang, H. Zhang, *Talanta* **75** (2008) 1245
6. Community Reference Laboratories, *CRLs view on state of the art analytical methods for national residue control plans*, CRL Guidance Paper, 2007, p. 8
7. G. B. Landerkin, H. Katznelson, *Appl. Microbiol.* **5** (1957) 152
8. A. C. Martel, S. Zeggane, P. Drajnudel, J. P. Faucon, M. Aubert, *Food Addit. Contam.* **23** (2006) 265
9. V. Čuláková, E. Kiss, J. Kubincová, S. Šilhár, *J. Food Nutr. Res.* **47** (2008) 139
10. G. Tayar, S. Rath, F. Guillermo, R. Reyes, *Food Control* **21** (2010) 620
11. F. Molino, R. Lázaro, C. Pérez, S. Bayarri, L. Corredera, A. Herrera, *Apidologie* **42** (2011) 391
12. M. Jimenez, J. J. Mateo, T. Huerta, M. Mateo, *J. Sci. Food Agric.* **64** (1994) 67
13. M. M. Cavia, M. A. Fernandez-Muino, S. R. Alonso-Torre, J. F. Huidobro, M. T. Sancho, *Food Chem.* **100** (2007) 1728.

Journal of the Serbian Chemical Society
JSCS-info@shd.org.rs • www.shd.org.rs/JSCS
J. Serb. Chem. Soc. *77* (7) 887–898 (2012)
JSCS–4318
UDC 535.563:532.74+519.6:544.351
Original scientific paper

Calculations of optical rotation: Influence of molecular structure

JIA YU[1], YU CAO[1], HANG SONG[1], XIANLONG WANG[2,3] and SHUN YAO[1]*

[1]School of Chemical Engineering, Sichuan University, Chengdu 610065, China, [2]School of Life Science and Technology, University of Electronic Science and Technology of China, Chengdu 610054, China and [3]Department of Chemistry, Bryn Mawr College, 101 N Merion Ave, Bryn Mawr, PA 19010, USA

(Received 5 September 2011)

Abstract: The *ab initio* Hartree–Fock (HF) method and the Density Functional Theory (DFT) were used to calculate the optical rotation of 26 chiral compounds. The effects of the theory and basis sets used for the calculation, the influence of the solvent on the geometry and the values of the calculated optical rotation are all discussed. The polarizable continuum model, included in the calculation, did not improve the accuracy effectively, but was superior to γ_s. The optical rotation of five- and six-membered cyclic compounds was calculated and 17 pyrrolidine or piperidine derivatives, which were calculated by the HF and DFT methods, gave acceptable predictions. The nitrogen atom dramatically affected the calculation results and it is necessary in the molecular structure in order to obtain an accurate computation result. Namely, when the nitrogen atom was substituted by an oxygen atom in the ring, the calculation result deteriorated.

Keywords: *ab initio*; chiral molecules; molecular structure; optical rotation; solvent effect.

INTRODUCTION

Optical rotation (OR) at the sodium D line ($[\alpha]_D$) is one of the most common experimental data that characterizes an optically active compound, and it can be correlated with the absolute configuration by reliable algorithms.[1] In recent years, there has been increasing interest in the calculation of the optical rotation at the sodium D line. Polavarapu[2] identified a “renaissance” in optical rotation. The first *ab initio* calculation of optical rotation was reported by Polavarapu and co-workers[3] in 1997 and subsequently more attention was paid to this calculation. In the beginning, most calculations were concentrated on small and rigid molecules for accuracy. Polavarapu and co-workers[4] calculated the optical rotation of small molecules: H_2O_2 and H_2S_2. With the development of computers and algorithms,

---

* Corresponding author. E-mail: cusack@scu.edu.cn
doi: 10.2298/JSC110905207Y

more calculations were directed to large and flexible molecules or natural product molecules, even to the determination of the absolute configuration of molecules.[5] Moreover, the absolute configuration of more complex molecules can be determined combined with other calculations.[6] Although great progress was made in these years with the development of quantum chemical models, accurate computation results remained unreliable. Hence, researchers still focus on improvement of the calculation accuracy,[7] and many calculation methods have demonstrated an encouraging agreement between the observed and predicted optical rotation.

The determination of the absolute configuration of chiral molecules is a challenging task. Optical rotation can be used to determine the absolute configuration of the molecules.[8] If calculation methods are easy and the results are sufficiently accurate, they will be helpful for the assignment of absolute configuration. Great effort should still be made in this field. Density functional theory (DFT) is widely used for the calculation of OR, and nowadays it has become a major trend. Several authors have reported the performance of DFT in the determination of the sodium D-line specific rotation $[\alpha]_D$ of a number of rigid chiral molecules. In addition, the coupled cluster theory was reported by Ruud *et al.*[9] Stephens *et al.*[10] reported that the *ab initio* calculation of the OR (and of electronic circular dichroism, ECD) provided reliable results only when the TDDFT method with extended basis sets (*i.e.*, including both polarization and diffuse functions) was used. Although this kind of method has been applied by many researchers and its availability has been approved, strong computational capability is compulsory when a large and complicated molecule is studied. The Hartree–Fock (HF) theory should be considered in the calculation of OR.

The specific rotation of a chiral molecule at a frequency ν is given by:[11–13]

$$\phi = \frac{16\pi^3 N \nu^2}{c^2} \gamma_s \beta \tag{1}$$

where N is the number of chiral molecules cm^{-3} in an isotropic solution and $\beta = 1/3\mathrm{Tr}[\beta_{\alpha\beta}]$, where $\beta_{\alpha\beta}$ is the electric dipole – magnetic dipole polarizability. $\beta_{\alpha\beta}$ is given by:

$$\beta_{\alpha\beta} = \frac{c}{3\pi h} \mathrm{Im}\left[\sum_{k \neq 0} \frac{\langle 0 | (\mu_{\mathrm{el}}^{\mathrm{e}})_\alpha | k \rangle \langle k | (\mu_{\mathrm{mag}}^{\mathrm{e}})_\beta | 0 \rangle}{\nu_{\mathrm{k0}}^2 - \nu^2} \right] \tag{2}$$

where 0 and k label the ground and excited electronic states, $\mu_{\mathrm{el}}^{\mathrm{e}}$ and $\mu_{\mathrm{mag}}^{\mathrm{e}}$ are the electronic electric and magnetic dipole operators, respectively and γ_s is the solvent effect. However, the inclusion of γ_s in the calculated ORs values leads to deterioration from the experiment data. The solvent correction is neglected ($\gamma_s = 1$) in the first calculation. Then next calculation is approximated by using the Lorentz expression: $\gamma_S = (n^2+2)/3$.[12,14] Optical rotations are usually measured using D line (589.3 nm) radiation.

Although the quantum mechanical origin of the optical rotation angle was described by Rosenfeld in 1928, Amos first realized the calculation of $\beta_{\alpha\beta}$ using *ab initio* methods in 1982. In this paper, our focus was on *ab initio* optical rotation studies of molecules with similar structures (pyrrolidine or piperidine derivatives), whereby attempts were made to find some relations between calculation methods and molecular structure. The accuracy of various types of methods and basis sets are discussed for five- or six-membered nitrogen-containing compounds. The application of the HF and DFT methodologies in the calculation of optical rotation is discussed and acceptable prediction was currently proved for 17 pyrrolidine or piperidine derivatives. Finally, the inclusion of polarizable continuum model (PCM) in the calculations is discussed and compared to inclusion of the solvent effect γ_S.

COMPUTATIONAL DETAILS

The OR was calculated by the HF and DFT methods utilizing two exchange-correlation functional, B3-LYP[15-17] (hybrid three-parameter Becke–Lee–Yang–Parr functional) and B3PW91[15,18,19] (hybrid three-parameter Becke–Perdew–Wang91 functional). Three basis sets were used in both the HF and DFT methods: 6-31G(d), 6-311+G(d) and 6-311++G(3df, 2pd). Another three basis sets were only used in the HF method: cc-pVDZ, cc-pVDZ, aug-cc-pVDZ. In order to characterize the accuracy of these methods in calculations of this kind of molecules, it is necessary to choose sufficient samples. Both rigid and flexible molecules were studied. Considering confirmation of the configuration of flexible molecules is difficult and is easily affected by the environment, 26 molecules were selected, all of which were heterocyclic compounds. Their structures are detailed in Fig. 1 and the values of their experimental optical rotation are listed in Table I.

All molecules were optimized at the B3LYP/6-31G(d) level, which is reported to be good enough for the optimization of molecular structure.[42] The calculation was focused on discussing whether specific structures of the molecules influence the calculation results. The specific rotations were calculated for the sodium D-line wavelength (589.3 nm). In order to improve the accuracy, PCM and the solvent effect γ_s were considered in some calculations.[43] Calculations in this investigation have been carried out following the protocol as below: if great difference existed between computation and experimental values, priority was given to regulation of the input conformation.

All calculations were performed using the Gaussian 03 program.[44]

RESULTS AND DISCUSSION

First, the calculation results for the 26 compounds are investigated and the calculation errors discussed, and the solvent effect is analyzed. Second, an attempt is made to discuss the relationship between the OR calculation result and molecular structure.

Calculation values with the DFT and HF methods

Values of $[\alpha]_D$ which neglect the solvent effect γ_S ($\gamma_S = 1$) were obtained by using HF and DFT and different basis sets are listed in Table SI of the Supplementary material to this paper. Absolute differences between calculated and experimental $[\alpha]_D$ values are also given. The largest deviations were obtained for molecules **7**, **8**, **10**, **11**, **19** and **20**. However these results do not mean that DFT or HF method is unsuitable for these molecules, because there may be many factors which could influence the calculation.

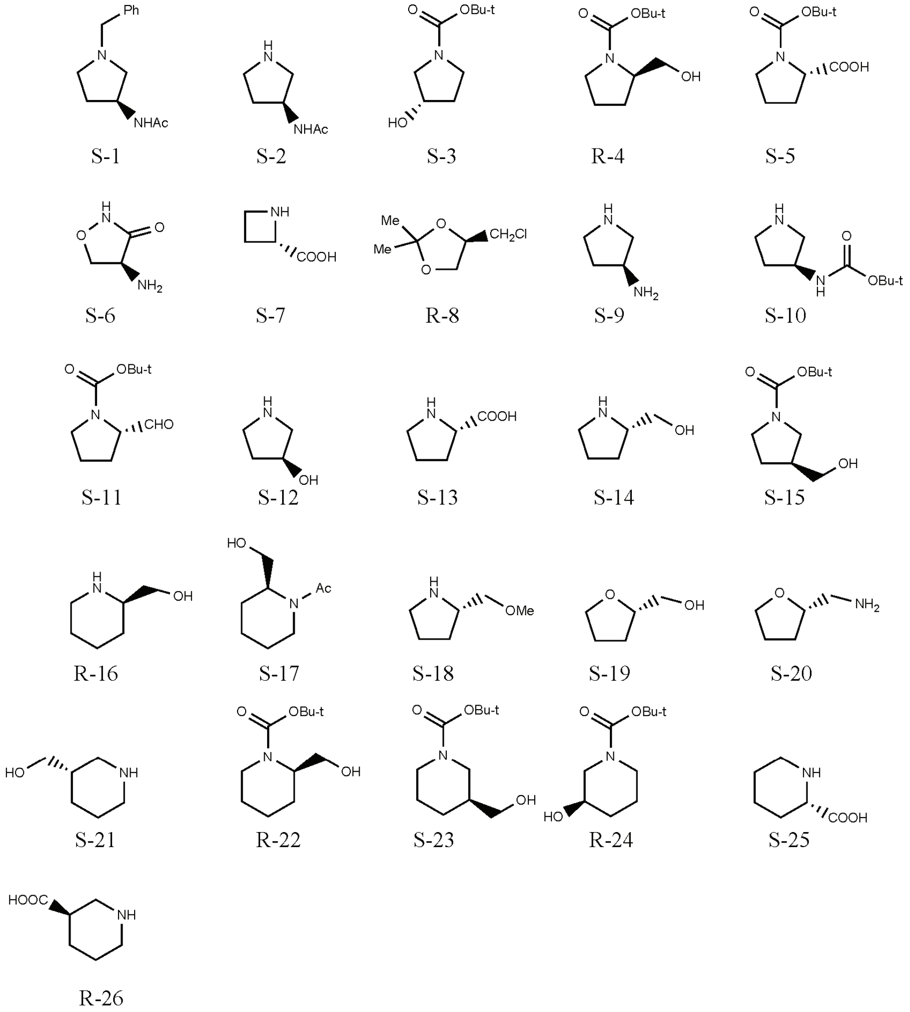

Fig. 1. Molecules **1**–**26**. The absolute configurations are those for which *ab initio* optical rotation calculations were performed (see Table SI in the Supplementary material to this paper).

TABLE I. Experimental specific rotations of compounds **1–26**

Compound	Configuration	t °C	c g (100 mL)$^{-1}$	Solvent	$[\alpha]_D$ ° dm^{-1} g^{-1} cm^3	Ref.
1	*S*	20	1.00	Chloroform	–19	20
2	*S*	20	1	Methanol	–46.5	21
3	*S*	27	1.02	Chloroform	22.75	22
4	*R*	20	3.0	Chloroform	44	23
5	*S*	24	1.40	Chloroform	–72.7	24
6	*S*	22	–	Water	–115	25
7	*S*	20	3.6	Water	–118	26
8	*R*	25	5.03	Benzene	35.9	27
9	*S*	20	–	Neat	–20	21
10	*S*	20	1	Ethanol	–21	21
11	*S*	23	1.1	Chloroform	–90.1	28
12	*S*	20	3.5	Ethanol	–6.5	21
13	*S*	25	0.83	Chloroform	–40.1	29
14	*S*	–	1.3	Chloroform	11.69	30
15	*S*	24	0.9	Chloroform	–6.5	31
16	*R*	20	2.38	Ethanol	–13.5	32
17	*S*	25	4.00	Chloroform	20.5	33
18	*S*	20	2.00	Benzene	3	34
19	*S*	20	–	Neat	2.3	21
20	*S*	20	5.05	Chloroform	12.15	35
21	*S*	21	18	–	–3.8	36
22	*R*	20	2	Chloroform	31.2	37
23	*S*	20	1	Chloroform	11.2	38
24	*R*	20	1.11	Chloroform	–10.8	39
25	*S*	22	1.0	Water	–25.9	40
26	*R*	23	–	–	–3.4	41

HF and DFT methods are compared in the calculation results listed in Table II. For molecules **2**, **4**, **5**, **13**, **15**, **16** and **24**–**26** the HF method gave accurate calculations and the range of derivations were **2**: 4.05–6.41; **4**: 0.6–2.65; **5**: 1.87–11.64; **13**: 7.42–17.9; **15**: 1.28–20.71; **16**: 4.79–35.89; **24**: 0.6–12.6; **25** :5.3–15.03 and **26**: 2.1–5.45. Conversely, for molecules **3**, **6**, **9**, **14**, **18** and **21**–**23** the DFT method had a better performance and the range of derivations were **3**: 0.92–42.93, **6**: 7.5–64.3; **9**: 1.97–83.88, **14**: 0.17–16.32, **18**: 2.66–15.97, **21**: 6.59–25.07, **22**: 0.75–24.65, **23**: 1.68–11.36. However, it should be registered that both the HF and DFT method could give acceptable computational results for molecules **2**–**6**, **9**, **13**–**16**, **18** and **21**–**26**.

Analysis of factors influencing the calculated data

Through the calculations of the OR of 26 molecules, it could be seen that the HF or DFT method were suitable for the molecules as follows: 1) which are all pyrrolidine derivatives or piperidine derivatives; 2) the chiral centers have short chains, such as –CH_2OH, –NHAc, –OH or –COOH; 3) weak electron-attracting-group, –H or –$COOC(CH_3)_3$, was linked to the nitrogen. However, bad calculation results were obtained for molecules **12**, **15** and **21**, which also belonged to this kind of molecule; hence, some other limits may exist. The differences between calculated and experimental $[\alpha]_D$ values can be attributed to many factors, such as: 1) error in the configuration; 2) solvent effect; 3) error in experimental $[\alpha]_D$ values, *etc*. Especially for the configuration, the computed optical rotation angles are very sensitive to geometry. For molecule **15**, initially neither the HF nor the DFT method could predict the sign correctly. Even for calculations with the big basis set, the correct sign was not given. This may result from errors in configuration. Hence, the input configuration was modified and then the calculation results gave the correct sign. Hence, properly optimized geometries are essential for the calculation of reliable rotation angles. Recently, Mazzeo *et al.*[45] thought that a higher level of theory may be required after geometry optimization by the commonly used DFT/B3LYP/6-31G(d). Thus, the importance of the optimized geometry can be seen.

TABLE II. Comparison of the $[\alpha]_D$ (dm^{-1} g^{-1} cm^3) obtained using the HF and DFT methods

Compd.	HF	$[\alpha]_D$	DFT	$[\alpha]_D$
1	6-311++G(3df,2pd)	20.49	B3PW91/6-311++G(3df,2pd)	17.38
2	6-311+G(d)	4.05	B3PW91/6-311++G(3df,2pd)	65.83
3	6-311++G(3df,2pd)	5.41	B3LYP/6-31G(d)	0.92
4	6-31G(d)	0.60	B3PW91/6-31G(d)	5.90
5	6-31G(d)	1.87	B3LYP/6-31G(d)	37.18
6	6-311++G(3df,2pd)	54.20	B3PW91/6-311++G(3df,2pd)	7.50
7	6-31G(d)	128.31	B3PW91/6-31G(d)	79.05
8	6-311++G(3df,2pd)	123.88	B3LYP/6-311++G(3df,2pd)	142.24
9	6-311++G(3df,2pd)	26.02	B3LYP/6-311+G(d)	1.97
10	6-31G(d)	55.28	B3LYP/6-31G(d)	67.36
11	6-31G(d)	113.16	B3PW91/6-31G(d)	118.42
12	6-31G(d)	17.50	B3PW91/6-31G(d)	38.73
13	6-311++G(3df,2pd)	7.42	B3PW91/6-31G(d)	55.15
14	6-31G(d)	2.59	B3LYP/6-31G(d)	0.17
15	6-31G(d)	9.73	B3PW91/6-31G(d)	26.62
16	6-31G(d)	4.79	B3LYP/6-31G(d)	4.95
17	6-311+G(d)	30.71	B3LYP/6-311+G(d)	34.5
18	6-31G(d)	15.47	B3PW91/6-311++G(3df,2pd)	2.66
19	6-311+G(d)	44.64	B3LYP/6-311+G(d)	52.52
20	6-31G(d)	49.70	B3PW91/6-31G(d)	74.13
21	6-31G(d)	15.63	B3LYP/6-31G(d)	14.19
22	6-31G(d)	14.06	B3LYP/6-31G(d)	0.75
23	6-311++G(3df,2pd)	4.54	B3LYP/6-311+G(d)	1.68
24	6-311+G(d)	0.60	B3PW91/6-311+G(d)	8.25
25	6-31G(d)	6.10	B3PW91/6-31G(d)	43.36
26	6-311++G(3df,2pd)	2.10	B3LYP/6-31G(d)	3.06

The studied molecules have a stable ring structure, short chains with low flexibility and an atomic electron that does not drift dramatically. The nitrogen atom may be very important for the obtained calculation results, and when the nitrogen atom was substituted by an oxygen atom in the ring, the calculation result deteriorated. For molecules **8, 19** and **20**, the derivation was about 50 to 120 degrees from the experiment value.

Consideration of the solvent effect in the calculations

Then both solvent effects γ_S and PCM were considered in a further HF calculation, the results of which are given in Table III. The effects of the addition of PCM and γ_S in the calculations of molecules **2, 3, 15** and **16** were compared. Comparison of the experimental $[\alpha]_D$ values with the calculated values for the 17 molecules is shown in Figs. 2 and 3. Comparison of solvent effect with γ_S and PCM included in the calculation is shown in Fig. 3. Inclusion of the solvent effect factor γ_S in the calculation led to a deterioration of the results for most of the molecules. PCM was also considered for some molecules (**2, 3, 15** and **16**) to improve the computation effect. However, the results differed from one another (Figs. 4 and 5). For molecules **2** and **16**, the calculations were especially improved on addition of PCM in the geometry optimization with the relative deviation decreasing from 8.7 to 1.5 % and from 34.5 to 7.8 %, respectively. However, the calculations of **3** and **15** deteriorated a little with PCM in the geometry optimization. It is clear that the calculations will be changed when PCM is introduced in the geometry optimization, but the variation is not large. Although it has been reported that PCM does not effectively contribute to the calculation.

TABLE III. Hartree–Fock method with the solvent effect included in the calculations

Compd.	γ_S	$[\alpha]_D$ / dm^{-1} g^{-1} cm^3	PCM	$[\alpha]_D$ / dm^{-1} g^{-1} cm^3
2	6-311++G(3df,2pd)	4.7	6-31G(d)	0.69
3	6-311++G(3df,2pd)	1.2	6-311++G(3df,2pd)	11.28
4	6-311++G(3df,2pd)	12.8		
5	6-31G(d)	28.9		
6	6-311++G(3df,2pd)	33.93		
9	–	–		
13	6-311++G(3df,2pd)	24.7		
14	6-31G(d)	7.8		
15	6-31G(d)	10.9	6-31G(d)	9.75
16	6-31G(d)	2.3	6-31G(d)	1.05
18	6-31G(d)	23.19		
21	–	–		
22	6-31G(d)	7.8		
23	6-311++G(3df,2pd)	2.1		
24	6-311++G(3df,2pd)	0.8		
25	6-31G(d)	16.77		
26	–	–		

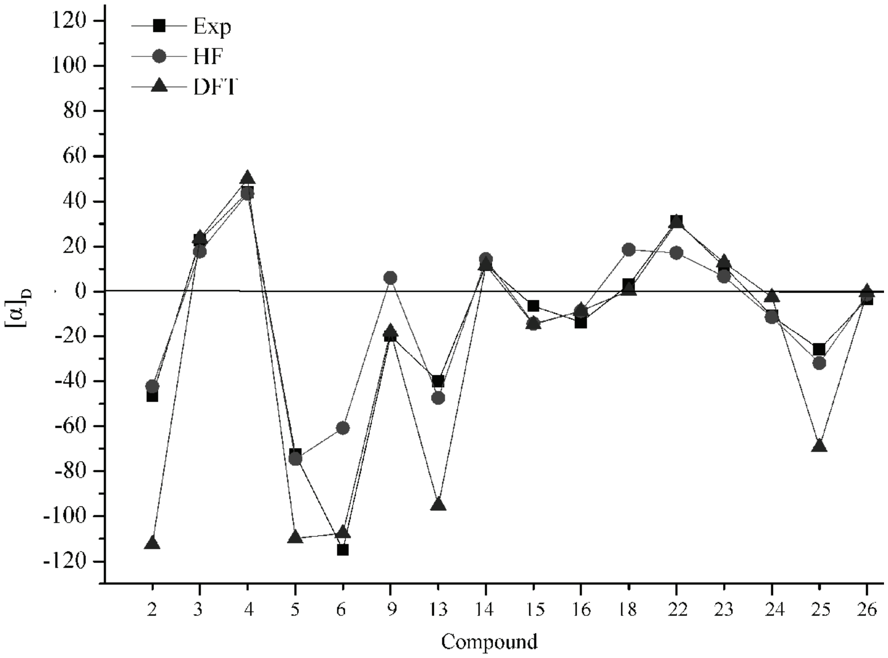

Fig. 2. Comparison of the $[\alpha]_D$ (dm^{-1} g^{-1} cm^3) of 17 molecules calculated by HF or DFT method with the experimental $[\alpha]_D$ values.

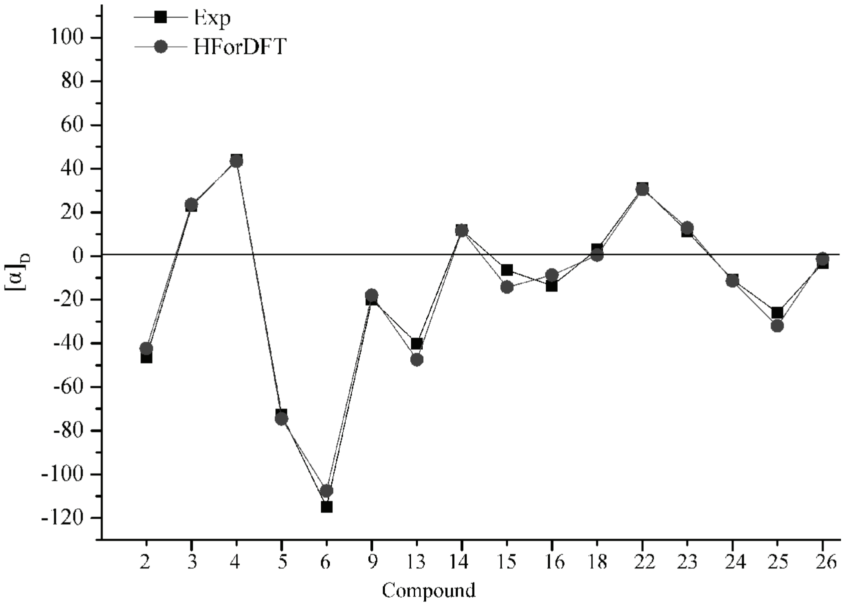

Fig. 3. Comparison of the $[\alpha]_D$ (dm^{-1} g^{-1} cm^3) calculated by the HF and DFT methods with the experimental $[\alpha]_D$ values.

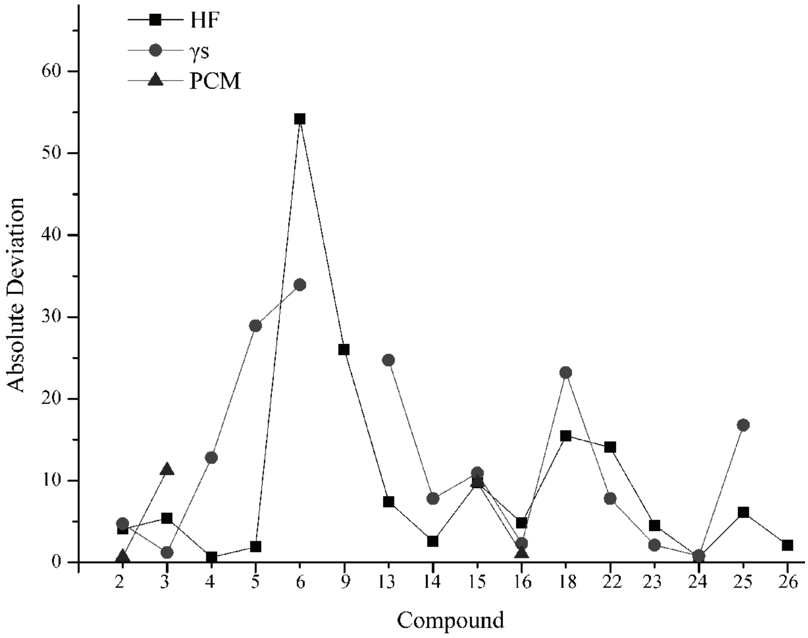

Fig. 4. Comparison of the $[\alpha]_D$ ($dm^{-1}\ g^{-1}\ cm^3$) calculated by the HF method including the solvent effect with the experimental $[\alpha]_D$ values.

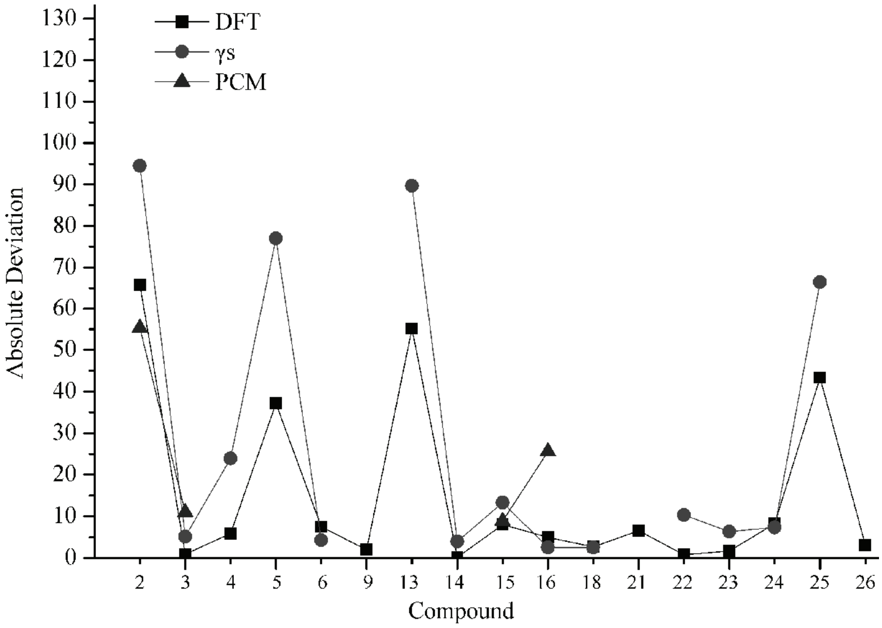

Fig. 5. Comparison of the $[\alpha]_D$ ($dm^{-1}\ g^{-1}\ cm^3$) calculated by the DFT method including the solvent effect with the experimental $[\alpha]_D$ values.

PCM is still a commonly used method to evaluate solvent effects in optical rotation calculations. In the present study, PCM worked well in some cases, such as for molecules **2, 10** and **16**, but led to a deterioration of the results in other cases. Thus, PCM is not ineffective and there may exist some rules to use this model, such as molecular structure, solvent, the property calculated, *etc*., which could produce desirable calculations, The addition of the factor γ_S to solve solvent effect may not be an effective way. It is clear that solvent effect γ_S changes the results dramatically, while inclusion of PCM in the calculation only produces a change of several degrees.

The chiral molecules in the present calculations were considered as being in the gaseous state, and the HF method gave admirable predictions. This may be because the experimental specific rotations were measured in a weak polar solvent that had little interaction with the molecules.

CONCLUSIONS

The accuracy of the HF and DFT methods was evaluated for the calculation of the optical rotation of 26 molecules. The HF method with six basis sets was employed for the calculations. In parallel, B3LYP and B3PW91 functionals with three basis sets have been performed. The result showed that for the 17 chiral molecules that have specific structures, the HF or DFT substantially gave acceptable predictions. Previous studies focused on the methods and the basis sets of the computation to improve accuracy, but the present study may prove that the structures of the molecules have a strong influence on the calculation values for an established method, or for a certain kind of molecules, some established method probably exists to give an accurate prediction. Our attention was no longer focused on the use of large basis sets or new methods to improve the accuracy of calculations for molecules that do not have similarity in their structure. For a large group of molecules, increasing the amount of computation to prove the accuracy have been widely discussed,[46] and in some cases, this is completely valid. However, for a certain kind of molecules, if an effective method can be found, it is still meaningful to decrease the amount of calculation and still obtain accurate calculation values.

Acknowledgement. The preparation of this paper was supported by the National Scientific Foundation of China (No. 81102344).

SUPPLEMENTARY MATERIAL

Comparison of $[\alpha]_D$ values obtained using HF and DFT methods with different basis sets are available electronically from http://www.shd.org.rs/JSCS/, or from the corresponding author on request.

И З В О Д

РАЧУНАЊЕ ОПТИЧКЕ РОТАЦИЈЕ: УТИЦАЈ МОЛЕКУЛСКЕ СТРУКТУРЕ

JIA YU[1], YU CAO[1], HANG SONG[1], XIANLONG WANG[2,3] и SHUN YAO[1]

[1]*Sichuan University, Chengdu 610065, China,* [2]*University of Electronic Science and Technology of China, Chengdu 610054, P. R. China и* [3]*Bryn Mawr College, Bryn Mawr, PA 19010, USA*

Ab initio Хартри–Фокова (HF) метода и теорија функције густине (DFT) су примењене за израчунавање оптичке ротације 26 једињења. Разматрани су утицај нивоа теорије и избора базних функција, као и утицај растварача на геометрију и вредност оптичке ротације. Модел континуиране поларизабилности није повећао тачност рачунања, али је дао боље резултате него γ_s. Израчунате су оптичке ротације за једињења са пето- и шесточланим прстеновима за 17 пиролидинских и пиперидинских деривата. Предвиђања на основу HF и DFT метода дају задовољавајуће резултате. Атом азота драматично утиче на резултате израчунавања, и такав атом је неопходан у молекулској структури да би се добили довољно тачни резултати. Наиме, када је атом азота у прстену замењен кисеоником, резултати израчунавања су постајали слабији.

(Примљено 5. септембра 2011)

REFERENCES

1. P. J. Stephens, F. J. Devlin, J. R. Cheeseman, M. J. Frisch, B. Mennucci, J. Tomasi, *Tetrahedron: Asymmetry* **11** (2000) 2443
2. P. L. Polavarapu, *Chirality* **14** (2002) 768
3. P. L. Polavarapu, *Mol. Phys.* **91** (1997) 551
4. P. L. Polavarapu, D. K. Chakraborty, *J. Chem. Phys.* **240** (1999) 1
5. P. J. Stephens, J. J. Pan, F. J. Devlin, J. R. Cheeseman, *J. Nat. Prod.* **71** (2008) 285
6. P. J. Stephens, F. J. Devlin, C. Villani, F. Gasparrini, S. L. Mortera, *Inorg. Chim. Acta* **361** (2008) 987
7. K. B. Wiber, Y. G. Wang, P. H. Vaccaro, J. R. Cheeseman, G. Trucks, M. J. Frischet, *J. Phys. Chem., A* **108** (2004) 32
8. B. Mennucci, M. Claps, A. Evidente, C. Rosini, *J. Org. Chem.* **72** (2007) 6680
9. K. Ruud, P. J. Stephens, F. J. Devlin, P. R. Taylor, J. R. Cheeseman, M. J. Frisch, *Chem. Phys. Lett.* **373** (2003) 606
10. P. J. Stephens, F. J Devlin, J. R. Cheeseman, M. J. Frisch, *J. Phys. Chem., A* **105** (2001) 5356
11. L. Rosenfeld, *Z. Phys.* **52** (1928) 161
12. E. U. Condon, *Rev. Mod. Phys.* **9** (1937) 432
13. E. Charney, *The Molecular Basis of Optical Activity: Optical Rotatory Dispersion and Circular Dichroism*, Wiley, New York, 1979, p. 19
14. J. A. Schellman, *Chem. Rev.* **75** (1975) 323
15. A. D. Becke, *Phys. Rev. A.* **38** (1988) 3098
16. C. Lee, W. Yang, R. G. Parr, *Phys. Rev., B* **37** (1988) 785
17. A. D. Becke, *J. Chem. Phys.* **98** (1993) 5648
18. J. F. Dobson, G. Vignale, M. P. Das, *Electronic Density Functional Theory: Recent Progress and New Directions*, Plenum, New York, 1998, p. 227
19. J. P. Perdew, *in Electronic Structure of Solids*, Akademie Verlag, Berlin, 1991, p. 11
20. T. Rosen, D. T. W. Chu, I. M. Lico, P. B. Fernandes, L. Shen, S. Borodkin, A. G. Pernet, *J. Med. Chem.* **31** (1988) 1586

21. *Alfa Aesar A Johnson Matthey Company*, Alfa Aesar reagent manual, 2008
22. B. D. Harris, K. L. Bhat, M. M. Joullié, *Synth. Commun.* **16** (1986) 1815
23. A. Carocci, G. Lentini, A. Catalano, M. M. Cavalluzzi, C. Bruno, M. Muraglia, N. A. Colabufo, N. Galeotti, F. Corbo, R. Matucci, C. Ghelardini, C. Franchini, *ChemMedChem* **5** (2010) 696
24. R. Conrow, P. S. Raymond, *J. Org. Chem.* **51** (1986) 938
25. C. H. Stammer, A. N. Wilson, F. W. Holly, K. Folkers, *J. Am. Chem. Soc.* **77** (1955) 2346
26. F. Couty, G. Evano, M. V. Sanchez, G. Bouzas, *J. Org. Chem.* **70** (2005) 9028
27. Y. Kawakami, T. Asai, K. Umeyama, Y. Yamashita, *J. Org. Chem.* **47** (1982) 3581
28. X. N. Song, Z. J. Yao, *Tetrahedron Asymm.* **66** (2010) 2589
29. N. Dai, F. A. Etzkorn, *J. Am. Chem. Soc.* **131** (2009) 13728
30. J. Katarzyńska, A. Mazur, M. Bilska, E. Adamek, M. Zimecki, S. Jankowski, J. Zabrocki, *J. Pept. Sci.* **14** (2008) 1283
31. R. N. Loy, E. N. Jacobsen, *J. Am. Chem. Soc.* **131** (2009) 2786
32. M. Kawaguchi, O. Hayashi, N. Sakai, M. Hamada, Y. Yamamoto, J. Oda, *Agric. Biol. Chem.* **50** (1986) 3107
33. E. J. Toone, J. B. Jones, *Can. J. Chem.* **65** (1987) 2722
34. D. Enders, P. Fey, H. Kipphardt, *Org. Prep. Proced. Int.* **17** (1985) 1
35. D. M. Musatow, V. S. Kublitskii, O. R. Malyshev, D. V. Kurilov, M. G. Vinogradov, *Russ. J. Org. Chem.* **43** (2007) 1813
36. P. Magnus, L. S. Thurston, *J. Org. Chem.* **56** (1991) 1166
37. M. Calmes, F. O. Escale, M. Rolland, J. Martinez, *Tetrahedron Asymmetry* **14** (2003) 1685
38. T. Kikuchi, M. R. Zhang, N. Ikota, K. Fukushi, T. Okamura, K. Suzuki, Y. Arano, T. Irie, *J. Med. Chem.* **48** (2005) 2577
39. M. Kamame, S. Yoshifuji, H. Sashida, *Chem. Pharm. Bull.* **56** (2008) 1310
40. G. H. P. Roos, K. A. Dastlik, *Synth. Commun.* **33** (2003) 2197
41. A. M. Akkerman, D. K. Dejonch, H. Veldstra, *Recl. Trav. Chim. Pays-Bas* **70** (1951) 899
42. D. C. Young, *Computational Chemistry: A Practical Guide for Applying Techniques to Real World Problems*, Wiley, New York, 2001, p. 206
43. B. Mennucci, J. Tomasi, R. Cammi, J. R. Cheeseman, M. J. Frisch, F. J. Devlin, S. Gabriel, P. J. Stephens, *J. Phys. Chem., A* **106** (2002) 6102
44. *Gaussian 03*, Revision A.1, Gaussian, Inc., Pittsburgh, PA, 2003
45. G. Mazzeo, E. Giorgio, R. Zanasi, N. Berova, C. Rosini, *J. Org. Chem.* **75** (2010) 4600
46. C. T. Campos, F. E. Jorge, T. P. Silva, M. R. Coppo, *Chem. Phys. Lett.* **494** (2010) 170.

JSCS@tmf.bg.ac.rs • www.shd.org.rs/JSCS

J. Serb. Chem. Soc. 77 (7) S106–S109 (2012) *Supplementary material*

SUPPLEMENTARY MATERIAL TO

Calculations of optical rotation: Influence of molecular structure

JIA YU[1], YU CAO[1], HANG SONG[1], XIANLONG WANG[2,3] and SHUN YAO[1]*

[1]*School of Chemical Engineering, Sichuan University, Chengdu 610065,* [2]*School of Life Science and Technology, University of Electronic Science and Technology of China, Chengdu 610054, P. R. China and* [3]*Department of Chemistry, Bryn Mawr College, 101 N Merion Ave, Bryn Mawr, PA 19010, USA*

J. Serb. Chem. Soc. 77 (7) (2012) 887–898

TABLE SI. Comparison of $[\alpha]_D$ (dm^{-1} g^{-1} cm^3) obtained using HF and DFT with different basis sets

Compd.	Configuration	Method	$[\alpha]_{cal}$	Expt.
1	*S*			–19
		HF/6-311++G(3df,2pd)	1.49	
		HF/aug-cc-pVDZ	–0.80	
		DFT/B3LYP/6-31G(d)	2.77	
		DFT/B3PW91/6-311++G(3df,2pd)	–1.62	
2	*S*			–46.5
		HF/6-311+G(d)	–42.45	
		HF/aug-cc-pVDZ	–43.12	
		DFT/B3LYP/6-311++G(3df,2pd)	–114.33	
		DFT/B3PW91/6-311++G(3df,2pd)	–112.33	
3	*S*			22.75
		HF/6-311++G(3df,2pd)	17.61	
		HF/aug-cc-pVDZ	14.56	
		DFT/B3LYP/6-311++G(3df,2pd)	20.48	
		DFT/B3PW91/6-311++G(3df,2pd)	23.67	
4	*R*			44
		HF/6-31G(d)	43.40	
		HF/aug-cc-pVDZ	42.13	
		DFT/B3LYP/6-31G(d)	49.90	
		DFT/B3PW91/6-31G(d)	54.71	
5	*S*			–72.7
		HF/6-31G(d)	–74.57	
		HF/cc-pVDZ	–79.09	
		DFT/B3LYP/6-31G(d)	–109.88	
		DFT/B3PW91/6-31G(d)	–111.71	

---

*Corresponding author. E-mail: cusack@scu.edu.cn

TABLE SI. Continued

Compd.	Conf.	Method	$[\alpha]_{cal}$	Expt.
6	*S*			–115
		HF/6-311++G(3df,2pd)	–60.82	
		HF/cc-pVTZ	–79.11	
		DFT/B3LYP/6-311+G(d)	–106.84	
		DFT/B3PW91/6-311++G(3df,2pd)	–107.50	
7	*S*			–118
		HF/6-31G(d)	10.30	
		HF/cc-pVDZ	19.91	
		DFT/B3LYP/6-31G(d)	–38.95	
		DFT/B3PW91/6-31G(d)	–31.04	
8	*R*			35.9
		HF/6-311++G(3df,2pd)	–87.98	
		HF/cc-pVDZ	–85.56	
		DFT/B3LYP/6-311++G(3df,2pd)	–106.34	
		DFT/B3PW91/6-311++G(3df,2pd)	–109.52	
9	*S*			–20
		HF/6-311++G(3df,2pd)	6.02	
		HF/aug-cc-pVDZ	3.70	
		DFT/B3LYP/6-311+G(d)	–18.03	
		DFT/B3PW91/6-311+G(d)	–1.16	
10	*S*			–21
		HF/6-31G(d)	–45.94	
		HF/cc-pVDZ	–49.62	
		DFT/B3LYP/6-311++G(3df,2pd)	–86.06	
		DFT/B3PW91/6-31G(d)	–73.19	
11	*S*			–90.1
		HF/6-31G(d)	23.06	
		HF/cc-pVDZ	40.22	
		DFT/B3LYP/6-31G(d)	28.37	
		DFT/B3PW91/6-31G(d)	28.32	
12	*S*			–6.5
		HF/6-31G(d)	–24.00	
		HF/cc-pVDZ	–23.87	
		DFT/B3LYP/6-31G(d)	–49.64	
		DFT/B3PW91/6-31G(d)	–45.23	

TABLE SI. Continued

Compd.	Conf.	Method	$[\alpha]_{cal}$	Expt.
13	*S*			–40.1
		HF/6-311++G(3df,2pd)	–47.52	
		HF/cc-pVTZ	–38.07	
		DFT/B3LYP/6-31G(d)	–100.51	
		DFT/B3PW91/6-31G(d)	–95.25	
14	*S*			11.69
		HF/6-31G(d)	14.28	
		HF/cc-pVTZ	11.06	
		DFT/B3LYP/6-31G(d)	11.52	
		DFT/B3PW91/6-31G(d)	13.56	
15	*S*			–6.5
		HF/6-31G(d)	–14.21	
		HF/cc-pVTZ	–3.93	
		DFT/B3LYP		
		DFT/B3LYP/6-31G(d)	–14.53	
		DFT/B3PW91/6-31G(d)	–15.34	
16	*R*			–13.5
		HF/6-31G(d)	–8.71	
		HF/cc-pVDZ	6.14	
		DFT/B3LYP/6-31G(d)	–8.55	
		DFT/B3PW91/6-31G(d)	–5.35	
17	*S*			20.5
		HF/6-311+G(d)	–10.21	
		HF/cc-pVTZ	–10.21	
		DFT/B3LYP/6-311+G(d)	–14.00	
		DFT/B3PW91/6-311+G(d)	–16.06	
18	*S*			3
		HF/6-311++G(3df,2pd)	–13.45	
		HF/cc-pVDZ	–2.51	
		DFT/B3LYP/6-311++G(3df,2pd)	0.27	
		DFT/B3PW91/6-311++G(3df,2pd)	0.34	
19	*S*			2.3
		HF/6-311+G(d)	46.94	
		HF/cc-pVTZ	58.03	
		DFT/B3LYP/6-311+G(d)	54.82	
		DFT/B3PW91/6-311+G(d)	55.75	

TABLE SI. Continued

Compd.	Conf.	Method	$[\alpha]_{cal}$	Expt.
20	*S*			12.15
		HF/6-31G(d)	61.85	
		HF/cc-pVDZ	51.74	
		DFT/B3LYP/6-31G(d)	87.43	
		DFT/B3PW91/6-31G(d)	86.28	
21	*S*			–3.8
		HF/6-31G(d)	–19.43	
		HF/cc-pVDZ	–26.99	
		DFT/B3LYP/6-31G(d)	–10.39	
		DFT/B3PW91/6-31G(d)	–14.51	
22	*R*			31.2
		HF/6-31G(d)	17.14	
		HF/cc-pVTZ	–421.52	
		DFT/B3LYP/6-31G(d)	32.06	
		DFT/B3PW91/6-31G(d)	30.45	
23	*S*			11.2
		HF/6-311++G(3df,2pd)	6.66	
		HF/cc-pVDZ	27.88	
		DFT/B3LYP/6-311+G(d)	12.88	
		DFT/B3PW91/6-311+G(d)	14.05	
24	*R*			–10.8
		HF/6-311+G(d)	–11.4	
		HF/cc-pVTZ	–7.7	
		DFT/B3LYP/6-311+G(d)	–2.29	
		DFT/B3PW91/6-311+G(d)	–2.55	
25	*S*			–26.7
		HF/6-31G(d)	–32.00	
		HF/cc-pVDZ	–23,13	
		DFT/B3LYP/6-31G(d)	–71.08	
		DFT/B3PW91/6-31G(d)	–69.26	
26	*R*			–3.4
		HF/6-311++G(3df,2pd)	–1.30	
		HF/aug-cc-pVDZ	–1.72	
		DFT/B3LYP/6-31G(d)	–0.34	
		DFT/B3PW91/6-31G(d)	–0.51	

Journal of the Serbian Chemical Society

JSCS-info@shd.org.rs • www.shd.org.rs/JSCS

J. Serb. Chem. Soc. 77 (7) 899–910 (2012)
JSCS–4319

UDC 544.6:543+546.817+
546.6.076.32:543.552:543.554
Original scientific paper

Nanomolar determination of Pb(II) ions using a selective templated electrode

MOHAMMAD MAZLOUM-ARDAKANI[1]*, MOHAMMAD KAZEM AMINI[2], MARZIEH DEHGHAN[3], ELHAM KORDI[3] and MOHAMMAD ALI SHEIKH-MOHSENI[1]

[1]*Department of Chemistry, Faculty of Science, Yazd University, Yazd, I. R. Iran,* [2]*Department of Chemistry, University of Isfahan, Isfahan, I. R. Iran and* [3]*Department of Chemistry, Payam Noor University, Ardakan Center, Ardakan, I. R. Iran*

(Received 30 August, revised 5 December 2011)

Abstract: A polypyrrole-modified electrode, prepared by electro-polymerization of pyrrole in the presence of methyl red as a dopant, was templated with respect to Pb^{2+} and applied for the potentiometric and voltammetric detection of this ion. The templating process improved the analytical response characteristics of the electrode, especially its selectivity with respect to Pb^{2+}. The improvement depended on both the incorporated ligand (dopant) and the templating process, with the latter being more vital. The potentiometric response of the electrode was linear within the Pb^{2+} concentration range of 2.0×10^{-6} to 5.0×10^{-2} M with a near-Nernstian slope of 28.6 mV dec^{-1} and a detection limit of 7.0×10^{-7} M. The electrode was also used for pre-concentration differential pulse anodic stripping voltammetry (DPASV) and the results showed that the peak currents for the incorporated lead species were dependent on the metal ion concentration in the range 1.0×10^{-8} to 1.0×10^{-3} M. The detection limit of the DPASV method was 3.5×10^{-9} M. The selectivity of the electrode with respect to some transition metal ions was investigated. The modified-templated electrode was used for the successful assay of lead in two standard reference material samples.

Keywords: templated polymers; lead; polypyrrole; potentiometry; voltammetry; nanomolar.

INTRODUCTION

Conducting polymers are very attractive due to their potential use as electrochromic devices, capacitors, gas separation membranes, anti-static membranes, catalysts, electromagnetic shielding devices and selective sensors.[1] The most important property of conducting polymers is their doping/imprinting ability with

---

* Corresponding author. E-mail: mazloum@yazduni.ac.ir
doi: 10.2298/JSC110830210M

various molecular and ionic species. Therefore, various recognition elements can be introduced into these polymers during the polymerization step.[2,3] Conducting polymers with specific affinities can be prepared in the presence of template molecules by chemical derivatization of the polymer with various compounds, or by doping the polymer with specific ligands.[4,5] Among different conducting polymers, polypyrrole (PPy) has found attractive applications as one of the fundamental building materials in the design of various analytical tools because of its good stability, facile synthesis, higher conductivity and versatility.[6,7] Following Dall'Olio *et al*. who initially deposited PPy by electrochemical polymerization of pyrrole from dilute sulfuric acid solution[8] and Diaz *et al*. for electrochemically synthesizing the first free-standing PPy films,[9] there has been an increasing interest in the application of electro-polymerized PPy for the development of various electrochemical sensors,[10] including voltammetric[11,12] and potentiometric[13–15] sensors.

The increasing presence of toxic pollutants in the environment has been perceived as a major problem in the last decades.[16] Modern medicine confirms that lead and its compounds are hazardous to people's nerve, blood, digestion, cardiovascular and other endocrine systems. Furthermore, unlike organic compounds, lead species are non-biodegradable that facilely accumulate in soils and waters. Pb^{2+} is one of the most common ions assayed in environmental samples, and there is an increasing interest in its determination because of its toxicological effects.[17]

A wide range of analytical techniques are used for the detection of Pb^{2+} in various samples, including atomic absorption spectrometry (AAS), atomic emission spectroscopy (AES), inductively coupled plasma mass spectrometry (ICP–MS)[18–21] and reflectance spectrometry.[22] These techniques can offer good limits of detection and wide linear ranges, but are very expensive and require adequate expertise. Therefore, the analysis is often limited to laboratory level only. The need for rapid and in-field analysis of trace heavy metal ions is of tremendous interest in environmental applications. The electrochemical methods for determination of Pb^{2+} require instrumentation of relatively low cost and low maintenance.[23–26] Using the differential pulse anodic stripping voltammetry (DPASV) technique, very low detection limits for many metal ions with wide linear ranges can be obtained.[27,28]

Among different modified electrodes and electrochemical sensors,[29,30] the technique of templating/imprinting polymers has shown considerable promise as a method of choice for preparing materials with the capability for recognition of molecules and ions.[31] Such polymers, besides their ease of production, low cost and stability in harsh environments, show high affinity and selectivity to the target species.[32]

In this study, the templating approach was used to develop a templated PPy-based sensor for potentiometric and voltammetric determination of Pb^{2+}. The method is based on the application of successive potential steps to the electropolymerized Methyl Red/PPy film (MR/PPy) in $Pb(NO_3)_2$ as the only electrolyte present in solution. During these steps, the membrane is templated with respect to Pb^{2+}. The resulting sensor exhibited a noticeable enhancement in the potentiometric and voltammetric response characteristics, extending the linear dynamic range and lowering the detection limit.

EXPERIMENTAL

Materials

Methyl Red (MR), potassium nitrate (KNO_3), lead (II) nitrate ($Pb(NO_3)_2$) and nitrate salts of all other cations were purchased from Merck and used without further purification. Pyrrole monomer (Fluka) was purified by distillation under reduced pressure and stored at a low temperature protected from light. The pH adjustment was made with dilute nitric acid and sodium hydroxide solutions as appropriate. Doubly distilled water was used throughout.

Apparatus

The electropolymerization and all the voltammetric measurements were performed using a potentiostat/galvanostat Autolab (model PGSTAT 302 N). A conventional three electrode cell, including a glassy carbon (GC) disk electrode of 2 mm diameter (Azar Electrode, Uromieh, Iran) modified with MR/PPy film (MR/PPy/GC) as the working electrode, a saturated double salt bridge $Hg/Hg_2Cl_2/KCl$ (SCE) from Metrohm as the reference electrode and a platinum wire (Metrohm) as the counter electrode, was used in the voltammetric experiments. The potential and pH measurements were performed on a pH/mV meter (Metrohm model 691). The MR/PPy/GC and SCE were used as indicator and references electrodes, respectively in the potentiometric measurements. All the potentials are quoted *versus* the reference electrode (SCE).

PPy Film electrode preparation

The GC disk working electrodes were polished with 0.3 µm alumina slurry and cleaned thoroughly with water. The electro-polymerization of PPy was performed from a deoxygenated aqueous solution containing 0.1 M pyrrole and 1.0×10^{-4} M Methyl Red on the polished GC surface using the potentiostatic method by application of a potential of +0.75 V for the desired period under an atmosphere of pure argon.

After the electro-polymerization, the electrode was washed with water and then subjected to several alternative reduction/oxidation steps in a solution containing 1.0×10^{-3} M $Pb(NO_3)_2$. The reduction and oxidation steps were performed potentiostatically at –0.4 and 0.5 V, respectively, each for a period of 5 min. The overall process was repeated three times, followed with an oxidation step for a period of 10 min. The prepared MR/PPy/GC electrode was then directly used for voltammetric measurement or conditioned in 1.0×10^{-3} M $Pb(NO_3)_2$ solution for at least 19 h prior to its use as the indicator electrodes for potentiometric measurements.

Potentiometric measurements

The MR/PPy/GC was used as the indicator electrode in conjunction with an SCE reference electrode. The analytical performance of the electrode was investigated by measuring its potential response in Pb^{2+} solutions, freshly prepared in the concentration range of 1.0×10^{-9} to 0.10 M by serial dilution of a stock 0.10 M solution of this salt. The solution was stirred and the potential was recorded when it attained a stable value. The data were plotted as the observed potential *vs*. the logarithm of the Pb^{2+} activity to construct a calibration plot.

DPASV Measurements

The voltammetric measurements were carried out using the modified MR/PPy/GC as the working electrode together with the reference and counter electrodes. The pre-concentration step was carried out by dipping the electrodes in the sample solution and applying a potential of –0.7 V *vs*. SCE for a period of 200 s. Then the electrode was washed with water and transferred to a cell containing 0.2 M potassium nitrate electrolyte solution at pH 2.0. The DPASV was performed in the potential range of –0.9 to –0.1 V at a scan rate of 100 mV s^{-1}.

Sample pretreatment

Two standard reference materials (SY-4, a CANMET standard rock and SGHM-2 (3484-86), an aluminous silicate standard from Institute of Geochemistry SB RAS, Irkutsk) were used for real sample analysis. The following procedure was used for pretreatment of these samples. To 0.3 g of each sample was added 25 mL of 2.0 M nitric acid and the resulting solution was heated for 3 h at 60 °C. Then the solution was filtered through a filter paper, neutralized with sodium hydroxide solution to pH 5.6 and after dilution to 100 mL, used for the voltammetric measurements.

RESULTS AND DISCUSSION

Electropolymerization of pyrrole and the templating process

A PPy film with incorporated Methyl Red was formed on the surface of a GC electrode from an aqueous solution containing 0.10 M pyrrole monomer and 1.0×10^{-4} M Methyl Red by using a constant potential of 0.75 V. During the electropolymerization, pyrrole was first oxidized to give the corresponding radical cations, followed by a coupling reaction to give oligomers and finally polymer on the electrode surface.

After the electro-polymerization step, the electrode was washed with water and transferred to a cell containing 1.0×10^{-3} M $Pb(NO_3)_2$, the only electrolyte present in solution, for the templating process. Then the electrode was subjected to three redox potential steps in this solution, as described in the experimental section. During these steps, the polymer backbone underwent successive reduction/oxidation reactions, resulting in generation of neutral/positively charged PPy chains, accordingly. During the reduction step, the polymer backbone became neutral, making the MR/PPy membrane negatively charged. Under this condition, Pb^{2+} present in solution was incorporated into the polymer. When the polymer was re-oxidized, the MR/PPy film became neutral and the incorporated metal species were expelled from the membrane. The templating process was found to be essential for obtaining high selectivity and better response characteristics in both potentiometric and voltammetric measurements.

Optimizing the electropolymerization and pre-concentration conditions

The voltammetric response characteristics of the modified electrodes strongly depended on the electropolymerization conditions. Therefore, the DPASV peak height was used as the criterion for selecting the optimum operating conditions in the electropolymerization process. The influence of various electropolymerization parameters and conditions, including the pyrrole and Methyl Red concentrations, the pH of the solution and polymerization charge or membrane thickness, were investigated.

The DPASV peak current depended on both the pyrrole and Methyl Red concentrations. Maximum response was observed for 0.10 M pyrrole and 1.0×10^{-4} M Methyl Red concentrations. The influence of pH of the electro-polymerization solution on the DPASV signal is shown in Fig. 1. As can be seen, the peak current increased with increasing pH of the solution up to 5.7 and then decreased slowly for higher pH values. Methyl Red is protonated at low pH values but is in anionic form at pH values higher than 5 (the pK_a of MR is 5.1), therefore MR can be incorporated into the PPy because of its anionic charge and the DPASV signal increased at pH values higher than 5. Since the pH of the polymerization solution containing 0.10 M pyrrole and 1.0×10^{-4} M MR was 5.6, there was no need to adjusting the solution pH.

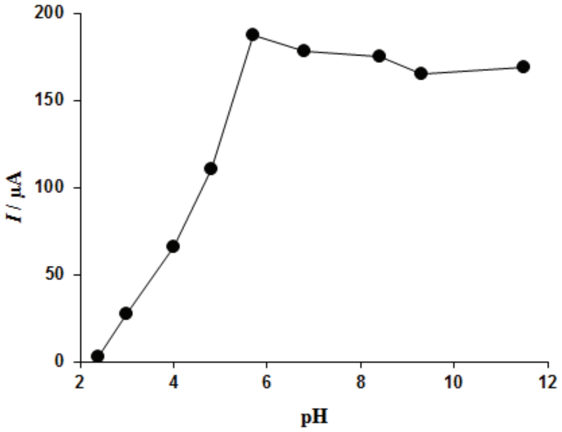

Fig. 1. Influence of pH of electro-polymerization solution on the DPASV signal.

The voltammetric response of the MR/PPy film electrode, expressed as the DPASV peak height, was influenced by the film thickness, which can be controlled by the polymerization time. It was found that maximum DPASV signal was observed when the polymerization time was 30 s. At films thinner than this (shorter polymerization time), the DPASV peak current decreased sharply, because there is not enough binding sites on the electrode for interaction with Pb^{2+}. Thicker films (longer polymerization time) increase the electrode resistance and pose mass transfer limitations to Pb^{2+}, during the accumulation and stripping steps, and thus, lower the sensitivity of the measurement.

The influence of the pre-concentration conditions was also investigated by varying the pH, applied potential and pre-concentration time for a 1.0×10^{-5} M Pb^{2+} solution (Fig. 2). The effect of pH on the pre-concentration of Pb^{2+} into the modified electrode was investigated by varying pH between 1.5 and 13 and measuring the DPASV signal. The results showed that the peak current was almost independent of pH in the range of 5.0–9.1, as shown in Fig. 2A. Interference from H^+ due to protonation of the coordination sites of the membrane at low pH values and the formation of insoluble species at high pH values are possible reasons for lower DPASV signal in these regions.

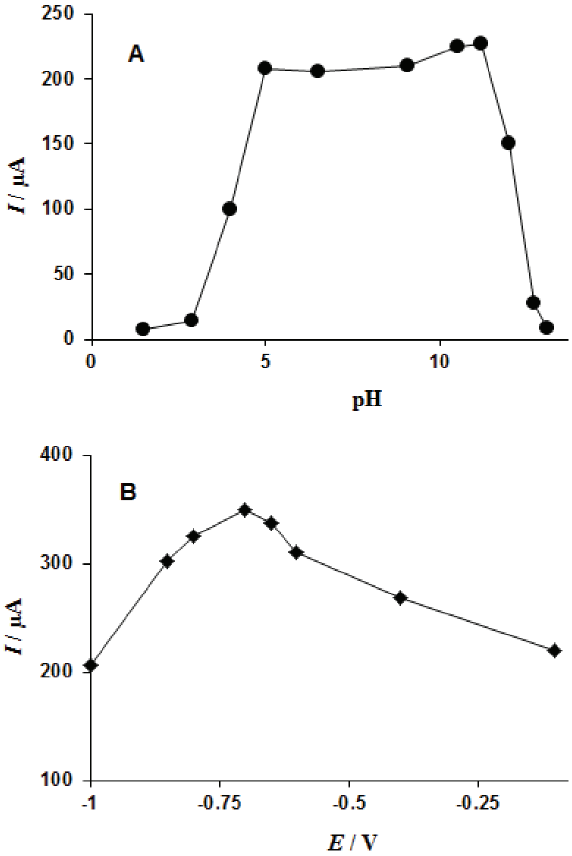

Fig. 2. Influence of the pre-concentration conditions on the DPASV signal; A) pH of the pre-concentration solution and B) applied pre-concentration potential.

Pre-concentration of lead species into the MR/PPy film strongly depended on the applied potential, as shown in Fig. 2B. The maximum DPASV signal was observed at an applied pre-concentration potential of –0.7 V. The reason for the lower efficiency at potentials more positive than –0.7 V is the incomplete reduction of PPy and consequently reduced pre-concentration of lead species into the membrane. Lower efficiency at potentials more negative than –0.7 V can be related to reduction of the azo group in Methyl Red and cleavage of the N=N bond of this compound.[33] The pre-concentration time depended on the concentration of Pb^{2+}, however, a 200 s period was determined to be sufficient for all the studied concentrations and no further improvement could be observed after this period.

Voltammetric response of the electrode

Voltammetric calibration. The modified-templated electrode was used for pre-concentration/DPASV measurement of Pb^{2+}. At the optimized conditions, the DPASV measurements were performed by transferring the electrode, after pre-concentration, into a cell containing 0.20 M potassium nitrate adjusted to pH 2.0, and scanning the potential from –0.9 to –0.1 V using a pulse amplitude of 50 mV and a scan rate of 100 mV s^{-1}. The DPASV peak current was dependent on log of the Pb^{2+} concentration over a wide concentration range of 1.0×10^{-8} to 1.0×10^{-3} M with a slope of 32.54 µA/ $\log c_{Pb^{2+}}$ (mol/l) and $R^2 = 0.992$, as shown by the calibration plot in Fig. 3. The *RSD* of DPASV for 5.0×10^{-7} M Pb^{2+} peak current was 5.1 % ($n = 7$) and the detection limit was determined to be 3.5×10^{-9} M Pb^{2+}.

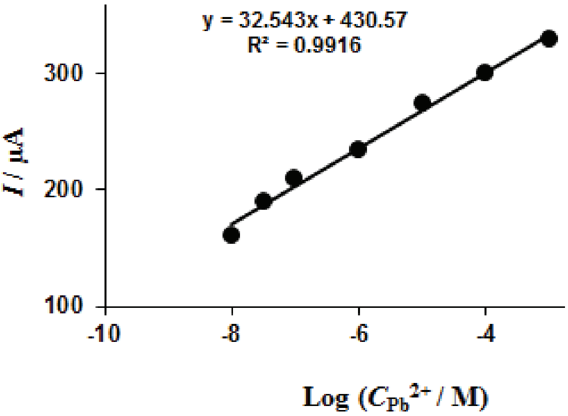

Fig. 3. Voltammetric calibration curve for the modified-templated electrode under the optimum conditions.

Interference study

Interference studies of several cationic species on the DPASV of Pb^{2+} were performed in mixture experiments. Pre-concentration was performed in solutions containing 1.0×10^{-5} M Pb^{2+} and different concentrations of interfering ions at a potential of –0.7 V for a period of 200 s and then DPASV was performed as usual. The results indicated that most of the ions did not interfere significantly; however, interference of Cu^{2+} was considerable.

Potentiometric response of the electrode

Before the potentiometric measurements, the modified-templated electrode was conditioned in 1.0×10^{-3} M lead(II) nitrate solution. After conditioning for approximately 19 h, a stable Nernstian response was obtained for Pb^{2+} solutions of various concentrations. To test the performance of the electrode characteristics, various operation parameters, such as working concentration range, selectivity, and the effect pH were investigated.

Effect of pH

The effect of the pH of the test solution on the potentiometric response of the templated electrode was examined in a 1.0×10^{-5} M Pb^{2+} solution adjusted to different pH values with dilute nitric acid or sodium hydroxide solutions. As illustrated in Fig. 4, the electrode can be used in the pH range of 5.2–10. A substantial increasing trend in the potential was observed at pH < 5.2, which may be due to participation of H^+ in the ion exchange processes on the polymer/solution interface.[34] The potential drop at high pH values (>10) may be because of precipitation of Pb^{2+}.

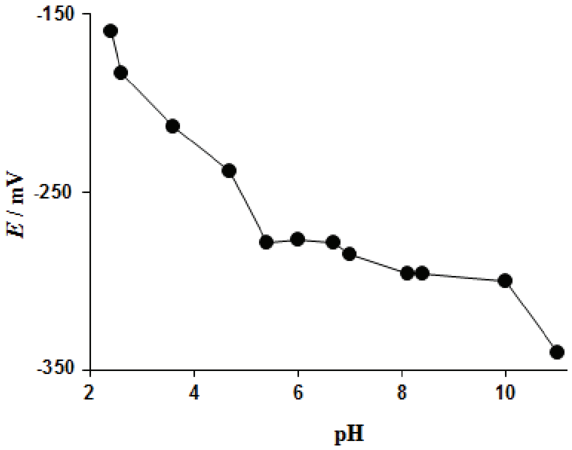

Fig. 4. Effect of the pH of the test solution on the potentiometric response of the templated electrode at 1.0×10^{-5} M Pb^{2+} solution.

Potentiometric calibration

The potentiometric response of the electrode was investigated in solutions of different Pb^{2+} concentrations at pH 5.6. The calibration plot of the electrode is shown in Fig. 5, indicating a linear response over the concentration range of 2.0×10^{-6} to 5.0×10^{-2} M with a Nernstian slope of 28.6 mV per decade of Pb^{2+} activity. The detection limit was 7.0×10^{-7} M Pb^{2+}. Comparison between the potentiometric response of the templated and untemplated electrodes, indicated a much improved sensitivity, dynamic range and detection limit for the templated electrode.

Potentiometric selectivity coefficient

The potentiometric selectivity of the templated and untemplated modified electrodes were studied by the separate solution method (SSM), according to IUPAC recommendations,[35] using 1.0×10^{-3} M Pb^{2+} and interfering ions. From the selectivity coefficients summarized in Table I, it is obvious that most of the metal ions examined on the templated electrode did not show obvious interferences in the determination of Pb^{2+}. However, copper ion showed a significant interference. The untemplated electrode showed lower selectivity for Pb^{2+} with respect to all of these ions. According to the results of Table I, the templating step has an important role in generating recognition sites for Pb^{2+}.

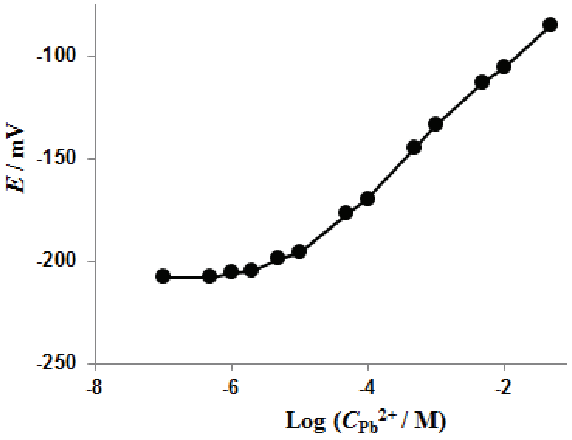

Fig. 5. Potentiometric calibration curve of the modified-templated electrode at pH 5.6.

TABLE I. Selectivity coefficients ($\log K_{\mathrm{Pb}^{2+},\mathrm{M}^{n+}}$) of the modified electrode for Pb^{2+} with respect to some other ions

Ion	Before templating	After templating
Cr^{3+}	–1.79	–2.27
Fe^{2+}	–3.16	–4.00
Ag^{+}	–3.76	–3.80
K^{+}	–1.37	–2.71
Cd^{2+}	–0.31	–3.74
Mg^{2+}	0.338	–0.135
Ca^{2+}	1.86	–0.96
Na^{+}	0.10	–0.72
Mn^{2+}	0.45	–0.24

Analytical application

The templated electrode was applied for the determination of the lead content in two standard ore samples by the voltammetric method and the results were compared with the certified concentration of lead in these samples (Table II). The samples were prepared as described in the Experimental section. The results show that, in spite of the presence of high concentrations of different components, including alkaline and alkaline earths, and significant concentrations of various transitions elements in these samples, there was a good agreement between the certified and measured concentrations of lead, indicating the capability of the modified electrode for the determination of lead in real samples.

TABLE II. Application of the electrode for the determination of the lead content (μg g^{-1}) of standard ore samples by DPASV, comparison between the determined and certified concentrations

Sample	Certified value	Found value (*n* = 4)
SY-4	10±1	10.9±1.0
3484-86 (SGHM-2)	$1.6\times10^{-3}\pm3.0\times10^{-4}$	$1.8\times10^{-3}\pm2.9\times10^{-4}$

CONCLUSIONS

The electrode modified with MR/PPy was studied as a potentiometric and voltammetric sensor for Pb^{2+}. The results indicated that the templating process performed by applying a potential step program to the electropolymerized MR/PPy membrane in a solution containing $Pb(NO_3)_2$ as the electrolyte improved the selectivity of the electrodes toward the Pb^{2+} ion. This process seems to rearrange the binding sites of both the PPy and the ligand, and therefore, generates chemical recognition elements in the modified polymer film. The proposed sensor was successfully applied for the measurement of Pb^{2+} using potentiometry in the range of 2.0×10^{-6} to 5.0×10^{-2} M and DPASV in the range of 1.0×10^{-8} to 1.0×10^{-3} M, with improved selectivity compared to the untemplated electrodes. It seems that by judicious selection of the chelating ligand and change of the polymerization and templating factors, it may be possible to induce better selectivity for Pb^{2+} and to extend this approach to other cationic species.

Acknowledgment. The authors would like to thank Payam Noor University Research Council (center of Ardakan), Yazd University Research Council, IUT Research Council and Excellence in Sensors for financial support of this research.

ИЗВОД

ОДРЕЂИВАЊЕ Pb(II) ЈОНА У НАНОМОЛАРНОМ РАСТВОРУ ПОМОЋУ ПОЛИМЕРНЕ ЕЛЕКТРОДЕ СА ПРЕТХОДНО ДЕФИНИСАНОМ СЕЛЕКТИВНОШЋУ

MOHAMMAD MAZLOUM-ARDAKANI[1], MOHAMMAD KAZEM AMINI[2], MARZIEH DEHGHAN[3], ELHAM KORDI[3]
и MOHAMMAD ALI SHEIKH-MOHSENI[1]

[1]*Department of Chemistry, Faculty of Science, Yazd University, Yazd, I.R. Iran,* [2]*Department of Chemistry, University of Isfahan, Isfahan, I.R. Iran и* [3]*Department of Chemistry, Payam Noor University, Ardakan Center, Ardakan, I.R. Iran*

Електрода која је претходно модификована електрополимеризацијом полипирола уз метиленско црвено као допант, додатно је електрохемијски допована/дедопована јонима Pb^{2+}, чиме јој је дефинисана селективност, а затим коришћена за потенциометријску и волтаметријску детекцију поменутих јона. Процес електрохемијског доповања/дедоповања побољшао је аналитичке карактеристике електроде, посебно њену селективност према Pb^{2+}. Степен побољшања зависи и од укљученог лиганда (допанта) и од електрохемијског доповања/дедоповања, при чему је други фактор значајнији. Потенциометријски одговор електроде је био линеаран у опсегу концентрације од $2{,}0\times10^{-6}$ to $5{,}0\times10^{-2}$ M са нагибом од 28,6 mV дек$^{-1}$, као што предвиђа Нернстова једначина, и границом детекције од $7{,}0\times10^{-7}$ M. Електрода је такође коришћена за диференцијалну пулсну анодну стрипинг волтаметрију (ДПАСВ) уз претходно укључивање олова из испитиваног раствора у полимерни филм. Резултати су показали да струја максимума зависи од концентрације металних јона у опсегу од $1{,}0\times10^{-8}$ до $1{,}0\times10^{-3}$ M. Граница детекције методе ДПАСВ је $3{,}5\times10^{-9}$ M. Испитивана је и селективност електроде у односу на поједине јоне прелазних метала. Модификована допована/дедопована електрода је успешно тестирана за одређивање олова у два стандардна референтна узорка.

(Примљено 30. августа, ревидирано 5. децембра 2011)

REFERENCES

1. J. Bobacka, *Electroanalysis* **18** (2006) 7
2. C. Pellicer, A. Gomez-Caballero, N. Unceta, M. A. Goicolea, R. J. Barrio, *Anal. Methods* **2** (2010) 1280
3. H. Zhu, Y. Wang, Y. Yuan, H. Zeng, *Anal. Methods* **3** (2011) 348
4. M. A. Rahman, M. S. Won, Y. B. Shim, *Anal. Chem.* **75** (2003) 1123
5. A. Ramanavicius, A. Ramanaviciene, A. Malinauskas, *Electrochim. Acta* **51** (2006) 6025
6. A. Ramanaviciene, A. Ramanavicius, *Crit. Rev. Anal. Chem.* **32** (2002) 245
7. S. Zhao, G. Zhang, L. Fu, L. Liu, X. Fang, F. Yang, *Electroanalysis* **23** (2011) 355
8. A. Dall'Olio, Y. Dascola, V. Varraca, V. Bocchi, *Compt. Rend., C* **267** (1968) 433
9. A. F. Diaz, K. K. Kanazawa, G. P. Gardini, *J. Chem. Soc. Chem. Commun.* **14** (1979) 635
10. M. E. G. Lyons, *Electroactive polymer electrochemistry. Part 2: Methods and applications*, Plenum Press, New York, 1996
11. D. W. M. Arrigan, M. J. Lowens, *Electroanalysis* **11** (1999) 647
12. A. Wanekaya, O. A. Sadik, *J. Electroanal. Chem.* **537** (2002) 135
13. N. Vazquez, J. Vobacka, A. Ibaska, *J. Solid State Electrochem.* **9** (2005) 865
14. G. A. Alvarez-Romero, M. E. Palomar-Pardave, M. T. Ramirez-Silva, *Anal. Bioanal. Chem.* **387** (2007) 1533
15. M. Sahin, Y. Sahin, A. Ozcan, *Sens. Actuators, B* **133** (2008) 5
16. S. Y. Bae, X. Zeng, G. M. Murray, *J. Anal. Atom. Spectrom.* **13** (1998) 1177
17. M. Mazloum Ardakani, M. Khayat Kashani, M. Salavati-Niasaria, A. A. Ensafi, *Sen. Actuators, B* **107** (2005) 438
18. S. M. Talebi, H. Safigholi, *J. Serb. Chem. Soc.* **72** (2007) 585
19. W. Chuachuad, J. F. Tyson, *J. Anal. Atom. Spectrom.* **20** (2005) 282
20. M. Tripkovic, M Todorovic, I. Holclajtner-Antunovic, S. Razic, A. Andrakandic, D. Markovic, *J. Serb. Chem. Soc.* **65** (2000) 323
21. L. Polo-Diez, J. Hernandez-Méndez, F. Pedraz-Penalva, *Analyst* **105** (1980) 37
22. Z. Yanaz, H. Filik, R. Apak, *Sens. Actuators, B* **147** (2010) 15
23. M. Mazloum Ardakani, P. Pourhakak, M. Salavati-Niasari, *Anal. Sci.* **22** (2006) 865
24. A. R. Zanganeh, M. K. Amini, *Electrochim. Acta* **52** (2007) 3822
25. H. Bessbousse, I. Nandhakumar, M. Decker, M. Barsbay, O. Cuscito, D. Lairez, M. C.

Clochard, T. L. Wade, *Anal. Methods* **3** (2011) 1351
26. M. M. Ardakany, A. A. Ensafi, H. Naeimi, A. Dastanpour, A. Shamlli, *Sens. Actuators, B* **96** (2003) 441
27. M. Javanbakht, F. Divsar, A. Badiei, F. Fatollahi, Y. Khaniani, M. R. Ganjali, P. Norouzi, M. Chaloosi, G. Mohammadi Ziarani, *Electrochim. Acta* **54** (2009) 5381
28. M. Mazloum Ardakani, Z. Akrami, H. Kazemian, H. R. Zare, *J. Anal. Chem.* **63** (2008) 184
29. M. Mazloum-Ardakani, H. Beitollahi, Z. Taleat, M. Salavati-Niasari, *J. Serb. Chem. Soc.* **76** (2011) 575
30. M. Mazloum-Ardakani, H. Beitollahi, M. A. Sheikh-Mohseni, H. Naeimi, N. Taghavinia, *Appl. Catal., A* **378** (2010) 195
31. A. R. Zanganeh, M. K. Amini, *Sens. Actuators, B* **135** (2008) 358
32. J. Steinke, D. C. Sherington, I. R. Dunkin, *Adv. Polym. Sci.* **123** (1995) 81
33. O. Abollino, M. Aceto, C. Sarzanini, E. Mentasti, *Electroanalysis* **11** (1999) 870
34. A. Michalska, K. Maksymiuk, *Electrochim. Acta* **44** (1999) 2125
35. Y. Umezawa, K. Umezawa, H. Sato, *Pure Appl. Chem.* **67** (1995) 507.

Journal of the Serbian Chemical Society
JSCS-info@shd.org.rs • www.shd.org.rs/JSCS

J. Serb. Chem. Soc. *77* (7) 911–917 (2012)
JSCS–4320

UDC 546.13+633.71-32+632.951:543.4/.5
Note

NOTE

Derivative spectrophotometric determination of acetamiprid in the presence of 6-chloronicotinic acid

VALÉRIA J. GUZSVÁNY[1*#], SANJA D. LAZIĆ[2], NATAŠA VIDAKOVIĆ[1]
and ZSIGMOND J. PAPP[1#]

[1]*Department of Chemistry, Biochemistry and Environmental Protection, Faculty of Sciences, University of Novi Sad, Trg D. Obradovića 3, 21000 Novi Sad, Serbia and* [2]*Faculty of Agriculture, University of Novi Sad, Trg D. Obradovića 8, 21000 Novi Sad, Serbia*

(Received 17 June 2011, revised 10 February 2012)

Abstract: A simple first-order derivative spectrophotometric method was developed for the simultaneous determination of acetamiprid and 6-chloronicotinic acid (6-CNA) at pH 7.0. By using the zero-crossing approach, acetamiprid was determined at 269.0 nm and 6-CNA at 216.0 nm with detection limits of 7.19×10^{-7} and 8.25×10^{-7} mol dm^{-3}, respectively, and relative standard deviations not exceeding 1.2 % in the case of model systems.

Keywords: derivative spectrophotometry; acetamiprid; 6-chloronicotinic acid.

INTRODUCTION

Acetamiprid ((*E*)-*N*^{1}-[(6-chloro-3-pyridyl)methyl]-*N*^{2}-cyano-*N*^{1}-methylacetamidine, Fig. 1a) belongs to the most efficient class of insecticides nowadays, called neonicotinoids, which account for about 24 % of the total insecticide market.[1] Since its launch in the mid-1990s, products containing acetamiprid have gained registrations for over 60 agricultural crops, including cotton, vegetables, potato, orchards, vines, citrus, tea, and ornamentals.[1] In addition, acetamiprid is also of interest for the control of termites and household pests.[1] Acetamiprid is marketed under a variety of names, including Mospilan, Dyken, Fertilan, Masuta, Mospildate, Suntamiprid and Vapcomere.[2]

6-Chloronicotinic acid (6-CNA), Fig. 1b, represents one of the synthetic precursors,[3] and also an intermediate of acetamiprid decomposition.[4–8] These facts impose the need for reliable analytical methods for the determination of these two compounds in their mixtures. The analytical techniques used most widely for acetamiprid determination are gas chromatography[9,10] and liquid

---

[*] Corresponding author. E-mail: valeria.guzsvany@dh.uns.ac.rs
[#] Serbian Chemical Society member.
doi: 10.2298/JSC110617015G

chromatography (LC) with diode array (DA),[4–7,11,12] mass spectrometric (MS),[6,7,13–20] and thermal lens spectrometric[21] detection. Some alternative techniques, such as enzyme-linked immunosorbent assay,[22] spectrophotometry,[23] colorimetry,[24] Fourier transform infrared spectroscopy[6] and voltammetry,[6,25] have also been employed to analyze different acetamiprid (and 6-CNA) containing samples.

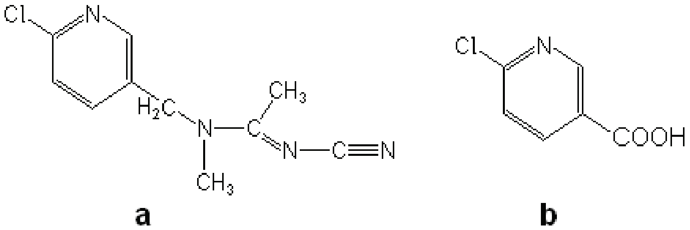

Fig. 1. Structural formula of a) acetamiprid and b) 6-CNA.

Due to the widespread availability of the instrumentation, simplicity of procedures, speed, precision and accuracy, spectrophotometric methods enjoy wide popularity. In addition, they are more economic and simpler, compared to methods such as chromatography and electrophoresis.[26] Except for a conference proceeding,[27] no spectrophotometric methods have hitherto been reported as papers for the simultaneous determination of acetamiprid and 6-CNA.

Several techniques have been proposed for the treatment of spectrophotometric data, with the objective of extracting the largest amount of analytical information from spectra composed of unresolved bands. Undoubtedly, a major success was achieved by the derivative treatment of the absorbance curves – plotting the first- or a higher-order mathematical derivative of the absorbance against wavelength ($dA/d\lambda$). Derivative spectrophotometry offers a convenient solution to a number of analytical problems, such as resolution of multicomponent systems, removal of sample turbidity, matrix background and enhancement of spectral details. For these reason, it has been applied in the analysis of different pharmaceuticals, foods, cosmetics and environmental samples.[26,28,29] The same method was also applied for the simultaneous determination of pesticides or pesticides and their degradation products.[30–36]

In this work, a rapid, environmentally acceptable and inexpensive first-order derivative spectrophotometric method was developed for the determination of acetamiprid and 6-CNA in their mixtures.

EXPERIMENTAL

Chemicals and solutions

All chemicals used were of analytical reagent grade. Pestanal quality (Riedel de Haën, Germany) was employed as the analytical standard of acetamiprid and 6-CNA. Stock solutions were prepared by dissolving the compounds in doubly distilled water to obtain a concentration of 5×10^{-4} mol dm^{-3}, which did not change over a long period when the solutions were kept in the dark at 4 °C. Britton–Robinson buffer solutions were prepared from a stock solution containing 0.04 mol dm^{-3} phosphoric, boric and acetic acids (all Merck), respectively, by adding 0.2 mol dm^{-3} sodium hydroxide (Merck) to the required pH values, covering the pH range of approx. 2–10.

Apparatus

Spectrophotometric measurements were performed on a PG Instruments T80+ UV–Vis double-beam spectrophotometer (PG Instruments, United Kingdom). A digital pH-meter (PHM 62, Radiometer, Denmark) and a combined glass electrode were used for pH measurements.

Procedures

Spectrophotometry. Characterization of the individual optical behavior of acetamiprid and 6-CNA was performed at the same molar concentration (4.34×10^{-5} mol dm^{-3}) in the pH range 2−10 and at wavelengths from 200 to 400 nm ($\Delta\lambda$ = 1 nm). Standard solutions for the calibration curves were prepared by the stepwise dilution of the stock solution to obtain concentrations in the range 3.69×10^{-6}–6.20×10^{-5} mol dm^{-3} for both compounds. Simultaneous derivative spectrophotometric determinations were realized at 269.0 nm (acetamiprid) and 216.0 nm (6-CNA).

pH Measurements. A digital pH-meter, a glass electrode and a saturated calomel electrode were used for all pH measurements. The glass electrode was previously calibrated using commercial buffer solutions (Hanna Instruments, USA) in two separate ranges 1.68−6.86 and 6.86−10.01.

Validation of the analytical method. The linearity for the developed derivative spectrophotometric method was checked in the concentration range of 3.69×10^{-6}–6.20×10^{-5} mol dm^{-3}. The limit of detection (*LOD*) and the limit of quantification (*LOQ*) were calculated using the following equations: $LOD = 3s/m$ and $LOQ = 10s/m$, where s is the standard deviation of the blank and m is the slope of the calibration curve.

Data processing. The experimental data were plotted using Origin 6.1 software package. The first derivative spectra were calculated using all data points in the range from 200 to 400 nm with $\Delta\lambda$ = 1 nm using the option differentiate. For noise reduction, the adjacent averaging method was tested using different smoothing factors (3, 5 and 9). Calibration equations were calculated using the linear fit option.

RESULTS AND DISCUSSION

To study the optical characteristics of the investigated compounds, the corresponding spectra were recorded in Britton–Robinson buffers (pH 2.0–10.0) in the wavelength range 200–400 nm. The representative spectra of acetamiprid and 6-CNA obtained at pH 7.0 are shown in Fig. 2. The spectrum of acetamiprid has two discrete absorption bands with maxima at 216.0 and 245.0 nm, of which the latter is much more intense. No significant changes in the absorption spectrum were observed in dependence on the pH of the solution. As was described earlier, the spectrum of 6-CNA also has two discrete, well-defined absorption bands with the maxima at 224.0 and 269.0 nm, the former band being more intense.[36,37] The shape of the 6-CNA spectra and the positions of its maxima depended significantly on the pH value, especially at pH < 4.0.[36,37] At higher pH values, no significant change was observed.[36,37] In this context, pH 7.0 was selected for further investigations. As can be seen from Fig. 2, the strong overlapping of the spectra of the investigated compounds hinders their conventional spectrophotometric determination in a mixture. Hence, derivative spectrophotometry was investigated to develop a method for their simultaneous determination.[27] The derivative spectra of solutions containing the individual analytes were investigated in order to optimize the derivative order. The first-order derivative spectrum showed the highest sensitivity and a good resolution for the simultaneous determination of the compounds. Higher derivative orders were discarded because the noise attenuation was less effective and the signal became distorted.

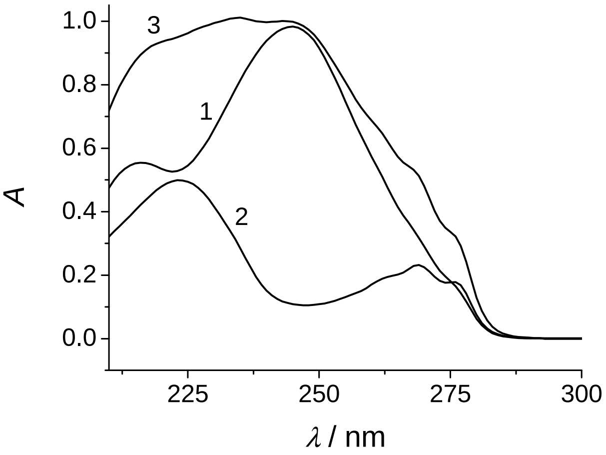

Fig. 2. Absorption spectra of acetamiprid (1), 6-CNA (2) and their mixture (3). Measurement parameters: $c_1 = c_2 = 4.34\times10^{-5}$ mol dm^{-3}, pH 7.0.

The main disadvantage of the derivative technique is that the signal/noise ratio becomes worse as the order of the derivative increases. Therefore, in practice, the derivative technique includes a certain degree of low-pass filtering or smoothing, to control the noise increase, which is an inevitable consequence of differentiation of the noise signal. The effect of smoothing of a peak-type signal is to reduce the noise, which is desirable. However, it distorts the signal, which is undesirable but unavoidable.[29] Thus, optimization of the smoothing factor is very important for obtaining the appropriate signals. In the present study, the adjacent averaging method was tested using smoothing factors of 3, 5 and 9, and the obtained curves were compared with the unsmoothed ones (Fig. 3). Smoothing factor 5 was selected, because this yielded good sensitivity, without significant sacrifice of the signal/noise ratio.

The smoothed first derivative spectrum of both compounds has more zero-crossings, of which those at 216.0 nm in case of acetamiprid and 269.0 nm in case of 6-CNA offer better sensitivity for the determination of the second compound (Fig. 3c). At these wavelengths, all the absorption is attributed to a single compound. The effect of the concentration of the analytes on both zero-crossing points was studied in the range of 3.69×10^{-6}–6.20×10^{-5} mol dm^{-3}. The zero-crossing values selected were independent of the concentration.

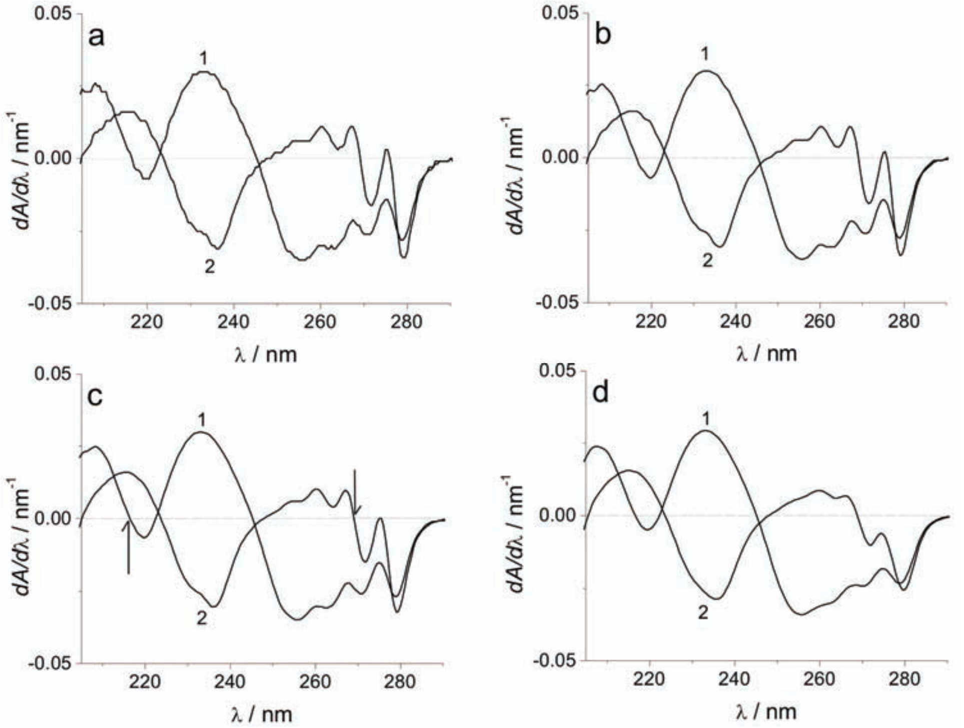

Fig. 3. Unsmoothed (a) and smoothed (b–d) first-order derivative spectra of acetamiprid (1) and 6-CNA (2). Measurement parameters: $c_1 = c_2 = 4.34\times10^{-5}$ mol dm^{-3}, pH 7.0; smoothing factors: 3 (b), 5 (c) and 9 (d).

Using the selected conditions, linear graphs of d*A*/d*λ* *vs*. analyte concentration were obtained in the concentration range of 3.69×10^{-6}–6.20×10^{-5} mol dm^{-3} for both analytes. The calculated values of the *LOD* were 7.19×10^{-7} and 8.25×10^{-7} for acetamiprid and 6-CNA, respectively. The relative standard deviation (*RSD*) values did not exceed 1.2 % (1.0 % for 6-CNA and 1.2 % for acetamiprid).

The good recoveries and low *RSD* values reflect the high accuracy and precision of the proposed derivative spectrophotometric method. The method is sensitive, simple, rapid and inexpensive, thus making it a convenient alternative tool for the determination of acetamiprid and 6-CNA in their mixtures.

Acknowledgements. The authors acknowledge the financial support of the Ministry of Education and Science of the Republic of Serbia (Project Nos. 172012 and TR 31038).

И З В О Д

ДЕРИВАТИВНО СПЕКТРОФОТОМЕТРИЈСКО ОДРЕЂИВАЊЕ АЦЕТАМИПРИДА У ПРИСУСТВУ 6-ХЛОРНИКОТИНСКЕ КИСЕЛИНЕ

VALÉRIA J. GUZSVÁNY[1], САЊА Д. ЛАЗИЋ[2], НАТАША ВИДАКОВИЋ[1] и ZSIGMOND J. PAPP[1]

[1]*Департман за хемију, биохемију и заштиту животне средине, Природно–математички факултет,*
Универзитет у Новом Саду, Трг Д. Обрадовића 3, 21000 Нови Сад и [2]*Пољопривредни факултет,*
Универзитет у Новом Саду, Трг Д. Обрадовића 8, 21000 Нови Сад

Предложена је једноставна дериватвна спектрофотометријска метода за истовремено одређивање ацетамиприда и 6-хлорникотинске киселине (6-CNA) при pH 7,0. Примењујући приступ нултог пресека ацетамиприд је одређиван у модел систему на 269,0 nm а 6-CNA на 216,0 nm, са границама детекције од $7{,}19\times10^{-7}$ и $8{,}25\times10^{-7}$ mol dm^{-3}, редом, и стандардном девијацијом мањом од 1,2 %.

(Примљено 17. јуна 2011, ревидирано 10. фебруара 2012)

REFERENCES

1. P. Jeschke, R. Nauen, M. Schindler, A. Elbert, *J. Agric. Food Chem.* **59** (2011) 2897
2. C. D. S. Tomlin, Ed., *The Pesticide Manual: A World Compendium*, 15th ed., British Crop Protection Council, Farnham, Surrey, UK, 2009
3. N. V. Kovganko, Zh. N. Kashkan, *Russ. J. Org. Chem.* **40** (2004) 1759
4. M. L. Dell'Arciprete, L. Santos-Juanes, A. Arques, R. Vicente, A. M. Amat, J. P. Furlong, D. O. Mártire, M. C. Gonzalez, *Photochem. Photobiol. Sci.* **8** (2009) 1016
5. M. L. Dell'Arciprete, L. Santos-Juanes, A. Arques, R. F. Vercher, A. M. Amat, J. P. Furlong, D. O. Mártire, M. C. Gonzalez, *Catal. Today* **151** (2010) 137
6. V. Guzsvány, M. Kádár, Zs. Papp, L. Bjelica, F. Gaál, K. Tóth, *Electroanalysis* **20** (2008) 291
7. V. Guzsvány, J. Csanádi, S. Lazić, F. Gaál, *J. Braz. Chem. Soc.* **20** (2009) 152
8. V. Guzsvány, Lj. Rajić, B. Jović, D. Orčić, J. Csanádi, S. Lazić, B. Abramović, *J. Environ. Sci. Heal., B* **47** (2012) 1919
9. M. Mateu-Sánchez, M. Moreno, F. J. Arrebola, J. L. Martinez-Vidal, *Anal. Sci.* **19** (2003) 701
10. M. Tokieda, M. Ozawa, S. Kobayashi, T. Gomyo, *J. Pest. Sci.* **22** (1999) 77
11. E. Watanabe, K. Baba, H. Eun, *J. Agric. Food Chem.* **55** (2007) 3798
12. S. Seccia, P. Fidente, D. Montesano, P. Morrica, *J. Chromatogr., A* **1214** (2008) 115
13. H. Obana, M. Okihashi, K. Akutsu, Y. Kitagawa, S. Hori, *J. Agric. Food Chem.* **51** (2003) 2501
14. I. Ferrer, E. M. Thurman, A. R. Fernandez-Alba, *Anal. Chem.* **77** (2005) 2818
15. S. Seccia, P. Fidente, D. A. Barbini, P. Moricca, *Anal. Chim. Acta* **553** (2005) 21
16. P. Fidente, S. Seccia, F. Vanni, P. Morrica, *J. Chromatogr., A* **1094** (2005) 175
17. A. Di Muccio, P. Fidente, D. A. Barbini, R. Dommarco, S. Seccia, P. Morrica, *J. Chromatogr., A* **1108** (2006) 1
18. S. Liu, Z. Zheng, F. Wei, Y. Ren, W. Gui, H. Wu, G. Zhu, *J. Agric. Food Chem.* **58** (2010) 3271
19. J.-Y. Park, J.-H. Choi, B.-M. Kim, J.-H. Park, S.-K. Cho, M. W. Ghafar, A. M. Abd El-Aty, J.-H. Shim, *Biomed. Chromatogr.* **25** (2011) 136
20. Z. Xiao, X. Li, X. Wang, J. Shen, S. Ding, *J. Chromatogr., B* **879** (2011) 117

21. V. Guzsvány, A. Madžgalj, P. Trebše, F. Gaál, M. Franko, *Environ. Chem. Lett.* **5** (2007) 203
22. S. Watanabe, S. Ito, Y. Kamata, N. Omoda, T. Yamazaki, H. Munakata, T. Kaneko, Y. Yuasa, *Anal. Chim. Acta* **427** (2001) 211
23. J. Fan, X.-J. Shao, Y.-F. Wei, J.-J. Wang, *Chin. J. Anal. Chem.* **36** (2008) 1411
24. Q. Xu, S. Du, G. Jin, H. Li, X. Y. Hu, *Microchim. Acta* **173** (2011) 323
25. F. F. Gaál, V. J. Guzsvány, L. J. Bjelica, *J. Serb. Chem. Soc.* **72** (2007) 1465
26. F. S. Rojas, C. B. Ojeda, *Anal. Chim. Acta* **635** (2009) 22
27. F. Gaál, V. Guzsvány, S. Lazić, N. Vidaković, in *Proceedings of the 12th Symposium on Analytical and Environmental Problems*, Szeged, Hungary, 2005, p. 88
28. C. B. Ojeda, F. S. Rojas, *Anal. Chim. Acta* **518** (2004) 1
29. G. V. Popović, L. B. Pfendt, V. M. Stefanović, *J. Serb. Chem. Soc.* **65** (2000) 457
30. B. F. Abramović, V. B. Anderluh, F. F. Gaál, D. V. Šojić, *J. Serb. Chem. Soc.* **72** (2007) 809
31. J. L. M. Vidal, M. D. G. Garcia, M. M. Galera, A. G. Frenich, *Anal. Lett.* **30** (1997) 2409
32. I. Baranowska, C. Pieszko, *Chem. Anal. (Warsaw)* **45** (2000) 583
33. I. Baranowska, C. Pieszko, *Anal. Lett.* **35** (2002) 473
34. T.-L. Kuo, D.-L. Lin, R. H. Liu, F. Moriya, Y. Hashimoto, *Forensic Sci. Int.* **121** (2001) 134
35. A. G. Frenich, M. M. Galera, J. L. M. Vidal, P. P. Vazquez, M. D. G. Garcia, *Anal. Lett.* **30** (1997) 341
36. V. Guzsvány, *PhD Thesis*, University of Novi Sad, Faculty of Sciences, 2006
37. V. J. Guzsvány, Zs. J. Papp, S. D. Lazić, F. F. Gaál, L. J. Bjelica, B. F. Abramović, *J. Serb. Chem. Soc.* **74** (2009) 1455.

Journal of the Serbian Chemical Society
eversion electronic
JSCS-info@shd.org.rs • www.shd.org.rs/JSCS

J. Serb. Chem. Soc. 77 (7) 919–935 (2012)
JSCS–4321

UDC 678.664’84+678.674:66.095.26:
532.14:536.5.004.12
Original scientific paper

Poly(urethane–siloxane)s based on hyperbranched polyester as crosslinking agent: synthesis and characterization

MARIJA V. PERGAL[1]*, JASNA V. DŽUNUZOVIĆ[1], SANJA OSTOJIĆ[2#], MIODRAG M. PERGAL[3#], ALEKSANDRA RADULOVIĆ[2] and SLOBODAN JOVANOVIĆ[4#]

[1]University of Belgrade, Institute of Chemistry, Technology and Metallurgy, Studentski trg 12–16, Belgrade 11000, Serbia, [2]University of Belgrade, Institute of General and Physical Chemistry, Studentski trg 12–16, Belgrade 11000, Serbia, [3]University of Belgrade, Faculty of Chemistry, Studentski trg 12–16, Belgrade 11000, Serbia and [4]University of Belgrade, Faculty of Technology and Metallurgy, Karnegijeva 4, Belgrade 11000, Serbia

(Received 13 October, revised 28 December 2011)

Abstract: A series of novel polyurethane crosslinked structures (PUs) was prepared from *α*,*ω*-dihydroxy-(ethylene oxide–poly(dimethylsiloxane)–ethylene oxide) (EO–PDMS–EO), 4,4’-methylenediphenyl diisocyanate and Boltorn® hyperbranched polyester of the third pseudo generation. The hydroxy-functional hyperbranched aliphatic polyester with 26 end groups was used as a crosslinking agent. In order to improve the compatibility of all the reactants during the synthesis, the PU samples were prepared by two-stage, step-growth polymerization in solution. The content of the soft EO–PDMS–EO segments was varied in the range from 15 to 40 wt. %. The influence of the EO–PDMS–EO content on the swelling behavior, crosslink density, hardness, and the thermal and surface properties of the synthesized PUs was investigated. The structure of the synthesized polyurethanes was confirmed by the presence of specific bands in the Fourier transform infrared spectra. Swelling studies were performed to determine the crosslink density and polyurethane networks with lower EO–PDMS–EO contents had higher crosslink densities. The glass transition temperature of the synthesized PUs, determined by differential scanning calorimetry, slightly increased from 50 to 58 °C on decreasing the EO–PDMS–EO content because of the higher crosslink density of the samples. Increasing the EO–PDMS–EO content led to better thermal stability, as was evidenced by the onset temperature of weight loss. The surface of the polyurethane networks became more hydrophobic with increasing EO–PDMS–EO content. The surface morphology of synthesized polyurethanes was analyzed by scanning electron microscopy.

Keywords: polyurethane networks; hyperbranched polyester; poly(dimethylsiloxane); crosslink density; thermal properties; surface properties.

---

* Corresponding author. E-mail: marijav@chem.bg.ac.rs
# Serbian Chemical Society member.

doi: 10.2298/JSC111013006P

INTRODUCTION

Polyurethanes (PUs) based on hyperbranched polyesters (HBPs) have attracted great attention due to their excellent mechanical properties and good biocompatibility. Additionally, the presence of a large number of end functional groups in HBPs, good compatibility with different materials, the presence of nanoscale cavities within the structure of HBPs contribute to the unique physical and chemical properties of polyurethane networks.[1,2] Potential applications of polyurethanes based on HBPs in the fields of coatings, drug delivery, membranes and nanomaterials have been reported.[1–4] Generally, PU networks are prepared using urethane prepolymers combined with crosslinkers having a functionality of three or more.[5] The HBPs which have a large number of end hydroxyl groups can react with the isocyanate groups of the urethane prepolymer and form networks.[6] In addition, they contain a large number of ester groups, which could create H-bonds with the carbonyl and amine groups of adjacent chains in the polyurethane networks. The properties of PU networks depend especially on the composition and chemical structure of all components, on the molecular weight of the soft segments and particularly on the nature of the employed crosslinking agent.[7]

The introduction of poly(dimethylsiloxane) (PDMS) into the polymer chains has the advantage of imparting some of the attractive properties of PDMS to polyurethanes, such as high flexibility, biocompatibility, excellent thermal, oxidative and hydrolytic stability, and low surface energy.[8–11] Combinations of polyurethanes and poly(dimethylsiloxane)s has attracted special attention due to the good thermal stability and high flexibility at low temperatures given by the PDMS part and the enhanced mechanical strength and abrasion characteristics conveyed by the polyurethane. However, PDMS has a low surface energy and a low value of the solubility parameter, which result in incompatibility of PDMS with other polymers. In order to overcome this, a mixture of macrodiols or a special type of macrodiols was used in order to increase the compatibility of the reactants and, therefore, to achieve better mechanical properties.[12–17]

Recently some papers dealing with the use of hyperbranched polymers for the synthesis of PU crosslinked structures have been published. Czech *et al.* and Okrasa *et al.*[18,19] synthesized polyurethane networks using Boltorn® HBP of the fourth pseudo generation polyethers or polyesters and 4,4’-methylenediphenyl diisocyanate (MDI) or 4,4’-methylenedicyclohexyl diisocyanate. Cao and Liu[20] prepared a series of novel hyperbranched polyurethanes using a second pseudo generation hyperbranched polyester as the crosslinker and investigated the phase transition behavior and the morphology of the products. Maji and Bhowmick[21] used Boltorn® HBPs of the second, third and fourth pseudo generations for the preparation of PUs. Moreover, the results of a study[22] are available on poly(urethane–siloxane) networks based on isophorone diisocyanate, *α*,*ω*-dihydroxybutyl-poly(dimethylsiloxane) and a hybrid diol containing hydrolysable Si–OC_2H_5 groups besides OH groups in which crosslinked structure was formed by silica domains. However, to the best of our knowledge, PDMS macrodiols have not been used for the preparation of poly(urethane–siloxane) crosslinked structures based on Boltorn® HBP of the third pseudo generation. Polyurethane networks prepared from this specific combination of reactants enables the exploitation of their good features and simultaneously introduces good thermal and surface properties, swelling ability, rubber elasticity and other properties which are important for different applications, especially for coatings.

In the work presented herein, a series of novel polyurethane crosslinked structures based on ethylene oxide–poly(dimethylsiloxane)–ethylene oxide (EO––PDMS–EO) as soft segments and 4,4'-methylenediphenyl diisocyanate and hyperbranched polyester of the third pseudo generation (BH-30) as components of the hard segments was prepared. In the synthesis of PU networks, the ethylene oxide blocks served as compatibilizers between the non-polar PDMS prepolymer and the polar MDI and BH-30. In addition, in order to improve the compatibility of all reactants during the synthesis, PU samples were prepared by two-step, step-growth polymerization in solution. The EO–PDMS–EO content was varied in the range from 15 to 40 wt. %. The influence of the EO–PDMS–EO content on the swelling behavior, hardness, and the thermal and surface properties of the synthesized PU samples were investigated.

EXPERIMENTAL

Materials

α,ω-Dihydroxy-(ethylene oxide–poly(dimethylsiloxane)–ethylene oxide) (α,ω-dihydroxy-(EO–PDMS–EO)), supplied by ABCR, (M_n = 1000 g mol^{-1}) was dried over molecular sieves (0.4 nm) before use. The number-average molecular weight (M_n) determined by ^1H--NMR spectroscopy,[23] was 1200 g mol^{-1} and this value was used in the calculations of the compositions of the reaction mixtures for the synthesis of the polyurethanes. The molecular weight of the central PDMS-block was 1090 g mol^{-1}, whereas the terminal ethylene oxide sequences consisted of one unit. 4,4'-Methylenediphenyl diisocyanate (MDI) (supplied by Aldrich) with an isocyanate content of 33.6 wt. %, was used as received. Commercially available Boltorn® hydroxy-functional aliphatic hyperbranched polyester of the third pseudo generation (BH-30) was kindly supplied by Perstorp Specialty Chemicals AB (Sweden) and dried at 50 °C under vacuum for 48 h prior to use. The aliphatic hyperbranched polyester is based on 2,2-bis(hydroxymethyl)propionic acid as the monomer and tetrafunctional ethoxylated pentaerythrytol as the core.[24] For the exact calculation of the amounts of all components necessary for the synthesis of polyurethanes, the value of the molecular weight determined by vapor pressure osmometry (M_n= 3080 g mol^{-1}) and hydroxyl number of BH-30 determined by the titration method (HN = 474.1 mg KOH g^{-1}) were used.[25] Consequently, the exact functionality, f_n, of the used BH-30 was calculated (f_n = 26). The solvent *N*-methylpyrrolidone (NMP), supplied by Across, was dried over calcium hydride and distilled before use. Tetrahydrofuran (THF), supplied by J. T. Baker, was refluxed with lithium aluminum hydride and distilled before use. Toluene (from Lach-Ner) was used as received. The catalyst was stannous octanoate ($Sn(Oct)_2$), supplied by Aldrich.

Synthesis of the polyurethanes

A series of polyurethanes was synthesized by two-stage, catalyzed step-growth polymerization in solution using α,ω-dihydroxy-(ethylene oxide–poly(dimethylsiloxane)–ethylene oxide) macrodiol, 4,4'-methylenediphenyl diisocyanate and a hyperbranched aliphatic polyester as the crosslinking agent. This series consisted of four samples (PU3-40, PU3-30, PU3-20 and PU3-15) of different EO–PDMS–EO contents. The last two numbers in the designation of the synthesized samples represent the weight percent of EO–PDMS–EO in the reactants. The mixture of solvents NMP/THF was used as the reaction medium. This solvent mixture and the used ratio (NMP/THF, 7/1 v/v) were found to be the best choice for the synthesis of the investigated PUs. The molar ratio of the reactive –NCO and –OH groups (from HBP and α,ω-dihydroxy-(EO–PDMS–EO)) for all samples was kept at a constant value of 1.05.[16] The amount of the catalyst was 0.15 mol % $Sn(Oct)_2$, based on α,ω-dihydroxy-(EO–PDMS–EO).[16] The composition of the synthesized PUs and weight of the reactants used for the synthesis of the PUs are presented in Table I. As an example, the synthesis of a PU network based on BH-30 with 40 wt. % soft EO–PDMS–EO segments (PU3-40 sample, Table I) is described.

TABLE I. Composition of the synthesized PUs and weight of reactants used for their preparation

Sample	Content of soft EO–PDMS–EO segment wt. %[a]	EO–PDMS–EO g	BH-30 g	MDI g
PU3-40	40	5.000	3.040	4.463
PU3-30	30	4.000	4.013	5.321
PU3-20	20	3.000	5.382	6.619
PU3-15	15	2.500	6.461	7.707

[a] Soft segment content = $[m(\text{EO–PDMS–EO})/(m(\text{MDI}) + m(\text{BH-30}) + m(\text{EO–PDMS–EO}))]\times100$

A four necked round-bottom flask equipped with a mechanical stirrer, an inlet for dry argon, a reflux condenser and a dropping funnel was charged with 5.000 g (4.167 mmol) of α,ω-dihydroxy-(EO–PDMS–EO), 4.463 g (17.85 mmol) of 4,4'-methylenediphenyl diisocyanate, 35 mL of NMP and 5 mL of THF. The flask was heated to 40 °C in a silicone oil bath and the reaction started by the introduction of 0.41 mL of a solution of stannous octanoate in NMP. The reaction mixture was stirred for 30 min at 40 °C to prepare the NCO-terminated prepolymer, which was considered to be obtained when the theoretical –NCO content (4.94 wt. %) was attained.[16] The content of –NCO groups during the reaction was determined using the dibutylamine back titration method.[26] In the second stage of reaction, 3.040 g (0.9870 mmol) of hyperbranched polyester was dissolved in 26 mL NMP and added drop-wise into the NCO-terminated prepolymer solution, and the reaction was continued at 40 °C for 1 h. The obtained mixture was then cast into glass dish, previously lubricated with a very small amount of silicone oil. The crosslinking reaction was continued in a force-draft oven at 50 °C for 50 h and 1 h at 110 °C and finally 10 h at 50 °C in a vacuum oven at 0.5 mm Hg. The polyurethane samples were obtained as yellow films (thickness of about 2 mm). The films were kept in a desiccator. Samples were maintained at room temperature for about two weeks before characterization.

Characterization of the polyurethanes

The FTIR spectra of the PUs were recorded on an ATR NICOLET 380 spectrometer. The scanning range was from 400 to 4000 cm^{-1} at a resolution of 4 cm^{-1} and 64 scans were collected for each sample.

Swelling measurements were performed on rectangular-shaped specimens, with dimension of 1.2×2.1×0.20 cm^3 (weighing approximately 0.20 g), by immersion of the samples in toluene for 48 h and in THF for 24 h at room temperature. The applied duration of the swelling measurements in both solvents was chosen because this was sufficient to achieve equilibrium swelling of the examined PUs, which was previously confirmed by separate periodical measurements of the weight of swollen samples until a constant mass was obtained. After swelling, the swollen samples were dried in vacuum oven at 0.5 mm Hg and 50 °C to remove the absorbed solvent and the weight of the deswollen specimens was measured. Data from three different specimens of each PU sample were averaged. Values of the equilibrium degree of swelling, q_e, were calculated using conventional gravimetric method and the following equation:

$$q_e = \frac{w - w_0}{w_0} \tag{1}$$

where, w_0 and w are the sample weights before and after swelling, respectively.

The crosslink density, ν, of the PUs was calculated according to the Flory–Rehner Equation: [27]

$$\nu = -\frac{\ln\left(1 - V_{PU}\right) + V_{PU} + \chi V_{PU}^2}{V_s\left(V_{PU}^{1/3} - \frac{V_{PU}}{2}\right)} \tag{2}$$

where, χ is the interaction parameter between the solvent (THF) and polymer, which is equal to 0.34,[28] V_s is the molar volume of THF (81.7 cm^3 mol^{-1})[28] and V_{PU} is the volume fraction of the crosslinked polymer in the swollen specimen, which was calculated from the density of the PUs (ρ_{PU} from 1.065 g cm^{-3} for PU3-15 to 1.149 g cm^{-3} for PU3-40), the density of THF (ρ_s = 0.889 g cm^{-3}),[29] and the weights of the swollen and deswollen PU samples.[27]

Differential scanning calorimetry (DSC) measurements were realized using a DSC Q1000V9.0 Build 275 thermal analyzer. The samples were analyzed under a nitrogen atmosphere from –90 to 230 °C, at a heating and cooling rate of 10 °C min^{-1}. The glass transition temperatures (T_g) of the PU networks were determined from the second heating run as an average of three measurements.

Thermogravimetric analysis (TGA) was performed using a TGA Q500 V6.3 Build 189 instrument under dynamic nitrogen, in the temperature range from 25 to 700 °C. The gas flow rate was 50 cm^3 min^{-1} and the heating rate was 10 °C min^{-1}. The weight of the samples was approximately 10 mg.

Wide angle X-ray scattering (WAXS) was performed using a PW1710 diffractometer with CuK$_\alpha$ radiation employing a copper anode (tube: 40 kV, 30 mA, λ = 0.154178 nm). The diffraction patterns were obtained in the Bragg angle range of 5–50°. The scan speed was 0.02 s per step in all measurements.

The hardness measurements were performed using a Shore A apparatus (Hildebrand, Germany) on polymer films. The results of the measurements were registered one second after penetration of the needle into the sample. The average of at least five measurements was used.

The surface morphology of the PU samples was analyzed by field emission scanning electron microscopy (SEM). The samples were adhered to aluminum sample holders and sputter coated with Au layer. The microphotographs of the PUs were obtained using a JEOL JSM-6610 instrument at a working distance of *ca*. 14 mm and an accelerating voltage of 20 or 30 kV.

Water contact angle measurements of the PU samples were performed on a Krüss DSA100 instrument using the sessile drop method. Single 20-μL drops of distilled water were deposited on the surface of the polymer films and the contact angles were measured after 30 s, at a temperature of 26 °C. In all cases, at least five measurements were made, and the average contact angle was then calculated.

RESULTS AND DISCUSSION

A series of novel polyurethanes with crosslinked structure based on *α*,*ω*-dihydroxy-(ethylene oxide–poly(dimethylsiloxane)–ethylene oxide), 4,4'-methylenediphenyl diisocyanate and Boltorn® hyperbranched polyester of the third pseudo generation was synthesized by two-stage, step-growth polymerization in solution. During the synthesis of all samples, the total molar ratio of –NCO and –OH groups (from HBP and *α*,*ω*-dihydroxy-(EO–PDMS–EO)) was kept constant. The chemical structures of *α*,*ω*-dihydroxy-(EO–PDMS–EO), MDI and the hyperbranched polyester of the third pseudo generation (BH-30) are shown in Fig. 1. The results obtained in a previous work showed that polymerization in the melt and incompatibility of the non-polar EO–PDMS–EO with polar reactants, *i.e.*, hyperbranched polyester of the second pseudo generation and MDI, led to the formation of heterogeneous PU networks.[30] Therefore, in this work a two-step, step-growth polymerization in solution was applied to improve the compatibility between reactants during the synthesis of the PU networks, using the mixture NMP/THF as the reaction medium. In the first stage of reaction, the NCO-terminated prepolymer was synthesized in an argon atmosphere by reacting hydroxy-terminated EO–PDMS–EO prepolymer with MDI until the theoretical –NCO content of 4.94 wt. % was attained. In the second stage of the reaction, the NCO–terminated prepolymer was reacted with multifunctional BH-30 as crosslinker to form the PU network. The EO–PDMS–EO content was varied in the range from 15 to 40 wt. % (Table I). Thus, a different degree of chemical crosslinking was in a controlled manner brought into the structure of the synthesized PUs through the hard segments (BH-30 and MDI).

FTIR Spectroscopy of the synthesized polyurethane networks

The structure of the synthesized polyurethanes was verified by FTIR spectroscopy. Typical infrared spectra of the hyperbranched polyester BH-30 and the polyurethane samples are presented in Fig. 2. In FTIR spectrum of the hyperbranched polyester, hydroxyl groups as a broad absorption band at 3300 cm^{-1} can be observed, while the characteristic peak at 1723 cm^{-1} was ascribed to the carbonyl ester groups. The IR absorption bands characteristic for the ether groups (1010–1120 cm^{-1}), C–O linkage of ester groups (1040–1210 cm^{-1}) and $–CH_2–$

and –CH_3 groups (2900–3000 cm^{-1}) can also be observed in the FTIR spectrum of BH-30.

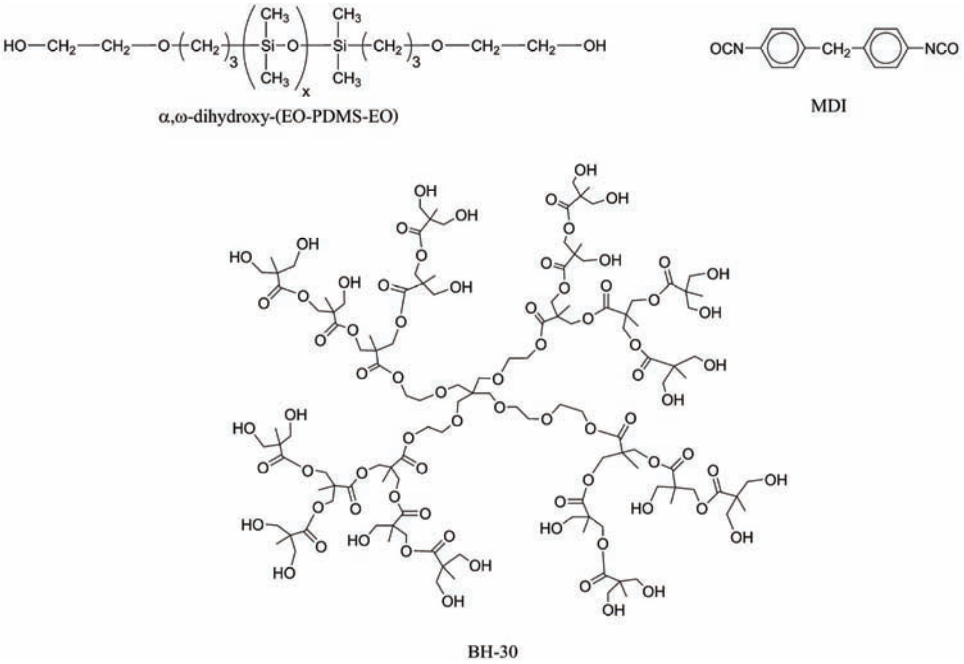

Fig. 1. Chemical structures of α,ω-dihydroxy-(EO–PDMS–EO), MDI and the hyperbranched polyester of the third pseudo generation (BH-30).

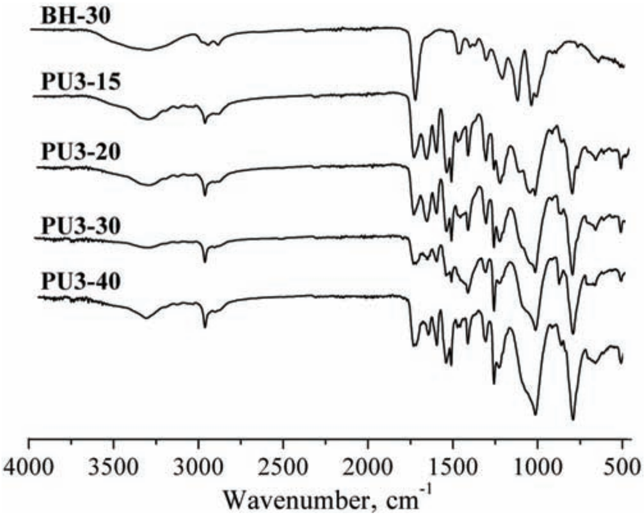

Fig. 2. FTIR Spectra of the hyperbranched polyester BH-30 and the synthesized polyurethanes.

In FTIR spectra of the synthesized polyurethane samples, the bands around 3310 cm^{-1} (H-bonded urethane N–H stretch) and 1710 cm^{-1} (H-bonded urethane C=O) were assigned to the urethane linkage. The amide II and amide III bands for polyurethanes appeared at 1537 and 1258 cm^{-1}, respectively. The carbonyl ester groups show a characteristic band at 1725 cm^{-1}. The intensive bands at 1016 and 1080 cm^{-1} correspond to the Si–O–Si and C–O–C groups. The absorption band at around 790 cm^{-1} was ascribed to the Si–CH$_3$ linkage. The rest of the bands at 2961, 2903 and 2875 cm^{-1} were assigned to the presence of symmetric and asymmetric –CH$_2$– and –CH$_3$ groups, while the bands at 1597 and 1413 cm^{-1} were assigned to the aromatic C=C. As shown in Fig. 2, none of the samples exhibited an apparent band at 2270 cm^{-1}, which means that all the –NCO groups were consumed during the reaction.

Swelling measurements and hardness of the synthesized polyurethane networks

The swelling behavior of the synthesized PU samples was investigated in THF and toluene. The values of equilibrium degree of swelling of the PUs determined in toluene and in THF are summarized in Table II. The equilibrium swellling degree of samples increased from 0.783 to 1.889 (in THF) and from 0.003 to 0.188 (in toluene) as the EO–PDMS–EO content increased from 15 to 40 wt. %. Therefore, the equilibrium degree of swelling was found with increasing soft EO–PDMS–EO content (Fig. 3). The solvent uptake was much higher after immersion of synthesized PUs in THF (Table II). Although the solubility parameters of THF and toluene are similar,[28] the results obtained in this work indicate that better solvatation of the PU samples was achieved in THF. The reason for this behavior is the difference in polarity between THF and toluene; hence, the polar THF can easily diffuse into the PU networks leading to better solvatation of the PU samples in THF.

TABLE II. The equilibrium swelling degree, q_e, crosslink density, v, glass transition temperature, T_g, and water contact angle of the synthesized PUs

Sample	q_e		$v\times10^4$ / mol cm^{-3}	$T_g{}^a$ / °C	Water contact angle, °
	THF	Toluene	THF		
PU3-40	1.8897±0.0050	0.1876±0.0031	3.76	52.1±0.1	93.9±0.9
PU3-30	1.5884±0.0044	0.1774±0.0020	5.92	57.0±0.2	87.3±1.1
PU3-20	0.8701±0.0040	0.1414±0.0031	17.95	58.2±0.1	86.6±0.8
PU3-15	0.7828±0.0035	0.0031±0.0007	23.11	50.4±0.1	87.0±1.1

[a] Determined by DSC analysis from the second heating run

Calculation of crosslink density of the synthesized PUs was performed using the results obtained from equilibrium swelling in THF according to the Flory–Rehner Equation.[27] These results are shown in Table II. It can be observed that the crosslink density of the PU samples increased with decreasing EO–PDMS–EO content. Additional crosslinking could have occurred through the formation of allophanates, which also would decrease the swelling ability of the PUs in THF. Thus, for the series of synthesized PUs, the polymers with a higher crosslink density values are less flexible and hence have a lower solvent uptake.

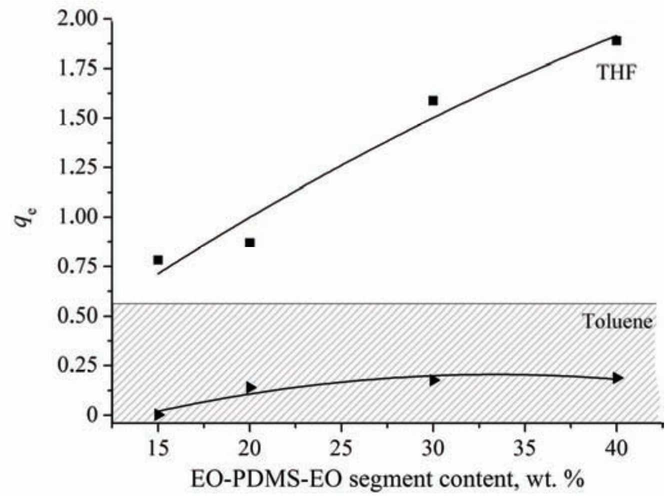

Fig. 3. Equilibrium degree of swelling, q_e, of the synthesized PUs determined in toluene and in THF *vs*. the content of EO–PDMS–EO.

The results of hardness measurements show that the hardness of the synthesized polyurethanes increased with decreasing EO–PDMS–EO content, from 83 Shore A to 88 Shore A. The PU samples with lower EO–PDMS–EO content showed slightly higher hardness because of the higher crosslink density of the samples.

Thermal properties of the synthesized polyurethane networks

Determination of the glass transition temperature (T_g) of the synthesized samples was performed using DSC at a heating rate of 10 ° min^{-1}, under a nitrogen atmosphere. The DSC curves of the synthesized PU samples obtained during the first and second heating runs are shown in Fig. 4. The broad endothermic peak around 150 °C, observed in the DSC curves during the first heating run, corresponds to H-bond interactions in PU samples.[2] This peak was absent in the curve obtained during the second heating run, indicating that the samples were completely cured. As a result, the T_g values of the polyurethane samples determined in the second run were higher in comparison with those obtained in the first run. According to the literature,[13] the EO–PDMS–EO prepolymer exhibits two T_gs, at –105 and –8 °C, while the T_g of BH-30 is 31 °C.[31] The T_g values of the PUs synthesized in this work, determined during the second heating run, were in the range from 50 to 58 °C (Table II). The obtained results show that the T_g values of these PU samples depended on the hard segment (MDI and BH-30) content. As the content of hard segments increased, the values of the T_g also increased, except for the last sample in PU series (sample PU3-15). The increase of T_g is due to the higher crosslink density of PUs. Crystallization or melt peaks were not observed for any of the samples.

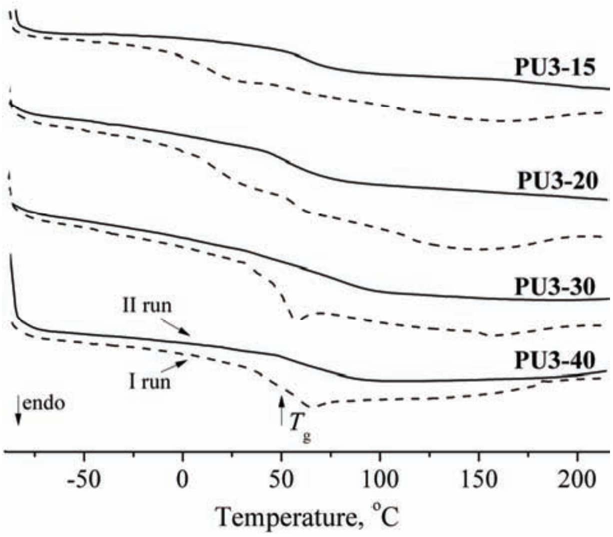

Fig. 4. DSC Thermograms of the synthesized polyurethane samples obtained during the first and second heating run.

The thermal stability of the synthesized PU samples was investigated by thermogravimetric (TG) analysis at heating rate of 10 °C min^{-1} under a dynamic nitrogen atmosphere. The recorded TG curves and the differential TG (DTG) curves for selected PU networks presented in Fig. 5, while some characteristic temperatures of thermal degradation and the temperatures corresponding to the DTG peaks are listed in Table III. From the presented results, it can be seen that weight loss of these PU networks started between 266 and 298 °C, as observed from the temperature of 15 % mass loss, and the temperature increased with increasing content of EO–PDMS–EO in the PU networks (except for the sample PU3-40). From Fig. 5 it is not possible to observe any specific trend in the thermal stability of the synthesized PU network between the temperatures corresponding to 15 and 50 % of weight loss. In the very short temperature range, between temperatures, which correspond to the 50 and 70 % of weight loss, thermal stability of PU samples increases with increasing crosslink density, which is in accordance with results given in the literature.[20,21] However, at higher temperatures, thermal stability increased with increasing soft segment content. From the obtained results, it can be concluded that mechanism of the thermal degradation of the synthesized PU samples is very complex and influenced by the soft EO–PDMS–EO content, *i.e.*, the crosslink density.

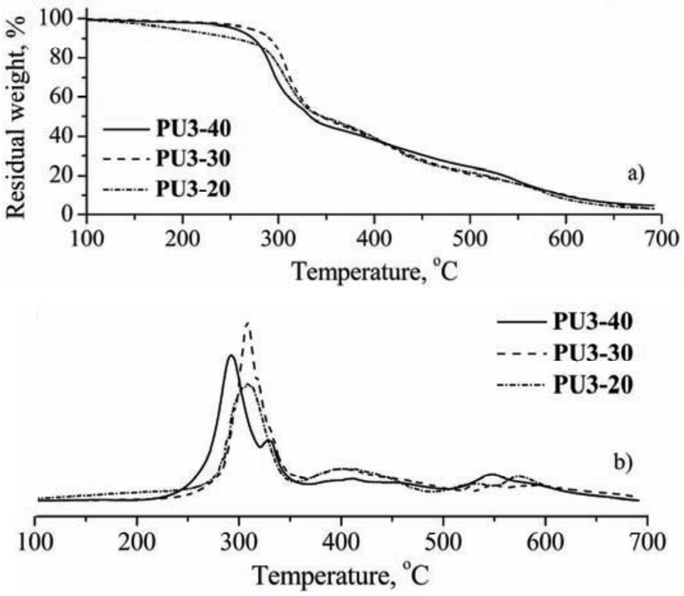

Fig. 5. TG and DTG Curves of the synthesized PU samples, determined at a heating rate of 10 °C min^{-1}, under a nitrogen atmosphere.

TABLE III. Characteristic temperatures of thermal degradation and temperatures of DTG peaks

Sample	$T_{15\%}$ / °C	$T_{50\%}$ / °C	$T_{70\%}$ / °C	$T_{95\%}$ / °C	T_{max} / °C
PU3-40	283	333	453	673	292/329/412/548
PU3-30	298	344	439	654	308/318/403/565
PU3-20	285	345	434	635	305/309/404/550
PU3-15	266	337	425	640	305/318/401/561

From the DTG curves presented in Fig. 5 and results listed in Table III, it could be concluded that thermal degradation of the synthesized PU networks is a four-step process in nitrogen. During the first step of the thermal degradation, urethane bonds, which are thermally the weakest links in the PU samples, decomposed, resulting in the dissociation to the original macrodiol and isocyanate, the formation of a primary or secondary amine, an alkene and carbon dioxide.[32] During the second step of the thermal degradation, the ester components decomposed, while PDMS degraded in the third step. Aromatic compounds decomposed in the temperature region 500–600 °C (Table III).

WAXS Analysis of the synthesized polyurethane networks

The X-ray diffractograms of the synthesized PU samples are given in Fig. 6. All diffractograms contain two amorphous halos at $2\theta = 12°$, arising from the phase-separated PDMS segments, and at $2\theta = 20°$, arising from the non PDMS-containing segments, *i.e.*, MDI and BH-30.[33] This behavior demonstrates that the

PDMS formed a completely separated phase in the polyurethanes at room temperature. There was no evidence of any crystallinity from WAXS analysis, which is consistent with the data obtained by DSC.

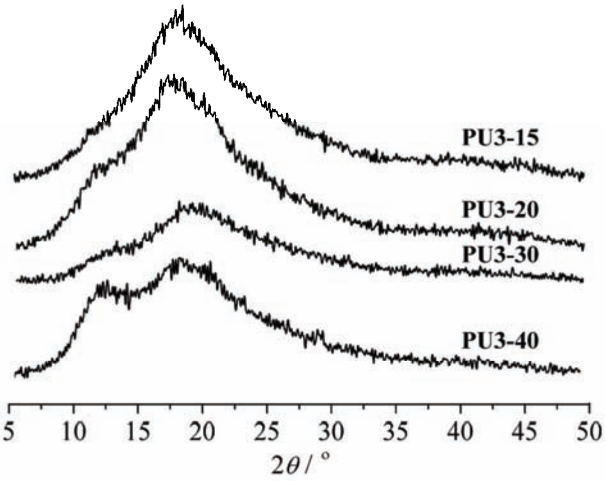

Fig. 6. X-Ray diffractograms of the synthesized polyurethane samples.

Investigation of morphology of the synthesized polyurethane networks

The surface morphology of PU films was investigated by scanning electron microscopy (SEM) and the obtained microphotographs of the PU samples are shown in Fig. 7. It is well known that polyurethanes based on PDMS show the presence of microphase-separated structures because of the large differences between solubility parameters of PDMS and the urethane components.[33] From the obtained results, it could be concluded that the surface morphology of the PU samples based on EO–PDMS–EO and the hyperbranched polyester is quite complex and significantly affected by the content of EO–PDMS–EO and the crosslink density. The SEM microphotographs showed that the hard domains had some physical associations/connectivity (hydrogen bonding) with each other, an effect that is thought to become more pronounced on the surface of the sample PU3-40. Furthermore, the SEM results of the samples PU3-30 and PU3-15 indicated increased homogeneity of the samples and improved compatibility of all components (Fig. 7). Therefore, the general view of the surface revealed a homogeneous structure, characteristic of the synthesized crosslinked polymers. The SEM results of the samples indicated increased phase mixing with increasing crosslink density of PUs.

The EDX analysis, performed to identify the type of the atoms present in the polyurethane samples at a depth of 100–1000 nm from the surface,[22] confirmed the presence of all expected elements (C, O, Si and N). The results obtained from

EDX analysis are displayed in Fig. 8 and tabulated in Table IV. It could be noticed that the N-percentage determined by EDX analysis on the surface of samples decreased with increasing EO–PDMS–EO content, *i.e.*, with decreasing urethane content. On the other hand, Si-percentage on the surface of samples increased with increasing of EO–PDMS–EO content. This suggests that there is increased content of PDMS on the surface of the PU samples, which confirms the tendency of PDMS to migrate to the surface of PU networks. Additional confirmation of this conclusion was obtained from theoretically calculated Si wt. % in the synthesized samples (from 4.54 for PU3-15 to 12.15 wt. % for PU3-40), which were smaller than the values experimentally determined by EDX surface analysis. These results are in agreement with data obtained by water contact angle measurements of the PU samples.

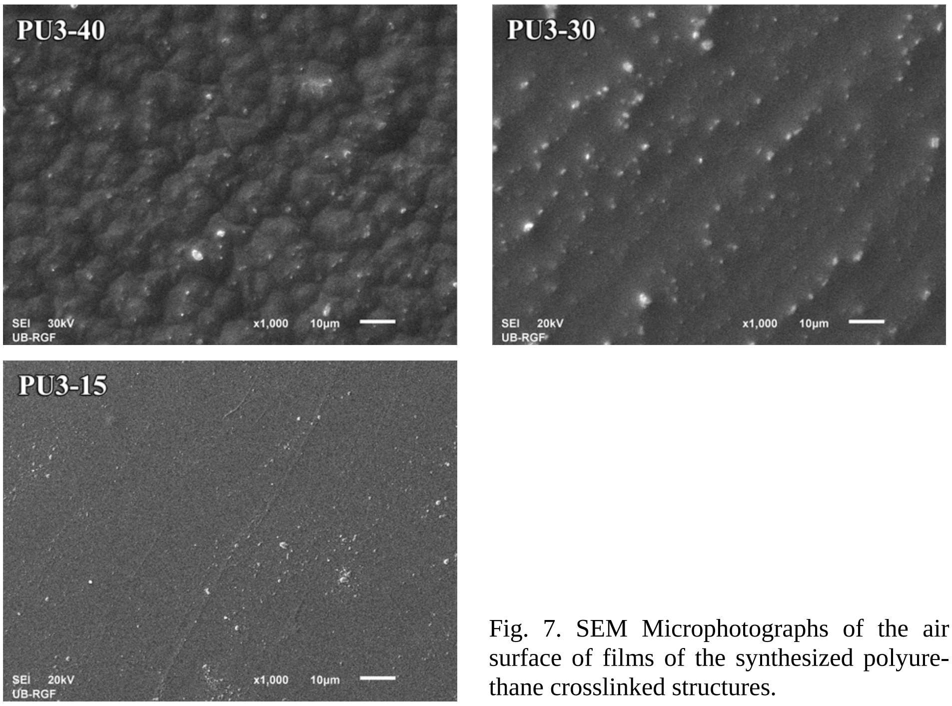

Fig. 7. SEM Microphotographs of the air surface of films of the synthesized polyurethane crosslinked structures.

Water contact angle of the synthesized polyurethane networks

The wettability and hydrophobicity of the surface of the synthesized PU samples were investigated by static water contact angle measurements and the obtained results are reported in Table II. Samples that have a water contact angle greater than 90° are considered hydrophobic. The value of the water contact angle for the PU networks increased from 86.6 to 93.9° with increasing content of EO–PDMS–EO in the polymers. This behavior may be ascribed to a tendency of the PDMS segments to migrate to the surface caused by the very low surface energy of PDMS, which hence covered most of the surface of the Pus, which resulted in a reduction of the surface tension. As expected, the wettability of the polyurethane networks decreased, *i.e.*, the hydrophobicity increased, with increasing weight fraction of EO–PDMS–EO.

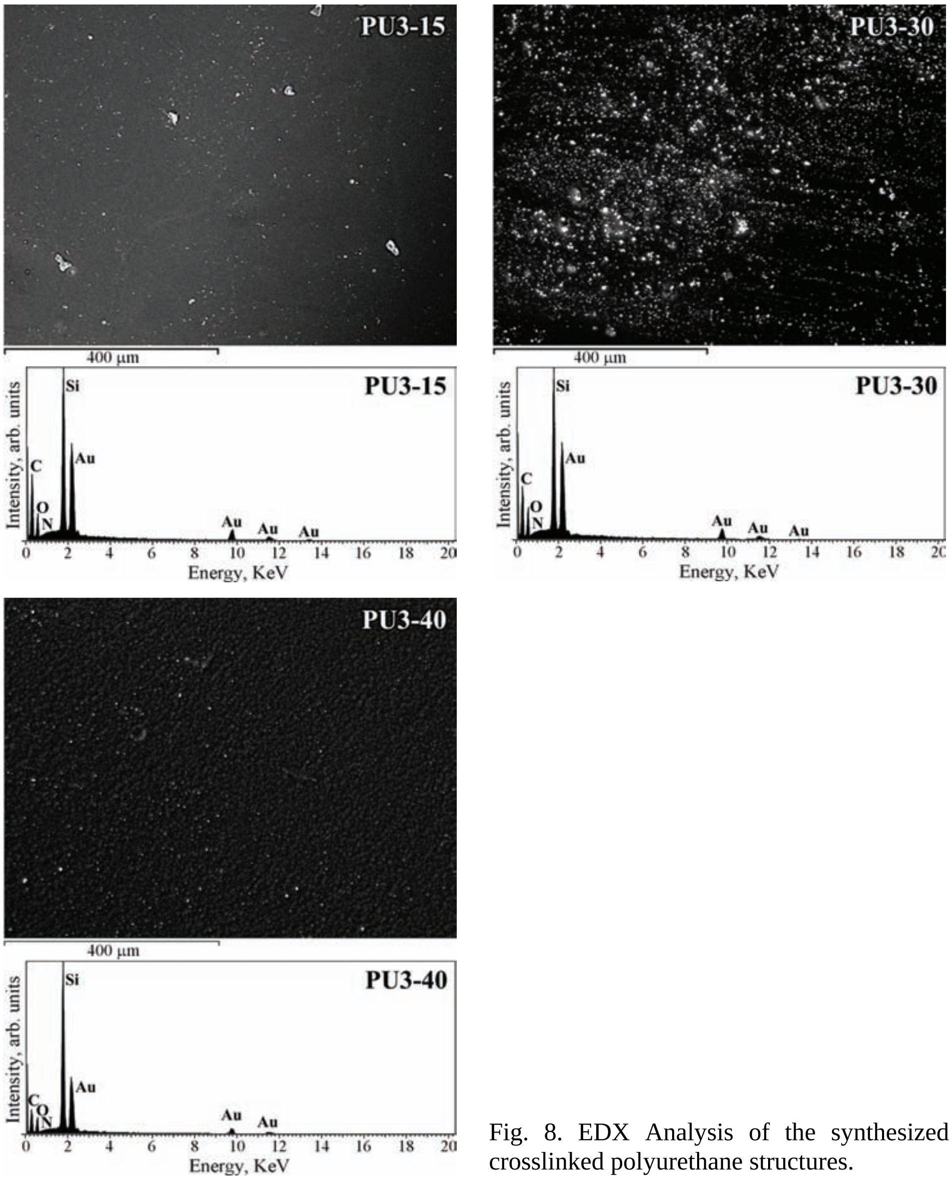

Fig. 8. EDX Analysis of the synthesized crosslinked polyurethane structures.

In comparison with the PUs based on BH-30 prepared by other authors, the PU networks synthesized in this study had a similar crosslink density.[21] In addition, the thermal stability of the synthesized PU networks was similar to the thermal stability of other PU networks based on PDMS[34] and slightly higher than the thermal stability of some PUs based on HBP.[35] In addition, a good waterproof performance of the synthesized PUs was obtained, which could be improved by increasing the EO–PDMS–EO content.

TABLE IV. Results of EDX analysis of the synthesized PUs

Element	PU3-15		PU3-30		PU3-40	
	wt. %	at. %	wt. %	at. %	wt. %	at. %
C K	60.34	69.72	54.56	60.77	52.63	63.64
N K	6.89	6.97	5.03	5.24	4.63	4.81
O K	23.36	18.69	27.25	27.46	24.19	21.96
Si K	9.41	4.62	13.28	6.53	18.55	9.59

CONCLUSIONS

Two-stage, step-growth polymerization in solution was used to prepare novel poly(urethane–siloxane) crosslinked structures based on a hyperbranched polyester of the third pseudo generation. In the first stage, 4,4'-methylenediphenyl diisocyanate was reacted with α,ω-dihydroxy-(ethylene oxide–poly(dimethylsiloxane)–ethylene oxide), which was followed by reaction of the obtained NCO-terminated prepolymer with a hydroxy-functional hyperbranched polyester in the second stage. In this manner, polyurethane crosslinked structures of different soft EO–PDMS–EO segment contents (15–40 wt. %) were synthesized. The formation of the expected structures was verified by FTIR spectroscopy. The influence of the EO–PDMS–EO content on some properties of the obtained polyurethane networks was investigated by DSC, WAXS, TGA, SEM, swelling measurements, as well as hardness and water contact angle measurements. The swelling behavior showed that the crosslink density of the polyurethane samples was enhanced by decreasing the EO–PDMS–EO content. The equilibrium degree of swelling of the synthesized PUs determined in toluene and in THF increased with increasing content of EO–PDMS–EO. The surface morphology of the synthesized polyurethanes, investigated by SEM analysis, revealed that phase mixing increased with the increase crosslink density of the PUs. The observed glass transition temperature of the PUs increased with decreasing EO–PDMS–EO content. Thermal stability of the synthesized PUs increased with increasing EO–PDMS–EO content at the beginning of thermal degradation. The surface of the polyurethane networks became more hydrophobic with increasing weight fraction of PDMS. Finally, it could be concluded that inclusion of the PDMS prepolymer with ethylene oxide sequences in the PUs based on hyperbranched polyester resulted in networks with good swelling behavior, thermal and surface properties in comparison to some similar PU networks presented in the literature and prepared from other types of macrodiols, which makes the synthesized PU networks good candidates for coatings, matrices for drugs encapsulation and composites.

Acknowledgement. This work was financially supported by the Ministry of Education and Science of the Republic of Serbia (Project No. 172062).

ИЗВОД

ПОЛИ(УРЕТАН-СИЛОКСАНИ) НА БАЗИ ХИПЕРРАЗГРАНАТОГ ПОЛИЕСТРА КАО УМРЕЖИВАЧА: СИНТЕЗА И КАРАКТЕРИЗАЦИЈА

МАРИЈА В. ПЕРГАЛ[1], ЈАСНА В. ЏУНУЗОВИЋ[1], САЊА ОСТОЈИЋ[2], МИОДРАГ М. ПЕРГАЛ[3], АЛЕКСАНДРА РАДУЛОВИЋ[2] и СЛОБОДАН ЈОВАНОВИЋ[4]

[1]Универзитет у Београду, Институт за хемију, технологију и металургију, Студентски трг 12–16, 11000 Београд, [2]Универзитет у Београду, Институт за општу и физичку хемију, Студентски трг 12–16, 11000 Београд, [3]Универзитет у Београду, Хемијски факултет, Студентски трг 12–16, 11000 Београд и [4]Универзитет у Београду, Технолошко–металуршки факултет, Карнегијева 4, 11000Београд

У овом раду приказана је синтеза, структура и нека својства нових умрежених полиуретана припремљених полазећи од α,ω-дихидрокси-(етиленоксид–поли(диметилсилоксан)––етиленоксид) претполимера (EO–PDMS–EO), 4,4’-метилендифенилдиизоцијаната и Boltorn® хиперразгранатог полиестра треће псеудо-генерације. Хиперразгранати хидрокси функционални алифатски полиестар са 26 крајњих група служио је као умрежавајући агенс при синтези полиуретана. У циљу побољшања компатибилности реактаната током синтезе, полиуретани су синтетисани двостепеном полимеризацијом у раствору. Садржај меког EO–PDMS–EO сегмента вариран је у опсегу од 15 до 40 мас. %. Испитан је утицај EO–PDMS–EO садржаја на понашање при бубрењу, густину умрежавања, тврдоћу, термичка и површинска својства синтетисаних полиуретана. Структура синтетисаних полиуретана потврђена је FTIR спектроскопијом. Понашање при бубрењу је испитивано како би се одредила густина умрежавања и показано је да полиуретанске мреже са нижим EO–PDMS–EO садржајем имају већу густину умрежавања. Резултати диференцијалне скенирајуће калориметрије показали су повећање температуре остакљивања полиуретана од 50 до 58 °C са смањењем EO–PDMS–EO садржаја као последицу веће густине умрежености узорака. Синтетисани полиуретани са већим садржајем EO–PDMS–EO сегмената показују бољу термичку стабилност, што је потврђено порастом почетне температуре деградације, одређене TG анализом. Хидрофобност површине полиуретана је расла са повећањем садржаја EO–PDMS–EO у одговарајућем узорку. Површинска морфологија синтетисаних полиуретана је анализирана скенирајућом електронском микроскопијом.

(Примљено 13. октобра, ревидирано 28. децембра 2011)

REFERENCES

1. D. K. Chattopadhyay, K. V. S. N. Raju, *Prog. Polym. Sci.* **32** (2007) 352
2. E. Žagar, M. Žigon, *Prog. Polym. Sci.* **36** (2011) 53
3. X. Zhang, *Polym. Int.* **60** (2011) 153
4. P. Kolhe, E. Misra, R. M. Kannan, S. Kannan, M. Lieh-Lai, *Int. J. Pharm.* **259** (2003) 143
5. Z. S. Petrović, J. Ferguson, *Prog. Polym. Sci.* **16** (1991) 695

6. P. Czech, L. Okrasa, G. Boiteux, F. Méchin, J. Ulanski, *J. Non-Cryst. Solids* **351** (2005) 2735
7. J. Dodge, *Polyurethanes and polyureas*, in *Synthesis Methods in Step-Growth Polymers*, M. E. Rogers, T. E. Long, Eds., Wiley, Hoboken, NJ, 2003, Ch. 4, p. 197–214
8. R. W. Hergenrother, Y. Xue-Hai, S. L. Cooper, *Biomaterials* **15** (1994) 635
9. D. J. Martin, G. F. Meijs, P. A. Gunatillake, S. P. Yozghatlian, G. M. Renwick, *J. Appl. Polym. Sci.* **71** (1999) 937
10. İ. Yilgör, J. McGrath, *Adv. Polym Sci.* **86** (1988) 1
11. A. Simmons, J. Hyvarinen, L. Poole-Warren, *Biomaterials* **27** (2006) 4484
12. P. A. Gunatillake, G. F. Meijs, S. J. McCarthy, R. Adhikari, *J. Appl. Polym. Sci.* **76** (2000) 2026
13. R. Hernandez, J. Weksler, A. Padsalgikar, T. Choi, E. Angelo, J. S. Lin, L.-C. Xu, C. A. Siedlecki, J. Runt, *Macromolecules* **41** (2008) 9767
14. J. P. Sheth, E. Yilgor, B. Erenturk, H. Ozhalici, I. Yilgor, G. L. Wilkes, *Polymer* **46** (2005) 8185
15. T. Choi, K. A. Masser, E. Moore, J. Weksler, A. Padsalgikar, J. Runt, *J. Polym. Sci.,B* **49** (2011) 865
16. M. V. Pergal, V. V. Antic, M. N. Govedarica, D. Gođevac, S. Ostojić, J. Djonlagic, *J. Appl. Polym. Sci.* **122** (2011) 2715
17. M. V. Pergal, V. V. Antić, G. Tovilović, J. Nestorov, D. Vasiljević-Radović, J. Djonlagić, *J. Biomat. Sci.: Polym. E.* (2011) 1, Article in Press, doi: 10.1163/092050611X589338
18. P. Czech, L. Okrasa, F. Méchin, G. Boiteux, J. Ulanski, *Polymer* **47** (2006) 7207
19. L. Okrasa, P. Czech, G. Boiteux, F. Méchin, J. Ulanski, *Polymer* **49** (2008) 2662
20. Q. Cao, P. Liu, *Eur. Polym. J.* **42** (2006) 2931
21. P. K. Maji, A. K. Bhowmick, *J. Polym. Sci., A* **47** (2009) 731
22. M. Alexandru, M. Cazacu, M. Cristea, A. Nistor, C. Grigoras, B. C. Simionescu, *J. Polym. Sci., A* **49** (2011) 1708
23. M. V. Vuckovic, V. V. Antic, M. N. Govedarica, J. Djonlagic, *J. Appl. Polym. Sci.* **115**, (2010) 3205
24. E. Malmström, M. Johansson, A. Hult, *Macromolecules* **28** (1995) 1698
25. J. Vuković, S. Jovanović, M. D. Lechner, V. Vodnik, Synthesis and molecular structure investigation of aliphatic hyperbranched polyesters, in Modern Trends in Macromolecular Chemistry, J. N. Lee, Ed., Nova Science Publishers, New York, 2009, pp. 39–59.
26. A. Marand, J. Dahlin, D. Karlsson, G. Skarping, M. Dalene, *J. Environ. Monit.* **6** (2004) 606
27. P. J. Flory, J. H. Rehner, *J. Chem. Phys.* **11** (1943) 521
28. E. A. Grulke, *Solubility parameter values*, in *Polymer Handbook*, 3rd ed., J. Brandrup, E. H. Immergut, Eds., Wiley, New York, 1989, Ch. 7, p. 519–559
29. D. Fleischer, *Physical Constants of the most common solvents*, in *Polymer Handbook*, 3rd ed., J. Brandrup, E. H. Immergut, Eds., Wiley, New York, 1989, Ch. 3, p. 29
30. J. Vuković, M. Pergal, S. Jovanović, V. Vodnik, *Hem. Ind.* **62** (2008) 353
31. J. Vuković, S. Jovanović, M. D. Lechner, V. Vodnik, *J. Appl. Polym. Sci.* **112** (2009) 2925
32. D. K. Chattopadhyay, D. C. Webster, *Prog. Polym. Sci.* **34** (2009) 1068
33. T. Choi, J. Weksler, A. Padsalgikar, J. Runt, *Polymer* **50** (2009) 2320
34. H. D. Hwang, H. J. Kim, *React. Funct. Polym.* **71** (2011) 655
35. A. Asif, W. Shi, X. Shen, K. Nie, *Polymer* **46** (2005) 11066.

Journal of the Serbian Chemical Society
JSCS-info@shd.org.rs • www.shd.org.rs/JSCS

J. Serb. Chem. Soc. 77 (7) 937–944 (2012)
JSCS–4322

UDC 66.017:510.644:669.14:669–122
Original scientific paper

Application of a Bayesian Artificial Neural Network and the Reversible Jump Markov Chain Monte Carlo Method to predict the grain size of hot strip low carbon steels

MOHSEN BOTLANI-ESFAHANI[1]* and MOHAMMAD REZA TOROGHINEJAD[2]

[1]*Department of Materials Engineering, Lenjan Branch, Islamic Azad University, Isfahan, Iran and* [2]*Department of Materials Engineering, Isfahan University of Technology, Isfahan, 84156-83111, Iran*

(Received 11 November 2011, revised 31 January 2012)

Abstract: An Artificial Neural Network (ANN) with Reversible Jump Markov Chain Monte Carlo (RJMCMC) simulation was used to predict the grain size of hot strip low carbon steels, as a function of steel composition. The results show good agreement with experimental data taken from the Mobarakeh Steel Company (MSC). The developed model is capable of recognizing the role and importance of elements in grain refinement. Furthermore, the effects of these elements, including manganese, silicon and vanadium, were investigated in the present study, which were in good agreement with the literature.

Keywords: artificial neural network; grain size; hot strip; low carbon steel.

INTRODUCTION

Grain size is an important aspect of microstructure with respect to mechanical properties of steels. The ferrite in low carbon steels is typically strengthened by grain refinement, precipitation hardening, and, to a lesser extent, solid-solution strengthening. Grain refinement is the most desirable strengthening mechanism because it improves not only strength but also toughness.[1] According to Equation (1), indicating the Hall–Petch Relation, fine grain sizes produce higher yield strengths, (σ_{yield}):[2]

$$\sigma_{\text{yield}} = \sigma_{\text{init}} + k_{\text{y}} d_{\alpha}^{-1/2} \tag{1}$$

where σ_{init} is the yield strength for a polycrystalline material, k_{y} is a constant and d_{α} is a measure of the ferrite grain size. Grain size also has an effect on the ultimate tensile strength by changing the work-hardening rate. Work-hardening occurs within the grains during plastic deformation according to Morrison:[3]

---

* Corresponding author. E-mail: botlani@iauln.ac.ir
doi: 10.2298/JSC111115011B

$$n = 5/(10 + d_\alpha^{-1/2}) \tag{2}$$

where n is work-hardening exponent and d_α is the grain size.

The main purpose of hot stripping is to refine the microstructure of steels, thereby enhancing both strength and toughness.[4] Ferrite mainly nucleates at the austenite grain boundaries and thus finer austenite grains results in finer ferrite grains. Further ferrite refinement could be achieved by transformation from deformed austenite grains because deformation increases the ferrite nucleation rate.[2]

Precise prediction of grain size and properties of hot stripped steel products depends on the thermo-mechanical behavior of the steel, microstructure evolution and phase transformation during hot rolling stages and the cooling period. These are complicated metallurgical phenomena and strongly depend on chemical composition, therefore development of a physical model to analysis these parameters and predict the final grain size is cumbersome. In addition, the accuracies of the hitherto developed models are somehow questionable and not suitable for practical purposes. On the other hand, estimating the final grain size of low carbon steel strips in terms of chemical composition is desirable from an engineering viewpoint. In the present work, by selecting more relevant inputs and using a hybrid Bayesian Artificial Neural Network (ANN) Model assisted with the Reversible Jump Markov Chain Monte Carlo (RJMCMC) Method, the final grain size in low carbon steel strips was predicted.

METHODS

Artificial Neural Network (ANN)

An artificial neural network model maps sets of input data onto a set of appropriate output data. It is a modification of the standard linear perceptron in that, it uses three or more layers of neurons with nonlinear activation functions. This makes it more powerful than the perceptron, and can distinguish data that is not linearly separable.[5] The basic ANN Model with k outputs is:

$$f_k(X,W) = w_{k_0} + \sum_{j=1}^{m} w_{kj} \tanh(w_{j_0} + \sum_{i=1}^{d} w_{ji} x_i) \tag{3}$$

where X is a d-dimensional input vector, W denotes the weights, and the indices i and j correspond to the input and hidden units, respectively.[6] The schematic architecture of an ANN Model is sketched in Fig. 1.

Traditionally, the complexity of an ANN is controlled with early stopping, whereby part of the data is used to train the network and the other part is used to control the complexity of the model.

Bayesian learning for an ANN

Early stopping is inefficient because the effective complexity may be much less than the number of parameters in the model. Within the Bayesian framework, the weights of the network are considered as random variables and the posterior distribution of the weights updated according to the Bayes' Rule:[7]

$$\text{Posterior}=\frac{\text{Likelihood}\times\text{Prior}}{\text{Evidence}} \tag{4}$$

This equation in terms of Artificial Neural Networks is:

$$p(\theta|D)=\frac{p(D|\theta)\,p(\theta)}{p(D)}\propto L(\theta|D)\,p(\theta) \tag{5}$$

where $p(\theta)$ is the prior distribution for the model parameters θ, $D = \{(\mathbf{x}^{(1)},\mathbf{y}^{(1)}),\ldots,(\mathbf{x}^{(n)},\mathbf{y}^{(n)})\}$ is the observed data and $L(\theta|D)$ is the likelihood function that gives the probability of the observed data as a function of the unknown model parameters.[6]

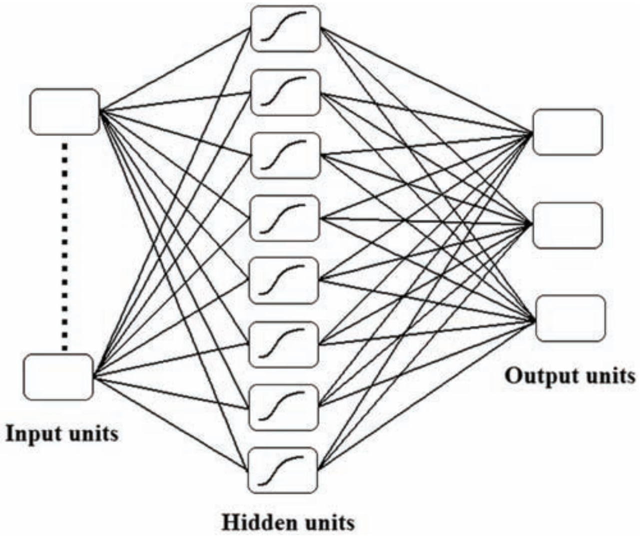

Fig. 1. Schematic structure of the ANN Model.

Reversible Jump Markov Chain Monte Carlo Method

Neal introduced an implementation of Bayesian learning for an ANN in which difficult integrations accompanied within this framework were performed using the Markov Chain Monte Carlo (MCMC) Method. In this application, samples (in model parameters space) are generated using the Markov Chain Monte Carlo Method to estimate the desired posterior distributions.[6]

In practical problems, as in the present study, it is usual to measure many variables, but it is not necessarily known which one of them is relevant and is required to solve the problem. To make the model more explainable or to reduce the measurement cost and computation time, it may be useful to select a model with a smaller set of input variables.[6] Consequently, the RJMCMC method is applied for this modeling. This algorithm allows jumps between models with different dimensional parameter spaces with respect to the number of inputs chosen in the model. The RJMCMC visits the models according to their posterior probability, which allows it to be used for model selection.[8]

Modeling database

Since an ANN Model is empirical, its performance depends on the dataset used for training. In this research, the data was taken from the Mobarakeh Steel Company (MSC) and consisted of 624 metallographic images. At this company, these images were classified into three groups according to ASTM (E-112), a standard that assigns larger numbers to finer grain structures. An example of such a database is shown in Fig. 2. Further information is also given in Table. I. The input parameters are chemical composition of the strips, which includes 14 elements. Additional input variables are given in Table. II.

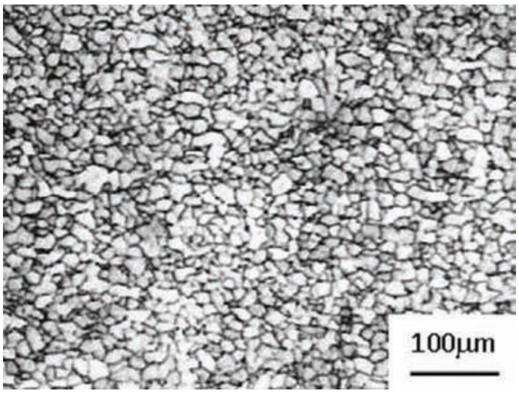

Fig. 2. One sample of data, microstructure of a produced steel with ASTM grain size No. 9.0.

TABLE I. Output data information

Number of samples	ASTM (E-112) grain No.
162	8.5
294	9
167	9.5

Model training

The modeling database was divided into training and test sets, which included 60 % and 40 % of the data, respectively. Training was started with a (14–8–3) architecture and model selection procedure was evaluated by an internal procedure of the RJMCMC algorithm, as mentioned above. The result of this training indicated a chain of network parameters. When this chain converged into a stable distribution, a sample of the chain (network parameters) was selected based on the minimum classification error of the model on the test dataset. This modeling was implemented by MCMC methods for Multilayer Perceptron (MLP) Network and Gaussian Process (GP).*

RESULTS AND DISCUSSION

Performance of the model

Calculation of the misclassification error on test data is a popular way to show the prediction accuracy (generalization) of a classifier model. This error is calculated according to:

---

* www.lce.hut.fi/research/mm/mcmcstuff/

$$\text{Misclassification error}=\frac{\sum\left|\text{Test data-Model result}\right|}{\text{Number of test data}}\times 100 \qquad (6)$$

The achieved model revealed a misclassification error of just 2.439 %, which is very low and indicates that the model has good generalization. More information about the misclassified error is available in Table. III.

TABLE II. Input parameter information

No.	Inputs	Min.	Max.	Mean	*SD*
1	C / wt. %	0.032	0.179	0.1272	0.0312
2	Si / wt. %	0.008	0.218	0.0637	0.0798
3	Mn / wt. %	0.191	1.15	0.6466	0.211
4	P / wt. %	0.002	0.025	0.0072	0.0022
5	S / wt. %	0.001	0.02	0.0089	0.0029
6	Cu / wt. %	0.004	0.078	0.03	0.0109
7	Al / wt. %	0.015	0.075	0.0454	0.0119
8	N / ppm	16	75	38	8.8
9	Nb / wt. %	0	0.045	0.0051	0.0105
10	V / wt. %	0	0.011	0.003	0.0014
11	Ti / wt. %	0	0.042	0.0017	0.0031
12	Mo / wt. %	0	0.019	0.0038	0.0045
13	Cr / wt. %	0.004	0.194	0.0131	0.012
14	Ni / wt. %	0.02	0.042	0.03	0.0034

TABLE III. Misclassified case for the number of misclassified 2

Test target data	Model result
9	8.5
9.5	9

Model results

As mentioned, the RJMCMC method can select potentially useful inputs according to the marginal probabilities of the inputs. The result of this analysis indicated the importance of the contents of Si, Mn and C on grain refinement, which were significantly greater than the concentrations of other elements. The most effective element for grain refinement was recognized to be that of vanadium. However, its concentration in these steels was very low.

For testing, the results of the model are depicted when the concentrations of elements are on their mean values, which are given in Table II and the micro-alloying elements (*i.e.*, Nb, Ti and V) are not present. The model result of this analysis is shown in Fig. 3. Manganese stabilizes austenite, therefore decreases the austenite to ferrite transformation temperature and hence refines the grain structure. In addition, manganese can enhance the precipitation strengthening of the vanadium micro-alloyed steels and to a lesser extent, niobium micro-alloyed steels.[1]

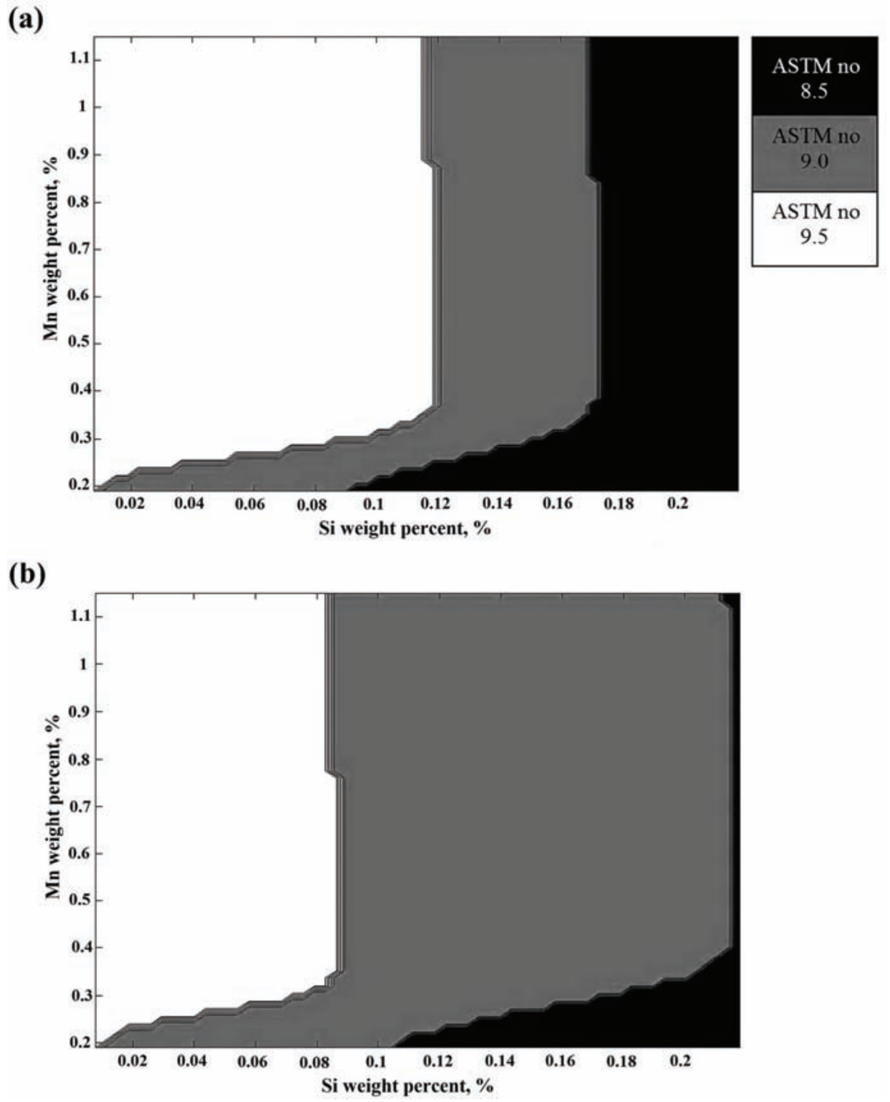

Fig. 3. Model results in respect to the silicon and manganese concentration in 0.015 wt. % C and 0.035 wt. % Al. a) Absence of micro-alloying elements (Nb, V and Ti). b) Minor addition of vanadium (0.008 wt. %) in the absence of the other micro-alloying elements (Nb and Ti).

Fig. 3a reveals the determining role of silicon on grain size in the absence of micro-alloying elements (*i.e.*, Nb, Ti and V). The figure shows that the silicon concentration divides the figure into three regions, including finer, mild and coarser grain structures. This figure also indicates that increasing Si content increases the grain size. This is because silicon is a ferrite stabilizer and promotes ferrite grain growth.[9] Fig. 3b shows that addition of small amount of vanadium, 0.008 wt. %, to steel severely contracts the coarser grain region. Vanadium acts as a scavenger for oxides, and forms nano-scale inter-phase precipitations. This is mainly due to the rapid rate of the austenite to ferrite transformation, which produces these nano-scale precipitates.[10] Furthermore, the addition of vanadium also reduces the finer grain area somewhat. This is because vanadium is strong carbide former and as the majority of such elements are ferrite stabilizers, it therefore promotes ferrite grain growth.[11] The net effect of this minor vanadium addition is to decrease the sensitivity of the grain size to the silicon content, and also reduction of coarse grain area.

CONCLUSIONS

A Bayesian ANN Model assisted by RJMCMC is capable of predicting the grain size of hot strip low carbon steels and can be used as a function of steel composition. The results are shown to be consistent with experimental data (acquired from Mobarakeh Steel Company data). Furthermore, the model recognizes the effects of relevant elements in grain refining. These are manganese, silicon and vanadium. The silicon concentration has a determining role, this effect has not been reported in the literature, and vanadium has a great impact on grain refining phenomena. The major advantage of this method, which was validated by literature in the present research, is the selection of useful inputs in complex problems with many inputs. As many problems in materials science and engineering are similar, this method could be useful for solving them.

Acknowledgment. . The authors wish to thank, Lenjan Branch, Islamic Azad University, and the Iranian Nanotechnology Initiative Council (INIC) for their supports as well as Isfahan Mobarakeh Steel Company for supplying experimental data.

ИЗВОД

ПРИМЕНА БАЈЕСОВИХ ВЕШТАЧКИХ НЕУРОНСКИХ МРЕЖА (ANN) И РЕВЕРЗИБИЛНЕ МОНТЕ КАРЛО МЕТОДЕ НА БАЗИ МАРКОВЉЕВИХ ЛАНАЦА (RJMCMC) ЗА ПРЕДВИЂАЊЕ ВЕЛИЧИНА ЗРНА У ТОПЛО ВАЉАНИМ ТРАКАМА ОД НИСКО УГЉЕНИЧНОГ ЧЕЛИКА

MOHSEN BOTLANI-ESFAHANI[1] и MOHAMMAD REZA TOROGHINEJAD[2]

[1]*Department of Materials Engineering, Lenjan Branch, Islamic Azad University, Isfahan, Iran* и [2]*Department of Materials Engineering, Isfahan University of Technology, Isfahan, 84156-83111, Iran*

Вештачке неуронске мреже (ANN) и реверзибилна Монте Карло Метода на бази Марковљевих ланаца (RJMCMC) су коришћени да би се предвидела величина зрна топло ваљаних трака од ниско-угљеничног челика у функцији њиховог састава. Резултати показују добро слагање са експерименталним подацима добијеним у *Mobarakeh* фабрици за производњу челика (MSC). Развијени модел има могућност идентификовања улоге и важности елемената за рафинацију зрна. Поред тога, ефекти ових елементата, укључујући манган, силицијум и ванадијум, су испитивани у овом раду и показују добру сагласност са подацима из литературе.

(Примљено 11. новембра 2011, ревидирано 31. јануара 2012)

REFERENCES

1. Keytosteel.com, *Control of high strength low alloy (HSLA) steel properties*, http:// //www.keytosteel.com (accessed in 2010)
2. S. V. Parker, *PhD Thesis*, University of Cambridge, UK, 1997
3. J. Ryu, *M. Sc. Thesis*, Pohang University of Science and Technology, Korea, 2008
4. I. Tamura, C. Ouchi, T. Tanaka, H. Sekine, *Thermomechanical processing of high strength low alloy steels*, Butterworth,London, UK, 1988
5. S. Haykin, *Neural networks: a comprehensive foundation*, 2nd ed., Prentice Hall International, Upper Saddle River, NJ, 1998
6. J. Lampinen, A. Vehtari, *Applied Computational Intelligence to Engineering and Business* , K. Wang, J Grundespenkis, A. Yerofeyev, Eds., Riga Technical University, Latvia, 2001, p. 7
7. M. Xu, G. Zeng, X. Xu, G. Huang, R. Jiang, W. Sun, *Water Air Soil Pollut.* **172** (2006) 167
8. A. Vehtari, J. Lampinen, *Neural Comput.* **14** (2002) 2439.
9. M. Umemoto, Z. G. Liu, K. Masuyama, K. Tsuchiya, *Sci. Mater*. **45** (2001) 391
10. H. K. D. H. Bhadeshia, R. W. K. Honeycombe, *Steels Microstructure and Properties*, 3rd ed., Elsevier, Oxford, UK, 2006
11. Y.-B. Zhang, D. Y. Ren, *Mater. Sci. Technol*. **19** (2003) 1029.

Journal of the Serbian Chemical Society
JSCS-info@shd.org.rs • www.shd.org.rs/JSCS

J. Serb. Chem. Soc. 77 (7) 945–957 (2012)
JSCS–4323

UDC 533.6.011+537.872:519.6:536.7
Original scientific paper

Numerical analysis and field study of the time-dependent exergy–energy of a gas–steam combined cycle

BAMDAD BARARI[1]*, ASHKAN ABBASIAN SHIRAZI[1], MOHSEN KESHAVARZI[1]
and IMAN ROSTAMSOWLAT[2]

[1]Mechanical Engineering Department, Shiraz University, Shiraz, Iran and [2]Mechanical Engineering Department, Islamic Azad University, Kazeroon branch, Kazeroon, Iran

(Received 8 July 2011, revised 9 February 2012)

Abstract: In this study, a time-dependent exergy analysis of the Fars Combined Power Plant Cycle was considered. The exergy analysis was used to investigate each part of the actual combined cycle by considering irreversibility from April 2006 to October 2010. Performance analysis was performed for each part by evaluating the exergy destruction in each month. By use of the exergy analysis, the aging of each part was evaluated with respect to time. In addition, the rate of lost work for each month was calculated and the variation of this parameter was considered as a function of aging rate. Finally, the effect of exergy destruction of each part on the exergy destruction of the whole cycle was investigated. The entire analysis was realized for Unit 3 and 4 of the gas turbine cycle that combine with Unit B of the steam cycle in the Fars Combined Power Plant Cycle located in the Fars Province in Iran.

Keywords: exergy analysis; exergy loss; combined power plant.

INTRODUCTION

The rapid improvement of gas turbine technology in the 1990s drove combined cycle thermal efficiency to nearly 60 % with natural gas as the fuel[1] and it will probably go even higher in the future. This high plant efficiency together with low emissions, and competitive capital and running costs made combined cycle gas turbine (CCGT) plants very popular prime movers for electricity generation. This increasing interest in CCGT plants led to more consideration being devoted the behavior of a plant after long service times. As a result, simulation codes were developed to predict the behavior of such power plants and their subsystems on a thermo-fluid dynamic basis.[2,3] Even under normal engine operating conditions, with good inlet filtration systems and using clean fuel, the flow path section in the gas turbine engine will become fouled, eroded, corroded and co-

---

* Corresponding author. E-mail: barari@shirazu.ac.ir

doi: 10.2298/JSC110708014B

vered with rust scale. Any failure or malfunctioning within the gas turbine would be magnified, as it would affect two CCGT plants simultaneously. Therefore, in combined cycles in which the gas turbine is connected to another plant, such as a steam cycle, the deterioration of the performance of the gas turbine engine would be increased. Exergy analysis based on the First and Second laws of Thermodynamics are significant tools to analyze energy systems. It also reveals inefficient thermodynamic processes. On the other hand, the Second Law of Thermodynamics deals with the quality of the energy and determines the maximum amount of work obtainable from an energy resource. Exergy analysis is performed in two main parts.[4] The first one is devoted to evaluating the system and determining inefficient processes based on exergy destruction calculations and the second one is based on making some changes and corrections in the processes based on avoidable and unavoidable exergy destructions. Exergy is defined as the maximum theoretical useful work that can be obtained as a system interacts with an equilibrium state. Exergy is generally not conserved like energy but is destroyed in the system. Exergy calculation shows the place in the system where losses occur and the magnitude of these losses. Exergy efficiency of a combined cycle power plant is usually lower than the thermal efficiency of the same plant.

In 1960, a primitive investigation of a combined cycle power plant was performed by Sieppel and Bereuter.[5] Czermak and Wunsch made a thermodynamic analysis of an actual combined power plant.[6] Wunsch mentioned that the efficiency of a combined cycle power plant is more related to the gas turbine parameters, such as maximum temperature and pressure ratio, than to the steam cycle parameters. Khaliq and Kaushik made a Second Law (exergy) analysis of a Rankine–Brayton cycle with a pre-heater. They also derived some correlation for the First and Second Law efficiency of the entire cycle and the exergy destruction for each part.[7] Ramaprabhu studied a computational model of a combined cycle power plant with an inlet air conditioning (fogging) system and applied it to an actual cycle in Arizona, USA.[8] Arrieta *et al*. investigated an actual combined cycle in Brazil and revealed that the ambient temperature, atmospheric pressure and air humidity have significant effects on the performance of a combined cycle.[9]

Cihan[10] used an exergy and energy analysis for a combined cycle power plant and reported that the combustion chambers, gas turbines and HRSG account for more than 85 % of the exergy losses. Sue and Chuang[11] performed a First and Second Law analysis of a combined cycle power plant with and without cogeneration using dual pressure HRSGs, turbine inlet air-cooling, absorption chilling and fuel gas preheating. Khaliq and Kaushik[12] investigated the effects of the steam pressure and pinch point in a gas turbine cogeneration system and reported higher First and Second Law efficiencies with reheat. The effect of reheat and intercooling on Second Law performance of a gas turbine cogeneration system has not received much attention in the literature, which was also registered by Khaliq and Kaushik. According to them, energy-based performance analyses are often misleading as they fail to identify the deviation from ideality. Ganapathy *et al*. performed an exergy and energy analysis for investigating a 50 MW steam cycle with coal as the fuel and declared that the energy assessment must be made through the energy quantity as well as the quality.[13] Erdem analyzed comparatively the performance of thermal power plants from an exergetic and energetic viewpoint in Turkey. By means of exergetic and energetic analyses, the thermodynamic inefficiencies of each plant were identified.[14] Irreversibility in a combined cycle power plant may be caused by several damages, such as fouling and erosion of the gas turbine blade, fouling in the compressor, deposition in the HRSG and condenser. Several papers in which these damages in combined cycle power plants were studied are available.[15–20]

There have been several studies on degradation in combined cycle in recent years but no study has been performed on a time dependent exergy analysis with modeling of aging. The purpose of this work was the use of time dependent exergy analysis for investigating each part of the Fars combined cycle plant by considering irreversibility. In addition, performance analysis was realized for each part by evaluating the exergy destruction during April 2006 to October 2010.

THEORY AND METHOD

Exergy can be divided into four distinct components. The two important ones are physical exergy and chemical exergy. In this study, the other two components, *i.e.*, kinetic exergy and potential exergy, were assumed negligible as the elevation and speed have negligible changes. The physical exergy is defined as the maximum theoretical useful work obtained as a system interacts with an equilibrium state. The chemical exergy is associated with the departure of the chemical composition of a system from its chemical equilibrium. The chemical exergy is an important part of exergy in combustion processes. Availability for any thermodynamic state can be calculated as:

$$av_{\mathrm{i}} = h_{\mathrm{i}} - h_{\mathrm{o}} - T_{\mathrm{o}}(s_{\mathrm{i}} - s_{\mathrm{o}}) \tag{1}$$

The physical exergy for that state is:

$$\dot{E}x_{\mathrm{ph,i}} = \dot{m}_{\mathrm{i}}\, av_{\mathrm{i}} \tag{2}$$

The chemical exergy of air, fuel and exhaust gas can be written, respectively, as:

$$\dot{E}_{\mathrm{ch,air}} = \dot{m}_{\mathrm{air}}\left(\frac{\bar{R}}{M_{\mathrm{air}}}\right)T_{\mathrm{o}}\left[y_{\mathrm{O_2,air}}\ln\left(\frac{y_{\mathrm{O_2,air}}}{y^{\mathrm{e}}_{\mathrm{O_2,air}}}\right) + y_{\mathrm{N_2,air}}\ln\left(\frac{y_{\mathrm{N_2,air}}}{y^{\mathrm{e}}_{\mathrm{N_2,air}}}\right)\right] \tag{3}$$

$$\dot{E}_{\mathrm{fuel,ch}} = \left(\frac{\dot{m}_{\mathrm{fuel}}}{M_{\mathrm{CH_4}}}\right)\left[g_{\mathrm{CH_4}} + 2g_{\mathrm{O_2}} - g_{\mathrm{CO_2}} - 2g_{\mathrm{H_2O(g)}} + RT_{\mathrm{o}}\ln\left(\frac{(y^{\mathrm{e}}_{\mathrm{O_2}})^2}{y^{\mathrm{e}}_{\mathrm{CO_2}}(\mathrm{y}^{\mathrm{e}}_{\mathrm{H_2O}})^2}\right)\right] \tag{4}$$

$$\dot{E}_{\text{ch,exhaust}} = \dot{m}_{\text{exhaust}}\left(\frac{\bar{R}}{M_{\text{exhaust}}}\right)T_{\text{o}} \times$$

$$\times\left[y_{\text{CO}_2}\ln\left(\frac{y_{\text{CO}_2}}{y^{\text{e}}_{\text{CO}_2}}\right)+y_{\text{H}_2\text{O}}\ln\left(\frac{y_{\text{H}_2\text{O}}}{y^{\text{e}}_{\text{H}_2\text{O}}}\right)+y_{\text{N}_2}\ln\left(\frac{y_{\text{N}_2}}{y^{\text{e}}_{\text{N}_2}}\right)+y_{\text{O}_2}\ln\left(\frac{y_{\text{O}_2}}{y^{\text{e}}_{\text{O}_2}}\right)\right] \quad (5)$$

where y_i^{e} is the equivalent mole ratio of constitute i of a gas mixture and for air, the values are given in Table I. $\bar{R}$ is the gas constant and g_i is the Gibbs function of a gas constitute. The Gibbs function of some gases at 298 K and 1 atm are:

$$g_{\text{CH}_4} = -50790,\ g_{\text{O}_2} = 0,\ g_{\text{CO}_2} = -394380 \text{ and } g_{\text{H}_2\text{O}} = -228590$$

Table 1. Molar mass and equivalent mole ratio of air components

Product	M / g mol^{-1}	y_{e}
N_2	28.17	0.7567
O_2	32	0.2035
H_2O gas	18	0.0303
CO_2	44	0.0003

Each device in the power plant constitutes a control volume and the associated equations of energy and exergy analysis are given below:

The Continuity Equation is expressed as:

$$\sum_{\text{i}}\dot{m}_{\text{i}} = \sum_{\text{e}}\dot{m}_{\text{e}} \quad (6)$$

where $\dot{m}$ is the mass flow rate and the subscripts i and e refer to the inlet and exit conditions, respectively.

First Law of Thermodynamics is in the following form:

$$\sum_{\text{i}}\dot{m}_{\text{i}}h_{\text{i}} + \dot{Q} = \sum_{\text{e}}\dot{m}_{\text{e}}h_{\text{e}} + \dot{W} \quad (7)$$

where $\dot{Q}$ is the heat transfer rate to the control volume, $\dot{W}$ is the work given out per unit time and h is the enthalpy. The kinetic and potential energy changes are omitted since they are negligibly small compared to the changes in enthalpy.

The exergy balance is presented as follow:

$$\dot{E}_{\text{Q}} - \dot{E}_{\text{W}} = \sum_{\text{e}}\dot{m}_{\text{e}}e_{\text{e}} - \sum_{\text{i}}\dot{m}_{\text{i}}e_{\text{i}} + \dot{E}_{\text{L}} \quad (8)$$

where e is the specific exergy and E_{L} is the exergy loss rate. E_{Q} and E_{W} are the exergy rates due to the heat input and mechanical energy, respectively, which are defined as:

$$\dot{E}_{\text{Q}} = \left(1 - \frac{T_{\text{o}}}{T_{\text{j}}}\right)\dot{Q}_{\text{j}} \quad (9)$$

$$\dot{E}_{\text{W}} = \dot{W} \quad (10)$$

where T is the absolute temperature and the subscripts j and o refer to the surface and environmental conditions, respectively. Exergy destruction in each component of a combined cycle, which is schematically shown in Fig. 1, can be calculated as below:

Exergy destruction for compressor is presented as:

$$\dot{E}_{\mathrm{L_{Comp}}} = \dot{W}_{\mathrm{C}} - (\dot{E}_2 - \dot{E}_1)\,, \tag{11}$$

for the combustion chamber as:

$$\dot{E}_{\mathrm{L_{C,Ch}}} = \dot{E}_{\mathrm{fuel}} - (\dot{E}_3 - \dot{E}_2)\,, \tag{12}$$

for the gas turbine as:

$$\dot{E}_{\mathrm{L_{GT}}} = (\dot{E}_3 - \dot{E}_4) - \dot{W}_{\mathrm{GT}}\,, \tag{13}$$

for the HRSG as:

$$\dot{E}_{\mathrm{L_{HRSG}}} = (\dot{E}_4 - \dot{E}_9) - (\dot{E}_5 - \dot{E}_8)\,, \tag{14}$$

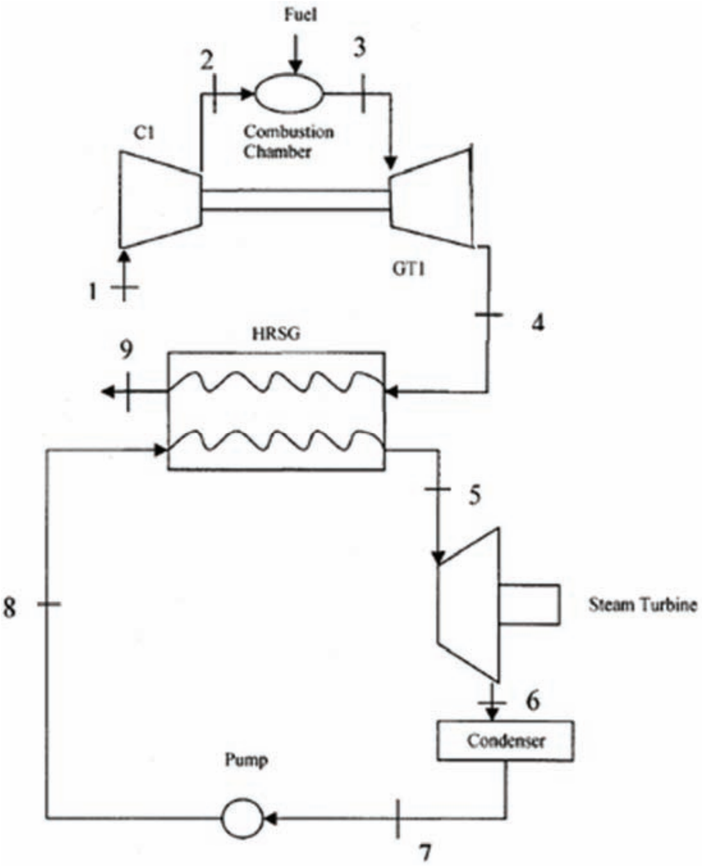

Fig. 1. The components of a combined cycle.

for the steam turbine as:

$$\dot{E}_{\mathrm{L_{ST}}} = (\dot{E}_5 - \dot{E}_6) - \dot{W}_{\mathrm{ST}}\ , \tag{15}$$

and for the condenser as:

$$\dot{E}_{\mathrm{L_{Cond}}} = (\dot{E}_7 - \dot{E}_6) \tag{16}$$

Finally, the Second Law efficiency could be written as follow:

$$\eta_{\mathrm{II}} = \frac{\sum\limits_{\mathrm{k}} \dot{E}_{\mathrm{W_k}}}{\dot{E}_{\mathrm{fuel}}} \tag{17}$$

The heat recovery steam generators (HRSG) of Unit 3 and 4 in the Fars Combined Cycle Power Plant, which combine Unit 3 and 4 of the gas cycle and Unit B of the steam cycle are shown in Fig. 2.

For calculations of the exergy loss of the components, the inlet and outlet states of each component are required. The inlet and outlet compressor pressure and temperature are included in gas cycle data sheets, therefore the inlet temperature and pressure of the combustion chamber are known. The outlet temperature and pressure of the gas turbine could also be obtained from the gas cycle data sheets. By neglecting the pressure drop in the combustion chamber, the combustion chamber outlet pressure has the same value as the combustion chamber inlet pressure. To obtain the combustion chamber outlet temperature, the energy balance in the combustion chamber can be used:

$$\dot{m}_{\mathrm{air}}\, h_2 + \dot{m}_{\mathrm{f}}\, LHV = \dot{m}_{\mathrm{mix}}\, h_3 \tag{18}$$

where *LHV* is the low heating value of the fuel, which for natural gas is 50020 kJ kg^{-1} In Eq. (18), m_{air}, m_{mix} and h_3 are unknown. $\dot{m}_{mix}$ can be related to m_{air} and m_{f} as follows:

$$\dot{m}_{\mathrm{mix}} = \dot{m}_{\mathrm{f}} + \dot{m}_{\mathrm{air}} \tag{19}$$

By estimating m_{air} in Eq. (19), m_{mix} can be obtained. By using this value, Eq. (18) can be solved. T_3 can be obtained from combustion equation as below:

$$a\mathrm{CH_4} + x(\mathrm{O_2} + 3.76\mathrm{N_2}) \rightarrow a\mathrm{CO_2} + b\mathrm{H_2O} + c\mathrm{N_2} + d\mathrm{O_2} \tag{20}$$

where

$$\begin{aligned} &a = \frac{\dot{m}_{\mathrm{fuel}}}{M_{\mathrm{fuel}}},\ x = \frac{\dot{m}_{\mathrm{air}}}{M_{\mathrm{air}} \times 4.76} \\ &c = 3.76x \\ &b = 2a \\ &d = x - 2a \end{aligned} \tag{21}$$

In this case, the mole fraction of each component in the mixture that entered the gas turbine can be calculated as follow:

$$y_{\mathrm{CO_2}} = a/n,\quad y_{\mathrm{H_2O}} = b/n,\quad y_{\mathrm{N_2}} = c/n,\quad y_{\mathrm{O_2}} = d/n \tag{22}$$

where:

$$n = a + b + c + d \tag{23}$$

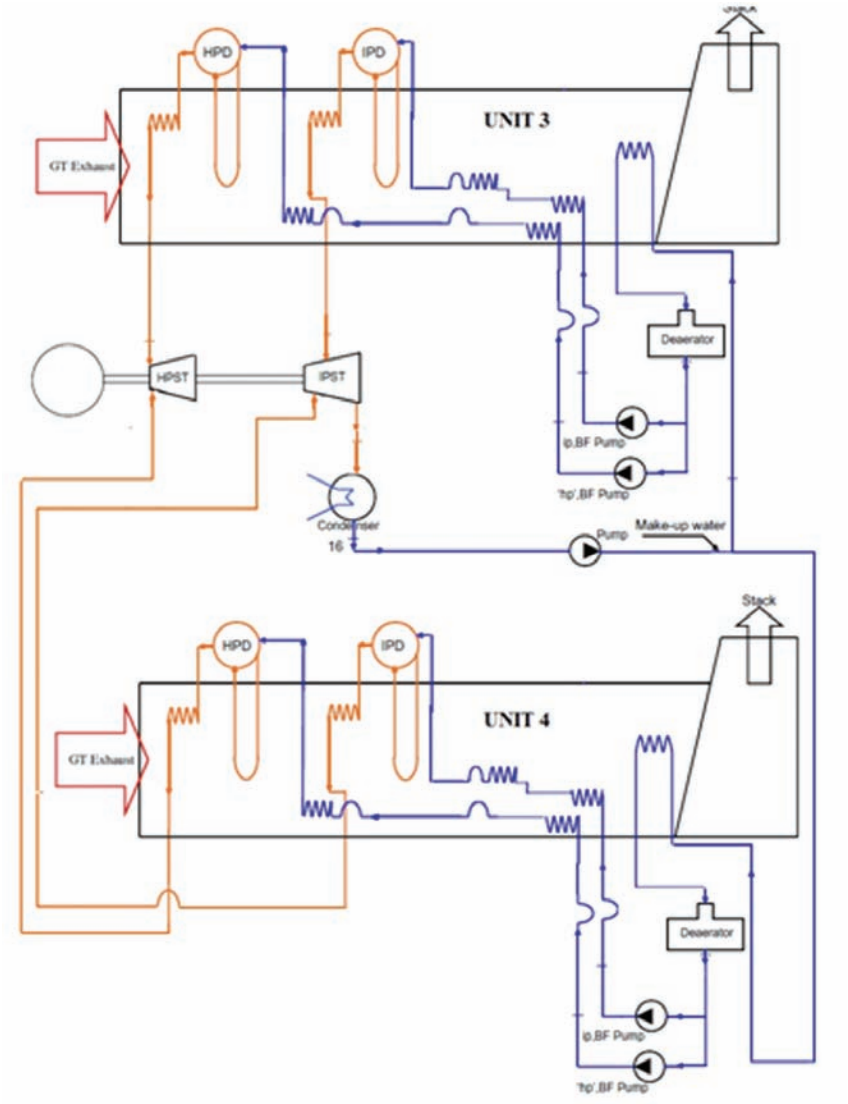

Fig. 2. HRSG of Unit 3 and 4 in the Fars Combined Cycle Power Plant.

$\bar{h}_3$, the combustion chamber outlet molar enthalpy, can be obtained by multiplying $\bar{h}_3$ and molar mass of the mixture, which is presented in Eq. (24):

$$\bar{h}_3 = h_3 M_{\text{mix}} \tag{24}$$

M_{mix} can be obtained by Eq. (24):

$$M_{\text{mix}} = \sum_i y_{\text{i}} M_{\text{i}} \tag{25}$$

The combustion chamber outlet molar enthalpy can also be calculated using the Gas Law as follow:

$$\bar{h}_3 = \sum_i y_\mathrm{i}\, \bar{h}_\mathrm{i}(T_3) \tag{26}$$

The molar enthalpy for each component of the mixture can be obtained from thermodynamic tables. By using the try and error process, T_3 can be obtained from Eq. (26).

The accuracy of the primitive estimation for m_air could be ensured from the output work correlation, which presented by Eq. (27):

$$W_\mathrm{net} + M_\mathrm{air}\left(h_2 - h_1\right) = M_\mathrm{mix}\left(h_3 - h_1\right) \tag{27}$$

If this equation is correct, the primitive estimation for m_air is also correct. The inlet and outlet state of the steam cycle components can be obtained from data that is held in the ANNEX room of the Fars Combined Power Plant complex.

Plant description

In 2003, one of the notable power plant projects in Iran was inaugurated. This project, which includes 22 Combined Cycle Power Plants, has not yet been completed.[21] One of these power plants, *i.e.*, the Fars Combined Power Plant, is located near the city of Shiraz. This power plant has six gas Units. Each two-gas unit combines with a steam unit by using HRSGs. As a result, this plant has six gas cycles and three steam cycles. The Siemens GE Frame 9 gas turbines of this combined cycle were installed in 1981. Each gas cycle output power, at 100 % load, is 100 MW. In each gas cycle, air is compressed to approximately 10 bars by an axial compressor from the ambient pressure of 0.86 bars. The compressed air enters into the combustion chamber. The flue gas from the combustion chamber enters the turbine at approximately 1550 K. The exhaust gas at 550 °C enters the HRSG without supplementary firing. Each dual pressure HRSG generates HP and LP at approximately 500 and 200 °C, respectively. The rated steam turbine power output is 130 MW at 100 % load. The expanded steam enters a condenser and transfers its heat to water. Then, the water flows through a cooling tower and releases its heat. The condensate water drops to the hot well at the bottom of the condenser and is pumped to the deaeriator by means of condensate extraction pumps. The feed water to the LP evaporator and HP first and second economizers is fed by a common two-pressure HP/LP pump, which take their suction from the feed water storage tank. The HP water discharge of the pump passing through HP economizers goes to the HP drum and, after evaporation, the separated saturated steam in the drum passes through the superheater. Finally, this steam goes to the steam turbine HP section and completes the cycle.

RESULTS AND DISCUSSION

In present study, an exergy analysis was realized for Units 3 and 4 gas turbine and Unit B steam turbine of the Fars Combined Power Plant. The data for the analysis were obtained from resources such as the archives of the power plant, log sheets of the gas cycle, daily reports of the steam and gas units and the daily fuel consumption of whole power plant. Results of the power output and exergy loss for Units 3 and 4, the entropy generation of the whole cycle by means of the power output and the Second Law efficiency, exergy loss for gas, steam and the whole cycle for each month and the exergy loss per MW for each component of the cycle are presented in this section.

Power output and exergy loss for the components of Units 3 and 4

The power output and exergy loss for different parts of Units 3 and 4 are presented, respectively, in Figs. S1 and S2 (Supplementary material to this paper). For a proper comparison, a factor of the exergy loss for each component was considered to obtain values in the same order of magnitude. Thus the exergy loss of the compressor, gas turbine, combustion chamber and HRSG were divided by 100, 250, 2000 and 500, respectively. From Figs. S1 and S2, the exergy loss of each part showed an approximately ascending trend with some oscillations. As observed in the figures, these oscillations were related to variations in the power output; therefore, the power output and the exergy loss for each part have a similar trend. This similarity was obtained due to the essence of exergy loss, which is directly related to power output and irreversibilities. In addition, it could be observed that with decreasing output power, the exergy loss of each part also decreased. The decreasing power output was caused by reduction in the fuel consumption, which descended the input exergy of the whole unit. This phenomenon affected directly the exergy loss of each part.

Entropy generation for the whole cycle based on the power output and Second Law efficiency

The entropy generation *vs*. power output is shown in Fig. S3 (Supplementary material to this paper). As can be seen, the entropy generation increased with increasing power output of the combined cycle. The entropy generation based on the Second Law efficiency is presented in Fig. S4 (Supplementary material to the paper), from which it can be seen that with increasing the Second Law efficiency, a greater part of the input fuel exergy is transformed to mechanical energy. Accordingly, the exergy losses and irreversibility become a minor part of the input exergy. This conclusion could be confirmed by Eq. (17). Two distinct trends can be seen in Fig. S4. The upper trend related to the time when Units 3 and 4 were working together and a lower when one of the Units was under maintenance. Based on the fact mentioned above in relation to Fig. S3, by decreasing the power output, lower entropy generation could be obtained for the whole cycle.

Exergy losses for Units 3 and 4 gas turbine, Unit B steam turbine and whole cycle based on time duration

Exergy losses *vs*. time duration for the whole cycle, Units 3 and 4 gas turbine and Unit B steam turbine are presented in Fig. 3. MI, CCI and HGP imply major inspection or overhaul of each unit, combustion chamber inspection and high temperature gas path, respectively. The black line is related to the exergy loss of the whole cycle, the blue line to the Unit B steam turbine, the green and orange lines present the exergy loss of Unit 3 and 4 gas turbine, respectively. From diagrams in Fig. 3, the exergy loss value for the steam cycle is much lower than the value in gas cycle. This event is due to the high exergy loss in the components of the gas cycle, such as combustion chamber, gas turbine and HRSG, which is in good correlation with previous studies. In Fig. 3, it can be seen that the whole cycle exergy loss has a rapid decrease caused by maintenance of some units. In addition, the exergy loss for each unit had an increasing trend with some oscillations. These oscillations were caused by fluctuations in the power output of each unit. In Fig. S5 (Supplementary material of the paper), non- dimensional analysis was realized by dividing the exergy loss by the power output of each unit, in order to eliminate power output effects. As a result, an increasing trend of exergy loss per MW for each unit was obtained. It is very obvious that after the maintenance period of each unit, the exergy loss per MW decreased, this reduction can be seen from the results for the whole cycle.

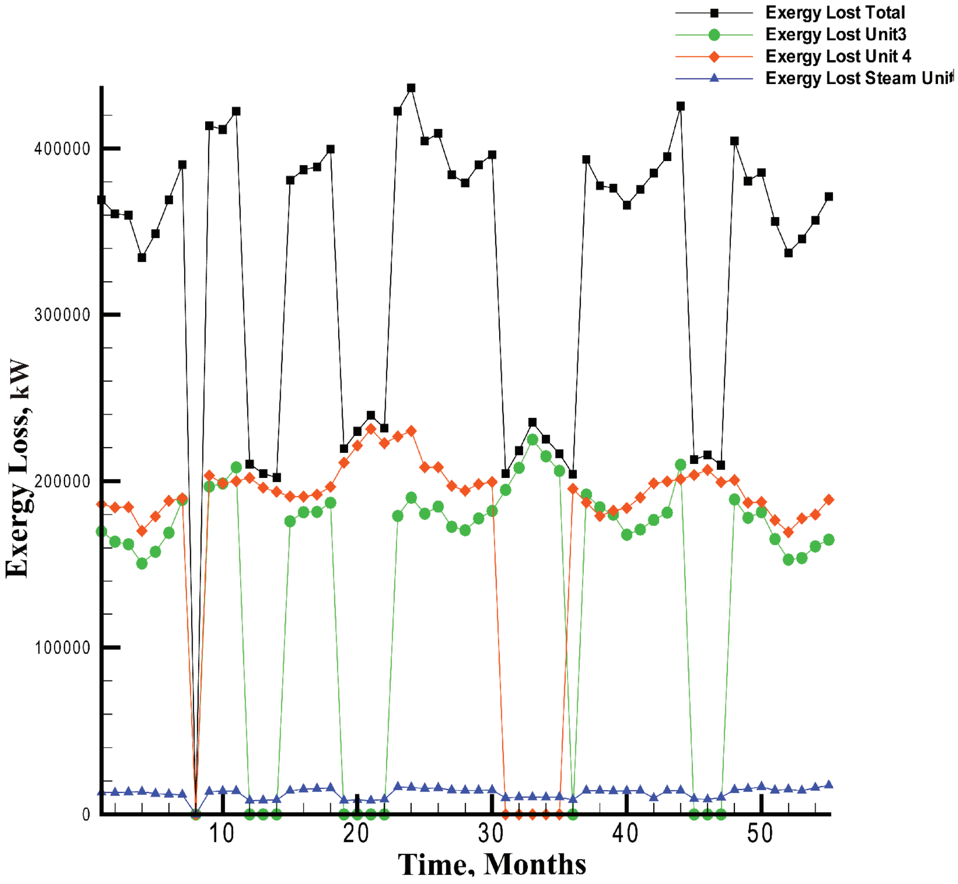

Fig. 3. Exergy losses *vs*. time for the whole cycle, Units 3 and 4 gas turbines and Unit B steam turbine.

Exergy loss per MW for each component in Unit 3, 4 and Unit B

In this section, exergy loss per MW for each component in Units 3, 4 and B is presented. Due to the low exergy loss in the condenser and pump, these parts are neglected in the exergy analysis. As a result, the exergy loss per MW for the compressors, gas and steam turbines, combustion chambers and HRSG were obtained and calculated.

Exergy loss per MW for compressors. The exergy losses per MW for the compressors are presented in Figs. S6 and S7 (Supplementary material to the paper). Based on the maintenance schedule, a major inspection (MI) of Unit 3 occurred from Oct 2007 to Jan 2008 and of Unit 4 from Oct 2008 to Feb 2009. As can be seen from Fig. S6, the exergy loss for the compressor of Unit 3 increased because of the MI because either the MI was not realized at the proper moment or improper maintenance was performed. In Fig. S7, a large reduction in exergy loss for compressor of Unit 4 could be noticed after the MI period because the MI was performed at the proper moment. In addition, the exergy loss for the compressor of Unit 3 is greater than that for the compressor of Unit 4; for this reason, the performance of Unit 4 is better than that of Unit 3.

Exergy loss per MW for the combustion chambers. Exergy losses per MW for the combustion chambers are presented in Figs. S8 and S9 (Supplementary material to the paper). As could be seen, exergy losses for the combustion chambers were greater than those from the other components. From the results presented Figs. S8 and S9, it could be stated that the MI process performed at the right moment, when the exergy losses had their highest values. In combustion chamber, CCI, MI and HGP process have the great effects on realizing a reduction of exergy loss for both Unit 3 and 4.

Exergy loss per MW for gas turbines and HRSGs. Exergy losses per MW for the gas turbines and HRSGs are presented in Figs. S10–S13 (Supplementary material to the paper). In all diagrams, after MI and the CCI process, the exergy loss for each component was reduced significantly. In addition, by means of the HGP process, the exergy loss was decreased because the HGP process improved the isentropic efficiency of the gas turbine, which reduced the irreversibility of the gas turbine and HRSG. As in the previous data, it is noticeable that exergy loss decreased after the maintenance process. In addition, Unit 3 had a faster trend in increasing the exergy loss than Unit 4.

Exergy loss per MW for the steam turbine. The exergy loss per MW for the steam turbine is presented in Fig. S14 (Supplementary material to the paper). Unexpected increasing trends in the exergy loss could be seen. This occurred when one of the gas units was under maintenance. In Fig. S14, a significant increase in exergy loss took place from month 31 to 35 when Unit 4 was under the MI process. Other increasing trend was related to maintenance of Unit 3. It is obvious that when Unit 4 was under overhaul, the exergy loss in the steam turbine was extensively increased. This event is the result of the mentioned proper operation of Unit 4 in the whole cycle. In addition, after the HGP period of Unit 3, an extreme reduction could be seen in exergy loss; hence, the high temperature gas path of Unit 3 might be the reason for the large exergy loses. Finally, by neglecting the maintenance periods, the exergy loss per MW during time has an ascending trend.

CONCLUSIONS

The combined power plant is one of the most important power generators in Iran and special consideration must be given for this type of power plant. In this study, an exergy analysis was performed for each component of Unit 3 and 4 gas cycle and Unit B steam cycle based on data from the Fars Combined Power Plant. The results showed that, the exergy loss in the components of Unit 3 and 4 increased with increasing power output and also increased with operation time. In addition, to consider time effect on exergy loss, the exergy loss was divided by MW to eliminate the MW effect. Finally, entropy generation of whole power plant based on MW and the Second Law efficiency were considered and calculated.

SUPPLEMENTARY MATERIAL

Figs. S1–S14 are available electronically from http://www.shd.org.rs/JSCS/, or from the corresponding author on request.

ИЗВОД

НУМЕРИЧКА АНАЛИЗА И ИНДУСТРИЈСКА ИСПИТИВАЊА ВРЕМЕНСКЕ ЗАВИСНОСТИ ЕКСЕГИЈА–ЕНЕРГИЈА КОД КОМБИНОВАНОГ ЦИКЛУСА ЗА ПРОИЗВОДЊУ ЕЛЕКТРИЧНЕ ЕНЕРГИЈЕ

ASHKAN ABBASIAN SHIRAZI[1], BAMDAD BARARI[1], MOHSEN KESHAVARZI[1] и IMAN ROSTAMSOWLAT[2]

[1]*Mechanical Engineering Department, Shiraz University, Shiraz, Iran и* [2]*Mechanical Engineering Department, Islamic Azad University, Kazeroon branch, Kazeroon, Iran*

Истраживање дато у овом раду анализира комерцијални комбиновани циклус за производњу електичне енергије у области Фарс у Ирану, употребом ексергетске анализе, при чему је промена ексергије разматрана у зависности од времена. Ексергетска анализа је употребљна да би се истражио сваки део комбинованог циклуса узимањем у обзир неповратности процеса који се дешава у сваком делу опреме у периоду од априла 2006 до октобра 2010. Анализа сваког дела опреме спроведена је прорачунавањем трансформације ексергије у анергију за сваки месец. Употребом ексергетске анализе смањење ефикасности опреме разматрано је у зависности од времена. Такође, израчуната је брзина умањења рада за сваки месец, при чему је умањење разматрано као функција времена употребљавања опреме. На крају, разматрано је како умањење ексергије за сваки део опреме утиче на умањење ексергије целог циклуса. Анализа је изведена за комерцијални комбиновани циклус у области Фарс у Ирану, у коме се електрична енергија производи употребом гасних турбина у постројењима 3 и 4, док се издувни гасови из гасних турбина комбинују са парним постројењем Б.

(Примљено 8. јула 2011, ревидирано 9. фебруара 2012)

REFERENCES

1. M. S. Briesch, R. L. Bannister, *J. Eng. Gas Turbines Power* **117** (1995) 734
2. M. R. Erbes, R. R. Gay, in *Proceeding of the Winter Annual Meeting of the ASME*, San Francisco, CA, USA, 1989, p. 223
3. J. Roy-Akins, *Proc. Inst. Mech. Eng. Part A: J. Power Energy* **209** (1995) 281
4. T. J. Kotas, *The Exergy Method of Thermal Plant Analysis*, Butterworth, Stoneham, MA, USA, 1985
5. C. Sieppel, R. Bereuter, *Brown Boveri Rev.* **47** (1960) 83
6. H. Czermak, A. Wunsch, in *Proceedings of ASME*, 1982, USA, paper No. 82 GT-323
7. A. Khaliq, S. C. Kaushikb, *Appl. Energy* **78** (2004) 179
8. V. Ramaprabhu, R. P. Roy, *J. Energ. Resour. - ASME* **126 (**2004) 231
9. F. R. P. Arrieta, L. E. E. Silva, *Appl. Energy* **80** (2005) 261
10. A. Cihan, K. Kahveci, *Int. J. Energy Res.* **30** (2006) 115
11. D. C. Sue, C. C. Chuang, *Energy* **29** (2004) 1183
12. A. Khaliq, S. C. Kaushik, *Appl. Therm. Eng.* **24** (2004) 1785
13. T. Ganapathy, N. Alagumurthi, R. P. Gakkhar, K. Murugesan, *J. Eng. Sci. Tech*. **2** (2009) 123
14. H. H. Erdem, A. V. Akkaya, *Int. J. Therm. Sci*. **48** (2009) 2179
15. A. Hamed, W. Tabakoff, D. Singh, *Int. J. Rotating Mach.* **4** (1998) 243
16. M. Morini, M. Pinelli, *J. Eng. Gas Turbines Power* ***132*** (2010) 032401-1
17. A. Hamed, W. Tabakoff, *J. Turbomach.* **127** (2005) 445
18. P. R. Spina, in *Proceedings of ASME Turbo Expo*, Amsterdam, Netherlands, 2002, ASME P. GT-2002-30275
19. D. E. Muir, H. I. H. Saravanamuttoo, D. J. Marshall, *J. Eng. Gas Turbines Power* **111** (1989) 244
20. A. R. Howell, R. P. Bonham, *Proc. Inst. Mech. Eng., C* **163** (1950) 235
21. M. Ameri, P. Ahmadi, S. Khanmohammadi, *Int. J. Energy Res.* **32** (2008) 175.

Journal of the Serbian Chemical Society
JSCS@tmf.bg.ac.rs • www.shd.org.rs/JSCS
J. Serb. Chem. Soc. 77 (7) S111–S118 (2012)
Supplementary material

SUPPLEMENTARY MATERIAL TO

Numerical analysis and field study of the time dependent exergy–energy of a gas–steam combined cycle

BAMDAD BARARI[1]*, ASHKAN ABBASIAN SHIRAZI[1], MOHSEN KESHAVARZI[1]
AND IMAN ROSTAMSOWLAT[2]

[1]Mechanical Engineering Department, Shiraz University, Shiraz, Iran and [2]Mechanical Engineering Department, Islamic Azad University, Kazeroon branch, Kazeroon, Iran

J. Serb. Chem. Soc. 77 (7) (2012) 945–957

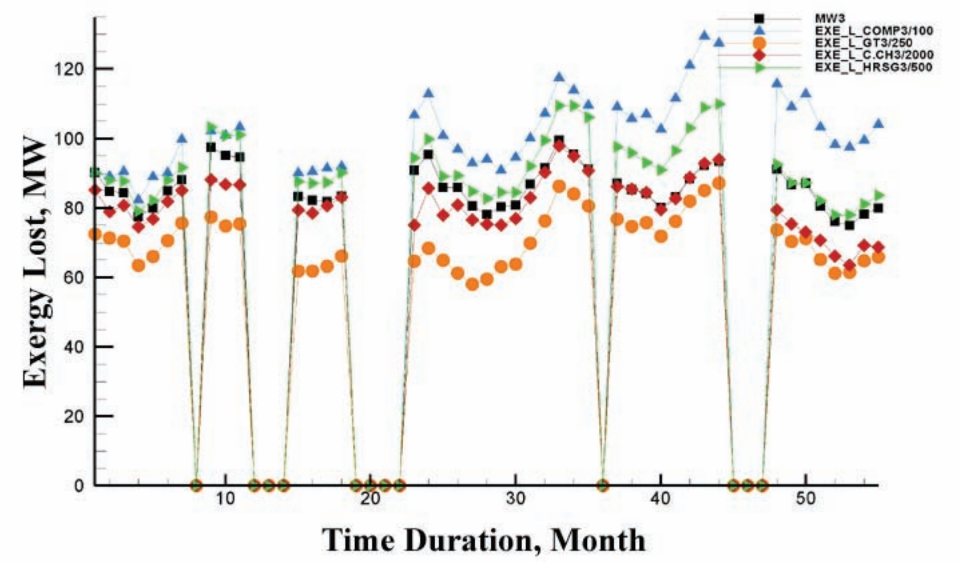

Fig. S1. Power output and exergy loss for different parts of Unit 3.

---

* Corresponding author. E-mail: barari@shirazu.ac.ir

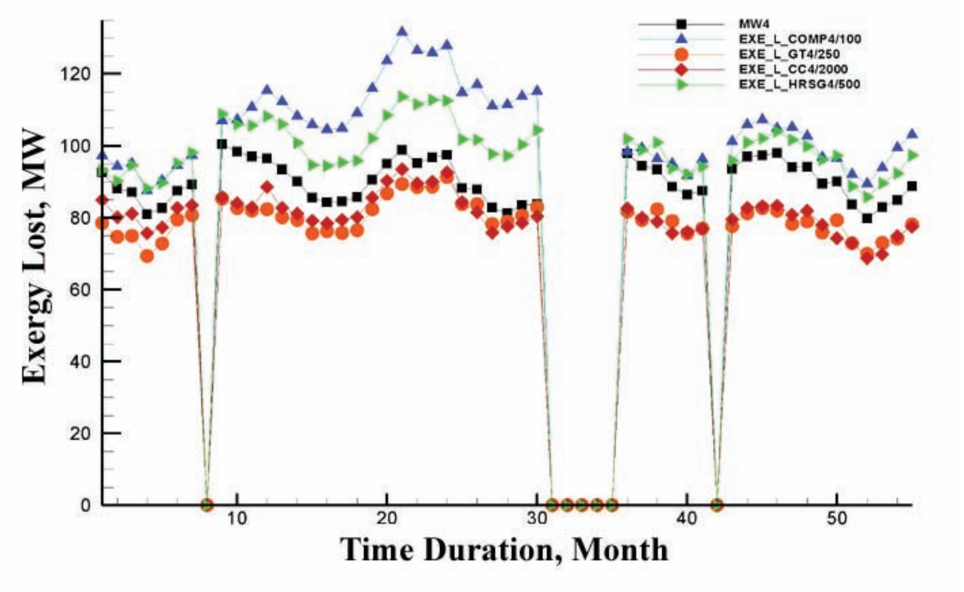

Fig. S2. Power output and exergy loss for different parts of Unit 4.

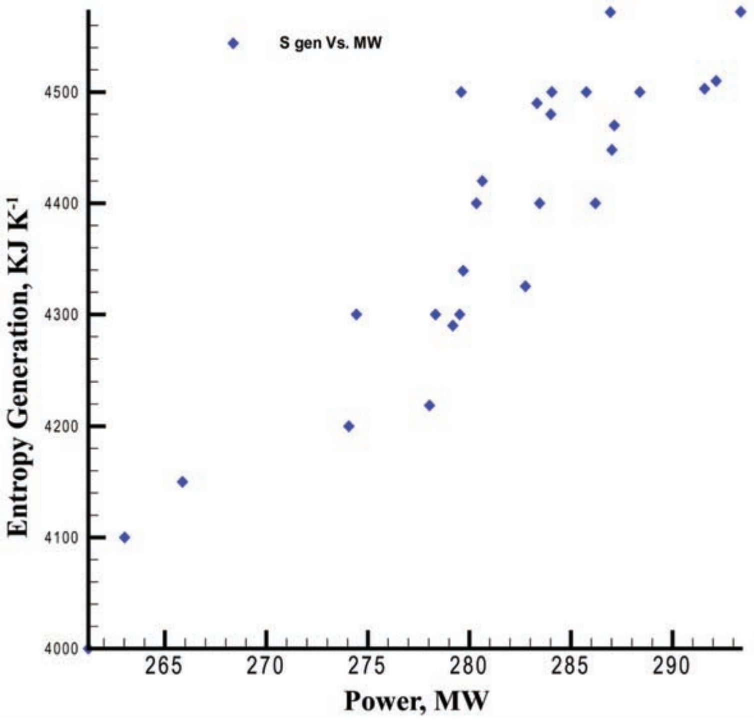

Fig. S3. Entropy generation *vs*. power output.

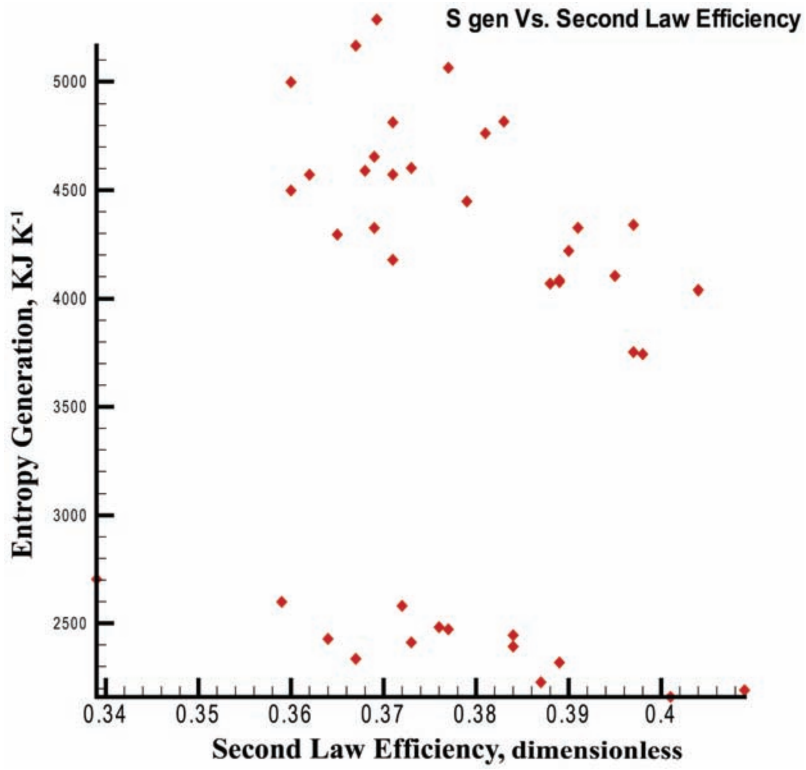

Fig. S4. Entropy generation *vs*. the Second Law efficiency.

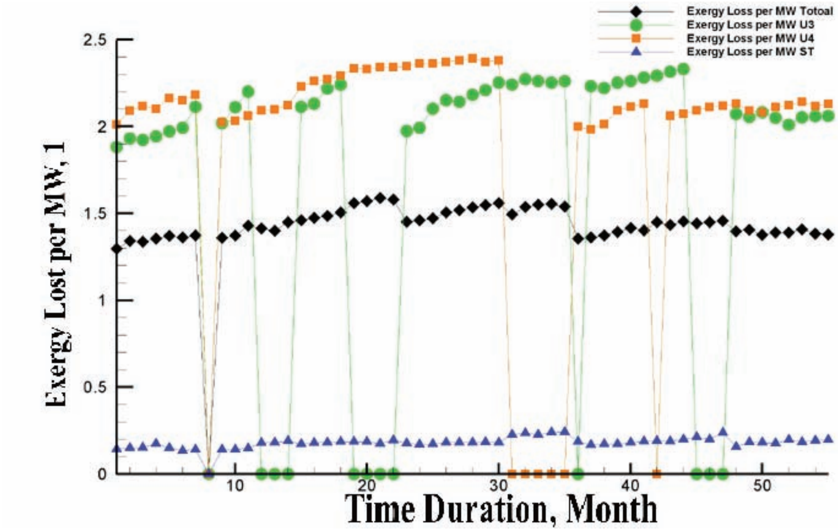

Fig. S5. Exergy losses per MW *vs*. time duration for the whole cycle, Unit 3 and 4 gas turbines and Unit B steam turbine.

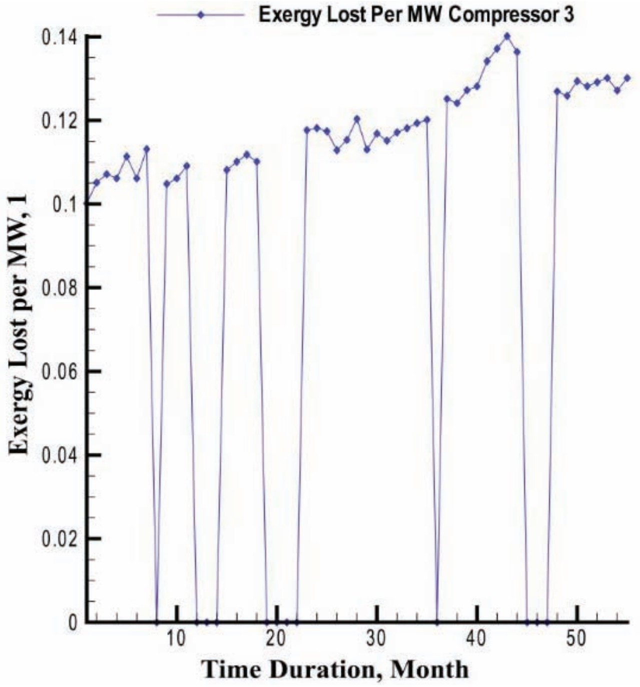

Fig. S6. Exergy losses per MW for the Unit 3compressor.

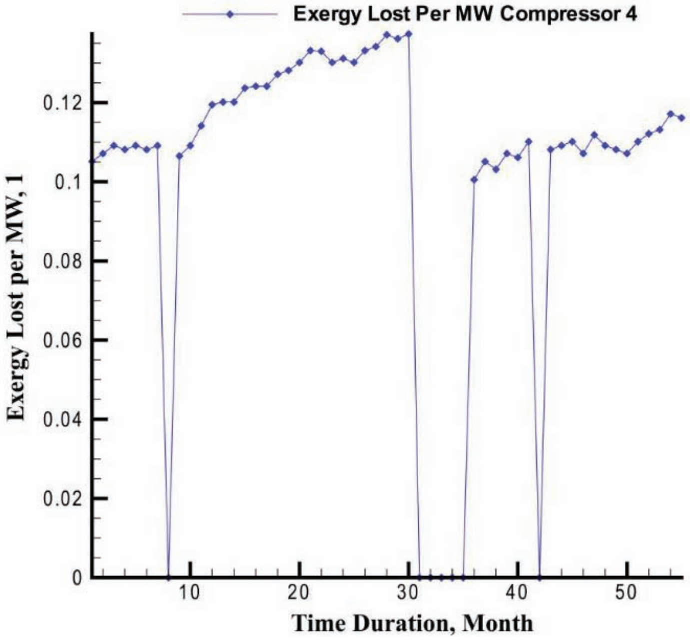

Fig. S7. Exergy losses per MW for the Unit 4compressor.

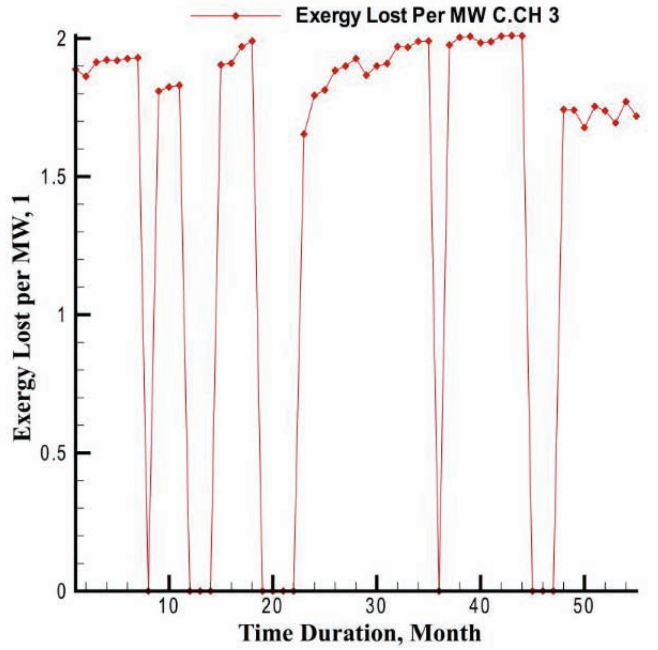

Fig. S8. Exergy losses per MW for the Unit 3combustion chamber.

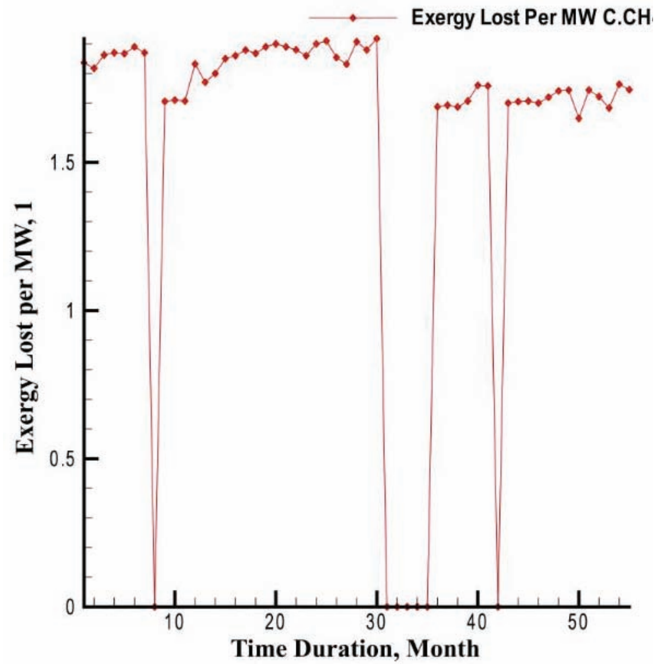

Fig. S9. Exergy losses per MW for the Unit 4 combustion chamber.

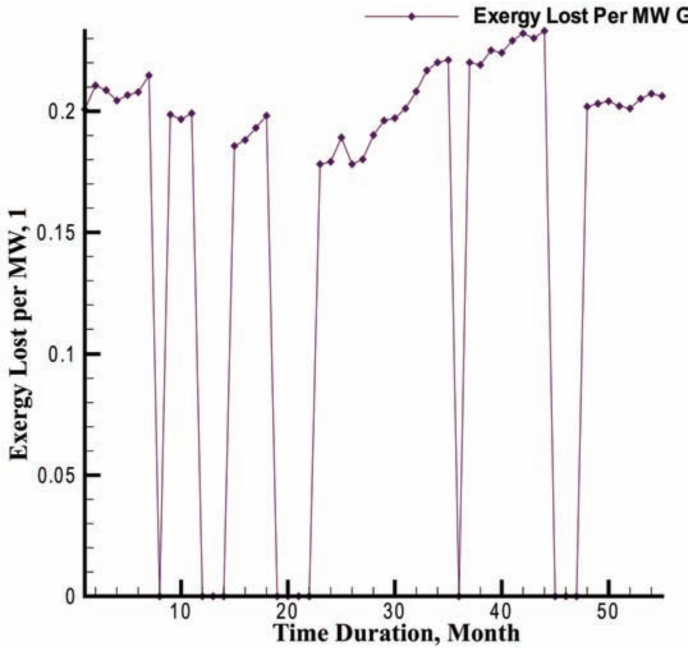

S. 10. Exergy losses per MW for the Unit 3 gas turbine.

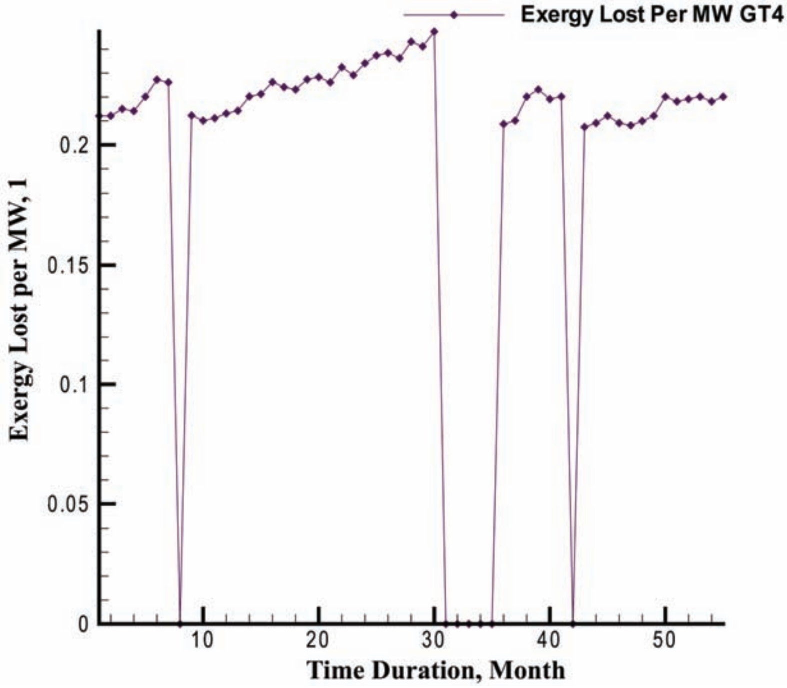

S. 11. Exergy losses per MW for the Unit 4 gas turbine.

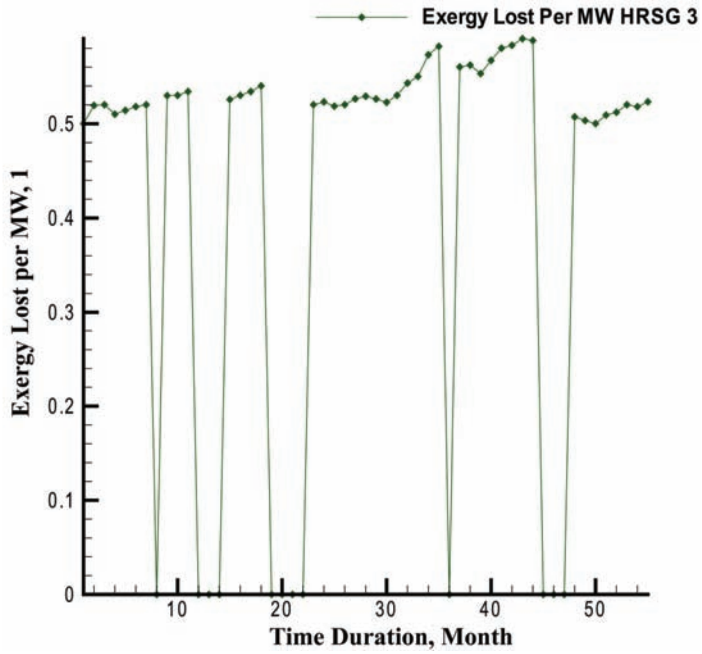

S. 12. Exergy losses per MW for the heat recovery steam generator of Unit 3.

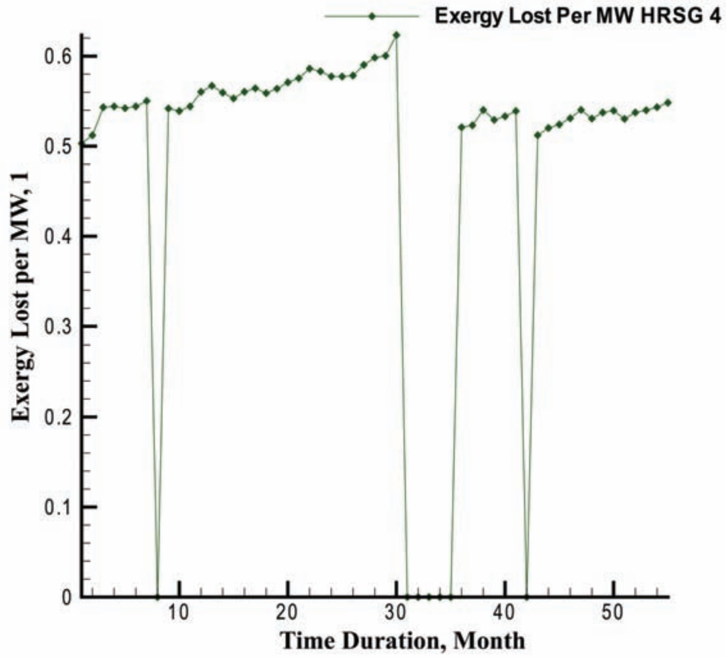

S. 13. Exergy losses per MW for the heat recovery steam generator of Unit 4.

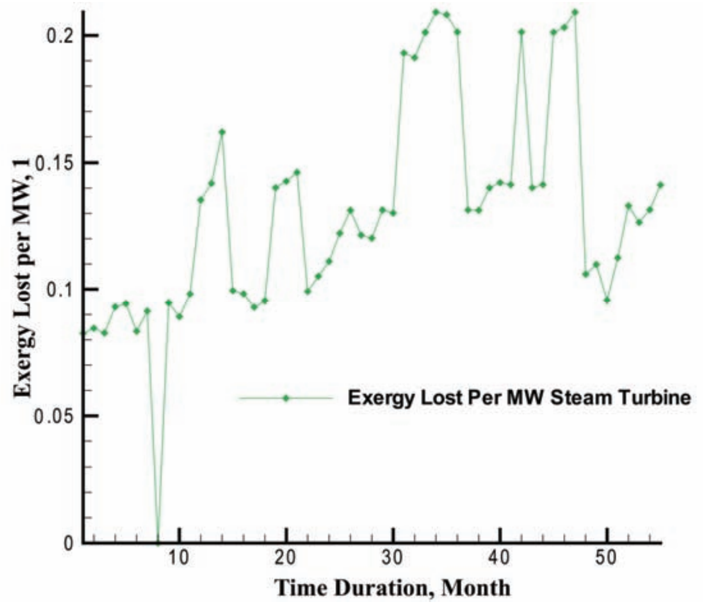

S. 14. Exergy losses per MW for the Unit B steam turbine.

Journal of the Serbian Chemical Society
JSCS-info@shd.org.rs • www.shd.org.rs/JSCS

J. Serb. Chem. Soc. 77 (7) 959–970 (2012)
JSCS–4324

UDC 546.56'47'711'72'76:504.53:
581.5(497.11)(23.0)
Original scientific paper

Heavy metal contents in *Veronica* species and soil from mountainous areas in Serbia

JELENA ŽIVKOVIĆ[1]*, SLAVICA RAŽIĆ[2#], JELENA ARSENIJEVIĆ[3] and ZORAN MAKSIMOVIĆ[3]

[1]*Institute for Medicinal Plant Research "Dr. Josif Pančić", Belgrade,* [2]*Department of Analytical Chemistry, School of Pharmacy, University of Belgrade, Belgrade and* [3]*Department of Pharmacognosy, School of Pharmacy, University of Belgrade, Belgrade, Serbia*

(Received 25 December 2011)

Abstract: This paper describes the relationships between the concentrations of selected trace elements in soil and their bioaccumulation in the aerial parts of three *Veronica* species (Plantaginaceae). Plant and soil samples were collected from three mountainous areas in Serbia, prepared by microwave-assisted acid digestion and analyzed by flame and flameless atomic absorption spectrometry. The total concentrations of Cu, Zn, Mn, Fe and Cr in the soil varied from 12.38 to 47.77, 62.78 to 138.00, 517.58 to 1675.78, 13574.22 to 35920.00 and 36.18 to 115.15 mg kg^{-1}, respectively, while those in the plants ranged from 6.04 to 12.8, 27.66 to 58.01, 25.38 to 89.25, 35.53 to 563.26 and 0.44 to 18.96 mg kg^{-1}, respectively. There were no significant differences in heavy metal concentrations between the tested *Veronica* species from the same location, indicating that their heavy metal uptake pattern was not species specific. In the case of Mn, despite its wide variation in the soil, the concentrations in the plant samples were uniform, which suggests the potential ability of the tested species to control Mn uptake and/or its translocation to the upper plant parts. Additionally, the lowest concentrations of Cu were obtained in plant samples collected from soil with the highest Fe concentrations, indicating that Cu availability to plants might be reduced due to high Fe contents in soil solution.

Keywords: atomic absorption spectroscopy; correlation analysis; trace elements; soil; plants.

INTRODUCTION

Environmental pollution and constant exposure to heavy metals are considered to be among the most important threats to human health today. The in-

---

* Corresponding author. E-mail: jelenazivkovic1@yahoo.com
\# Serbian Chemical Society member.
doi: 10.2298/JSC111225221Z

creased and still growing levels of heavy metals in the environment are a consequence of their utilization in various industrial activities.[1] As “miners” of the Earth’s crust, plants absorb numerous elements from the soil. Some of them are referred to as essentials because they are required by plants to complete their life cycle. Certain heavy metals, such as iron, manganese, copper and zinc, are known as micronutritients because they are required by plants in minute quantities, while other have proven to have a stimulatory effect on plants growth, but are not considered essential. Moreover, plants also absorb elements, such as chromium, which have no known biological function and are even known to be toxic at low concentrations.[2] Due to their non-biodegradable nature, heavy metals tend to accumulate in biological compartments and move through the food chains. Although some of them are micronutrients, in high concentrations they are toxic to various life forms.[1]

Inorganic trace pollutants exhibit their influence in many different ways. Being active in diverse metabolic processes, they enter the plant tissues and could be stored as inactive compounds in cells and on the surface of cell membranes. Apart from the specific mechanism of the target plant tissue, it was reported that trace elements, even in higher concentrations, may affect the chemical composition of plants without causing readily visible injury.[3] Accordingly, they are particularly responsible for the medicinal and nutritional properties of foods and medicinal plant products, as well as their toxicity.

The main objective of this study was, therefore, to determine the levels of several heavy metals (Cu, Zn, Mn, Fe and Cr) in three *Veronica* species (Plantaginaceae) growing wild in Serbia (*Veronica jacquinii* Baumg., *Veronica teucrium* L. and *Veronica urticifolia* Jacq.). Additionally, in order to explore the uptake patterns of specific metals in the plants, corresponding soil samples were analyzed.

The major external source of heavy metals in soils is usually pollution caused by anthropogenic activities, such as metal mining, smelting and processing or the use of fossil fuels. Additionally, diffuse pollution by wet and dry deposition has resulted in the long-term accumulation of heavy metals in many parts of the world. On the other hand, some high metal concentrations in soils are of natural origin, resulting from weathering of the underlying bedrock.[4] Since soils on different types of parent rock contain different levels of elements, especially heavy metals,[5] three mountainous areas with different geological settings were selected as the target sites. The first investigation site is located in the northern part of Serbia where acidic soils derived on albite-muscovite schist and granite gneiss are prevalent. The reverse process (alkalization) occurs in the second investigated site located on Mt. Stol, where the bedrock consists primarily of limestone and the third investigation site is located on Mt. Goč, one of the serpentine sites in central Serbia.

Veronica species were selected for the present investigation having in mind their widespread use in a traditional medicine worldwide, mostly as diuretics, for their wound-healing properties, in medical treatment of influenza and other respiratory diseases, as well as expectorants and antiscorbutic agents.[6] Extracts obtained from the above-ground parts of various *Veronica* species are used as folk remedies for the treatment of various inflammatory ailments, including rheumatism.[7] In addition, the stems and leaves of some *Veronica* species are edible, either raw or cooked.[8]

Numerous studies on the identification of secondary metabolites in *Veronica* species have already been published, with iridoid glucosides, phenylethanoid and flavonoid glycosides being mainly reported,[9–12] but only a few refer to the determination of inorganic components,[13,14] or relationship between the inorganic content of a herb and corresponding soil.[15,16] Zurayk *et al*. evaluated the role of some *Veronica* hydrophytes (*V. beccabunga*, *V. lysimachioides*, *V. anagalloides*) in the aquatic phytoremediation of Cr.[17] In addition, Abu Ziada *et al*. determined that *V. anagalis–aquatica* had the highest value of ferric ion content, among five common macrohydrophytes.[14] Wang *et al*. showed that *V. didyma* exhibited a high accumulation ability for Zn.[15] While previous investigations were primarily realized with *Veronica* species that were grown on polluted areas, plant samples from relatively clean environments were selected for this study.

This work, to the best of our knowledge, is the first report of the metal accumulation ability of *V. jacquinii* Baumg., *V. teucrium* L. and *V. urticifolia* Jacq. This paper gives new information about the content of certain elements, their correlations in these species and also in conjunction with their concentrations in the soil.

EXPERIMENTAL

All chemicals were of analytical reagent grade. For the preparation of all solutions, double distilled water was used. Stock solutions of Cu, Mn, Zn, Fe and Cr salts (1 g L^{-1}) were purchased from Merck (Germany). Working solutions were obtained by suitable dilution of the corresponding stock solution with 2.5 % HNO_3. Nitric acid (65 %, v/v) was provided by Merck (Germany), a solution of H_2O_2 (30 %, v/v) and KCl from Zorka Pharma Šabac (Serbia).

Acidity of soil samples was measured using a pHM 240 Radiometer analytical pH-meter. For the microwave-assisted acid digestion of the plants and soil samples, a closed-vessel, high-pressure microwave digester-CEM MDS-2000 was used.

The determination of Cu, Zn, Mn, and Fe was performed with a Perkin–Elmer model 5000 atomic absorption spectrophotometer under optimized measurement conditions using suitable hollow cathode lamps. The signals were measured with background correction (deuterium lamp) at the optimal flame (A–A_c) height.[18] The determination of Cr was performed using a Perkin–Elmer model 5000 atomic absorption spectrophotometer with a graphite furnace HGA 400 Automatic Burner Control, with pyrolytic graphite tubes. The optimal temperatures were set as follows: drying, pyrolysis, atomisation and cleaning – 110, 1650, 2500 and 2650 °C, respectively.[19]

The plant materials (aerial flowering parts of three *Veronica* species; eleven samples) were collected in June 2008 and 2009 from mountainous areas in Serbia: Goč in central Serbia, Vršačke planine in southern Banat and Stol in eastern Serbia (Table I). Bulk soil samples were collected at the same locations from areas with the greatest vegetation cover. In the case of plant samples 2, 3, 4, 10 and 11, soil was collected from the location approximately 20–30 cm from the plant root, and for the remaining plant samples, from within 10 m (depth of 0–15 cm) of where a particular plant was growing.

TABLE I. A list of the plant species and sampling locations

Location	Species	Description of sampling site	Coordinates	Bedrock (Marković)[40]
Mt. Goč	*V. urticifolia*	Meadow	N 43° 33’ 39.2’’ E 20° 44’ 24.8’’ H 870 m	Serpentinite
Mt. Goč	*V. urticifolia*	Sawmill	N 43° 33’ 29.5’’ E 20° 44’ 53.3’’ H 840 m	Serpentinite
Mt. Goč	*V. urticifolia*	Ball park	N 43° 33’ 28.6’’ E 20° 44’ 53.3’’ H 858 m	Serpentinite
Mt. Goč	*V. urticifolia*	Meadow	N 43° 33’ 32.8’’ E 20° 45’ 04.4’’ H 844 m	Serpentinite
Mt. Goč	*V. jacquinii*	Meadow	N 43° 33’ 39.2’’ E 20° 44’ 24.8’’ H 870 m	Serpentinite
Mt. Vršačke planine	*V. teucrium*	Hillside road (light traffic)	N 45° 07’ 11.7’’ E 21° 19’ 47.1’’ H 293 m	Amygdaloidal and Augen gneiss
Mt. Vršačke planine	*V. teucrium*	Forest path	N 45° 07’ 10.5’’ E 21° 19’ 57.6’’ H 291 m	Amygdaloidal and Augen gneiss
Mt. Vršačke planine	*V. teucrium*	Forest path	N 45° 07’ 18.5’’ E 21° 21’ 10.0’’ H 418 m	Amygdaloidal and Augen gneiss
Mt. Vršačke planine	*V. jacquinii*	Mountain lodge	N 45° 07’ 37.7’’ E 21° 20’ 31.9’’ H 357 m	Amygdaloidal and Augen gneiss
Mt. Stol	*V. jacquinii*	Forest	N 44° 10’ 08.3’’ E 22° 07’ 41.8’’ H 831 m	Limestone
Mt. Stol	*V. teucrium*	Mountain lodge	N 44° 10’ 19.6’’ E 22° 07’ 30.0’’ H 855 m	Limestone

Both plant and soil samples were air-dried at room temperature and ground. Prior to the microwave-assisted digestion procedure, acidity measurements were performed on the soil samples. The pH values of the soil samples were measured in the supernatant of suspensions.

For the determination of real acidity, soil samples and distilled water were mixed in the ratio of 1:2.5. For the determination of the potential acidity, the same ratio was applied, but with addition of 1 M KCl solution, in order to make available the H^+ that were adsorbed on the colloidal soil particles.

The plant and soil samples were then subjected to microwave-assisted acid digestion according to the procedure presented elsewhere.[19] Each sample (about 0.5 g dry weight) was digested with 2 mL hydrogen peroxide (30 % v/v) and 7 ml nitric acid in a microwave oven. After filtration, the obtained solutions were transferred into 25 ml volumetric flasks and diluted to the volume with redistilled water. One sample blank containing the same amounts of acid and oxidant was processed along with each set of samples. Wavelengths and method detection limits used for measuring (both in flame and graphite furnace atomic absorption spectroscopy) were as follows: 324.7 nm/0.05 mg L^{-1} (Cu), 213.9 nm/0.05 mg L^{-1} (Zn), 279.5 nm/ 0.05 mg L^{-1} (Mn), 248.3 nm/0.05 ml L^{-1} (Fe) and 357.6 nm/0.005 mg L^{-1} (Cr).

Accuracy of the methods applied for determination of Cr, Mn, Fe, Zn and Cu after microwave-assisted acid digestion of plants and soil samples was checked by analysis of standard reference materials (NIST SRM 1547–Peach Leaves and NIST SRM 2711–Montana II Soil) and good recoveries (89.0–115.3 %) were obtained. Concentrations of different elements in these samples were determined by external calibration by using corresponding calibration curves. The calculations of the standard deviations as well as correlation and regression analysis were performed using the statistical functions of Microsoft Excel, MS Office 2007.

RESULTS AND DISCUSSION

The concentrations of Zn, Cu, Mn, Fe and Cr were measured in samples of the aerial parts of three *Veronica* species growing on mountainous regions in Serbia. As heavy metal concentrations in plants depend mainly on their concentrations in the soil in which they grew or were cultivated,[20] the measurements were also performed for the corresponding soil samples. The results of the determinations of heavy metals in the analyzed plant and soil samples are summarized in Table II. Bearing in mind the diverse chemical properties of the various elements, each of them will be discussed in relation to its significance in terms of their essentiality and toxicity.

Analysis of heavy metal contents in Veronica *species*

Chromium is a toxic, non-essential element for plants; hence, there is no specific mechanism for its uptake. A possible pathway could involve the carriers used for the uptake of the metals essential for plant metabolism.[21] According to Pawlisz,[22] the regular Cr content in plants usually ranges from 0.006 to 18 mg kg^{-1}. According to the present findings, the Cr content in the investigated plant samples varied between 0.44 and 18.96 mg kg^{-1}. Samples from Mt. Vršačke planine contained the lowest chromium levels (0.44–0.59 mg kg^{-1}) in the investigated set, while the highest value was obtained for plant sample 3 (Mt. Goč). Zurayk *et al*. showed that *V. beccabunga* L., *V. lysimachioides* L. and *V. anagalloides* L. may be used as bio-indicators of Cr pollution and found that Cr was predominantly accumulated in the roots.[17] The translocation of chromium from roots to shoots is extremely limited and its accumulation by roots is 100-fold higher than by shoots, regardless of the investigated species. According to Chaney *et al*. any plant species that accumulates Cr in shoots to levels higher than 5 mg kg^{-1} is of interest as a possible hyperaccumulator.[23] From the results of the present investigation, the same could be concluded for species *V. urticifolia* and *V. jacquinii* when grown on serpentinite soil.

TABLE II. Metal content measured in the plant and soil samples after microwave-assisted acid digestion (expressed in mg kg^{-1} of dry weight)

Sample	Cr		Zn		Cu		Fe		Mn	
	Plant	Soil	Plant	Soil	Plant	Soil	Plant	Soil	Plant	Soil
1	3.55	111.33	46.69	88.87	8.40	24.41	102.73	13574.20	49.5	517.58
2	5.18	115.15	34.53	105.15	11.17	21.91	182.82	18226.40	30.47	665.97
3	18.96	97.13	31.41	91.06	10.83	31.36	563.26	14164.30	43.33	536.22
4	2.48	95.74	33.04	94.98	10.10	30.40	100.95	17667.20	38.55	750.38
5	7.43	111.33	55.76	88.87	10.33	24.41	175.55	13574.20	27.88	517.58
6	0.59	54.19	31.66	112.43	6.64	29.53	158.29	33580.00	34.21	803.53
7	0.53	48.86	27.66	63.29	7.17	12.38	143.44	26560.00	32.27	927.37
8	0.44	48.93	58.01	62.78	6.69	14.63	98.18	22100.00	89.25	1675.78
9	0.48	65.86	31.61	125.87	6.04	22.97	97.62	35920.00	33.00	980.20
10	1.62	53.08	39.59	138.00	12.18	47.77	35.53	20169.90	25.38	923.57
11	3.84	36.18	35.45	78.84	12.80	29.05	118.16	15435.70	36.43	639.00
Min	0.44	36.18	27.66	62.78	6.04	12.38	35.53	13574.22	25.38	517.58
Max	18.96	115.15	58.01	138.00	12.80	47.77	563.26	35920.00	89.25	1675.78
x_{sr}	4.10	76.16	38.67	95.47	9.30	26.26	161.50	20997.44	40.02	812.47
SD	5.420	30.040	10.312	23.668	2.407	9.427	139.770	7876.856	17.707	332.371
Max/Min	43.09	3.18	2.10	2.20	2.12	3.86	15.85	2.65	3.52	3.24

Manganese ions activate numerous enzymes in plant cells. The most important role of this element in green plants is its involvement in the process of decomposition of water molecules with the release of oxygen.[24] To fulfil its metabolic functions, Mn is only necessary at low concentration (20 mg kg^{-1} dry mass).[25] In the studied plant samples, the amount of Mn was relatively uniform (from 25.38 to 49.5 mg kg^{-1}), with the exception of sample 8 (89.25 mg kg^{-1}), where soil was also loaded with this element. The obtained values are close to those found by Mezyk and Wieckowski, when the Mn content in *V. officinalis* was 52.3 mg kg^{-1}.[13] The uniformity of Mn concentrations in plant samples despite the wide range of Mn concentrations in soil could be explained by an inner mechanisms of the tested *Veronica* species to control/prevent Mn uptake into the roots and/or avoid Mn translocation and accumulation into the upper plant parts. These mechanisms are controlled by their request for micronutrients and their capacity to absorb and eliminate toxic elements.

Zinc is important as a component of enzymes for protein synthesis and energy production, as well for maintaining the structural integrity of biological membranes.[26] It is not highly phytotoxic and the toxicity limits (300 to 400 mg kg^{-1}) depend on the plant species and growth stage.[3] For medicinal plants, WHO limits have not yet been established for Zn. According to Allaway,[20] the range of this element in agricultural products should be between 15 and 200 ppm. According to the present findings, the values of the Zn concentration in all plant species at the studied locations ranged from 27.66 to 58.01 mg kg^{-1}.

Copper is essential for photosynthesis and mitochondrial respiration, carbon and nitrogen metabolism, oxidative stress protection and is required for cell wall synthesis.[26] The content of Cu in plant samples varied between 6.04 and 12.8 mg kg^{-1}, depending on the location where the samples were collected. Medium values of 10.17, 6.64 and 12.49 mg kg^{-1} were obtained in the samples from Mt. Goč, Mt. Vršačke planine and Mt. Stol, respectively. The lowest concentrations of copper were obtained from Mt. Vršačke planine where the highest iron concentrations were recorded. These results are in accordance with literature data that copper availability to plants might be reduced due to high iron contents in the soil solution.[27] In well-aerated soil, Fe occurs mostly in the form of Fe^{3+} oxides or hydroxides,[28] which are known as efficient sorbents for inorganic cations, such as Cu.[29] According to Allaway,[20] the range of Cu in agricultural products should be between 4 to 15 ppm.

Iron is one of the key elements for normal enzyme functions, especially those involved in redox processes, such as synthesis of the porphyrin (chlorophyll and haeme biosynthesis), reduction of nitrite and sulphate, and N_2-fixation (as part of leghemoglobin).[30] The iron content in the investigated *Veronica* species ranged from 35.53 to 563.26 mg kg^{-1}, with the highest concentrations being recorded in the samples from Mt. Goč.

The ratio of Fe/Mn in vegetal tissue should be between 1.5 and 2.5 since both elements are involved in metabolic processes; hence, they must be present in suitable proportions for adequate plant growth.[3] In the present study for most of the tested plant samples (with the exception of samples 1 and 10), this ratio was not within the expected range.

Analysis of heavy metal contents in soil

The heavy metal content of soil is dependent on both natural and anthropogenic sources in the local ecosystems. While natural forms are usually found in relatively low concentrations, the number and intensity of anthropogenic sources have increased the local environmental heavy metal concentrations in recent decades.[31]

The acidity of the soil indirectly affects the availability and toxicity of heavy metals, causing a minimal or a maximal effect depending on the pH range.[32] Their mobility in soil is generally low, especially when the soil is more alkaline.[33] The obtained pH values for the real and potential acidity of the analyzed soils ranged from 5.24 to 7.43 and from 4.09 to 7.09, respectively (Table III). With the exception of sample 4, the soil samples from Mt. Vršačke planine had slightly lower real acidity values compared to the other samples. The average pH values were 6.62, 5.91 and 6.97 for Mt. Goč, Mt. Vršačke planine and Mt. Stol, respectively. The latter is situated in the Carpathian part of eastern Serbia, in the vicinity of the town of Bor. The processing of ore in the Copper Mining and Smelting Complex Bor causes massive air contamination by sulphur dioxide. The high concentrations of this air pollutant lead to the formation of acid rain. The effect of acid rain on the environment depends greatly on the ability of soils to neutralize the acid. Alkaline or basic soils, such as those rich in limestone, calcium carbonate, can neutralize the acid directly. This may be the explanation for the slightly higher pH values of the soil samples from Mt. Stol having underlying limestone.

TABLE III. Acidity of the soil samples

Soil sample	Location	pH	
		Real acidity	Potential acidity
S1	Mt. Goč	6.77	5.44
S2	Mt. Goč	6.39	5.28
S3	Mt. Goč	7.43	7.09
S4	Mt. Goč	5.87	4.74
S5	Mt. Vršačke planine	6.09	4.87
S6	Mt. Vršačke planine	6.14	5.43
S7	Mt. Vršačke planine	6.18	5.41
S8	Mt. Vršačke planine	5.24	4.09
S9	Mt. Stol	7.18	6.45
S10	Mt. Stol	6.76	5.80

In the investigated soil samples, the Cr concentrations ranged from 36.18 to 115.15 mg kg^{-1} and the highest were recorded in the samples collected on Mt. Goč (from 95.74 to 115.15 mg kg^{-1}), which is in a good accordance with previous research.[34] This location is one of the serpentinite sites in central Serbia,[35] and high levels of potentially phytotoxic elements (Ni, Cr and Co) is one of the characteristics of this soil type.[36]

In the soil samples, the levels of Cu varied from 12.38 to 47.77 mg kg^{-1}. The elevated copper concentrations in the samples from Mt. Stol in comparison to the others could be explained by potential pollution as a result of industrial emissions from mines (Bor).

The zinc content in the analyzed soils was higher in samples 6 and 9 than in samples 7 and 8 (Mt. Vršačke planine), showing the possible influence of anthropological activities. Location 9 is close to the mountain lodge, while location 6 is near by the main road. Location 7 and 8 are in the forest region and free of any anthropological activities.

According to Adriano,[37] the regular Mn content for most soil types ranges from 500–1000 mg kg^{-1}. The present results for the total Mn content in the soils varied widely, from 517.58 to 1675.78 mg kg^{-1} and were higher at locations from Mt. Vršačke planine.

Iron was the most abundant trace element in the analyzed soil samples, with values over a wide range, from 13574.2 to 35920.0 mg kg^{-1}. The highest concentrations were recorded in soil samples collected from Mt. Vršačke planine (22100 to 35920 mg kg^{-1}). These results are in agreement with earlier findings that gneiss soils contain high amounts of iron.[38]

For the potentially hazardous elements (Cu, Zn and Cr), the bioconcentration factor (*BCF*), also known as the plant uptake factor, was calculated as the ratio of a particular element in plant to its concentration in the soil (Table IV).[19] With the exception of the *BCF* value for Cr in sample 3, which was close to the allowed limit, all the calculated *BCF* values were lower than the maximum value recommended by the Idaho National Engineering and Environmental Laboratory (Cu = = 0.80, Zn = 1.50 and Cr = 0.19), suggesting the absence of significant pollution.[39]

TABLE IV. Calculated *BCF* values for toxic elements Cu, Cr and Zn

Sample	Cu	Cr	Zn
1	0.34	0.03	0.52
2	0.51	0.04	0.33
3	0.34	0.19	0.35
4	0.33	0.03	0.35
5	0.42	0.07	0.63
6	0.22	0.01	0.23
7	0.58	0.01	0.44
8	0.46	0.01	0.92
9	0.26	0.01	0.25
10	0.25	0.03	0.29
11	0.44	0.16	0.45

Correlation analysis

Correlation analysis has been used to establish relationships between heavy metal concentrations in tested plant and soil samples and several conclusions could be extracted from the obtained results (Table V). No direct correlation was identified between the content of the analyzed trace metals in the soil and *Veronica* species, except in the case of the Mn concentrations ($r = 0.694$, $p <$ < 0.05). The chromium content was in a strong positive correlation to the Fe content in plant samples ($r = 0.928$, $p < 0.001$). This is in agreement with the synergistic interactions between Cr and Fe already reported in the literature.[3]

Furthermore, a high correlation ($r = 0.721$, $p < 0.05$) was found between the Cu and Zn contents in the soil samples, indicating that the general contamination sources for these metals were primarily traffic and industrial activities.

TABLE V. Correlation analysis of the concentrations of elements measured in *Veronica* species and soil samples

Sample	Element	Plant					Soil			
		Cu	Fe	Mn	Zn	Cr	Cu	Fe	Mn	Zn
Plant	Fe	0.172	–	–	–	–	–	–	–	–
	Mn	–0.383	–0.001	–	–	–	–	–	–	–
	Zn	–0.028	–0.238	0.558	–	–	–	–	–	–
	Cr	0.442	0.928^{a}	–0.077	–0.060	–	–	–	–	–
Soil	Cu	0.601	0.011	–0.436	–0.154	–0.442	–	–	–	–
	Fe	-0.728^{b}	–0.281	–0.076	–0.397	–0.558	–0.189	–	–	–
	Mn	–0.512	–0.368	0.694^{b}	0.307	–0.519	–0.327	0.448	–	–
	Zn	0.147	–0.158	–0.554	–0.283	–0.085	0.721^{b}	0.328	–0.199	–
	Cr	0.194	0.355	–0.164	0.183	–0.491	–0.022	–0.511	–0.574	0.081

[a]Significant at $p < 0.001$; [b]significant at $p < 0.05$

CONCLUSIONS

This study of heavy metal contents did not show any significant variation between the tested *Veronica* species from the same location, indicating that their heavy metal uptake pattern was not species specific. The results of the study confirmed that *V. urticifolia* and *V. jacquinii* are promising Cr hyperaccumulator plants. Further research needs to be performed to determine the Cr content in different organs of *Veronica* species from serpentine soil, in order to determine the translocation of Cr from the roots to the tops of the plants. The contents of the measured elements in the soil samples were in the expected ranges for the particular biogeochemical backgrounds.

Acknowledgements. This work was supported by Grant Nos. 143012 and III43009 from the Ministry of Education and Science of the Republic of Serbia. The authors also wish to thank MSc Svetlana Đogo and Mrs Latinka Slavkovic for their professional assistance.

ИЗВОД

СПОСОБНОСТ АКУМУЛАЦИЈЕ ТЕШКИХ МЕТАЛА *Veronica* ВРСТА СА ПЛАНИНСКИХ ЛОКАЛИТЕТА У СРБИЈИ

ЈЕЛЕНА ЖИВКОВИЋ[1], СЛАВИЦА РАЖИЋ[2], ЈЕЛЕНА АРСЕНИЈЕВИЋ[3] и ЗОРАН МАКСИМОВИЋ[3]

[1]*Инсшишуш за йроучавање лековишоī биља ''Др Јосиф Панчић'', Беоīрад,* [2]*Кашедра за аналишичку хемију, Фармацеушски факулшеш, Универзишеш у Беоīраду, Беоīрад и* [3]*Кашедра за фармакоīнозију, Фармацеушски факулшеш, Универзишеш у Беоīраду, Беоīрад*

У овом раду приказан је однос садржаја одабраних елемената у траговима у земљишту и њихове биоакумулације у надземним деловима три *Veronica* врсте (Plantaginaceae). Биљни и узорци земљишта сакупљени су са три планинска локалитета у Србији, подвргнути су микроталасној дигестији у киселој средини и анализирани применом пламене и електротермалне атомске апсорпционе спектроскопије. Укупна концентрација Cu, Zn, Mn, Fe и Cr у узорцима земљишта варира од 12,38 до 47,77, 62,78 до 138,00, 517,58 до 1675,78, 13574,22 до 35920,00 и 36,18 до 115,15 mg kg^{-1}, док се у биљним узорцима креће у опсегу од 6,04 до 12,8, 27,66 до 58,01, 25,38 до 89,25, 35,53 до 563,26 и 0,44 до 18,96 mg kg^{-1}, редом. Нису показане

значајне разлике у концентрацији тешких метала између тестираних *Veronica* врста са истих локалитета, што показује да модел усвајања тешких метала није карактеристика врсте. Упркос великих варирања концентрације Mn у земљишту, концентрација у биљним узорцима је униформна, што указује на потенцијалну могућност тестираних врста да контролишу преузимање Mn или његов транспорт до надземних делова биљке. Најнижа концентрација Cu добијена је у биљним узорцима сакупљеним на земљишту са највећом Fe концентрацијом, сугеришући да је доступност Cu биљкама редукована услед високог садржаја Fe у земљишном раствору.

(Примљено 25. децембра 2011)

REFERENCES

1. B. Kiran, A. Kaushik, C. P. Kaushik, *Process Biochem.* **43** (2008) 598
2. J. R. Peralta-Videa, M. L. Lopez, M. Narayan, G. Saupe, J. Gardea-Torresdey, *Int. J. Biochem. Cell Biol.* **41** (2009) 1665
3. A. Kabata-Pendias, H. Pendias, *Trace elements in soil and plants*, CRC Press, Boca Raton, FL, USA, 2001
4. B. Nowack, J. M. Obrecht, M. Schluep, R. Schulin, W. Hansmann, V. Köppel, *J. Environ. Qual.* **30** (2001) 916
5. A. Pasieczna, J. Lis, *J. Geochem. Explor.* **66** (1999) 219
6. U. S. Harput, I. Saracogly, M. Inoue, Y. Ogihara, *Biol. Pharm. Bull.* **25** (2002) 483
7. E. Küpeli, U. S. Harput, M. Varel, E. Yesilada, I. Saracogly, *J. Ethnopharm.* **102** (2005) 170
8. F. Couplan, *The Encyclopedia of edible plants of North America*, McGraw-Hill, New Canaan, CT, USA, 1998, pp. 393–394
9. D. C. Albach, R. J. Grayer, S. R. Jensen, F. Özgökce, N. C. Veitch, *Phytochemistry* **64** (2003) 1295
10. S. R. Jensen, D. C. Albach, T. Ohno, R. J. Grayer, *Biochem. Syst. Ecol.* **33** (2005) 1031
11. U. S. Harput, I. Saracogly, M. Inoue, Y. Ogihara, *Chem. Pharm. Bull.* **50** (2002a) 869
12. U. S. Harput, I. Saracogly, A. Nagatsu, Y. Ogihara, *Chem. Pharm. Bull.* **50** (2002b) 1106
13. Z. Mezyk, S. K. Wieckowski, *Pol. J. Environ. Stud.* **8** (1999) 129
14. M. E. Abu Ziada, I. A. Mashaly, M. Abd El-Monem, M. Torky, *J. Appl. Sci.* **8** (2008) 1395
15. G. Wang, L. Wang, Z. Li, J. Ding, D. Liu, *Chin. J. Ecol.* **24** (2005) 639
16. A. Samecka-Cymerman, A. J. Kempers, *Arch. Environ. Contam. Toxicol* **53** (2007) 198
17. R. Zurayk, B. Sukkariyah, R. Baalbaki, *Water Air Soil Poll.* **127** (2000) 373
18. S. Ražić, A. Onjia, S. Đogo, L. Slavković, A. Popović, *Talanta* **67** (2005) 233
19. S. Ražić, S. Đogo, L. Slavković, *J. Serb. Chem. Soc.* **71** (2006) 1095
20. W. H. Allaway, *Adv. Agron.* **20** (1968) 235
21. A. K. Shanker, C. Cervantes, H. Loza-Tavera, S. Avudainayagam, *Environ. Int.* **31** (2005) 739
22. A. V. Pawlisz, *Environ. Toxic. Water* **12** (1997) 123
23. R. L. Chaney, M. Malik, Y. M. Li, S. L. Brown, E. P. Brewer, J. S. Angle, A. J. M. Baker, *Current Opin. Biotech.* **8** (1997) 279
24. M. N. V. Prasad, J. Hagemeyer, *Heavy Metal Stress in Plants*, Spinger-Verlag, Berlin, Heidelberg, 1999, pp. 157–181
25. T. Dučić, A. Polle, *Braz. J. Plant Physiol.* **17** (2005) 103
26. R. Hänsch, R. R. Mendel, *Curr. Opin. Plant Biol.* **12** (2009) 259
27. S. Mallick, G. Sinam, R. K. Mishra, S. Sinha, *Ecotoxicol. Environ. Saf.* **73** (2010) 987
28. W. L. Lindsay, A. P. Schwab, *J. Plant Nutr.* **5** (1982) 821

29. S. Ražić, S. Đogo, *Chemosphere* **78** (2010) 451
30. Z. M. N. V. Prasad, J. Hagemeyer, *Heavy Metal Stress in Plants,* Spinger-Verlag, Berlin, Heidelberg, 1999, pp. 232–247
31. M. Koch, W. Rotard, *Water Sci. Technol.* **43** (2001) 67
32. M. H. Wong, *Chemosphere* **50** (2003) 775
33. W. Rosselli, C. Keller, K. Boschi, *Plant Soil* **256** (2003) 265
34. D. Obratov-Petković, I. Bjedov, S. Belanović, *Bull. Fac. Forestry* **98** (2008) 143
35. B. Dudić, T. Rakić, J. Šinžar-Sekulić, V. Atanacković, B. Stevanović, *Arch. Biol. Sci.* **59** (2007) 341
36. E. Kazakou, P. G. Dimitrakopoulos, A. J. M. Baker, R. D. Reeves, A. Y. Troumbis, *Biol. Rev.* **83** (2008) 495
37. D. C. Adriano, *Trace Elements in the Terrestrial Environment*, Springer, New York, 1986, pp. 263–277
38. D. C. Cooper, D. Field, *Earth Planet. Sci. Lett.* **35** (1977) 105
39. Idaho National Engineering and Environmental Laboratory, *Development of plant uptake and bioconcentration factors*, http://www.ar.inel.gov/ (assessed on 25/12/2011)
40. B. Marković, Z. Obradinović, M. Veselinović, J. Anđelković, P. Stevanović, M. Rakić, *Basic geological map of the Federal Republic of Yugoslavia*, 1:100.000 (Osnovna geološka karta SFRJ, 1:100.000), Savezni geološki zavod, Belgrade, Serbia (in Serbian, English and Russian summaries), 1984.

Journal of the Serbian Chemical Society
JSCS-info@shd.org.rs • www.shd.org.rs/JSCS
J. Serb. Chem. Soc. 77 (7) 971–981 (2012)
JSCS–4325
UDC 631.85+631.454+631.8+631.42
Original scientific paper

Fractionation of soil phosphorus in a long-term phosphate fertilization

NASSER RAMDAN AMAIZAH[1], DRAGAN ČAKMAK[2], ELMIRA SALJNIKOV[2],
GORAN ROGLIĆ[1], VESNA MRVIĆ[2], RADA KRGOVIĆ[2] and DRAGAN MANOJLOVIĆ[1]*

[1]*Faculty of Chemistry, University of Belgrade, Studentski trg 12–16, 11000 Belgrade, Serbia and* [2]*Institute of Soil Science, Teodora Drajzera 7, 11000, Belgrade, Serbia*

(Received 27 September, revised 28 November 2011)

Abstract: The changes in inorganic and organic phosphorus (P) fractions of soil resulting from long-term fertilization (40 years) were investigated. In order to improve understanding of the sink and sources of phosphorus, P-fractions were extracted from soil samples from depths of 0–30 and 30–60 cm with different amounts of monoammonium-phosphate (MAP) and then determined. The studied soil was of the Stagnosol type. Phosphate fertilizer was applied in 26, 39 and 52 kg P ha^{-1} amounts during a period of 40 years. Samples were subjected to sequential extraction according to a modified Chang and Jackson method and the Community Bureau of Reference (BCR) sequential extraction procedure in order to extract different forms of phosphorus. The certified reference material CRM 684 (river sediment extractable phosphorus) was used to confirm the accuracy of the instrument and of both employed methods. Furthermore, the association of phosphorus with substrates was provided by comparison of the results of sequential methods of phosphorus species with the sequential extraction of metals (Fe, Al, Mn and Ca). The results of continuous fertilization during 40 years indicated increases of all forms phosphorus in the soil except of phosphorus bound to calcium and organic phosphorus. Application of higher amounts of P-fertilizer resulted in the dominance of the Al–P fraction in the studied soil, which indicated that this fraction was the most responsible for the migration of phosphorus along the soil profile.

Keywords: phosphorus; soil fertilization; sequential extraction; CRM 684.

INTRODUCTION

Phosphates, the most abundant form of phosphorus in the environment, are available for assimilation; thus, they have been traditionally used as fertilizers.[1] For long-term sustainability of cropping, adequate amounts of P through fertilization are needed. It was reported that the addition of inorganic P fertilizers increases the concentration of inorganic P in soil.[2] Phosphorus fertilization given in

---

* Corresponding author. E-mail: manojlo@chem.bg.ac.rs

doi: 10.2298/JSC110927208A

the form of manure, on the other hand, was found to increase the concentration of organic phosphorus.[3] More than 90 % of the total phosphorus in soils is present as insoluble and fixed forms, including the primary phosphate minerals, humus P, insoluble Ca-, Fe-, and Al-phosphates and phosphorus fixed by hydrous oxides and silicate minerals.[4] Guggenberger *et al*.[5] found that fertilization increased the labile organic P pool, but the type of fertilizer did not seem to be of any particular importance. The cumulative accumulation of available P in agricultural soils may partially saturate the soil capacity for P sorption, resulting in an increase of P leaching into the subsoil layers[6] or may sometimes reach a depth of more than 90 cm,[7] suggesting that erosion, rather than leaching, could cause a threat to water bodies.[8] Such a leaching process is especially effective in a Stagnosol type of soil, with a clear E horizon due to its lower adsorption capacity, with relatively shallow ground water.[9,10] Fertilization is an essential part of soil management as plants absorb P from the soil solution or soluble P is lost in runoff, hence, mobile P dissolves or desorbs from the solid phase to the solution.[11] In soil where fertilizers were not used, the concentration of phosphorus was gradually decreased to the level where the addition of P is a necessity for plants. Fertilization with mineral P and the inorganic pools explain 96 % of the variation in the level of available phosphorous.[12]

To characterize soil inorganic P in detail, Chang and Jackson[13] developed a sequential fractionation procedure based on the ability of selected extractants to distinguish between phosphorus in different pools. Originally, their procedure was thought to solubilize separately P in discrete minerals. The discovery of ligand exchange by Hingston *et al*.[14] created a new theoretical basis for this approach. In the light of current knowledge, it is clear that the procedure that Chang and Jackson developed separates different P pools according to the surface the P is bound too. The first extraction step aims at removing the loosely bound P and exchangeable Ca^{2+}, possibly interfering with the subsequent extraction steps. The use of NH_4F in the second extraction step is based on the ability of fluoride to form a stable complex with Al and to extract selectively Al-bounded P. Several modifications of the fractionation procedure had been published.[15–17] It was discovered that the Chang and Jackson fractionation procedure was not applicable to calcareous soils or sediments. Based on their work, a fractionation procedure for calcareous soils was further developed. Another widely used fractionation procedure was developed by Hedley *et al*.[18] The BCR extraction method according to the European Program, Standards, Measurements and Testing (SMT) standard protocol was applied for the determination of total P in soil samples. The BCR method is a non-specific extraction procedure developed for the determination of P in freshwater sediments. It was developed within the SMT protocol and used for a certification campaign for reference materials. A detailed description of the SMT protocol was given by Ruban.[19]

The aim of this study was to compare different forms of phosphorus in soil after 40 years of fertilization strategies. In the period of 40 years, phosphate fertilizer was applied in amounts of 26, 39 and 52 kg P ha^{-1}, but the added amount of urea was limited. Speciation of phosphorus was performed using two sequential extraction procedures: a modified Chang and Jackson[20] and the BCR procedure.[19] The goal of this study was to establish the most active form of P in a long-term mineral fertilization experiment, as well as to monitor the movement of different phosphorus forms along the soil profile.

EXPERIMENTAL

Site description

The investigation was conducted at the Varna experimental station, 44°41'38" and 19°39'10" (near Belgrade, Serbia) where a wide range of different fertilization treatments has been undertaken since 1968. The soil type was Stagnosol, a loam textured Pseudogley developed on Pliocene loam and clay materials under aquatic conditions at 109 m above sea level. Detailed descriptions of the studied site and the soil characteristics were given in a previous paper.[21] The experiment was arranged as a randomized block design, with each treatment randomized in three blocks for a total of 12 plots (5 by 11 m). Composite samples of five soil subsamples were taken from two depths: surface (0–30 cm) and subsurface (30–60 cm) layers in the spring of 2008. Three different amounts of $NH_4H_2PO_4$ fertilizer (MAP) were applied during the 40-year experiment (26, 39 and 52 kg P ha^{-1}) in combination with a constant amount of N (urea, 60 kg ha^{-1}) and K (KCl, 50 kg ha^{-1}). The mineralogical composition of the studied soil was illite (50–70 %), vermiculite (10–30 %), and other clay minerals (kaolinite, chlorite, feldspar, quartz, and amphibolites). The cultivated cops were winter wheat (*Triticum aestivum* L.) and corn (*Zea maize* L.) with crop residues removed. The soil cultivation was performed by a standard plowing to a depth of 25 cm. The results were compared with those obtained from the soil samples where only N and K fertilizer was used.

Sequential extraction procedures

A portion of each soil sample (air-dried) was subjected to sequential extraction. Speciation of phosphorus was realized using two sequential extraction procedures: a modified Chang and Jackson[20] and the BCR procedure.[19] Details are given in Table I. Furthermore, the soil was subjected to a 5-phase sequential extraction[22] in order to study the substrates (Fe, Al, Mn and Ca) of phosphorus and metals. Details are given in Table II.

TABLE I. Reagents and corresponding P fractions for the two sequential extraction procedures used in this study

Procedure	Step 1	Step 2	Step 3	Step 4	Step 5	Step 6
Manojlovic *et al.* 2007	1 M NH_4Cl, water soluble P	0.5 M NH_4F, Al bound P	0.1 M NaOH, Fe bound P	0.3 M Na dithionite, Na citrate, reducible P	0.1 M NaOH, occluded P	0.25 M H_2SO_4, Ca bound P
BCR (Ruban *et al.*, 2001)	1 M NaOH, NaOH-P	3.5 M HCl, HCl-P	1 M NaOH, inorganic P	1M HCl + calcination, Organic P	3.5 M HCl + calcinations, conc. HCl-P	–

The certified reference material CRM 684 (river sediment extractable phosphorus, from the Po River, Italy) was used.

TABLE II. Reagents used in the sequential extraction procedure employed to study the substrate metals (Fe, Al, Mn and Ca) and phosphorus

Procedure	Step 1	Step 2	Step 3	Step 4	Step 5
Petrovic *et al.* 2009	1 M CH_3COONH_4, exchangeable	1 M $NH_2OH\cdot HCl$, bound to carbonates and easily reducible	0.2 M $(NH_4)_2C_2O_4$ and 0.2 M $H_2C_2O_4$, moderately reducible	30 % H_2O_2 + 3.2 M CH_3COONH_4, organic sulfide	6 M HCl, residual

Reagents and instruments

All chemicals were of analytical reagent grade and were supplied by Merck (Darmstadt, Germany). A stock standard solution of orthophosphate (100 mg P^{-1}) was prepared from KH_2PO_4. Various solutions were prepared by dilution of the stock phosphorus solution. Calibration standards were prepared from multi-element standard stock solutions. These multi-element standards and blanks were prepared in the same matrix as the extracting reagents in order to minimize matrix effects.

The content of phosphorus and metals in all extracts were determined by inductively coupled plasma atomic emission spectrometry, iCAP 6500 Duo (Thermoscientific, United Kingdom).

Statistical analysis

Statistical analyses were performed using SPSS (version) 16 software. The effects of treatments on all variables were tested by ANOVA. The significance of their correlations was analyzed *via* the Pearson correlation matrix (SPSS, 2007).

RESULTS AND DISCUSSIONS

Modified Chang and Jakson method

The obtained results are presented in Table III.

Phosphorus extractable by NH_4Cl (water-soluble P). The content of phosphorus soluble in ammonium chloride solution (NH_4Cl) was low, about 1 % of the total content of mineral phosphorus. Fertilization with mineral phosphorus increased the content of water-soluble phosphorus in comparison with the control sample (6 times for sample treated by 52 kg P ha^{-1}, 0–30 cm depth). This significant increase was directly related to the accumulation of P[23] and was influenced by the processes of saturation of free spaces for adsorption of P in soil.[24]

The increase of water soluble P was lower for samples of 30–60 cm depth, which could be explained by P fixation during through-soil leaching.

Phosphorus bound to aluminum (Al–P). Phosphorus bound to aluminum (Al–P) represented a significant part of the mineral phosphorus. The recorded relative increase of Al–P *versus* the other mineral forms of P (from 16.08 % in the control to 34.51 % in the treatment with 52 kg P ha^{-1}) indicated the strong effect of fer-

TABLE III. Sequential analysis by a modified Chang and Jackson method. Forms of phosphorous in Stagnosol in a long-term phosphate fertilization experiment; *m* in mg kg^{-1}; *w* – ratio to control; w_{min} – content of mineral P in %; a, b, c, d – the identical letters show no significant difference between the different fertilization treatments

kg P ha^{-1}	Treatment																	
	NH_4Cl–P			Al–P			Fe–P			Reducible P			Occluded P			Ca–P		
	m	*w*	w_{min}	*m*	*w*	w_{min}	*m*	*w*	w_{min}	*m*	*w*	w_{min}	*m*	*w*	w_{min}	*m*	*w*	w_{min}
	Depth: 0–30 cm																	
0	3.08a	1.0	0.8	63.77a	16.1	1.0	0.30a	0.07	1.0	143.08a	36.1	1.0	46.94ab	11.8	1.0	139.35a	35.1	1.0
26	5.35a	1.7	1.2	100.80b	23.4	1.6	0.54b	0.13	1.8	125.04a	29.1	0.9	32.57a	7.6	0.8	165.75a	38.5	1.2
39	9.96b	3.2	0.6	130.16c	23.8	2.0	0.44ab	0.08	1.5	195.57b	35.7	1.4	67.37c	12.3	1.4	144.50a	26.4	1.0
52	19.38c	6.3	1.1	194.88d	34.5	3.1	0.46b	0.08	1.5	176.07b	31.2	1.2	60.70bc	10.7	1.3	126.33a	22.4	0.9
P	< 0.01			< 0.001			< 0.001			< 0.01			< 0.05			–		
	Depth: 30–60 cm																	
0	2.69a	1.0	0.8	48.50a	14.4	1.0	0.30a	0.09	1.0	120.27a	35.6	1.0	33.93a	10.0	1.0	132.15a	39.11	1.00
26	3.71a	1.4	0.9	63.33ab	15.9	1.3	0.41a	0.10	1.4	130.44a	32.6	1.1	44.73a	11.2	1.3	157.02a	39.29	1.19
39	5.38a	2.0	1.4	78.96b	19.8	1.6	0.31a	0.08	1.0	172.10b	43.1	1.4	56.67b	14.2	1.7	137.91a	34.51	1.04
52	4.67a	1.7	1.1	83.78b	19.2	1.7	0.28a	0.06	0.9	116.37a	26.6	1.0	47.47a	10.9	1.4	184.15a	42.17	1.39
P	–			< 0.01						< 0.01			< 0.05					
Correlation coefficient between two depths	0.518 ($P < 0.05$)			0.876 ($P < 0.01$)			0.405			0.405			0.254			0.385		

tilization exactly on this form of phosphorus. This was confirmed by the significant absolute increase of Al–P according to the applied fertilizer (three times more in 52 kg P ha^{-1} compared to the control). In acidic mineral soils, as in the present case, P is fixed mainly by aluminum and iron while in alkaline soils by calcium.[25]

The phosphorus movement along the depth was very limited and slow due to its strong binding. However, the increase in the absolute and relative values (from 14.35 % in the control to 19.18 % in the treatment with 52 kg P ha^{-1}), as well as the high coefficient of correlation between the first and second depths, indicate its mobility.

Phosphorus bound to iron (Fe–P). Phosphate bound to iron represented a very small fraction (about 0.1 %) of the mineral Al forms, probably due to its binding to reducible and occluded forms of P, similarly as the labile fraction of Fe–P is included in the Al–P phase. However, in spite of the small amounts, application of P-fertilizer increased its content compared to the control for the first depth, 0–30 cm (Table III). The percentage of Fe–P compared to the other mineral forms changed very little.

Reducible phosphorus (R-P). The reducible-P was well represented in the fraction compared to other mineral forms of P (about 30 %). Noticeably, the portion of this P *versus* the other forms in the first depth was the greatest in the control treatment, while in the higher fertilizer treatments, it was similar to the values of Al–P (Table III). The absolute content of R-P in soil between treatments was different. However, no clear tendency of the increase in its content for each treatment was observed, especially for the second depth.

Occluded phosphorus (O-P). The occluded phosphorus fraction represented about 10 % of the mineral forms of P. Fertilization resulted in irregular increases in the content of occluded P, probably due to irregularities of the field conditions and the processes that influence the content of O-P. Changes in the content of O-P were not detected.

Phosphorus bound to calcium (Ca–P). Phosphorus bound to calcium was a significant fraction within the studied soil. For the second depth, its portion in the mineral forms of P was the greatest (42.17 % in the treatment with 52 kg P ha^{-1}). The absolute content of Ca–P did not show significant differences for both depths (Table III). The absence of the effect of P-fertilization in acidic soils was also recorded in another paper.[26] A possible explanation lies in the fact that Ca–P was localized within the mineral apatite and thus, weakly changeable. However, the relative increase of Ca–P for the second depth comparing to the other mineral P forms indicated a significantly reduced binding of phosphorous with Al in the second depth.

BCR sequential analysis

The BCR analysis is not a classic sequential analysis. Less specific means for isolation of the first two fractions are used in comparison with the Chang and Jackson method. The share of NaOH–P (Al–Fe–Mn bound P) and HCl–P (Ca–P) fractions increased for both depths and depended on the amount of added fertilizer (Table IV). The results obtained for the fertilized samples indicated the leaching of the NaOH fraction from the first to the second depth.

The fraction of organic phosphorous (Org-P) represented about 20–30 % of the sum of the inorganic and organic P. The relative amount of organic P decreased from 28.9 to 20.3 %, correspondingly to the application rate of the fertilizer in the first depth, while in the second depth, this decrease was not linear (Table IV). However, for the second depth, the two highest rates of treatment with fertilizer resulted in higher contents of Org-P in comparison with the first depth. The absolute content of Org-P was not changed, which indicates that phosphorus from the fertilizer did not transform to organic P.

The content of concHCl-P showed a linear increase with depth through both layers, with the increase in the greater depth indicating greater fixation of P.

The certified reference material CRM 684 (river sediment extractable phosphorus, BCR, Community Bureau of Reference, Brussels, Belgium) was used to confirm the accuracy of the employed method. The results of phosphorous determination in the reference material showed very good agreement with the declared value (Table V).

Determination of substrates of metals and phosphorus

The results for the phosphorus sequential extraction methods were compared to the results for the sequential extraction of metals and a better assessment of substrates (Fe, Al, Mn and Ca) associated with phosphorus was thereby provided.

The most important correlations found between the contents of the different phosphorus forms and corresponding substrates are presented in Tables VI and VII.

The very high correlation between the applied P and aluminum from the second and the third phase confirms the importance of the aluminum present in soils for the chemodynamics of phosphorus. Regardless of the applied phosphorus extraction method, very high correlations between contents of aluminum and most phosphorus forms were obtained.

Aluminum from the second phase (aluminum II) is a typical representative of the clay minerals present in the examined samples and it could be extracted by an acid hydroxyamine solution, together with manganese oxides and the associated form of P. The role of aluminum II and manganese II confirmed the good correlation with different forms of P (Tables VI and VII).

Oxalate/oxalic acid (the extraction solution for phase III) is very efficient in the extraction of different forms of phosphorus associated with colloid amor-

TABLE IV. Results of the BCR method. Forms of phosphorous in Stagnosol in a long-term phosphate fertilization experiment; m in mg kg^{-1}; w – ratio to control; w_{IP+OP} – sum of IP + organic P, %; a, b, c – the identical letters show no significant difference between the different fertilization treatments

kg P ha^{-1}	Treatment											
	NaOH–P		HCl–P		IP			Organic P			Conc. HCl–P	
	m	w	m	w	m	w	w_{IP+OP}	w	m	w_{IP+OP}	m	w
Depth: 0–30 cm												
0	523.33a	1.00	366.7a	1.00	990.0a	1.00	71.0	403.3	1.0	28.9	892.0a	1.0
26	806.67b	1.54	533.3b	1.45	1200.0ab	1.21	76.3	373.3a	0.9	23.7	1127.7ab	1.3
39	1033.33b	1.97	683.3c	1.86	1473.3bc	1.49	79.6	376.7	0.9	20.6	1188.3b	1.3
52	1003.33b	1.97	753.3c	2.05	1600.0c	1.61	79.7	406.7	1.1	20.3	1374.0c	1.5
P	< 0.001		< 0.001			< 0.05			–		< 0.01	
Depth: 30–60 cm												
0	583.33a	1.00	340.0a	1.00	946.7a	1.00	71.0	386.7ab	1.0	29.0	813.7a	1.0
26	890.00b	1.52	420.0a	1.23	1020.0a	1.08	74.5	350.0a	0.9	25.6	958.3ab	1.2
39	1210.00c	2.07	546.7b	1.61	1093.3a	1.15	73.7	390.0ab	1.1	26.3	1048.7bc	1.3
52	1196.67c	2.05	586.7b	1.64	1226.7a	1.30	72.0	476.7b	1.2	28.0	1068.0c	1.3
P	< 0.01		< 0.05			–			–		–	
Correlation coefficient between two depths	0.901 (P < 0.01)		0.865 (P < 0.01)			0.483			–0.075		0.799 (P < 0.01)	

phous aluminum oxides and iron oxides. This fraction in the examined samples represents a significant substrate of phosphorus and the highest increasing content of phosphorus due to fertilization. This is conformed by the very high correlation factor.

TABLE V. Results of the BCR method. Forms of phosphorous in the certified reference material (CRM 684)

Phosphorous forms	NaOH-P	HCl-P	Inorganic P	Organic P	Conc. HCl-P
Declared, mg kg^{-1}	550±21	536±26	1113±24	209±9	1373±35
Found, mg kg^{-1}	587±11	530±11	1145±10	224±5	1401±10

TABLE VI. The correlation of extracted phosphorus by the modified Chang and Jackson method with various substrates

Parameter	Correlation coefficient, *r*	*P* value
Added P / Al II	0.9663	0.000
NH_4Cl-P / Al II	0.8502	0.000
Al-P / Al II	0.9037	0.000
Added P / Mn II	0.6911	0.013
NH_4Cl-P / Mn II	0.6599	0.020
Al-P / Mn II	0.7380	0.006
Al-P / Al III	0.8255	0.001
Red-P / Al III	0.5778	0.049
Added P / Al III	0.9546	0.000

TABLE VII. The correlation of extracted phosphorus by the BCR method with various substrates

Parameter	Correlation coefficient, *r*	*P* value
NaOH-P / Al II	0.8936	0.000
HCl-P / Al II	0.9120	0.000
IP / Al II	0.8931	0.000
concHCl-P / Al II	0.8879	0.000
NaOH-P / Mn II	0.6383	0.025
HCl-P / Mn II	0.7321	0.007
NaOH-P / Al III	0.9122	0.000
HCl-P / Al III	0.8945	0.000
IP / Al III	0.8709	0.000
concHCl-P / Al III	0.8721	0.000

Although most of iron oxides are present in phase III (there is no strong correlation with phosphorus), their role in the chemodynamics of phosphorus should not be ignored, especially because aluminum has a tendency to co-precipitate with iron oxide.

In addition, considering the soil type, the low correlations with calcium were expected.

CONCLUSIONS

Long-term fertilization with monoammonium-phosphate (MAP) influenced the content of all forms of P except P bound to Ca as determined by a modified Chang and Jackson method. The 40-year long fertilization period did not affect the content of organic P in soils. On the contrary, the results obtained by the BCR method showed that the contents of NaOH–P and HCl–P fractions were increased, as well as leaching along the soil profile.

Fertilization considerably increased the content of available P, especially of P bound to Al. Application of higher amounts of P-fertilizer resulted in the dominance of the Al–P fraction in the studied soil. A regular influence of fertilization on the second depth (30–60 cm) was established only for Al–P.

The application of mineral P fertilizer on the soil produced a significant increase in the bioavailable phosphorus. Most of this phosphorus was bound to clay minerals (hydrated oxides of aluminum and manganese from second and third phase) and remained in bioavailable forms.

ИЗВОД

ФРАКЦИОНИСАЊЕ ФОСФОРА У ЗЕМЉИШТУ НАКОН ДУГОТРАЈНЕ ПРИМЕНЕ ФОСФОРНОГ ЂУБРИВА

NASER RAMDAN AMAIZAH[1], ДРАГАН ЧАКМАК[2], ЕЛМИРА САЉНИКОВ[2], ГОРАН РОГЛИЋ[1], ВЕСНА МРВИЋ[2], РАДА КРГОВИЋ[2] И ДРАГАН МАНОЈЛОВИЋ[1]

[1]*Хемијски факултет, Универзитет у Београду, Студентски трг 12–16, 11000 Београд и*
[2]*Институт за земљиште, Теодора Драјзера 7, 11000, Београд*

У овом раду испитиване су промене у фракцијама неорганског и органског фосфора (P) у земљишту које су изазване 40 годишњим ђубрењем амонијум-фосфатом (MAP). Ђубриво је додавано у количинама од 26, 39 и 52 kg P по хектару земљишта. У циљу праћења мобилности фосфора, екстраховане су фосфорне фракције са две различите дубине земљишта: површински слој од 0–30 cm и дубина од 30–60 cm. Тип испитиваног земљишта је Стагносол. Узорци су у циљу екстраховања различитих облика фосфора подвргнути секвенцијалној екстракцији и то на два начина: према модификованој *Chang* и *Jackson* методи и BCR методи. Сертификовани референтни материјал CRM 684 (речни седимент) је коришћен за праћење тачности обе коришћене методе. Осим тога је проучено везивање фосфора са супстратима (Fe, Al, Mn и Ca) који су екстраховани секвенцијалном екстракцијом метала. Резултати указују да континуално 40 годишње ђубрење доводи до повећања садржаја свих облика фосфора у земљишту осим фосфора који је везан за калцијум и органског фосфора. Применом веће количине фосфорног ђубрива долази до доминације фракције фосфора везаног за алуминијум у испитиваном земљишту што указује да је та фракција најодговорнија за миграцију фосфора кроз земљиште.

(Примљено 27. септембра, ревидирано 28. новембра 2011)

REFERENCES

1. I. Aydin, F. Aydin, A. Saydut, C. Hamamci, *J. Hazard. Mater*. **168** (2009) 664
2. K. W. Perrot, S. U. Sarathchandra, J .E. Waller, *Aust. J. Soil Res.* **28** (1990) 593
3. A. N. Sharpley, R. W. McDowell, P. J. A. Kleinman, *Soil Sci. Soc. Am. J.* **68** (2004) 2048

4. K. Mengel, E. A. Kirkby, *Principles of Plant Nutrition*, 5th ed., Kluwer, Dordrecht, Boston, London, 2001, p. 453
5. G. Guggenberger, B. T. Christensen, G. Rubak, *J. Plant Nutr. Soil Sci.* **163** (2000) 151
6. P. S. Hooda, A. R. Rendell, A. C. Edwards, P. J. A. Withers, M. N. Aitken, V. W. Truesdale, *Environ. Qual. J.* **29** (2000) 1166
7. C. Chang, T. G. Sommerfeldt, T. Entz, *Environ. Qual. J.* **20** (1991) 475
8. Q. Zhou, Y. Zhu, *Geoderma 115* (2003) 45
9. G. Tyler, *Geoderma* **119** (2004) 277
10. R. Väänänen, J. Hristov, N. Taskanen, H. Hatikainen, M. Nieminen, H. IIvesniemi, *Boreal Environ. Res.* **13** (2008) 553
11. M. A. Tabatabai, D. L. Sparks, *Chemical Processes in Soils*, Soil Science Society of America, Inc. Madison, Wisconsin, USA, 2005, p. 273
12. M. A. Beck, P. A. Sanchez, *Soil Sci.* **34** (1994) 1424
13. C. Chang, M. L. Jackson *Soil Sci.* **84** (1957) 133
14. F. J. Hingston, R. J. Atkinson, A. M. Posner, J. P. Quirk, *Nature* **215** (1967) 1459
15. C. V. Fife, *Soil Sci.* **87** (1959) 83
16. A. Popovic, D. Djordjevic, *J. Serb. Chem. Soc.* **70** (2005) 1497
17. D. Manojlovic, M. Todorovic, J. Jovicic, V. D. Krsmanovic, P. A. Pfendt, R. Golubovic, *Desalination* **213** (2007) 104
18. M. J. Hedley, J. W. B Stewart, B. S. Chauhan, *Soil Sci. Soc. Am. J.* **46** (1982) 970
19. V. Ruban, J. F. Lopez-Sanchez, P. Pardo, G. Rauret, H. Muntau, P. Quevauviller, *J. Environ. Monit.* **3** (2001) 121
20. G. Petersen, R. Rey, *Sci. Soc. Am. J.* **30** (1966) 563
21. D. Cakmak, E. Saljnikov, V. Mrvic, M. Jakovljevic, Z. Marjanovic, B. Sikiric, S. Maksimovic, *Environ. Qual. J.* **39** (2010) 541
22. Dj. Petrovic, M. Todorovic, D. Manojlovic, V. D. Krsmanovic, *Pol. J. Environ. Stud.* **18** (2009) 873
23. A. Jaakola, H. Hartikainen, R. Lemola, *Agric. Food Sci. Finl.* **6** (1997) 313
24. S. Van Der Zee, M. M. Nederlof, W. Van Riemsdijk, F. De Haan. *J. Environ. Qual.* **17** (1988) 682
25. T. Peltovuori, R. Uusitalo, T. Kauppila, *Geoderma* **110** (2002) 35
26. H. Hartikainen, *J. Agric. Sci. Finl.* **61** (1989) 55.